HIGH TEMPERATURE OXIDATION OF Ti_3Al-BASED INTERMETALLIC ALLOYS

by

TAPAS KUMAR RAY

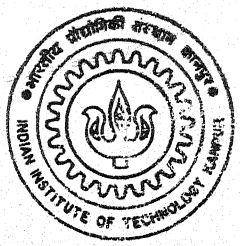

DEPARTMENT OF MATERIALS AND METALLURGICAL ENGINEERING

INDIAN INSTITUTE OF TECHNOLOGY KANPUR

APRIL, 1995

HIGH TEMPRATURE OXIDATION OF Ti_3Al-BASED INTERMETALLIC ALLOYS

A THESIS SUBMITTED

IN PARTIAL FULFILMENT OF THE REQUIREMENTS

FOR THE DEGREE OF

DOCTOR OF PHILOSOPHY

By

Tapas Kumar Ray

to the

DEPARTMENT OF MATERIALS AND METALLURGICAL ENGINEERING

INDIAN INSTITUTE OF TECHNOLOGY

KANPUR–208016 INDIA

APRIL 1995

DEDICATED

TO

My Parents

and

Shri Abani Mohan Chatterjee

and

Shri Akshoy Kumar Chatterjee

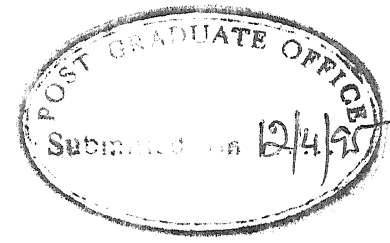

CERTIFICATE

It is certified that the work contained in the thesis entitled "HIGH TEMPERATURE OXIDATION OF Ti_3Al-BASED INTERMETALLIC ALLOYS" by **Tapas Kumar Ray** has been carried out under our supervision and that this work has not been submitted elsewhere for a degree.

(R. Balasubramaniam)
Assistant Professor

(A. Ghosh)
Professor

Department of Materials and Metallurgical Engineering

Indian Institute of Technology

Kanpur - 208016

ACKNOWLEDGEMENTS

The author wishes to take this opportunity to express his heartfelt reverence and gratitude to his supervisors Professor A. Ghosh and Dr. R. Balasubramaniam for their guidance, valuable suggestions and encouragement which brought forth the culmination of the study.

Author also wishes to acknowledge Dr.D. Banerjee and Dr.A.K. Gogia of DMRL, Hyderabad, and Dr.A. Pandey and Dr.V.N. Shukla of Texas Instruments, USA for providing the samples and rendering some other help.

Sincere thanks and appreciation are due to Dr.S.K. Choudhary and Mr.A. Sharma for various help and cooperation throughout the entire programme.

The author is grateful to Mr.B.D. Biswas who not only typed the manuscript but shared feelings at many odd moments. Thanks are also due to Mr.V.P. Gupta for tracing the figures.

Cooperation and help received from Dr.M.N. Mungole, M/s K.P. Mukherjee, P.K. Pal, U.S. Singh, D.P. Tripathi, Ram Avtar, K.S. Vamra, R.C. Sharma and S.B. Shukla are thankfully acknowledged.

Author would also like to thank his friends G.G.Roy, S.Ghosh, B. Bhattacharyay, N.K. Nath, K.K. Singh, C.N. Thakur, M. Sujata, S. Suwas, S. Ghosh Choudhary, K.S. Rao, S. Basu Mallick, A.K. Singh, S. Bhattacharyay, S. Mukhopadhyay, and Dr.S.N. Maiti for their support, help and encouragement.

Continued encouragements received from Professors A.K. Biswas, R.K. Ray and Dr.D. Bandyopadhyay and Dr.S.K. Dutta are also sincerely acknowledged.

The author is grateful to Dr.(Mrs) R. Ghosh, Mrs M. Biswas Dr.(Mrs) S. Biswas, Sudeshna and Avidipto who with their affectio and love made his stay a memorable one.

He had also the privilege to be associated with many othe friends and well wishers whose names have not been mentioned here.

Finally, the author is greatly indebted to his beloved famil members, relatives, and friends whose continued encouragement an support enabled him to complete the study.

Tapas Kumar Ra

LIST OF CONTENTS

CHAPTER Page

CHAPTER Page

CHAPTER Page

CHAPTER Page

LIST OF FIGURES

LIST OF TABLES

LIST OF SYMBOLS

a_M : activity of metal M

C_i : concentration of species i

C_e : concentration of electronic defect

C_h : concentration of electron hole

D_i : diffusion coefficient of species i, $m^2 s^{-1}$

D_{av} : average diffusion coefficient, $m^2 s^{-1}$

k_c : rate constant for cubic law

k_i : instantaneous parabolic rate constant, $kg^2\ m^{-4}\ s^{-1}$

k_l : linear rate constant, $kg\ m^{-2}\ s^{-1}$

k_m : power law rate constant

k_p : parabolic rate constant, $kg^2\ m^{-4}\ s^{-1}$

k'_p : averaged parabolic rate constant, $kg^2\ m^{-4}\ s^{-1}$

K : equilibrium constant

m : power law exponent

p_{O_2}, p_{N_2}, p_{CO_2} : partial pressure of gaseous species in a gas mixture, atm

$p^e_{O_2}$, $p^e_{N_2}$, $p^e_{CO_2}$: equilibrium partial pressure of gaseous species in a gas mixture, atm

N : number

P : average weight fraction of oxygen in oxide scale

Q : activation energy, $kJ\ mole^{-1}$

Q_{eff} : effective activation energy, $kJ\ mole^{-1}$

R : gas constant

t : time

t_i : instantaneous time

T : temperature, K

ΔG^{o} : change in standard free energy of a reaction, kJ $mole^{-1}$

$\frac{\Delta W}{A}$: weight gain per unit surface area of specimen at any time t = t, kg m^{-2}

x : scale thickness

X_B : mole fraction of solute B

X_B^* : critical solute content for internal to external oxidation

y : stoichiometric factor

ρ_{ox} : average density of oxide scale, kg m^{-3}

μ_{O_2} : chemical potential of oxygen

$\mu_{O_2}^e$: equilibrium chemical potential of oxygen

SYNOPSIS

Titanium aluminides based on Ti_3Al (designated as α_2) and TiAl (designated as γ) compounds have the potential to become a class of high temperature structural materials. They have been attracting increasing attention over the last 10 to 15 years as candidate materials for the next generation gas turbine engines and air frame components over the conventional two phase ($\alpha+\beta$) titanium alloys and nickel base superalloys. The current state-of-art development limits application of the most advanced titanium alloys to 600°C, because of lack of adequate strength and oxidation resistance above this temperature. Titanium alloys also suffer from limitations in damage tolerance, creep strength, and undergo rapid oxidation in turbine engine compressor application. Apart from increasing service temperatures, further advancement of aerospace systems and turbine engine technology call for introduction of structures with lighter weight for achieving higher thrust-to-weight ratio. Lower density alloys play a pivotal role in allowing this advancement. Currently, the materials most suited to these demanding needs are titanium aluminides based on Ti_3Al, and TiAl.

Low ductility and toughness at low to intermediate temperatures were important barriers to application for quite some time. However, this has been largely solved through chemistry control by alloying additions, and manipulation of microstructure. Niobium has proven to be the most effective addition for increasing room temperature ductility of binary Ti_3Al by stabilizing the ductile high temperature β-phase. Efforts are underway to make the above alloy class an engineering material.

Thus a key factor in increasing maximum use temperature is enhanced oxidation resistance while retaining adequate levels of creep strength. Particularly, once the desirable crystal structure of a material has been obtained and subsequent mechanical properties have been achieved, then the focus should be on oxidation and corrosion resistance. Therefore, the study of high temperature oxidation of titanium aluminides is important. This is specially so for Ti_3Al-based alloys, since here the lack of oxidation resistance primarily limits the maximum service temperature.

The thesis consists of six chapters. Chapter 1 briefly discusses the advantages and disadvantages of titanium aluminide as a high temperature material. It also records the salient features of structure and mechanical properties of important high temperature alloys including alloys based on Ti_3Al and TiAl.

Chapter 2 contains literature review on :

(i) structure, phase relations and mechanical properties of Ti-Al and Ti-Al-Nb alloys,

(ii) fundamentals of oxidation of metals and alloys,

(iii) thermodynamics and kinetics of oxidation and nitridation of Ti-Al-Nb system.

The findings of the review reveal that some controversies on several aspects of oxidation of such alloys exist. In the present investigation attempts were made to focus on some of these controversial issues, and throw further lights on the same for resolution of controversies.

Chapter 3 describes details of specimen, apparatus and experimental techniques. In the present investigation high temperature isothermal oxidation of three Ti_3Al-based alloys, viz., Ti-25Al, Ti-24Al-15Nb and Ti-25Al-11Nb (atom pct) has been studied. Some experiments have also been conducted to elucidate nitriding behaviour of these alloys. Various gases and gas mixtures employed were oxygen, nitrogen, oxygen-nitrogen, oxygen-argon and nitrogen-carbon dioxide at a total pressure of 1 atmosphere. The experiments in oxygen were carried out at several temperatures in the range of 1000 to 1300K, and in other gases and gas mixtures mostly at two temperatures, viz. 1200 and 1300K. Out of two niobium containing alloys, emphasis was given for Ti-24Al-15Nb since this composition has not been properly investigated so far. Time of exposure in reactive environments ranged between 4 to 6 hr mostly. However, in some cases, 10 hr and 24 hr exposure times were also employed.

Polished samples of length, width and thickness varying between 13 to 16 mm, 9 to 12 mm and 0.5 to 1.5 mm respectively were employed for experiments. Sample was hung inside the furnace from a Cahn 1000 electrobalance to measure weight gain as function of time. The scales formed after exposure were examined by visual observation, X-ray diffraction, scanning electron microscope with energy dispersive X-ray analysis, and optical microscope. Some microhardness measurements were also made in the alloys adjacent to alloy/scale interface.

Chapter 4 presents experimental results as well as processing of weight gain per unit area ($\frac{\Delta W}{A}$) vs time of exposure (t) data for determination of rate constant, as well as for assessment of

applicability of parabolic rate law and power law of oxidation. The principal reaction was oxidation. However, in nitrogen bearing atmospheres some nitridation was also observed.

The salient findings were:

(i) Amongst duplicate sets reproducibility of $(\frac{\Delta W}{A})$ vs t data was fairly good, and the values of parabolic rate constant (k_p) obtained by linear regression fitting of $(\frac{\Delta W}{A})^2$ vs t data, were also fairly reproducible. However, the instantaneous parabolic rate constant (k_i) was not independent of time. k_i also did not exhibit any systematic pattern of variation with time. Hence obedience to parabolic rate law was approximate only.

(ii) Another rate constant (k_m) was obtained by linear regression fitting of log $(\frac{\Delta W}{A})$ vs log t data based on the equation;

$$(\frac{\Delta W}{A})^m = k_m . t \qquad \ldots(1)$$

The scatter in data fitting was large. Moreover, both k_m and m exhibited large scatter as well as significant irreproducibility amongst duplicate sets. The values of m ranged between 1 to 1.86 as against the value of 2 for parabolic rate law. Hence, the oxidation behaviour may be stated as 'paralinear'.

(iii) In view of good reproducibility of parabolic rate constant (k_p) amongst duplicate sets as well as for comparison with literature, it was employed for further interpretation of kinetic data.

Chapter 5 contains discussions of results. It has been broadly divided into two parts viz.:

(i) oxidation behaviour in oxygen,

(ii) oxidation and nitridation behaviour in O_2-N_2, O_2-Ar, N_2 and N_2-CO_2.

The findings may be summarized as follows :

(i) The k_p for oxidation of Ti-24Al- 15Nb and Ti-25Al-11Nb in oxygen were almost the same at the same temperature. In general k_p values for Ti-25Al were 2 to 8 times larger as compared to those for Nb-containing alloys in the temperature range of 1100 to 1300K.

(ii) Temperature dependence of k_p followed Arrhenius type equation. The 'effective activation energy' (Q_{eff}) was 289 kJ/mole for Ti-25Al in the temperature range of 1000 to 1300K. For Ti-24Al-15Nb and Ti-25Al-11Nb Q_{eff} values were 329 and 330 kJ/mole respectively in the range of 1100 to 1300K.

(iii) The greyish or bluish scales were usually observed to be adherent and protective than the yellowish ones. In general, the scales were porous. These were thinner, adherent and more compact for Nb-containing alloys. On the other hand, Ti-25Al showed significant scale spallation above 1100K.

(iv) The scales formed on these alloys were predominantly composed of TiO_2. However, Al_2O_3 was also present as minor oxide. The outer scale in Ti-25Al was TiO_2, whereas in Nb-containing alloys it was mostly a mixture of Al_2O_3 and TiO_2. Nb was also detected by EDX in the inner scale. Improved oxidation resistance of Nb-containing alloys was attributed to the doping effect of Nb in reducing defect concentration of TiO_2.

(v) At 1200K, in O_2-Ar gas mixtures, k_p for Ti-24Al-15Nb was found to be proportional to square root of p_{O_2} in the range of 0.2

to 1 atm. However in O_2-N_2 mixture, decrease of k_p was much more, and approximately by an order of magnitude when p_{O_2} was lowered from 1 to 0.5 atm, and then became almost independent of p_{O_2}. On the other hand, in Ti-25Al, k_p values were approximately the same for O_2-Ar as well as O_2-N_2 gas mixtures as in only O_2.

(vi) In 20 pct O_2 + 80 pct N_2 gas mixture, k_p for Ti-24Al-15Nb was approximately an order of magnitude lower at all temperatures as compared to those in O_2. However, for Ti-25Al, k_p was similar in magnitude in O_2-N_2 mixture as in only O_2. Q_{eff} for oxidation of Ti-24Al-15Nb in 20 O_2 + 80 N_2 mixture was 274 kJ/mole in the temperature range of 1100 to 1300 K. However, for Ti-25Al, Q_{eff} was 351 kJ/mole in the temperature range between 1150 and 1300K.

(vii) For Nb-containing alloys, in addition to TiO_2 and Al_2O_3, TiN was also found in the scales formed in O_2-N_2 mixtures. TiN could not be detected in scale formed in Ti-25Al at 1300K, but was found at 1150K. The nitride layer seemed to have played an additional beneficial role in improving oxidation resistance of Nb-containing alloys whereas it showed no effect on Ti-25Al.

(viii) Some experiments were conducted in nitrogen at 1300K. However, some oxidation also occurred in addition to nitridation, although special efforts were made to remove traces of oxygen and other oxidants. The rate of nitridation was slower than rate of oxidation by more that an order of magnitude (i.e. k_p lower by about 2 orders of magnitude).

(ix) In sequential oxidation studies at 1300K, nitrogen pretreatment was observed to be beneficial for Ti-24Al-15Nb in lowering weight gain during oxidation in oxygen and O_2-N_2 gas

mixture. For Ti-25Al, N_2-pretreatment showed no effect. Presence of nitrogen in gas mixture has already been found to be beneficial for Nb-containing alloys. Thus additional beneficial effect may be attributed to the initial nitride layer formed during N_2-pretreatment. On the other hand O_2-pretreatment was beneficial for Ti-25Al only. Amount of Al_2O_3 was more in O_2-pretreated specimen than that in N_2-pretreated specimen, and this seemed to have lowered the rate.

(x) Rapid weight gain was recorded in N_2 containing 5 pct CO_2 for Ti-25Al. k_p was more than 2 orders of magnitude larger as compared to that in only nitrogen. The scale formed in the gas mixture was much thicker, non-adherent and porous which resulted in scale permeability and cracking and rapid oxidation by CO_2. On the other hand, the effect of CO_2 on Ti-24Al-15Nb was negligible, and the scale was compact and adherent. Thermodynamic considerations assisted in explanation of the differing behaviours in the two alloys.

(xi) Considerable subscale hardening was observed in Ti-25Al and Ti-24Al-15Nb alloys after exposure in O_2, N_2 and 20 O_2 + 80 N_2 gas mixtures at 1300K. From hardness profiles, values of diffusion coefficient (D) were evaluated making some simplifying assumptions; and have been found to be close to those reported in literature.

Chapter 6 presents summary and conclusions of the present study as well as suggestions for further work.

CHAPTER 1

INTRODUCTION

Titanium aluminides based on Ti_3Al (designated as α_2) and TiAl (designated as γ) compounds have the potential to become a class of high temperature structural materials. They have been drawing an increasing attention over the last 10 to 15 years as candidate materials for the next generation gas turbine engines and air frame components over the conventional two phase (i.e. $\alpha+\beta$) titanium alloys and nickel based superalloys. This class of alloys has concentration of aluminium exceeding roughly 20 atom pct. With such a high aluminium content, the resulting phases are intermetallic compounds, having ordered structures.

Intermetallic compounds can be defined as ordered alloy phases formed between two or more metallic elements[1]. An alloy phase is ordered if two or more sublattices are required to describe its atomic structure[2].

The system based on Ti_3Al is an intermetallic compound having an ordered hexagonal (i.e. DO_{19}) structure. This intermetallic is the oldest and comprehensively studied titanium aluminide. The first major research effort to develop an alloy based on this compound was made by McAndrew and Simcoe[3] in the 1950s when high temperature materials were required for the rapidly developing turbine engine industry. They concentrated on Ti-Al-Nb alloys and identified niobium as a potential addition for enhancing the ductility and oxidation resistance of higher aluminium containing

alloys. Research on Ti_3Al-based alloys grew slowly in the 1960s and early 1970s. While some promising mechanical properties were reported, interest waned as nickel based superalloys matured and served the engine designer's requirements.

As turbine engine designs matured, more attention was paid on developing materials which increased engine efficiency through lighter weight and higher operating temperatures. Furthermore, the oil crisis in the early 1970s spurred a resurgence in the research of these low density alloys. At this time, large efforts were directed towards the development of Ti_3Al-based alloys. By the end of the 1970s, nearly 20 years after McAndrew and Simcoe[3], the reference alloy known as Ti-24Al-11Nb (atom pct) was identified by Blackburn et al[4]. Further research centered around α_2-based (i.e.Ti_3Al) alloys developed to the present time, have two phase structure ($\alpha_2+\beta$/B2) with composition based on Ti-(23-25)Al-(10-30) Nb in atom pct. The alloy developmental activities have been reviewed in literature[5-13].

1.1 IMPORTANCE OF TITANIUM ALUMINIDES

The current state-of-art development limits application of even the most advanced titanium alloys to 600^{o}C, because of lack of adequate strength and oxidation resistance above this temperature[14]. Titanium alloys also suffer from limitations in damage tolerance, creep strength, and undergo rapid oxidation in turbine engine compressor application[12-13]. Apart from increasing service temperatures, further advancement of aerospace systems and turbine engine technology call for introduction of lighter weight structures for achieving higher thrust-to-weight ratio. Lower

density alloys play a pivotal role in allowing this advancement. Currently, the materials most suited to these demanding needs are α_2 titanium alloys based on Ti_3Al, and γ alloys based on TiAl[8,11,12].

The above alloy classes are attractive candidates for application in advanced aerospace, gas turbine engine and airframe components due to the following attributes[6-9,15,16] :

(i) high melting point

(ii) high strength to-weight-ratio

(iii) high elastic modulus

(iv) ordered crystal structure

(v) high temperature specific strength

(vi) high temperature creep rupture strength

High temperature properties such as strength retention, creep/stress rupture life, and high temperature fatigue resistance are improved over conventional titanium alloys, because of the generally slow diffusion in ordered alloys[6,12,17]. Table 1.1 compares some of the properties of Ti_3Al and TiAl alloys with those of conventional alloys and superalloys[6,8,11,12,16].

The original applications of α_2 class alloys envisaged compressor vanes, blades and disks, impellers and nozzle components in gas turbine engines. Other applications in airframe components such as, skins and ducts have also been considered[7,8,15].

Despite all the above attributes of ordered structure that allow for the higher temperature capability of these alloys, it may be noted that an ordered structure suffers from limited ductility, low fracture toughness, and low impact resistance. The brittleness

at low temperatures exhibited by these alloys in bulk polycrystalline form was found to be due to lack of an adequate number of slip systems, accentuated by planar slip.

Table 1.1 Comparison of Properties of Titanium Aluminides with Conventional Titanium Alloys and Superalloys

Property	Ti-base	Ti_3Al base	TiAl base	Superalloys
Structure	hcp/bcc	DO_{19}	$L1_o$	fcc/$L1_2$
Density (g/cm^3)	4.5	4.1-4.7	3.7-3.9	8.3
Elastic Modulus (GPa)	96-100	100-145	160-176	206
Yield Strength (MPa)	380-1150	700-990	400-650	-
Tensile Strength (MPa)	480-1200	800-1140	450-800	-
Ductility (% El. at RT)	10-25	2-10	1-4	3-5
Ductility (% El. at HT)	12-50	10-20	10-60	10-20
Fracture Toughness ($MPa\sqrt{m}$)	High	13-30	10-20	25
Creep Limit (^oC)	600	760	1000	1090
Oxidation Limit (^oC)	600	650	900	1090

Low ductility and toughness at low to intermediate temperatures were important barriers to application for quite some time. However, this has been largely solved through chemistry control by alloying additions, and manipulation of microstructure. Niobium has proven to be the most effective addition for increasing

room temperature ductility of binary Ti_3Al[18-20] by stabilizing the ductile high temperature β-phase. The effects of niobium on ductility of binary Ti_3Al have been reviewed in the literature[9,11,12]. Efforts are underway to make the above alloy class an engineering material.

Another negative feature of titanium aluminides is that the oxidation resistance is lower than desirable at elevated temperatures. These alloys would be very attractive for aerospace applications if they are more oxidation resistant. Although the alloys possess good high-temperature mechanical properties, these are reactive towards oxygen, nitrogen etc[21,22]. It appears that the maximum service temperature for these alloys would be usually limited not by creep strength but by oxidation and the accompanying embrittlement[23,24]. Ti_3Al-based alloys are limited by creep to temperatures below 815^{o}C, and by oxidation to temperatures below 650^{o}C[25].

Thus a key factor in increasing maximum use temperature is enhanced oxidation resistance while retaining adequate levels of creep strength. Particularly, once the desirable crystal structure of a material has been obtained and subsequent mechanical properties have been achieved, then the focus should be on oxidation and corrosion resistance. Therefore, the study of high temperature oxidation of titanium aluminides is important. This is specially so for Ti_3Al-based alloys, since here the lack of oxidation resistance primarily limits the maximum service temperature (Table 1.1).

1.2 OBJECTIVE OF THE PRESENT STUDY

Some studies on high temperature oxidation of Ti_3Al-based alloys have been carried out over the years. These have been reviewed in chapter 2. The findings of the review reveal that some controversies on several aspects of oxidation of such alloys exist. In the present investigation attempts were made to focus on some of these controversial issues, and throw further lights on the same for resolution of controversies. It was decided to investigate the following aspects of high temperature isothermal oxidation of Ti_3Al-based titanium aluminides with and without niobium :

(i) elucidation of high temperature oxidation kinetics of the above alloys exposed in various gaseous environments at different temperatures

(ii) influence of nitrogen on oxidation behaviour, also further understanding of nitridation kinetics

(iii) assessment of reliability of processing of rate data on the basis of parabolic law vis-a-vis power law

(iv) understanding the nature of scale formation and mechanisms governing high temperature oxidation

(iv) correlation between the observed kinetics and probable mechanisms; elucidation of role of niobium.

1.3 PLAN OF WORK

(i) procurement of Ti_3Al-based aluminide alloys from various sources

(ii) sectioning and preparation of oxidation samples from the above alloys

(iii) characterization of alloys

(iv) isothermal oxidation experiments and measurement of oxidation rates

(v) visual observation of scales formed after oxidation experiments

(vi) characterization of scales :

a) X-ray diffraction studies of scales

b) observation of surface scale morphology using scanning electron microscope (SEM)

c) nickel plating on the oxidized samples to prevent spallation of poorly adhered scales, some oxidized samples were nickel plated by electroless nickel plating technique

d) cross sectional metallography of scale using SEM and elemental analysis of scales by energy dispersive X-ray (EDX) analysis technique

e) optical metallography of scale cross section

(vii) microhardness measurements of substrate to study the extent of solid solution hardening and environmental embrittlement

(viii) interpretation of results.

CHAPTER 2

LITERATURE REVIEW

2.1 STRUCTURE, PHYSICAL AND MECHANICAL PROPERTIES OF ALUMINIDES

There are about 300 intermetallic compounds with high melting temperatures. Intermetallic compounds (e.g. aluminides and silicides)whose nature when judged from the view point of bonding character, fall between metal and ceramics . The majority of aluminides formed by two elements A and B, can be classified into three different stoichiometric combinations with compositions around A_3B, A_2B, and AB. Within each stoichiometric group, the compounds may have different crystal structure. Anton et al[26] have provided the list of some high temperature intermetallic compounds, classified according to stoichiometry and crystal structure. Respective melting points and densities have also been included in the list.

At present aluminide alloys based on nickel, iron and titanium have either been developed to a stage or close to ready for commercial application. Some of them contain sufficient amount of aluminium to form thin film of alumina (Al_2O_3) in oxidizing environments, that are often compact and protective. These materials have low densities, relatively high melting points, and good high temperature mechanical properties such as strength retention, creep/stress rupture and fatigue resistance. By far the greatest impediment in exploitation of these materials is brittleness at room temperature. However, some remedial measures

have been found out that offer the possibility of engineering applications. Liu et al[6] have extensively reviewed research and development on these aluminides and have summarized their possible applications. Table 2.1 lists the properties of some important aluminides[6].

Table 2.1 Comparison of Properties of Some Important Aluminide Alloys

Alloys	Melting point (^{o}C)	Density (g/cm^3)	Yield strength (MPa)	R.T. ductility (%)	Creep limit (^{o}C)
Ti_3Al	1600	4.20	700-990	2-10	760
TiAl	1460	3.91	400-650	1-4	1000
Ni_3Al	1390	7.50	250-500	2-50	760
NiAl	1640	5.86	250-475	2	1200
Fe_3Al	1540	6.72	385-392	2-12	700
FeAl	1250	5.56	360-380	2-17	827

2.2 STRUCTURE AND PHASE RELATIONS IN Ti-Al AND Ti-Al-Nb SYSTEMS

2.2.1 Ti-Al System

In the binary Ti-Al system, apart from disordered haxagonal α(Ti), disordered b.c.c. β(Ti) and disordered f.c.c. α(Al) terminal solid solutions, at least three intermetallics with compositions Ti_3Al, TiAl and Al_3Ti are known to exist. In addition to these, a number of long period superstructures of the type Al_2Ti, Ti_5Al_{11} and Ti_9Al_{23} have been reported, but their existence is still doubtful[6,27]. The Ti-Al system is still controversial and

many versions are available. The most recent binary Ti-Al phase diagram is shown in Fig.2.1 which was synthesized by Gama[28] from different sources.

The room temperature equilibrium phase of Ti_3Al is referred to as the α_2 phase. This phase has an ordered DO_{19} hexagonal structure. Fig.2.2 shows the ordered arrangement of atoms in Ti_3Al. It has a wide composition range from 22 atom pct to 39 atom pct Al. The stoichiometric composition Ti_3Al is stable upto about 1090^oC[6]. With 32 atom pct Al, the compound becomes congruently disordered at 1180^oC.

2.2.2 Ti-Al-Nb System

Responses of Ti_3Al intermetallic to alloying elements is similar to those for conventional titanium alloys. The alloying elements are either α or β stabilizers. Various β stabilizing elements (e.g. Nb, V and Mo) have been added to the base Ti_3Al alloy during the past several years to improve room temperature ductility. Niobium has been proven to be the most effective addition for this purpose. Generally, the majority of the material properties improve with increase in niobium content except creep property[11]. Once the niobium content reaches 10 atom pct, the high temperature β phase is retained to room temperature[7] along with the α_2 phase.

The equilibrium phase constituents and transformation sequences in the Ti-Al-Nb ternary system, centered around α_2 phase, are still not understood[9,12,29]. Different versions of Ti_3Al-Nb pseudo-binary diagrams are available in the literature[9,12,29]. Fig.2.3 shows some of the preliminary Ti_3Al-Nb pseudo-binary

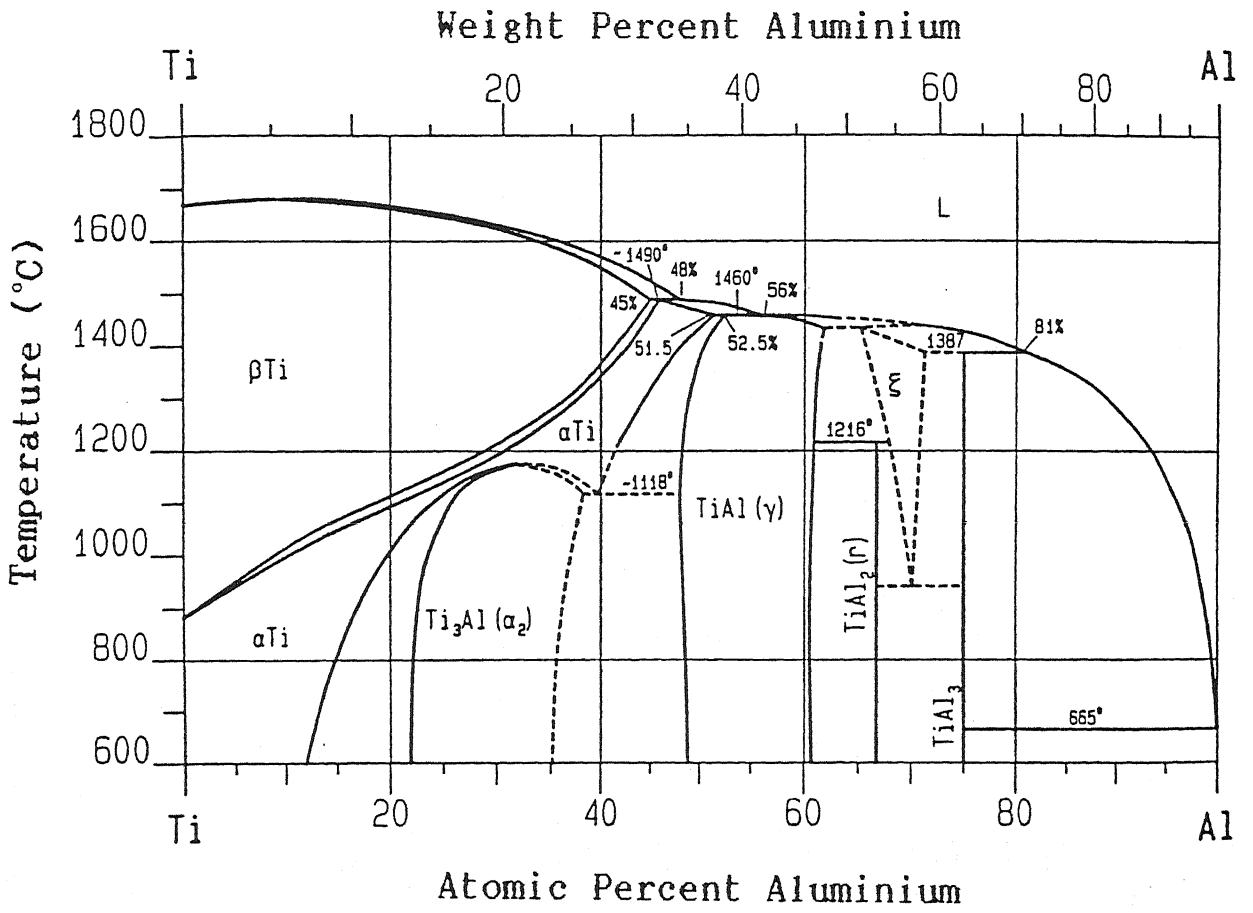

Fig.2.1: Binary phase diagram for the Ti-Al system[28]

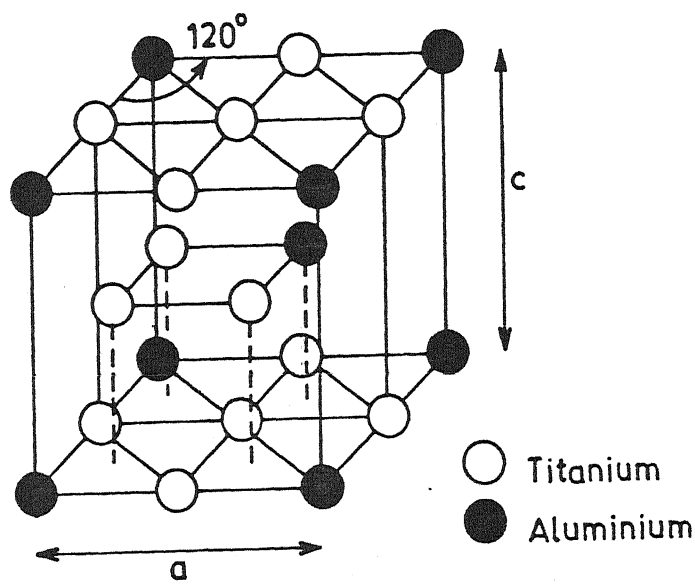

Fig.2.2: Ordered hexagonal DO_{19} structure of Ti_3Al

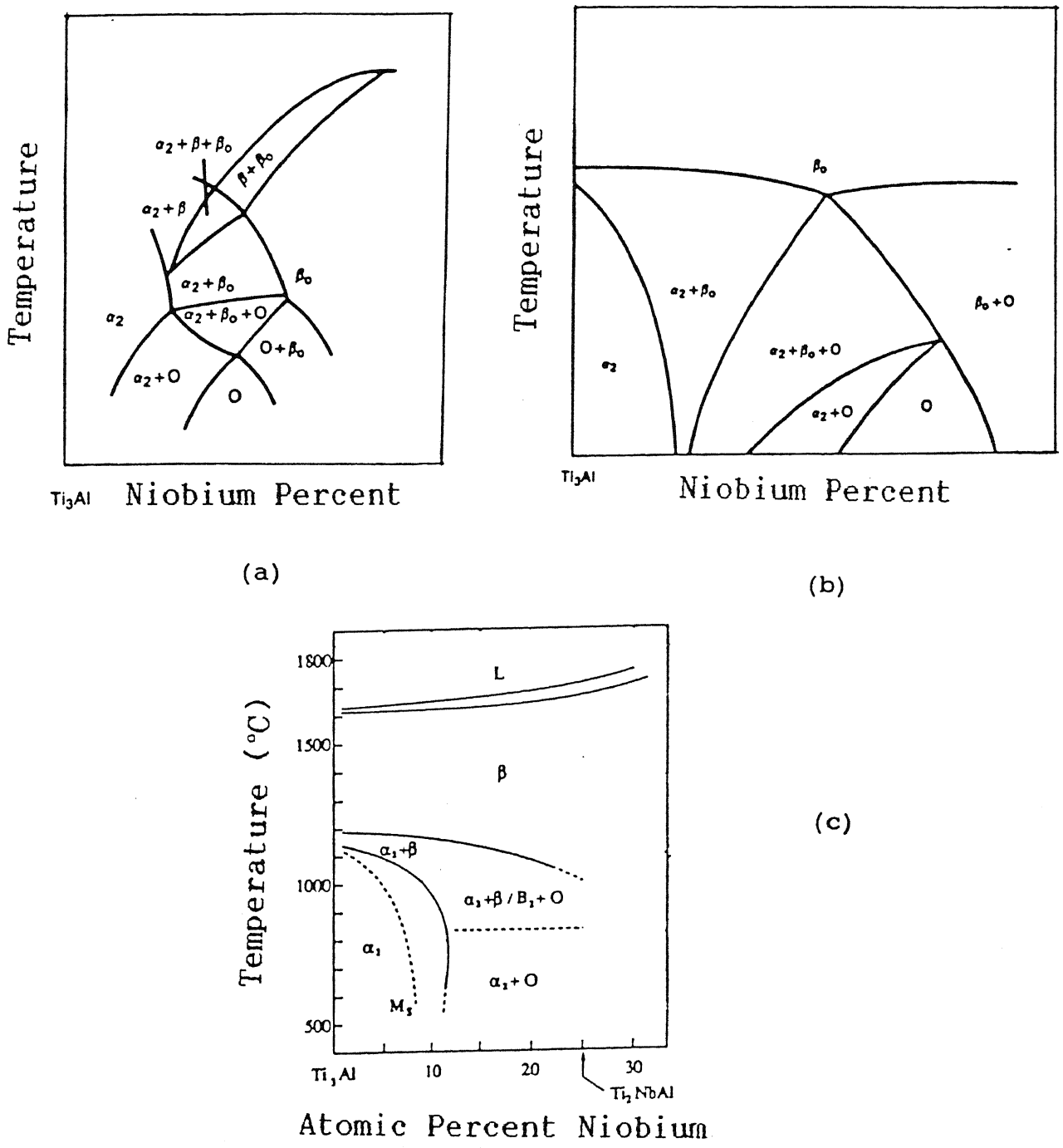

Fig.2.3: Different versions of Ti_3Al-Nb pseudo-binary phase diagrams (a) schematic, after Banerjee et al[29], (b) schematic after Rawe[9], (c) after Kim and Froes[12]

diagrams. A rigorous evaluation of high temperature stability in the Ti-Al-Nb system is in progress, and has been reported by Gama[28] in a recent compilation.

Recent studies by Banerjee et al[29] have shown that niobium addition to the Ti_3Al composition results not only in stabilization/ordering of the bcc β phase (B2 structure, also designated as β_O), but also in a distortion of the hexagonal α_2 phase to an orthorhombic phase (designated O), which appear to have potential for higher temperature applications. This new phase has drawn an increasing attention and hoped to be explored in detail in the coming years. The O phase appears at Nb levels exceeding 12 atom pct for Al contents of 24 to 25 atom pct. Muraleedharan et al[30] have reported detailed studies on phase transformations of Ti-24Al-15Nb alloy. Substitution of Ti by Nb increases the number of slip systems. Niobium may partly be replaced by other elements for strength improvement (e.g. V, Mo, Ta), creep resistance (e.g. Mo), and oxidation resistance (e.g. Ta, Mo)[13].

The α_2 alloys developed so far are two phase (α_2 + β/B2) alloys with compositions based on Ti-(23-25)Al-(8-30)Nb[11]. Alloy compositions with engineering significance are Ti-24Al-11Nb, Ti-25Al-10Nb-3V-1Mo, Ti-25Al-17Nb-1Mo and Ti-23.5Al-24Nb. The numbers denote atom pct of respective elements added to titanium. Properties of various α_2-based (i.e. Ti_3Al-based) titanium aluminides is presented in Table 2.2[6,12].

2.3 FUNDAMENTALS OF OXIDATION OF METALS AND ALLOYS

In general, metals and alloys form stable oxides under exposure to air or oxygen at elevated temperatures. For some metals

and alloys, the reactivity with atmospheric oxygen (i.e. oxidation) is a primary obstacle to their engineering applications, specially at high temperatures. There are books available on fundamentals of

Table 2.2 Room Temperature Properties and Elevated Creep Rupture Life of Some Ti_3Al-Based Alloys With Various Microstructures Controlled by Thermomechanical Processing

Alloys	Microstructure*	YS (MPa)	UTS (MPa)	El (%)	K_{IC} (MPa$\sqrt{m}$)	Creep rupture**
Ti-25Al	E	538	538	0.3	-	-
Ti-24Al-11Nb	W	787	824	0.7	-	44.7
	FW	761	967	4.8	-	-
Ti-24Al-14Nb	W	831	977	2.1	-	59.5
Ti-25Al-10Nb-3V-1Mo	W	825	1042	2.2	13.5	>360
	FW+P	942	1097	2.7	-	-
Ti-24.5Al-17Nb	W	952	1010	5.8	28.3	62
Ti-25Al-17Nb-1Mo	FW	989	1133	3.4	20.9	476

* E- equiaxed α_2 grain; W- widmanstatten; FW- fine widmanstatten; P- primary α_2 grain.

** Time to rupture in hour at 923K and 380 MPa.

oxidation of metals and alloys, e.g. by Birks and Meier[31], Kubaschewski and Hopkins[32], Scully[33], Kofstad[34] etc. On the basis of these some important aspects of high temperature oxidation of metals and alloys have been briefly presented here for the sake of completeness.

When a clean metal is exposed to reacting gases, the initial process is adsorption of gas on the metal surface. This is followed

by nucleation, and growth of nucleii of the reaction products. They grow laterally to cover the metal surface as a film. Thus metal and the gas are separated by reaction products. In order for the reaction to proceed further, one or both reactants must penetrate the scale. Therefore, the mechanism by which the reactants may penetrate the oxide layers is considered to be an important part of the mechanism of high temperature oxidation. Since all metal oxides are ionic in nature, transport of neutral metal or non-metal atoms through the oxide scale has been ruled out.

2.3.1 Mechanisms of Oxidation

Various mechanisms are available to explain the migration of ions through ionic solids, which may be divided into stoichiometric crystals or non-stoichiometric crystals. Ionic mobility in stoichiometric crystals is explained by the existence of ionic vacancies and interstitials, and migration of electrons is neglected.

Fig.2.4 is a simplified representation of mechanism of high temperature oxidation[31]. The kinetic steps are :

1. transport of O_2 in gas to oxide/gas interface
2. reaction at oxide/gas interface
3. transport of ions and electrons through oxide scale
4. reaction at metal/oxide interface
5. diffusion of metal (in case of alloy oxidation) to metal/oxide interface
6. diffusion of oxygen into metal.

The above is valid for non-porous oxide scales. If it is porous then oxygen molecules can diffuse through pores.

The cation migration leads to scale formation at scale/gas interface, whereas anion migration results in the scale formation at the metal/scale interface. Mobilities of ions and electrons are possible due to presence of point defects in oxide scale, either vacancies or interstitials. Cations can move only through cation vacancies and cation interstitials. Anions can move only through anion vacancies or anion interstitials. Larger is concentration of a particular type of defect, greater is the mobility of the corresponding ion through the scale.

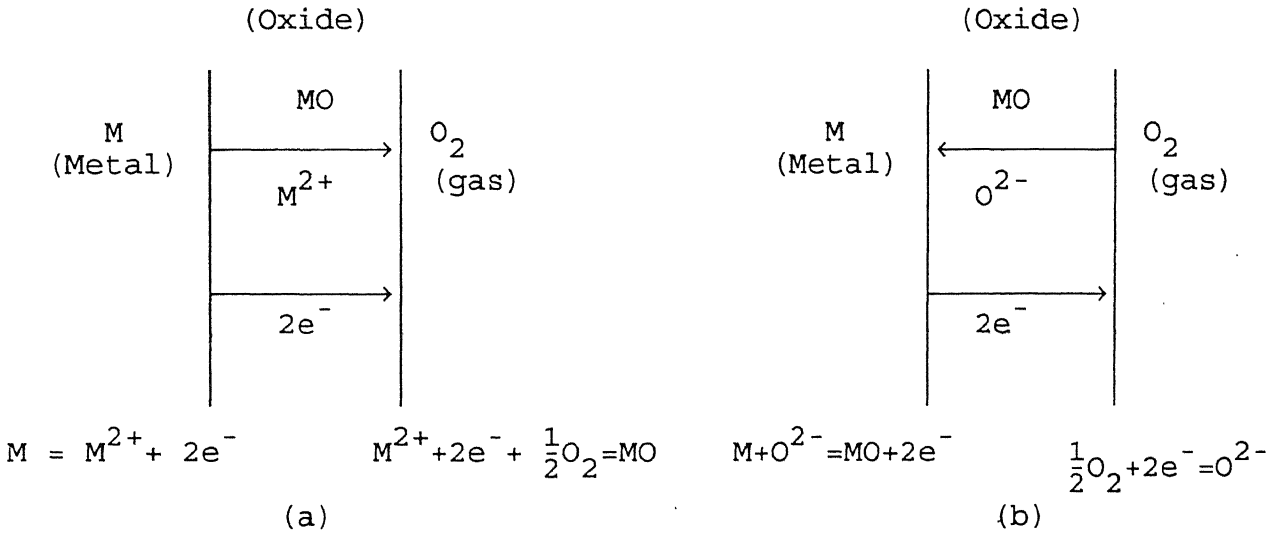

Fig.2.4: Interfacial reaction and transport processes through oxide scale during high temperature oxidation[31] (a) cation mobile, (b) anion mobile.

Simultaneous migration of electrons is possible since the oxides formed during oxidation have non-stoichiometry to different extents. Non-stoichiometric oxides are semiconductors, and exhibit either negative (i.e. n-type) or positive (i.e. p-type) conduction. In n-type oxides, the conduction electrons are mobile. It is a

consequence of either excess of metal or deficit of non-metal in the lattice. Some of the n-type oxides are ZnO, TiO_2, Nb_2O_5 etc. In p-type oxides, charge transfer is by electron hole conduction. It arises from either a deficit of metal or an excess of non-metal. NiO, Al_2O_3, Cr_2O_3, FeO are some of the oxides which show p-type behaviour. Deviation from stoichiometry in the case of Cr_2O_3 and Al_2O_3 is very small.

For n-type oxides, it can be theoretically derived that the equilibrium concentration of electronic defect (C_e) depends on partial pressure of oxygen in the gas as follows :

1. doubly charged defects (interstitials or vacancies),

$$C_e \propto p_{O_2}^{-1/6} \qquad \ldots(2.1)$$

2. singly charged defects,

$$C_e \propto p_{O_2}^{-1/4} \qquad \ldots(2.2)$$

3. neutral defects, C_e is independent of p_{O_2}

For p-type oxides, it can be theoretically derived that the equilibrium concentration of electron hole (C_h) depends on partial pressure of oxygen in the gas as follows :

1. doubly charged defects,

$$C_h \propto p_{O_2}^{1/6} \qquad \ldots(2.3)$$

2. singly charged defects,

$$C_h \propto p_{O_2}^{1/4} \qquad \ldots(2.4)$$

Since electrons and electron holes have mobilities several orders of magnitude larger than cations and anions, the motion of the former would basically determine electrical conductivity (σ) through the oxide. Assuming σ to be proportional to C_e, Eqs.(2.1) to (2.2) theoretically predict dependence of σ on p_{O_2}. Experimental measurements on σ as function of p_{O_2} for some metal oxides have confirmed above predictions.

2.3.2 Oxidation Rate Laws

Assuming that the oxide scale is of uniform density, a plot of weight gain per unit surface area vs time will have the same nature as that of oxide thickness vs time plot. Furthermore, weight gain is easier to measure than the film thickness, especially if thickness is very small. The following rate laws in terms of weight gain per unit surface area $(\frac{\Delta W}{A})$ and time of oxidation (t) have been experimentally observed.

1. Linear rate law : Here rate of oxidation is independent of time. This is expected when either transport of O_2 in gas (i.e. kinetic step 1 as given earlier), and/or rate of reactions at oxide/gas interface or metal/oxide interface (i.e. kinetic steps 2, 4) are rate controlling. The linear relationship is :

$$(\frac{\Delta W}{A}) = k_l t \qquad \ldots(2.5)$$

Where, k_l is linear rate constant. This law has been found to be obeyed when the scale is very thin such as at initial stages of oxidation.

2. Parabolic rate law : Here the rate of oxidation is inversely proportional to square root of time. This is expected to be valid when diffusion through the scale is the rate determining step. However such expectation is valid under idealized condition when the scale is uniform throughout in composition. Rate control by diffusion through oxide is likely when the scale has some thickness. The parabolic relationship is :

$$(\frac{\Delta W}{A})^2 = k_p t \qquad \ldots(2.6)$$

The straight line may not intersect the zero point of the co-ordinate axes since the parabolic law is not generally valid at the initial stage. Then the more general form of parabolic equation may be employed, viz.

$$(\frac{\Delta W}{A})^2 = k_p t + C \qquad \ldots(2.7)$$

Where, k_p is parabolic rate constant and C is also a constant.

Parabolic rate law has been found to be obeyed approximately in many investigations of high temperature oxidation of metals and alloys. Whether it is strictly obeyed or not, usually the investigators interprete observed rates on the basis of Eq.2.6.

Other rate laws such as, logarithmic law, is obeyed for formation of very thin films and at low temperature. Experimental values have occasionally been found to agree with a cubic relationship :

$$(\frac{\Delta W}{A})^3 = k_c t \qquad \ldots(2.8)$$

where k_c is the rate constant.

Under certain conditions, some systems might even show composite kinetics. For example, it would perhaps show parabolic behaviour to start with and then continue linearly. This has been termed as 'paralinear' or 'quasi-linear'. Here the predominant mechanism is ionic diffusion but the film is sufficiently brittle to crack from time to time.

During growth of oxide scale, it may crack under stress. Then the rate gets enhanced suddenly. Spalling of scale leads to sudden loss of weight consequently enhancing the rate. These can be detected if weight gain is recorded continuously as function of time. These are schematically illustrated in Fig.2.5[31].

2.3.3 Derivation of Parabolic Rate Law[35]

The following relation could be considered for oxidation of metal as :

$$\rho_{ox}\ \Delta x = (\frac{\Delta W}{A})/P \qquad \ldots(2.9)$$

Where, Δx is thickness of oxide film, ρ_{ox} is the density of oxide, $(\frac{\Delta W}{A})$ is the weight gain per unit surface area of the specimen, and P is average weight fraction of oxygen in the oxide film. Again, from Fick's first law,

$$\frac{d}{dt}(\frac{\Delta W}{A}) = -\frac{D_i}{\alpha}\frac{\delta C_i}{\delta x} \qquad \ldots(2.10)$$

Assuming that the oxidation is controlled by diffusion through oxide scale. Here, D_i is diffusion coefficient of controlling diffusing species i, and C_i is concentration of i in mass per unit volume. α is a stoichiometric factor resulting from the fact that the product solid is not the same as the diffusing species.

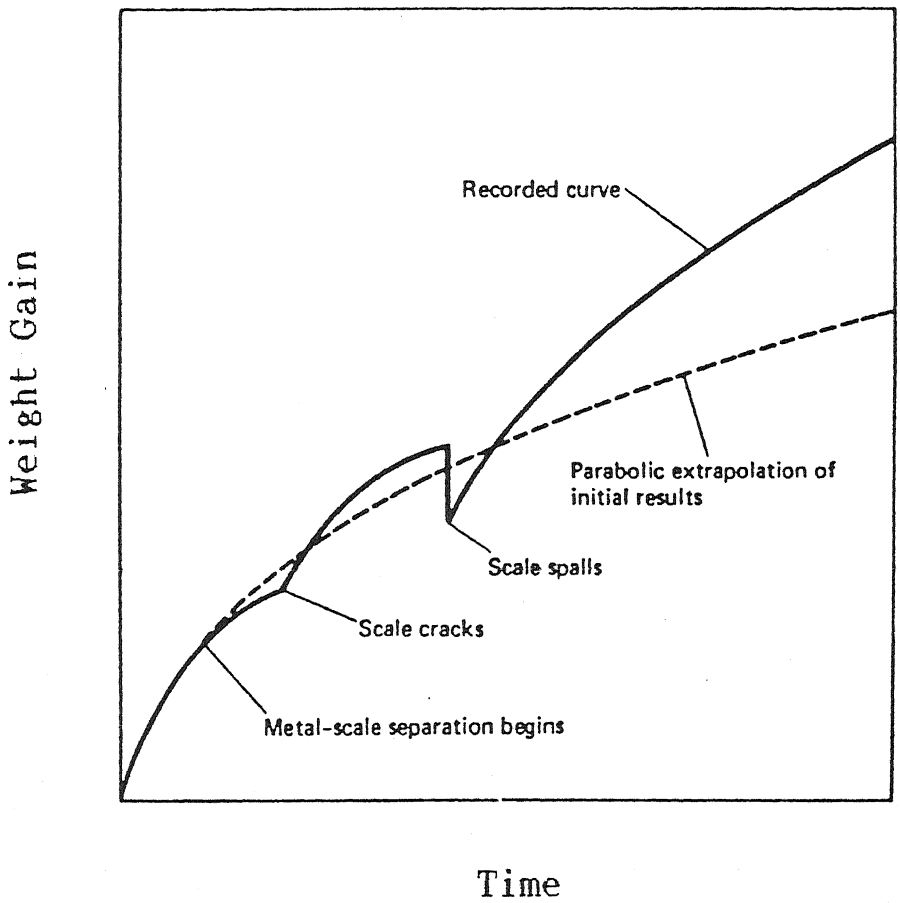

Fig.2.5: Schematic diagram showing possible features (exaggerated) that would be revealed if weight gain is recorded continuously[31]

Combining Eqs.(2.9) and (2.10),

$$\frac{d(\Delta x)}{dt} = \frac{D_i}{P\ \rho_{ox}\ \alpha}\ \frac{\delta C_i}{\delta x} \qquad \ldots(2.11)$$

Assuming D_i and P to be constants and noting that the boundary conditions at the two interfaces of oxide scale are fixed by thermodynamic equilibria, Eq.2.11 may be written as :

$$\frac{d(\Delta x)}{dt} = \frac{D_i\ (C_1 - C_2)}{P\ \rho_{ox}\ \alpha\ \Delta x} \qquad \ldots(2.12)$$

Where, C_1, C_2 are concentrations at the two interfaces. Integrating between limits : t = 0, $\Delta x = 0$; t = t, $\Delta x = \Delta x$,

$$(\Delta x)^2 = \frac{2D_i\ (C_1 - C_2)}{P\ \rho_{ox}\ \alpha}\ t \qquad \ldots(2.13)$$

or,
$$\left[\frac{(\frac{\Delta W}{A})}{\rho_{ox}\ P}\right]^2 = \frac{2D_i(C_1 - C_2)}{P\ \ \rho_{ox}\ \alpha}\ t \qquad \ldots(2.14)$$

or,
$$(\frac{\Delta W}{A})^2 = k_p t \qquad \ldots(2.6)$$

where k_p is parabolic rate constant given as :

$$k_p = \frac{2D_i P\ \rho_{ox}}{\alpha}\ (C_1 - C_2) \qquad \ldots(2.15)$$

2.3.4 Wagner's Theory of Oxidation

Wagner's[36] theory attempts to relate D_i of Eq.2.15 with physical and physico-chemical parameters. For this he made several simplifying assumptions. They are as follows :

1. oxide is compact and perfectly adherent to the substrate
2. migration of ions or electrons through the oxide layer is the rate controlling step
3. thermodynamic equilibrium exists at both the metal/oxide and oxide/gas interfaces
4. local thermodynamic equilibrium is established throughout the scale
5. scale is thick with small deviation from stoichiometry
6. dissolution of oxygen in the metal may be neglected.

Diffusion of ions sets up an electric field across the scale resulting in consequent transport of electrons from metal/oxide interface to oxide/gas interface through the scale. To maintain electroneutrality, the relative motions of cations, anions and electrons are balanced such that no net charge transfer occur as well as local electroneutrality is maintained. Originally, Wagner considered migration of cations, anions and electrons. However, mobility of electrons is high in the majority of oxides and hence is not rate controlling. Again, the mobilities of the cations and anions usually differ by several orders of magnitude. Thus to simplify the treatment, the role of the slower moving ionic species in oxidation was ignored.

When the cations are mobile, it was derived by Wagner[36] that the parabolic rate constant could be related to other parameters as follows :

$$k_p = \frac{1}{Z_C^2 F^2 C_M} \int_{\mu_M''}^{\mu_M'} \frac{\sigma_c \sigma_e}{\sigma_c + \sigma_e} d\mu_M \qquad \ldots(2.16)$$

where, Z_C is cationic charge, F is the Faraday constant, C_M is concentration of metal in the oxide scale. σ_c and σ_e are the partial electrical conductivities of cations and electrons respectively, μ'_M and μ''_M are the chemical potentials of metal at the metal/oxide and oxide/gas interfaces respectively, and k_p is the parabolic rate constant.

Generally the transport numbers of electrons, or electronic defects are close to unity. Compared to this, the transport numbers of cations or anions are negligibly small. So, Eq.2.16 may be simplified to,

$$k_p = \frac{1}{Z_C^2 \, F^2 \, C_M} \int_{\mu''_M}^{\mu'_M} \sigma_c \, d\mu_M \qquad \ldots(2.17)$$

k_p has also been related to diffusion coefficient of metal as :

$$k_p = \frac{1}{RT} \int_{\mu''_M}^{\mu'_M} D_M \, d\mu_M \qquad \ldots(2.18)$$

where, D_M is the diffusion coefficient of metal M through the scale. It is also assumed that D_M is a function of chemical potential of M i.e. μ_M. Thus, parabolic rate constant can be theoretically calculated knowing the relevant diffusion coefficient value as a function of chemical potential of the mobile species. Such data are incomplete and frequently not available. Moreover, it is usually easier to measure the parabolic rate constant directly without performing experiments to measure diffusion coefficient. Therefore, Wagner's analysis provides a complete mechanistic

understanding of high temperature oxidation under the conditions set out, but is rarely employed for quantitative estimation of parabolic rate constant.

In connection with oxidation of copper to Cu_2O, which is a p-type semiconducting oxide, Wagner[35] assumed copper ion vacancy as the ionic defect. Through thermodynamic analysis he showed that concentration of vacancy is proportional to $p_{O_2}^{1/8}$ at equilibrium. Wagner and Gruenewald[37] made experimental measurements and showed that the rate of oxidation of copper at 1273K was essentially a linear function of the seventh root of the oxygen pressure in the gas phase. The agreement of calculated and observed rates were also found to be excellent.

Birks and Meier[31] have reviewed studies on oxidation of cobalt to CoO, which is a metal deficit p-type semiconductor forming cation vacancies and electron. The dependence of vacancy concentration on p_{O_2} is governed by nature of vacancy i.e., doubly charged or singly charged or neutral. Experimental measurements showed k_p to vary as $p_{O_2}^{1/3}$ approximately. This has been taken as confirmation that singly charged and neutral vacancies are important.

Fueki and Wagner[38] derived some equations on the basis of which D_M (Eq.2.18) can be obtained from experimental data of variation of k_p as function of external partial pressure of oxygen. Mrowec and Przybylski[39] calculated diffusion coefficient of cobalt through CoO from their oxidation experiments with the help of the above. They obtained :

$$D_{Co} = 50 \times 10^{-8} \exp\left(-\frac{19100}{T}\right) m^2 s^{-1} \quad \text{(ref.39)} \qquad \ldots(2.19)$$

This may be compared with tracer diffusivity measurements by other investigators[40,41].

$$D_{Co} = 52 \times 10^{-8} \exp\left(-\frac{19200}{T}\right) m^2 s^{-1} \quad \text{(ref.40)} \qquad \ldots(2.20)$$

$$D_{Co} = 50 \times 10^{-8} \exp\left(-\frac{19400}{T}\right) m^2 s^{-1} \quad \text{(ref.41)} \qquad \ldots(2.21)$$

The excellent agreement may be noted. These and other studies studies validate Wagner's[36] theory of oxidation for parabolic rate

2.3.5 Oxidation of Pure Metals

It is difficult to illustrate completely any single mode of rate control during oxidation process. For example, when a metal is exposed at high temperature to an oxidizing environment, the initial rate is expected to be very large since the oxide layer is very thin. Strictly speaking the parabolic law, if extrapolated to zero scale thickness, predicts an infinite initial rate. This is not possible. So, the initial stage of oxidation must be controlled by some process other than ionic transport, such as surface reaction step. Observation of the initial period is very difficult, since some oxide scale forms even during heating the sample to temperature.

Once the oxidation of metal is controlled by ionic diffusion, the parabolic law has been found to be obeyed for a period whose duration depends on factors such as, sample geometry and natures of scale. In metal oxidation there are systems (e.g. Ni) where scale forms as a single layer, (e.g. NiO). Multiple scale layers also form in some systems e.g. Fe, Co, etc. Some metals form volatile

oxides as well, e.g. oxidation of Cr results in Cr_2O_3 formation which under certain conditions evaporates and leads to scale thinning.

Some metals exhibit significant oxygen solubilities. For example, Ti forms a number of stable oxides, and has high oxygen solubilities. Oxidation of Ti in the temperature range of 873 to 1273K was found to obey parabolic law but the rate was a combination of two processes, oxide scale growth and oxygen dissolution into the metal. Linear oxidation is observed in some systems (e.g. Nb) after some time due to scale cracking under stress. This has been termed as 'breakaway' linear oxidation.

2.3.6 Oxidation of Alloys

Alloy oxidation is more complex than oxidation of pure metal as a result of some, or all of the following :

(i) the metals in the alloys will have different affinities for oxygen

(ii) there may be a degree of solid solubility between the oxides

(iii) different mobilities of various metal ions in the oxide phases

(iv) different diffusivities of metals in the alloy

(v) precipitation of subsurface oxides of one or more alloying elements (internal oxidation) may occur due to dissolution of oxygen into the alloy.

Alloy oxidation has been classified into two groups :

1. noble parent with base alloying elements and,
2. base parent metal with base alloying elements.

The efforts for development of oxidation resistance in alloy

are based on the idea of addition of an element which will get selectively oxidized and provide a protective scale. The requirement is that the oxide of alloying element be more stable than the oxide of the base metal. Another requirement is that the concentration of the alloying element for oxidation resistance must be sufficient for the formation of its oxide as an external scale rather than an internal precipitate. Fig.2.6 illustrates schematically the two possibilities for the simple case where the oxygen partial pressure is too low to oxidize the parent metal[42].

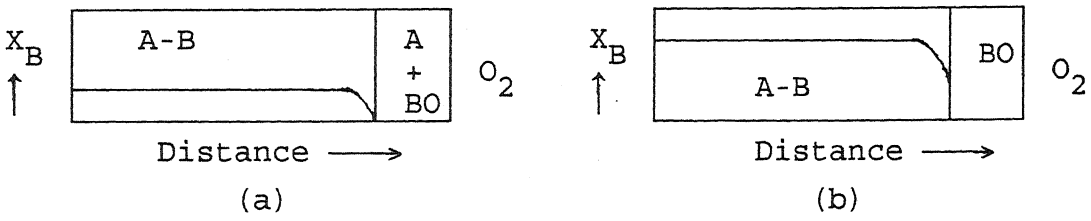

Fig.2.6: Schematic representation of oxidation of a noble metal A, containing a reactive metal B[42]
(a) dilute alloy showing internal oxidation of B
(b) concentrated alloy showing external BO scale formation.

2.3.7 Internal Oxidation

Internal oxidation occurs by inward diffusion of oxygen into an alloy causing subsurface precipitation of one or more oxides of alloying elements. This occurs if :

(i) oxide of solute metal is more stable than the parent metal oxide

(ii) parent metal has appreciable solubility and diffusivity for oxygen

(iii) solute concentration is low, so that it cannot diffuse outwards rapidly enough to form an external oxide scale

(iv) surface layer does not prevent the dissolution of oxygen into the alloy at the start of oxidation.

2.3.8 Transition from Internal to External Oxidation

According to Wagner's[43] criterion, the critical solute concentration (X_B^*) for the transition from internal to external oxidation can be expressed as :

$$X_B^* = \left(\frac{\pi \; g^* \; X_O \; D_O \; V_M}{2 \; \nu \; D_B \; V_{ox}} \right)^{1/2} \qquad \ldots(2.22)$$

Where, $X_O \; D_O$ is oxygen permeability in A

D_B is diffusivity of solute B in A,

g^* is a factor determined by the volume fraction of oxide required for transition (often $\simeq 0.3$)

ν is O/B ratio in the oxide

V_M and V_{ox} are molar volume of the alloy and oxide respectively.

It is clear from the above equation that the critical solute content (X_B^*) for external scale formation increases with the solubility and diffusivity of oxygen and decreases with an increase in the solute diffusivity in the alloy. Transition will occur at lower solute concentration for those conditions which decrease the inward flux of oxygen e.g. lower X_O (i.e. lower p_{O_2}), and those which increase the outward flux of B, e.g. cold working the alloy (which increases D_B by increasing the contribution of short-circuit diffusion). In Ti-Al binary system, the lack of informations on

precise values of oxygen solubility and oxygen and aluminium diffusivities in the alloys pose difficulties to evaluate the conditions for internal oxidation. However, thermodynamic calculation showed that Al level needed to stabilize Al_2O_3 in this system is more than 50 atom pct[44]. Experimental observation by Meier et al[45] revealed that continuous Al_2O_3 scale was formed in Ti-Al alloy containg more than 55 atom pct Al in oxygen upto 1273K. This was in good agreement with the thermodynamically estimated value.

However, for most systems, oxide of the parent metal can also form in the ambient condition and grows till the more stable solute oxide (i.e. BO) becomes continuous and hinders the growth of the 'transient oxide'. This is illustrated schematically in Fig.2.7[42].

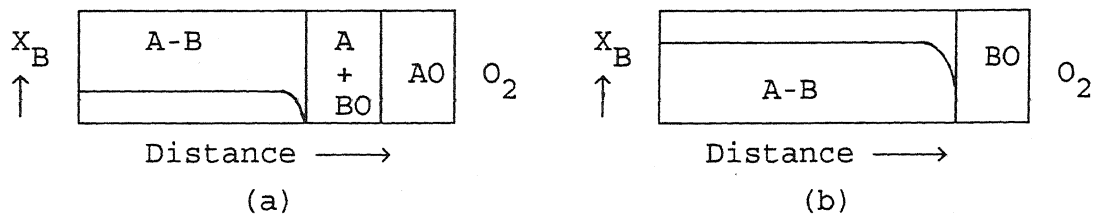

Fig.2.7: Schematic representation of oxidation of A-B with both AO and BO stable[42] (BO stabler)
(a) dilute alloy, internal oxidation of B under the layer of AO
(b) concentrated alloy showing external BO scale

2.3.9 Factors Affecting Alloy Oxidation

In high temperature oxidation, stress generation is an important phenomenon. Growth stresses develop during isothermal oxidation. Thermal stresses arise due to differential thermal expansion or contraction between the substrate and the scale during

temperature cycling. The followings are some of the causes due to which growth stresses occur :

(i) volume differences between the oxide and the metal from which it forms

(ii) formation of oxide within the scale

(iii) compositional change in the oxide or alloy

(iv) epitaxial stresses

Specific volume difference between the oxide and the metal is the principal source of growth stresses. The sign of the stress in the oxide is indicated by a simple parameter known as Pilling-Bedworth ratio (PBR).

However, this mechanism would only seem to be feasible if the oxide forms at the scale/metal interface.

$$PBR = \frac{V \text{ (per metal ion in oxide)}}{V \text{ (per metal atom in metal)}} \qquad \ldots(2.23)$$

For PBR < 1, oxide volume is insufficient resulting in porous and unprotective scale. For PBR > 2, large compressive stresses are likely, leading to buckling and flaking off scale. Oxide tends to be protective when PBR is equal to unity or slightly greater than unity.

The stresses developed during oxidation may be accommodated by a number of mechanisms. Some of these are :

(i) cracking of the scale

(ii) oxide spallation

(iii) plastic deformation of the oxide

To achieve good resistance to oxidation, diffusion through the

growing scale must be as low as possible. An ideal protective scale should :

(i) form externally

(ii) be closely stoichiometric, so that diffusion through the oxide is slow

(iii) be free from cracks, pores and other defects

(iv) be resistant to spalling

(v) be chemically stable so that it does not react further with the environment leading to scale thinning

2.4 THERMODYNAMICS OF OXIDATION AND NITRIDATION OF Ti-Al-Nb ALLOYS

Irrespective of whether α_2 (i.e. Ti_3Al) based or γ (i.e. TiAl) based alloys are used in monolithic form or as composites, the issue of their oxidation is still of concern. The addition of Nb to binary Ti-Al improves the low temperature ductility. In general, it has been found to enhance oxidation resistance as well. Metallic materials can be protected against high temperature oxidation only by formation of a protective oxide film such as Al_2O_3, Cr_2O_3, and SiO_2. These oxides have a sufficiently slow growth rate due to low defect concentration. Out of these oxides Al_2O_3 is favoured as a protective oxide.

One of the prerequisites for protectiveness of Al_2O_3 scale is that it should be most stable of all possible oxides, so that it does not get reduced by the base metal or other constituents of the alloy. Furthermore, thermodynamic factors dominate the Al_2O_3 scale formation in Ti-based alloys[44]. In this section thermodynamic aspects of oxidation and nitridation of the above alloy system would be discussed briefly.

2.4.1 Phase Diagram of Ti-Al-Nb-O Systems

The binary Ti-Al and ternary Ti-Al-Nb phase diagrams have already been presented earlier. Fig.2.8 shows the Ti-O phase diagram after Murray and Wriedt[46]. The major stable oxides in Ti-O system are TiO, Ti_2O_3, Ti_3O_4, Ti_4O_7, and TiO_2. In a recent study Pajunen and Kivilahti[47] evaluated Ti-O phase diagram by optimizing thermodynamic and phase diagram informations. However, the claim for good agreement of calculated Ti-O phase diagram with experimental one is doubtful in view of their use of questionable free energy values.

Thermodynamically the different oxides of Ti are expected to form as a sequence of layers. However, out of several polymorphic forms, rutile structure of TiO_2 has been commonly found below 1273K in oxygen at near atmospheric pressure[34]. This may be due to kinetic reasons which cause faster oxygen dissolution and consequent rutile formation, as compared to the rates of formation of lower oxides.

Pure Al forms Al_2O_3, which is closely stoichiometric due to large band gap (about 9.9 eV) and a high lattice energy[34]. However, it has several polymorphic forms. The binary Nb-O has a stable monoxide (NbO), and dioxide (NbO_2). In addition to these, Nb_2O_5 exists in polymorphic forms.

So far as Ti-Al-O system is concerned, not much studies are available. Glazova[48] provided Ti-Al-O isothermal section at 1073K. Luthra[44] estimated isothermal section of Ti-Al-O at 1073K with the help of thermodynamic data in order to calculate the minimum aluminium content needed to stabilize Al_2O_3 in binary Ti-Al alloys. This is shown in Fig.2.9. Based on EPMA measurements of oxidized

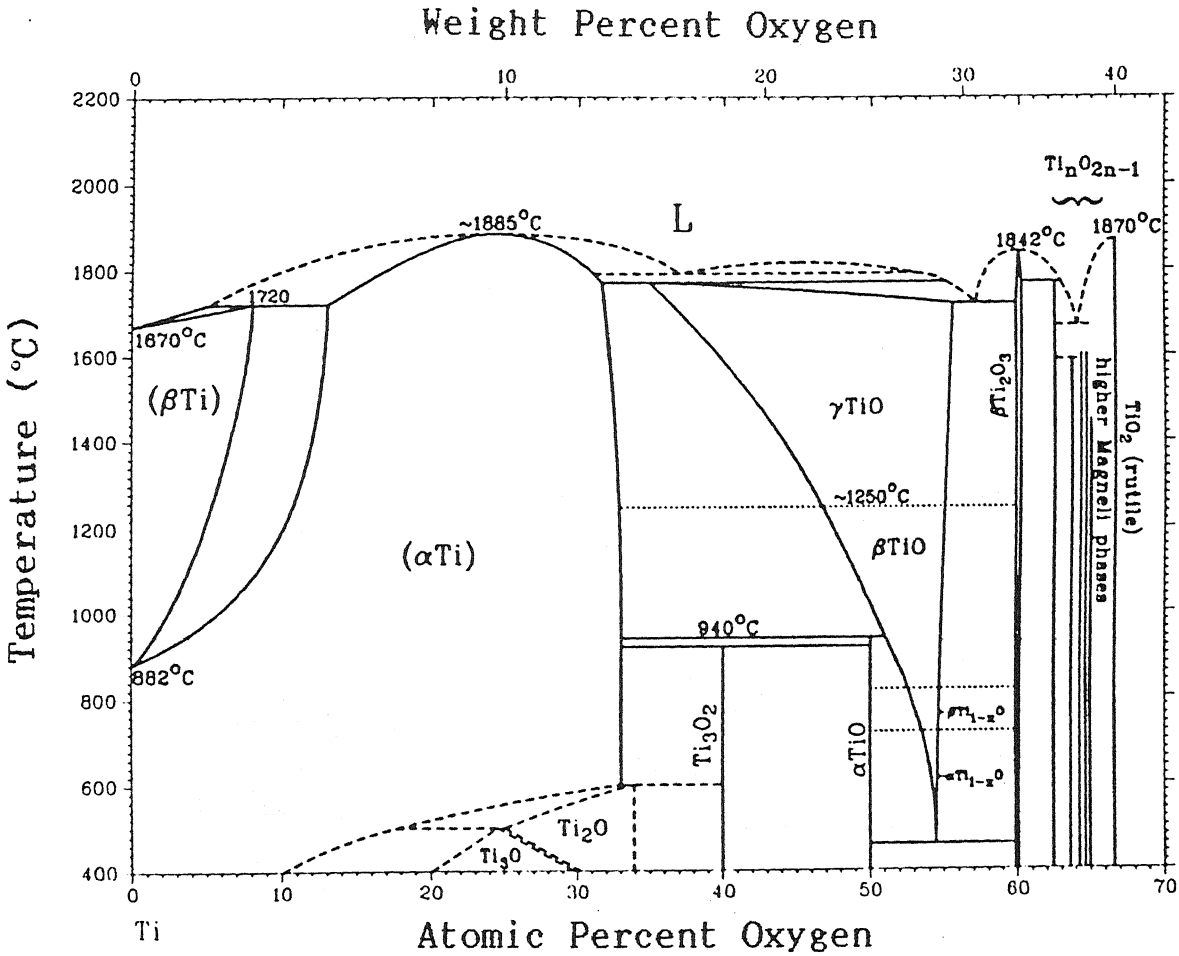

Fig.2.8: Binary Ti-O phase diagram after Murray and Wriedt[46]

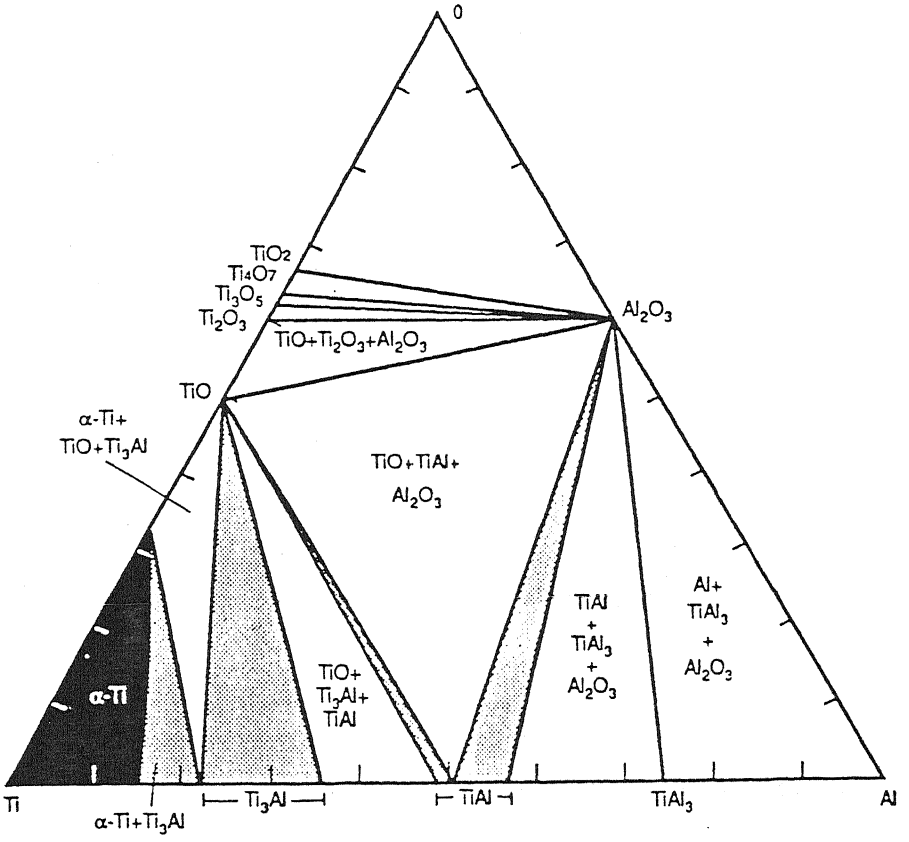

Fig.2.9: Isothermal section of Ti-Al-O phase diagram at 1073 K[44]

TiAl specimen, Becker et al[49] compared the recently published Al-Ti-O phase diagrams[44,50] and reported some discrepancies. However the Al-Ti-O phase diagram provided by them[49] was incomplete with several uncertainties. Recently Zhang et al[51] determined an isothermal section of Ti-Al-O at 1373K using equilibrated samples and diffusion couples. Various phases such as TiO, α (Ti,Al,O), α_2 and γ were found to be at equilibrium with Al_2O_3. However, the phase boundaries were somewhat uncertain. In a recent compilation Hoch and Lin[52] reviewed the studies on Ti-Al-O system, and reported the existence of several ternary oxides in addition to many binaries. Thermodynamic calculation showed that the ternary oxide $TiAl_2O_5$ became stable at temperatures above 1283K[50]. From the above discussion it can be concluded that discrepancies are there in existing ternary Ti-Al-O phase diagrams and are not well established.

The solubility of oxygen in the low temperature α-Ti (c.p.h structure) is about 31.9 atom pct and stabilizes α-Ti with respect to high temperature β modification (b.c.c. structure) (Fig.2.8). In β-Ti, the solubility of oxygen increases with temperature to about 8 atom pct at 1973K. Zhang et al[51] found the maximum solubility of oxygen in α_2 (i.e. Ti_3Al) to be 12±3 atom pct at 1373K.

2.4.2 Thermodynamic Analysis

The purpose of this is to try to predict relative stabilities of various oxides that are likely to form during oxidation of these alloys. Table 2.3 is a compilation of standard free energies of formation (i.e. ΔG^O) of several oxides and nitrides per mole of compound as function of temperature from various

sources[53-55]. ΔG^o values from different sources have been compared at 1200K in Table 2.4. The values are fairly in agreement demonstrating broad reliability of free energy data.

Analysis of thermodynamic criteria for relative stabilities of oxides may be carried out as follows. For example, we consider relative stabilities of TiO and Al_2O_3.

$$2Ti(s) + O_2(g) = 2TiO(s) \qquad \Delta G_f^o(TiO) \qquad ...(2.24)$$

$$\frac{4}{3}Al(s,l) + O_2(g) = \frac{2}{3}Al_2O_3(s) \qquad \Delta G_f^o(Al_2O_3) \qquad ...(2.25)$$

Subtracting, Eq.2.25 from Eq.2.24 we get,

$$2Ti(s) + \frac{2}{3}Al_2O_3(s) = 2TiO(s) + \frac{4}{3}Al(s,l) \qquad \Delta G_{26}^o \qquad ...(2.26)$$

$$\Delta G_{26}^o = \Delta G_f^o(TiO) - \Delta G_f^o(Al_2O_3) \qquad ...(2.27)$$

If Ti, Al, TiO and Al_2O_3 are all pure, then Al_2O_3 is stabler than TiO, if ΔG_{26}^o is positive.

i.e. $\Delta G_f^o(TiO) > \Delta G_f^o(Al_2O_3)$

However these are values of ΔG_f^o per mole of oxygen. Table 2.5 reports these values for various oxides.

Actually it is the chemical potential of oxygen (i.e. μ_{O_2}) which is the most fundamental criterion. Let us designate μ_{O_2} in equilibrium with Ti and TiO_2 be $\mu_{O_2}^e(Ti)$ and μ_{O_2} in equilibrium with Al and Al_2O_3 be $\mu_{O_2}^e(Al)$ where superscript e denotes equilibrium. Al_2O_3 would be stabler than TiO if,

$$\mu_{O_2}^e(Al) < \mu_{O_2}^e(Ti)$$

Table 2.3 Standard Free Energy of Formation per mole of Compound

$\Delta G^{\circ}_{T} = a + bT \log T + c\,T$, kJ/mole

Reaction	ΔG° (kJ) a	$bx10^{3}$	$cx10^{3}$	± (kJ)	Temperature (K)	Ref. No.
$2Al(s,l) + \frac{3}{2}O_2(g) = Al_2O_3(s)$	-1698.5	-15.7	386.0	16.7	923 - 1800	53
$Al(l) + \frac{1}{2}N_2(g) = AlN(s)$	- 327.2	-	115.6	4.2	873 - 2273	54
$Nb(s) + \frac{1}{2}O_2(g) = NbO(s)$	- 415.9	-24.1	161.2	8.4	298 -	53
$Nb(s) + O_2(g) = NbO_2(s)$	- 784.0	-	167.0	10.5	298 - 2423	54
$2Nb(s) + \frac{5}{2}O_2(g) = Nb_2O_5(s)$	-1921.4*	-29.3	655.2	-	298 - 1785	55
$NbO(s) + \frac{1}{2}O_2(g) = NbO_2(s)$	- 387.4	-24.1	166.4	8.4	298 -	53
$2NbO_2(s) + \frac{1}{2}O_2(g) = Nb_2O_5(s)$	- 313.3	-24.1	144.2	10.5	298 -	53
$Nb(s) + \frac{1}{2}N_2(g) = NbN(s)$	- 251.2	-	77.8	-	298 - 2323	54
$Ti(s) + \frac{1}{2}O(g) = TiO(s)$	- 511.9	-	89.2	16.7	600 - 2000	53
$2Ti(s) + \frac{3}{2}O_2(g) = Ti_2O_3(s)$	-1530.9*	-56.3	682.8	-	473 - 1150	55
$2Ti(s) + \frac{3}{2}O_2(g) = Ti_2O_3(s)$	-1545.4*	-36.2	133.8	-	1150 - 1800	55
$3Ti(s) + \frac{3}{2}O_2(g) = Ti_3O_5(s)$	-2448.8*	-33.3	668.0	-	450 - 1150	55
$Ti(s) + O_2(g) = TiO_2(s)$	- 946.9*	-23.3	345.9	-	298 - 1150	55
$Ti(s) + O_2(g) = TiO_2(s)$	- 954.1*	-13.9	286.6	-	1150 - 1800	55
$2TiO(s) + \frac{1}{2}O_2(g) = Ti_2O_3(s)$	- 477.8	-	79.7	16.7	298 - 2000	53
$\frac{3}{2}Ti_2O_3(s) + \frac{1}{4}O_2(g) = Ti_3O_5(s)$	- 185.2	-	41.3	6.3	700 - 2000	53
$\frac{1}{3}Ti_3O_5(s) + \frac{1}{6}O_2(g) = TiO_2(s)$	- 101.8	-	32.1	4.2	298 - 2123	53
$Ti(s) + \frac{1}{2}N_2(g) = TiN(s)$	- 342.4*	-13.9	193.1	-	298 - 1150	55
$Ti(s) + \frac{1}{2}N_2(g) = TiN(s)$	- 359.2*	- 4.5	133.4	-	1150 - 1800	55

* Contributions of higher order terms were adjusted with constant a considering an average temperature of 1150K

Table 2.4 Comparison of Standard Free Energy of Formation Data (kJ/mole) From Different Sources at 1200K

Compound	Kubaschewski et al[53]	Turkdogan[54]	Wicks and Block[55]
Al_2O_3	-1293.3 ± 16.74	-1295.7 ± 2.1	-1295.2
TiO_2	-	-728.2 ± 2.1	-727.9
TiO	-404.9 ± 16.74	-425.9 ± 20.9	-404.8
Ti_2O_3	-	-1192.8 ± 10.5	-1190.3
Ti_3O_5	-	-1930.4 ± 20.9	-1929.1
Nb_2O_5	-	-1385.3 ± 12.6	-1348.9
NbO_2	-	-583.6 ± 10.5	-582.3
NbO	-311.4	-310.4 ± 20.9	-
TiN	-224.1 ± 16.74	-224.5 ± 6.3	-225.2
NbN	-	-136.8	-137.5

Table 2.5 Standard Free Energy of Formation/Reaction per mole O_2 or N_2

$\Delta G^o_T = a + bT \log T + c\,T$, kJ/mole O_2 or kJ/mole N_2

Reaction	y	ΔG^o (kJ) a	$bx10^3$	$cx10^3$	± (kJ)	Temperature (K)	Ref. No.
$\frac{4}{3}Al(s,l)+O_2(g)=\frac{2}{3}Al_2O_3(s)$	$\frac{4}{3}$	-1132.3	-10.5	257.4	11.2	923 - 1800	53
$2Al(l)+N_2(g)=2AlN(s)$	2	- 654.4	-	231.2	8.4	873 - 2273	54
$2Nb(s)+O_2(g)=2NbO(s)$	2	- 831.7	-48.1	322.3	11.2	298 -	53
$Nb(s)+O_2(g)=NbO_2(s)$	1	- 784.0	-	167.0	10.5	298 - 2423	54
$\frac{4}{5}Nb(s)+O_2(g)=Nb_2O_5(s)$	$\frac{4}{5}$	- 768.6*	-11.7	262.1	-	298 - 1785	55
$2NbO(s)+O_2(g)=2NbO_2(s)$	2	- 774.8	-48.1	332.8	16.7	298 -	53
$4NbO_2(s)+O_2(g)=2Nb_2O_5(s)$	4	- 626.6	-48.1	288.4	21.0	298 -	53
$2Nb(s)+N_2(g)=2NbN(s)$	2	- 502.3	-	155.7	-	298 - 2323	54
$2Ti(s)+O_2(g)=2TiO(s)$	2	-1023.9	-	178.3	11.2	600 - 2000	53
$\frac{4}{3}Ti(s)+O_2(g)=\frac{2}{3}Ti_2O_3(s)$	$\frac{4}{3}$	-1020.6*	-37.5	455.2	-	473 - 1150	55
$\frac{4}{3}Ti(s)+O_2(g)=\frac{2}{3}Ti_2O_3(s)$	$\frac{4}{3}$	-1030.2*	-24.1	89.2	-	1150 - 1800	55
$\frac{6}{5}Ti(s)+O_2(g)=\frac{2}{3}Ti_3O_5(s)$	$\frac{6}{5}$	- 988.1*	- 2.0	194.6	-	1150 - 1400	55
$Ti(s)+O_2(g)=TiO_2(s)$	1	- 946.9*	-23.3	345.9	-	298 - 1150	55
$Ti(s)+O_2(g)=TiO_2(s)$	1	- 954.1*	-13.9	286.6	-	1150 - 1800	55
$4TiO(s)+O_2(g)=2Ti_2O_3(s)$	4	- 955.7	-	159.4	11.2	298 - 2000	53
$6Ti_2O_3(s)+O_2(g)=4Ti_3O_5(s)$	6	- 740.9	-	165.0	25.2	700 - 2000	53
$2Ti_3O_5(s)+O_2(g)=6TiO_2(s)$	2	- 611.2	-	192.6	25.2	298 - 2123	53
$2Ti(s)+N_2(g)=2TiN(s)$	2	- 684.9*	-27.9	386.2	-	298 - 1150	55
$2Ti(s)+N_2(g)=2TiN(s)$	2	- 718.3*	- 9.0	266.8	-	1150 - 1800	55

* Contributions of higher order terms were adjusted with constant a considering an average temperature of 1150K

Since $\mu^e_{O_2} = RT \ln p^e_{O_2}$, $p^e_{O_2}(Al) < p^e_{O_2}(Ti)$, where these are p_{O_2} in equilibrium with respective metal and oxide. For the reaction,

$$yM + O_2 = M_yO_2 \qquad \ldots(2.28)$$

$$\Delta G^o_{28} = \Delta G^o_f (M_yO_2) = - RT \ln K = - RT \ln \left\{ \frac{\left(a_{M_yO_2}\right)}{[a_M]^y \, p^e_{O_2}} \right\} \qquad \ldots(2.29)$$

Assuming that M_yO_2 is pure, $a_{M_yO_2} = 1$

$$\text{So,} \quad \Delta G^o_f (M_yO_2) = RT \ln p^e_{O_2} + y\, R\, T \ln [a_M] \qquad \ldots(2.30)$$

$$= \mu^e_{O_2} + y\, R\, T \ln [a_M] \qquad \ldots(2.31)$$

Calculation of $\mu^e_{O_2}$ or $p^e_{O_2}$ therefore require values of y and a_M besides ΔG^o_f. Table 2.5 presents values of y. For a_M, activity vs composition relationship in Ti-Al and Ti-Al-Nb alloys at different temperatures are required. Luthra[44] compiled the calculated activities of Ti and Al in Ti-Al alloys from various sources as function of composition at 1073K. This is reproduced in Fig.2.10. Rahmel and Spencer[50] also compiled the activities of Ti and Al in the Ti-Al system as a function of composition at various temperatures. The data corresponding to 1173K are also shown in Fig.2.10.

In Ti-N binary system, α-Ti is stabilized by nitrogen. The maximum solubility of nitrogen in α-Ti is between 6.5 and 7.4 wt pct[56]. In β-Ti the solubility of nitrogen is about 1.9 wt pct. The

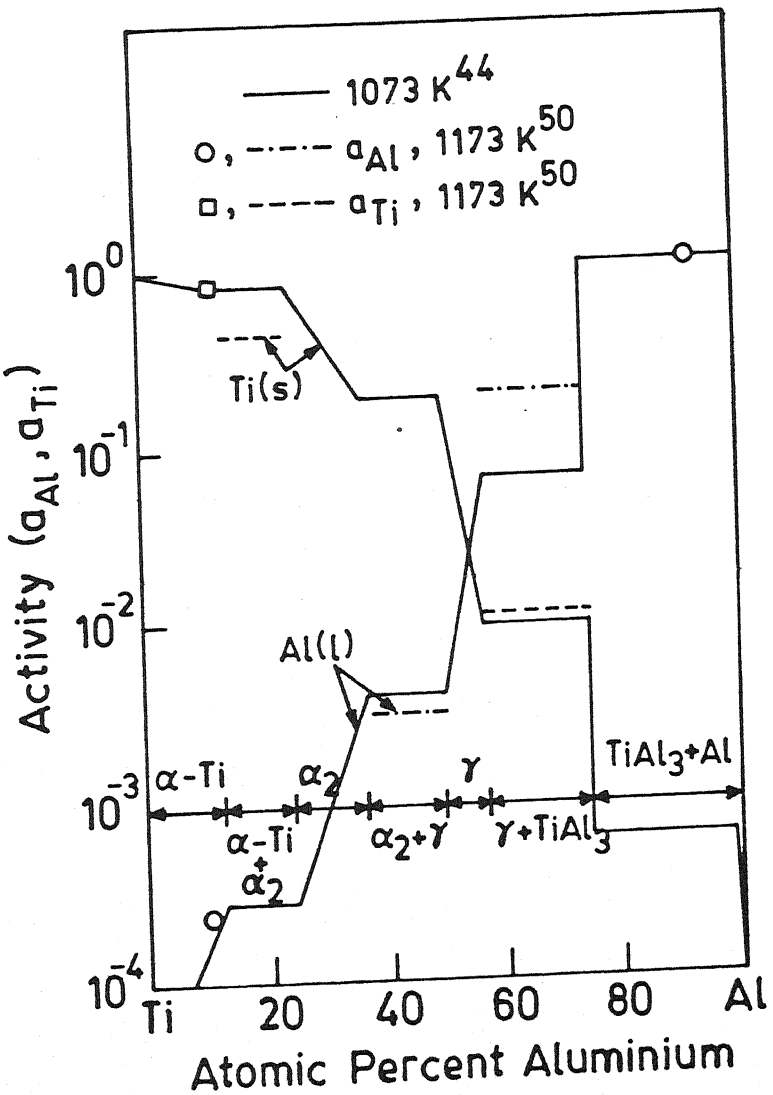

Fig.2.10: Calculated activities of aluminium and titanium as function of composition for binary Ti-Al system[44,50]

solubility of nitrogen in Al and Nb is very small.

The following type of exchange reactions is to be considered for nitride formation in Ti-Al-Nb alloys :

$$TiO(s) + \frac{1}{2} N_2(g) = TiN(s) + \frac{1}{2} O_2(g) \qquad \Delta G^o_{32} \qquad ...(2.32)$$

$$\Delta G^o_{32} = \Delta G^o_f(TiN) - \Delta G^o_f(TiO) \qquad ...(2.33)$$

$$\frac{1}{2} Al_2O_3(s) + \frac{1}{2} N_2(g) = AlN(s) + \frac{3}{4} O_2(g) \qquad \Delta G^o_{34} \qquad ...(2.34)$$

$$\Delta G^o_{34} = \Delta G^o_f(AlN) - \frac{1}{2} \Delta G^o_f(Al_2O_3) \qquad ...(2.35)$$

Here nitrogen and oxygen are competing with each other for the metal. Values of ΔG^o have already been reported in Table 2.3.

$$\Delta G^o_{34} = - RT \ln K_{34} \qquad ...(2.36)$$

where, K_{34} = equilibrium constant. The expression for equilibrium constant may be illustrated with the help of reaction (2.34)

Now,
$$K_{34} = \left\{ \frac{a_{AlN} \; p_{O_2}^{3/4}}{\left(a_{Al_2O_3}\right)^{1/2} \; p_{N_2}^{1/2}} \right\}_e \qquad ...(2.37)$$

Taking $a_{AlN} = 1 = a_{Al_2O_3}$,

$$K_{34} = \left\{ \frac{p_{O_2}^{3/4}}{p_{N_2}^{1/2}} \right\}_e \qquad ...(2.38)$$

or,
$$\log K_{34} = \frac{3}{4} \log (p^e_{O_2}) - \frac{1}{2} \log (p^e_{N_2}) \qquad ...(2.39)$$

nitridation of Ti-4.32Nb (wt pct) alloy. The weighted average parabolic rate constant was expressed as :

$$k'_p = \sum_{i=1}^{N} (k_i t_i) \,/\, \sum_{i=1}^{N} t_i \qquad \ldots(2.40)$$

where k_i (denotes instantaneous parabolic rate constant) and the respective time t_i were obtained from the slope of the plot of $(\frac{\Delta W}{A})^2$ vs t data.

During oxidation of titanium a change in parabolic rate constant with time was noticed by Chaze and Coddet[59]. At lower temperatures (below 823K), the rate constant decreased with time whereas at higher temperatures (above 873K) the rate constant increased with time. The rate constant was stabilized after prolonged exposure time (500 hr). The investigators[59] also commented that the large scatter in the published values of the rate constant and activation energies could be attributed to the above behaviour pattern.

Kahveci et al[60] noted nearly parabolic oxidation rate upto 1123K for Ti-Al alloys with 26 to 49 atom pct Al. According to them at higher temperatures (above 1250K), deviation from parabolic oxidation behaviour was reflected by the abrupt discontinuities in slopes of the weight gain versus time plots. These discontinuities were proposed by Welsch and Kahveci[61] to be due to formation of intermediate oxides of titanium (TiO, Ti_2O_3) as loose, powdery substance at temperatures above 1093K. Complex oxidation behaviour involving two or more rates depending on temperature and exposure time was observed by Sankaran et al[62] in Ti-14Al-21Nb (wt pct).

Wallace et al[63] studied isothermal oxidation behaviour of Ti-33Al-6Nb-1.4Ta (wt pct) in air from 923 to 1273K and in oxygen from 1073 to 1273K. Parabolic rate law was employed as follows.

$$(\frac{\Delta W}{A})^2 = k_p t \qquad \ldots(2.6)$$

where $(\frac{\Delta W}{A})$ and t, and k_p have their usual meaning. The instantaneous parabolic rate constant (k_i) was determined from the following equation :

$$k_i = 2(\frac{\Delta W}{A}) \frac{d(\frac{\Delta W}{A})}{dt} \qquad \ldots(2.41)$$

If k_i is constant with time, then the rate law would be parabolic.

The investigators[63] observed that in oxygen, the k_i decreased quickly during the initial period and became constant for the remainder of the exposure ensuring parabolic rate. When exposed in air, although the weight gain appeared parabolic, k_i decreased continuously throughout the entire exposure time. Fig.2.11 shows this. The formation of porosity in the titanium oxide was held to be responsible for this. With increasing porosity, the weight gain rate, and therefore, k_i would decrease. It is noted that based on this analysis, a parabolic fit to the weight gain curve would produce only an average rate constant that would also depend on the interval of the curve considered.

In a similar study the investigators[64] observed complex oxidation behaviour of Ti-25Al-10Nb-3V-1Mo (atom pct) in air over the temperature range of 923 to 1273K. At oxidation temperatures below 1173K, the parabolic oxidation was preceeded by an initial period of non-parabolic oxidation, the duration of which varied

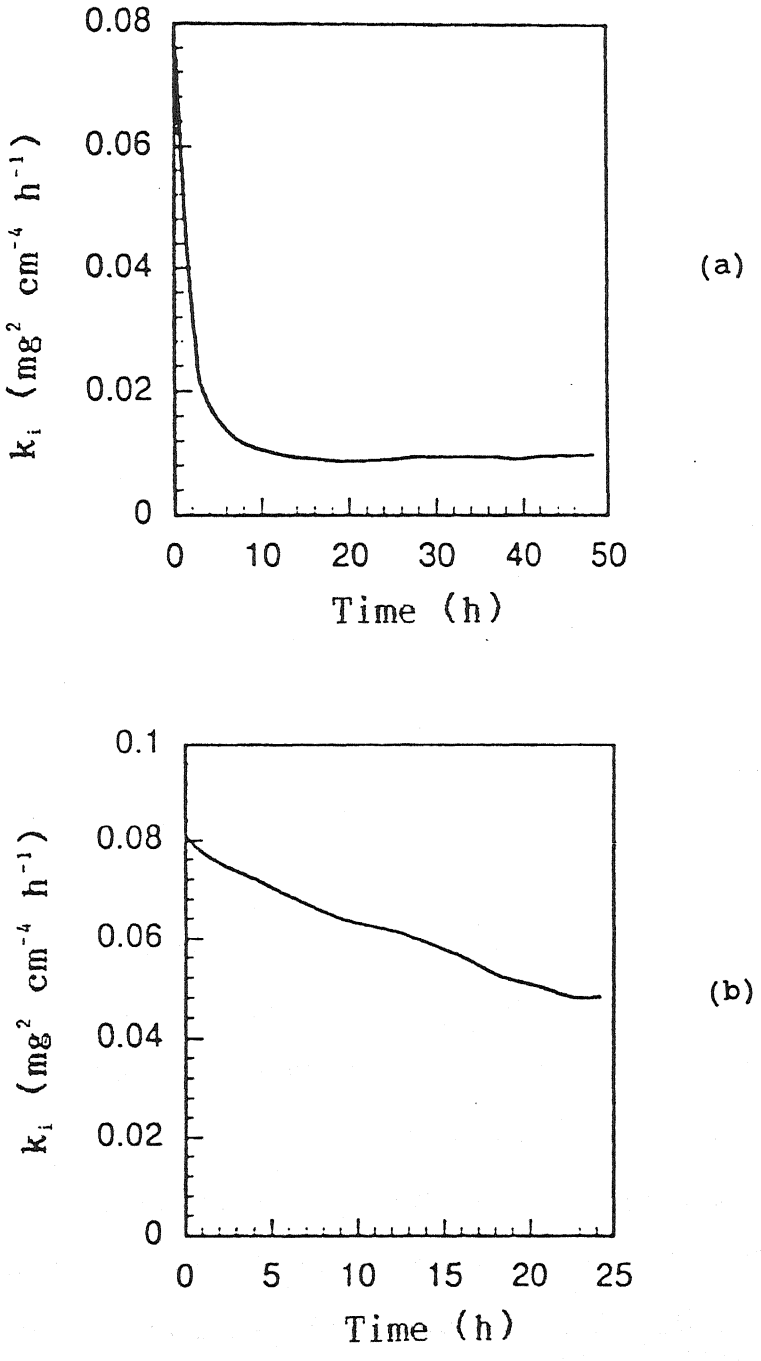

Fig.2.11: k_i versus time plots for oxidation of Ti-33Al-6Nb-1.4Ta at 1273 K[63] (a) in oxygen, (b) in air

from 20 hr at 973K to 2 hr at 1173K. This was evident from the fact that k_i initially decresed with time before becoming constant. Two distinct periods of parabolic oxidation separated by a non-parabolic transition period were observed during oxidation at or above 1173K.

Schaeffer[65] studied oxidation behaviour of two α_2 alloys (viz. Ti-25Al-10Nb-3V-1Mo and Ti-24.5Al-12.5Nb-1.5Mo (atom pct) in flowing air, and obtained the rate constants from the slopes of log-log plots of $(\frac{\Delta W}{A})$ vs time. The slopes ranged from 0.47 at 866K to 0.62 at 978K for 12.5Nb-1.5Mo alloy. This corresponded to near parabolic (0.5) rate. For 10Nb-3V-1Mo and Ti-6242 alloys, the slopes were about 0.85 at 866K and 921K and 0.65 at 978K. This indicated mixed kinetics. Although the slopes were similar at 978K, the 12.5Nb-1.5Mo alloy oxidized approximately at 4 times slower rate than 10Nb-3V-1Mo alloy.

2.5.2 Titania and Alumina Forming Kinetics

The formation of alumina as an external scale is beneficial towards promotion of oxidation resistance. The criterion for critical aluminium content needed for selective oxidation of Al was developed by Wagner[43], and has been described in earlier sec.2.3.8. Perkins et al[66] discussed the various factors deciding the ability of Ti-Al alloys to form an external alumina scale. One investigation[67] reported that for a fixed value of parabolic rate constant (10^{-8} $kg^2m^{-4}s^{-1}$), the growth rate of Al_2O_3 is slow upto 1573K as compared to that of SiO_2 and Cr_2O_3 and would appear to have the best potential for protecting Ti-alloys from oxidation. This idea is presented in Fig.2.12.

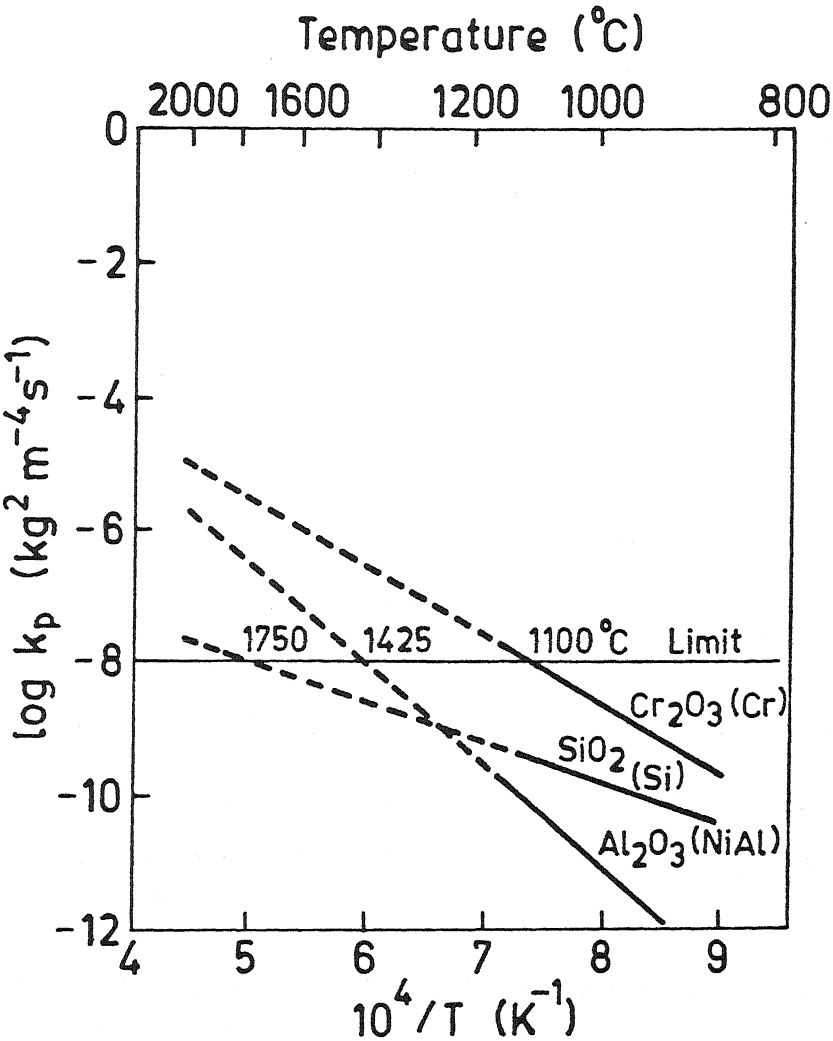

Fig.2.12: log k_p versus 1/T plots for oxidation demonstrating effect of protective oxide scales[67]

The amount of Al present in Ti-Al alloys decides whether alumina or titania formation will predominantly govern the kinetics of oxidation. Comparing the observed k_p values with purely Al_2O_3 or TiO_2 forming kinetics, one may be able to arrive at the dominant feature of the oxidation process. In this regard several investigators[60,61,68] compared the observed k_p values obtained from oxidation of titanium aluminides with purely Al_2O_3 and purely TiO_2 forming kinetics. This is illustrated in Fig.2.13 reproduced from Kim[69]. Choudhury et al[68] indicated (from the k_p values for oxidation of Ti_3Al) that the mass transport through TiO_2 was the rate controlling step. Increasing Al content or addition of Nb to Ti_3Al or TiAl tend to shift the kinetics towards Al_2O_3 formation (Fig.2.13).

2.6 CHARACTERISTICS OF SCALE FORMED AFTER OXIDATION

Table 2.6 summarizes some of the earlier studies on high temperature oxidation of Ti-Al-Nb system. The characteristics of scales formed after oxidation have been examined by various techniques. Usually most of the earlier investigators employed scanning electron microscope (SEM) and optical microscope for examining the scale morphologies. The phases were identified by X-ray diffraction (XRD) and the chemical composition was obtained by energy dispersive X-ray (EDX) analysis, and by electron probe microanalyser (EPMA). For XRD studies, the scales were either characterized intact or powders were prepared by mechanically removing the scale. In some cases both were employed.

The oxidation behaviour of metals and alloys is related to nature of the scales or product formed. During the parabolic

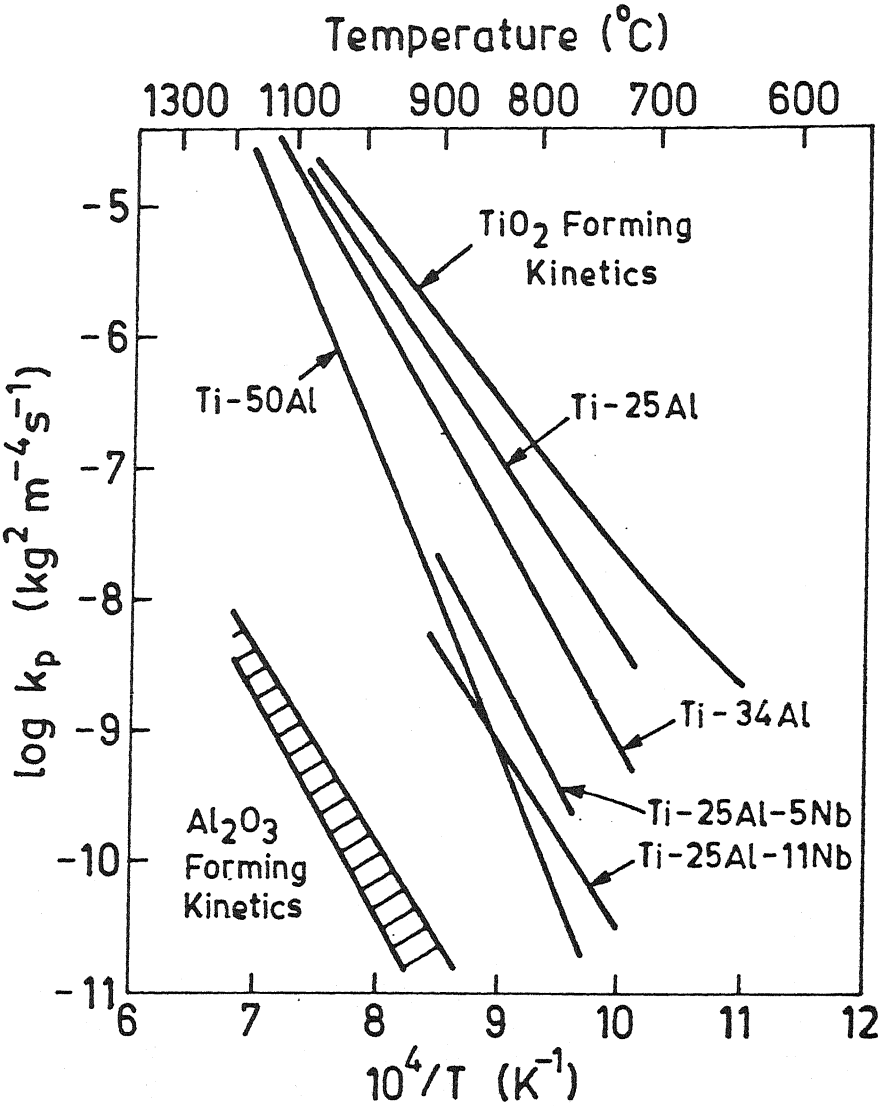

Fig.2.13: log k_p versus 1/T plots for oxidation of some titanium aluminides compared with purely TiO_2 and purely Al_2O_3 forming kinetics[69]

Table 2.6 Experimental Conditions and Some Features of High Temperature Oxidation of Ti-Al-Nb Systems

References	Alloy composition	Temperature(K)	Gas composition	Measurement technique	Rate law	Nb-beneficial?	Nature of scale	Remarks
Choudhury et al (68)	Ti-36Al(wt%) with Nb,Hf, etc.addition	1073-1473	air, O_2, gas mix of O_2 with N_2 or Ar or both & in changing environment	isothermal	parabolic, occasionally linear	yes	multilayer scale-TiO_2, Al_2O_3, α_2 and γ; no nitride identified	N_2 found to be detrimental
Strafford and Towell (82)	Ti	1173-1273	N_2(passed through Ti sponge)	isothermal	parabolic, occasionally linear	-	golden colour; adherent to substrate	extensive nitrogen dissolution in substrate
Rawe and Rosa (58)	Ti-4.32Nb (wt%)	1173-1473	air or N_2 for pre-nitrided sample and only in air	isothermal	parabolic	-	outer scale TiO_2 for all samples; inner scale consisted TiO_2 Ti_2O, ε-TiN and TiN	N_2 played beneficial role
Subrahmanyam (25)	Ti-14Al-24Nb (wt%)	1273-1373	air	cyclic	-	no	mostly TiO_2; minor Al_2O_3 and Nb_2O_5	Nb_2O_5 in scale detrimental
Welsch and Kahveci (61)	Ti-Al(25-49), Ti-25Al-21Nb (atom%)	873-1373	O_2	isothermal	parabolic upto 1123K, & linear at higher temperatures	yes	thin adherent scale (mostly rutile) at 873K and thick stratified scale at 1373K; mixture of TiO_2 and Al_2O_3 at surface and TiO_2-Nb_2O_5 in inner scale	internal oxidation observed
Meier et al (45)	Ti-Al(26-64 atom%)	1073-1573	O_2 & air	isothermal	parabolic	-	outermost scale virtually pure TiO_2 with islands of Al_2O_3 in alloys < 59 at% Al	internal oxidation in alloys with β but not in Ti-25Al

References	Alloy composition	Temperature(K)	Gas composition	Measurement technique	Rate law	Nb-beneficial	Nature of scale	Remarks
Wiedemann (78)	Ti-14Al-21Nb (wt%)	922-1366	air	isothermal	parabolic with two distinct transition	yes	mixture of Ti and Al oxide at surface; below that TiO_2; mixture of Ti and Nb oxide (not identified by XRD) near substrate; below that Ti and Nb nitride layer	N_2 played a subtle role in controlling oxygen activity
Maki et al (72)	TiAl-Nb	973-1173	air	-	non parabolic	yes	TiO_2, Al_2O_3 and TiO_2+ Al_2O_3 from surface inward	Nb enhances Al_2O_3 formation
Wallace et al (64)	Ti-25Al-10Nb-3V-1Mo (atom%)	923-1273	air (hydrocarbon <0.1 ppm)	isothermal	two distinct parabolic rates	yes	primarily TiO_2 doped with Nb; top layer Al_2O_3 and thin bottom layer of TiN	-
Becker et al (49)	Ti-36Al, Ti-35Al-0.1C, Ti-35Al-1.4V, Ti-35Al-5Nb-0.1C (wt%)	973-1273	air, O_2, & O_2+ Ar (mixture)	isothermal	close to parabolic at 1173K, linear with short transition at 1273K	yes	TiN and Ti_2AlN beneath the scale in Ti-Al-Nb alloy in air at 1223K; thin uniform scale with smaller crystal in TiAl	role of N_2 not clear; no role of p_{O_2}
Chen et al (76)	Ti-Al-Nb (wide range)	1173-1473	air (humidity 40%)	isothermal	parabolic, linear for high Nb alloy	yes (for high or low Ti/Nb ratio)	outer scale non-compact dominantly TiO_2+Al_2O_3; for low Al content (Ti, Nb)O_2+Al_2O_3 formed protective scale	occurrence of Nb_2O_5 detrimental
Takasaki et al (80)	Ti-42Al(atom%)	1073-1273	air	isothermal, also continuous heating	parabolic	-	outer oxide TiO_2 and inner scale a mixture of TiO_2 and Al_2O_3	in situ XRD of growing scale

Contd. Table 2.6

References	Alloy composition	Temperature(K)	Gas composition	Measurement technique	Rate law	Nb-beneficial	Nature of scale	Remarks
Schaeffer (65)	Ti-25Al-10Nb-3V-1Mo and Ti-24.5Al-12.5Nb-1.5Mo (atom%)	866-978	air	isothermal	near parabolic, some cases mixed	-	tinted blue fine grain oxide in V containing alloy; thick and dark grey scale with rutile over grown a dark porous oxide in Mo containing alloy	interstitial layer containing O,N and C
Shida and Anada (81)	Ti-Al(20-60 wt%)	1073-1173	air	isothermal	alloys upto 34.9 wt% Al showed parabolic initially and linear at later stage	-	porous multilayer scale consisting $TiO_2/Al_2O_3/TiO_2+Al_2O_3$/internal oxide from outer surface	Al_2O_3 internal oxide grew as stringers

oxidation period of titanium, Kofstad et al[57] noticed a very thin and extremely adherent grey scale. The oxide colour changed to white and yellow during the linear period with poor adherence to the metal. The oxide formed in all the cases was found to be TiO_2. In fact the morphologies and chemical composition of scales are influenced by some factors such as alloying elements, gas composition etc.

2.6.1 Effect of Alloying Elements Particularly Niobium

The oxidation of alloys and intermetallics in the binary Ti-Al system has been the subject of several earlier studies. The scale formed upon oxidation in such cases was mostly multilayered. Ti_3Al as well as TiAl have poor oxidation resistance as compared to $TiAl_3$[22,70] because at low Al content, the external scale of the former was not protective Al_2O_3 film but rather TiO_2 or a mixture of TiO_2 and Al_2O_3. Best oxidation resistance is obtained by Al_2O_3 scale formation. The temperature should be high enough to promote Al_2O_3 formation and the Al content must be sufficiently high to develop and maintain an Al_2O_3 layer. The main weakness of Al_2O_3 scale is the susceptibility to cracking and spalling which is caused due to stresses. Addition of a third element may improve the adherence and reduce the growth rate[71].

Internal oxidation of Al prevents the formation of protective Al_2O_3 scale. The critical concentration of Al needed for the transition from internal to external oxidation have been considered on the basis of Wagner's[43] equation, which has already been discussed in sec.2.3.8. Perkins et al[66] listed various ways which enhance the ability of Ti-Al alloys to form an external Al_2O_3

scale. It has been shown that Al_2O_3 could be formed if a third element was added to binary Ti-Al alloys to slow down the rate of transient oxidation and/or to decrease the permeability of oxygen and nitrogen[45,67]. Effective addition to Ti-Al alloys in decreasing order included Re, Mo, Cr, W, V and Nb. However best overall behaviour was exhibited by Ti-Al-Cr system[45].

In general, the addition of Nb to Ti-Al alloys was observed to be beneficial for oxidation resistance by several investigators as noted in Table 2.6. The positive role of Nb has been interpreted in many ways. According to some authors[61,62,64,68] the addition of Nb reduced the point defect concentration of titania scale which decreases diffusion rate through titania. While some investigators[49,63,72,73] proposed that Nb promotes the formation of protective Al_2O_3. Hoch[73] determined the activity ratios of Al and Ti in Nb containing Ti-36Al(wt pct) alloys and observed higher value of the ratios as compared to those in alloys without Nb.

Hauffe[74] reported that the addition of Nb not only improved oxidation resistance but discontinuities in the slopes of weight gain curves were also eliminated. The modification of defect structure of TiO_2 caused by niobium ions has also been proposed. However, the mechanism is not properly understood.

On the contrary Subrahmanyam[25] reported detrimental effect of Nb. According to the investigator, the presence of Nb_2O_5 in scale was found to be one of the factors leading to spallation. The concentration of Nb also influenced the oxidation behaviour. Addition of 5 wt pct Nb to TiAl caused Al_2O_3 formation at the metal/scale interface even at 1173-1223K. Becker et al[49] held

gradual enrichment of Nb in the alloy during the transient oxidation to be responsible for this. According to Singheiser et al[75] the oxidation rate was parabolic and rate constant values decreased with increasing Nb content and became independent for Nb addition greater than 10 atom pct. In another study Chen et al[76] reported that the oxidation resistance of Ti-Al-Nb system was reduced dramatically when the ratio of Ti to Nb was either too high or too low. The occurrence of Nb_2O_5 for high Nb alloys always led to a decrease in the oxidation resistance. Oxidation at 1173K showed predominantly TiO_2 at Al content lower than 45 atom pct and/or Ti/Nb ratio greater than 5 to 6.

2.6.2 Effect of Gas Composition

Composition of the oxidizing atmosphere is another factor which influences oxidation of titanium and its alloys. Oxidation in air can be significantly different than that in oxygen as compiled in the Table 2.6 and also reported elsewhere[59,77].

The oxidation of Ti-Al (upto 10 wt pct)[59] and Ti-4.32 Nb (wt pct)[58,77] alloy in air showed an improved oxidation resistance than that in O_2. According to Rawe and Rosa[58] the oxidation resistance in air was comparable to that of nitrogen pretreated alloy and was considerably higher than that in pure oxygen. The formation of titanium nitrde seemed to hinder oxidation rate. However Chaze and Coddet[59] could not detect any nitride in the scale. As per Becker et al[49] oxidation of TiAl in air can lead to nitride formation beneath the oxide scale and under certain conditions this favours protective Al_2O_3 formation at the metal/scale interface. However in general, nitridation was found to be detrimental with the

consequence of rapid oxidation in air than in O_2. They also observed that oxygen pressure in the range of 0.01-1 bar in O_2-Ar mixture did not influence the oxidation rate.

Wiedemann et al[78] provided probable explanation for the presence of nitride layer. For the reaction :

$$2TiN + O_2 = 2TiO + N_2 \qquad \ldots(2.42)$$

the equilibrium p_{O_2}/p_{N_2} is $5x10^{-16}$ at 1255K. The presence of TiN implied the ratio to be lower than this indicating a strong oxygen activity gradient across the oxide, as would be present in compact oxide.

Rapid oxidation of Ti-36 Al (wt pct) alloy upon exposure to air was attributed to the presence of nitrogen in air by Choudhury et al[68]. They also noticed that fast oxidation kinetics was not caused by hydrocarbon, CO, CO_2, or water vapour impurities present in air. The investigators also studied the effect of N_2 or air on preoxidized sample and observed a time dependent increase in the rate in N_2 as well as in air. However, no nitrogen containing phases were identified in the scale. Various mechanisms towards the role played by N_2 in the oxidation process have been listed by them.

Meier et al[45] have presented the alloy regimes in Ti-Al binary phase diagrams where alloys exhibited formation of protective Al_2O_3 scale upon oxidation. These alloys lie in γ (TiAl) phase field. This agrees with the findings of some other investigators as well. To obtain further understanding of effect of nitrogen, the investigators implanted TiAl by N^+-ions and then exposed in pure O_2 and found accelerated oxidation rate which was not explained properly.

As observed by Wallace et al[63] the instantaneous rate constant (k_i) vs time (t) plot of Ti-33Al-6Nb-1.4Ta (wt pct) exposed in O_2 was consistent with parabolic rate law while that in air showed different behaviour. Brady et al[79] found parabolic oxidation rate in air and near parabolic oxidation rate in pure O_2. The presence or absence of N_2 in the environment appeared to affect both the rate as well as the mechanism of oxidation of 25Nb-25Ti-50Al[79]. Schaeffer[65] studied oxidation of Ti-25Al-10Nb-3V-1Mo and Ti-24.5Al-12.5Nb-1.5Mo in air at temperatures between 866 and 978K. A white imaging layer had been seen underneath a thin oxide layer. Secondary ion mass spectroscopy (SIMS) and X-ray photoelectron spectroscopy (XPS) examinations revealed the white layer to be a layer as Ti (O,N,C). The investigator suggested that the layer slowed down oxidation rate of Ti_3Al-based alloys in air than in oxygen.

Takasaki et al[80] carried out in situ X-ray diffraction study during heating up and during isothermal heating of Ti-42Al (atom pct) at 1073 and 1273K in static air. They observed TiO_2 as the outer scale and a mixture of TiO_2 and Al_2O_3 as inner one. TiO_2 scale formed during heating up (at a rate of 0.33 K s^{-1}) at about 973K and then Al_2O_3 at about 1273K. For isothermal heating upto 7.2 ks, TiO_2 scale slowly grew up at 1073K but Al_2O_3 did not appear while both TiO_2 and Al_2O_3 grew up drastically at 1273K. After oxidation of Ti_3Al in air at 1173K Shida and Anada[81] observed multilayered scale. The various sublayers were in the order of $TiO_2/Al_2O_3/TiO_2+Al_2O_3$/internal oxide from the outer surface to the Ti_3Al matrix. Porosity was present in all these layers.

2.6.3 Influences of other factors

Sample surface preparation prior to oxidation can influence the oxidation rate, reaction product morphologies etc. Choudhury et al[68] observed that heavily surface-cold-worked samples of cast TiAl exhibited improved oxidation resistance compared to that of polished specimens in oxygen at 1223K. In another study Kahveci et al[60] noticed similar oxidation behaviour of Ti alloys with 25 and 34 atom pct Al in ground as well as in electropolished condition. Very little work have been carried out to see the effect of alloy microstructure on oxidation behaviour.

As Wagner[43] model describes, retaining a large amount of phase having a high diffusivity of aluminium could be beneficial for oxidation resistance. The high temperature phase in Ti-Cr alloys is a Cr-rich beta. According to Perkins et al[67] the optimum composition of Ti-44Al-32Cr (atom pct) provided the best balance of microstructure and oxidation resistance from 1073 to 1573K. Alloys containing mainly β solid solution exhibited severe internal oxidation under titania scale whereas alloys consisting primarily of Ti_3Al showed little or no internal oxidation[45]. The diffusivity of Al is high in beta phase. Hence, the ability to form alumina decreases as the amount of retained beta is decreased[66].

2.7 ENVIRONMENTAL EMBRITTLEMENT AND SOME REMEDIAL MEASURES

2.7.1 Environmental Embrittlement and Solid Solution Hardening of the Subscale

Titanium and its alloys have high affinity for oxygen and nitrogen. Dissolution of the same plays an important role during the oxidation process. A simple assessment of the amount of

dissolved oxygen or nitrogen could be made from the microhardness measurements taken from the metal/oxide interface to the interior of the metal[57,59,77,82]. The oxygen and nitrogen penetration into the metal increased with increasing reaction temperature and exposure time[82]. The relative importance of the dissolution process was observed to be decreasing with exposure time[57].

Kofstad et al[57] concluded that initial period of oxidation of Ti is primarily due to oxygen dissolution in the metal. When the oxygen content in the layer next to the metal/oxide interface reaches $TiO_{0.35}$, heavy oxide formation begins involving nucleation of the oxide (possibly TiO) followed by rapid oxidation to TiO_2 eventually attaining a linear rate. Increase in oxygen content in the metal was indicated by an increase in hardness value.

A significant increase of the observed maximum hardness near the interface and increased depth of penetration was found by Strafford and Towell[82] during nitridation of titanium, due to increasing temperature and exposure time. Rawe and Rosa[58] indicated that the drop in Vicker's hardness values from the surface to the interior followed, at least quantitatively, the oxygen profile determined by electron microprobe analysis. A reduction in the amount of dissolved oxygen in binary Ti-Al (Al upto 10 wt pct) during oxidation in air compared with that in oxygen was observed by Chaze and Coddet[59].

Kahveci et al[60] found oxygen enriched alloy substrate of about 30 μm thick in Ti-Al alloys oxidized for 24 hr at 1373K. It contained internally oxidized porous Al-rich channels. This enabled rapid mass transport along their surfaces which resulted in

mechanical weakening of the alloy surface layer. A well defined oxygen embrittled layer has been observed in Ti-26Al and Ti-34Al oxidized in dry oxygen at 1123K for 24 hr[61]. Internal oxidation in the oxygen affected alloy surface layer was also observed in Ti_3Al-Nb alloy due to the presence of β phase[45]. Diffusivity of oxygen in β phase is higher than α or α_2. Therefore, internal aluminium oxidation zone penetrated deeper along β lamellae, thus providing paths for crack propagation[61]. Dissolved oxygen concentration may go as high as 33 atom pct corresponding to O/Ti ratio of 0.5, but experimentally determined values lie below 25 pct[61]. Oxygen has strong α-stabilizing effect[46]. So, small oxygen concentration can destabilize the ductile β phase in Ti_3Al-Nb alloy and transform it into brittle α or α_2 phase.

During elevated temperature exposure in air, significant solid solution hardening near the surface of Ti-24Al-11Nb (atom pct) was observed by Balsone[23] from microhardness profile. This caused bulk alloy embrittlement leading to surface crack formation, which initiated premature failure in a transgranular mode. On the other hand, Wallace et al[63] did not observe a clear increase in hardness near the oxide/metal interface of Ti-33Al-6Nb-1.4Ta (wt pct) exposed for 24 hr in air at 1173K.

Becker et al[49] observed preferential oxidation of Al in γ alloys with 35-36Al (wt pct) during exposure in air and oxygen, which resulted in formation of a brittle oxygen rich α_2 phase layer beneath the scale. At α_2/γ interface the maximum oxygen content was about 5 atom pct which could reach upto 20 atom pct at the scale/α_2 interface. Saitoh and Mino[24] observed that slight

oxidation (exposure in hot air) of super α_2 (i.e.Ti_3Al-10Nb-3V-1Mo) caused loss in ductility which was more serious than oxidation itself. McKee[83] found a zone of embrittled 'alpha case' of 60 μm formed in Ti_3Al based alloys, exposed to air at 1088K for 1000 hr.

2.7.2 Surface Coating as a Remedial Measure

The α_2 alloys are particularly prone to subsurface embrittlement due to dissolution of oxygen, nitrogen etc. in the metal lattice during elevated temperature exposure. Either alloying or a protective coating could alleviate this problem. Several investigators[25,78,83,84] studied the influence of coating on oxidation behaviour. According to Subrahmanyam[25], an aluminide ($TiAl_3$) coating on Ti_3Al-Nb alloy surface can withstand much higher temperature compared to the creep limit of 1088K for Ti_3Al. Beneficial effect of pack aluminizing was also observed by Smialek et al[85]. Coating of oxides of various elements (such as Mg,Y, Zr,etc.) and fluorides of Ca and Y on the specimens, with glassy coatings as top coats, was found to exhibit good film integrity and reduced oxidation[78].

Grahle et al[84] applied coatings of aluminium and aluminium oxide on Ti_3Al. Aluminium coating of 0.2 μm thick reduced the oxidation rate below that of uncoated γ TiAl. They observed lowest oxidation rate after coating Ti_3Al with 0.6 μm aluminium oxide.

McKee[83] employed plasma sprayed coatings of FeCrAlY and CoCr, over a thin diffusion barrier of Cr or W, on Ti_3Al-based intermetallic compounds. Coatings were found to be adherent and protective for periods of at least 1000 hr during rapid thermal cycling in air at 1088K. Subsurface embrittlement was not observed.

CHAPTER 3

EXPERIMENTAL TECHNIQUES

3.1 SAMPLE PREPARATION AND CHARACTERIZATION

3.1.1 Materials

In the present study, three Ti_3Al-based (α_2) titanium aluminides were employed. Two pancakes of Ti-25Al and Ti-24Al-15Nb (atom pct) each of 150 mm dia and 15 mm height were provided by Defence Metallurgical Research Laboratory (DMRL), Hyderabad. These were produced by consumable vacuum-arc melting technique. The chamber was evacuated, flushed with argon and again evacuated. A few thin sheets (0.5 mm thick) of Ti-25Al-11Nb (atom pct) were obtained from Texas Instruments Inc., USA (designated as TI). Alloys from DMRL will now onwards be designated as alloys A (Ti-25Al) and B (Ti-24Al-15Nb) respectively, and alloy from Texas Instruments as alloy C (Ti-25Al-11Nb). At DMRL, the alloys were melted 4 times to minimize inhomogeneities while TI's sheet was produced by proprietory processing technique. Table 3.1 lists the alloy compositions as provided by the suppliers. Alloys were used for oxidation studies in as received condition without any further heat treatment.

3.1.2 Sample Preparation

The pancakes were cut into smaller pieces by diamond wheel. Rectangular oxidation samples were cut from these smaller pieces as well as from thin sheets using a low speed Buehler Isocut saw. The thickness of the sections varied from 0.5 mm (for TI's

Table 3.1 Chemical Compositions of Ti_3Al-Based Titanium Aluminides

Elements*		Alloy A		Alloy B		Alloy C	
		atom pct	wt.pct	atom pct	wt.pct	atom pct	wt.pct
Nominal composition	Al	24.28	15.3	24.69	13.4	25.47	14.4
	Nb	-	-	15.54	29.04	11.35	22.1
Typical interstitial content (ppm)	O	1550		1400		<800	
	N	100		120		<80	
	H	20		25		<10	

* Rest Ti (by balance)

sample) to 1.2 mm. A few trial sections were cut using the electric dicharge cutting method. However this method was very time consuming and not employed further. A 2 mm dia hole was made at the top of the sample with a tungsten carbide drill so that the specimen could be hung inside the furnace. Special tungsten carbide drills were employed since the materials were very hard and brittle, particularly alloy A (Ti-25Al). Conventional drills (e.g. high speed drill) did not work.

After sectioning, the sample surfaces were ground by mechanical abrasion successively through 220, 400 and 600 grit SiC papers. Measurements of dimensions of the samples were made by Vernier callipers with vernier constant of 0.02 mm. Close control of the sample dimensions was difficult due to its hardness and brittleness. The thickness, width and breadth of samples varied from 0.5 to 1.5, 9 to 12 and 13 to 16 mm respectively. Total geome-

tric surface area of the samples varied from 2.7 to 4.5 cm^2. The sample was then degreased using soap solution and acetone, washed throughly in water, rinsed with acetone and alcohol, and dried by hot air blown.

3.1.3 Metallography of as Received Samples

Microstructural observations of as received alloys were carried out following conventional metallography technique. Specimens were ground upto 600 grit SiC paper. Final polishing was done using 0.3 μm alumina powder. The polished samples were then etched with standard Kroll's reagent[86] (1 pct HF, 9 pct HNO_3, 90 pct H_2O). Metallographic observations were made using an optical microscope (Leitz Metallux 3, Leitz Wetzlar, Germany). Elemental line scan of the major constituents e.g. Ti, Al and Nb were performed in a JEOL JSM 840A Scaning Electron Microscope (SEM) attached with Kevex Energy Dispersive X-ray (EDX) analyser to check chemical homogeneity. Photomicrographs would be shown later.

3.2 APPARATUS FOR ISOTHERMAL OXIDATION EXPERIMENTS

The thermogravimetric technique was employed for kinetic measurements. The apparatus consisted of a furnace, a Cahn 1000 electro balance, and gas train. These are described below. Fig.3.1 is the photograph of the experimental set-up employed for the present investigation. In Fig.3.2 the thermogravimetry set-up with Cahn electrobalance has been shown schematically.

3.2.1 Furnace with Accessories

A platinum-20 pct Rhodium wire-wound vertical furnace of 210 mm length was employed to carry out the oxidation tests. The

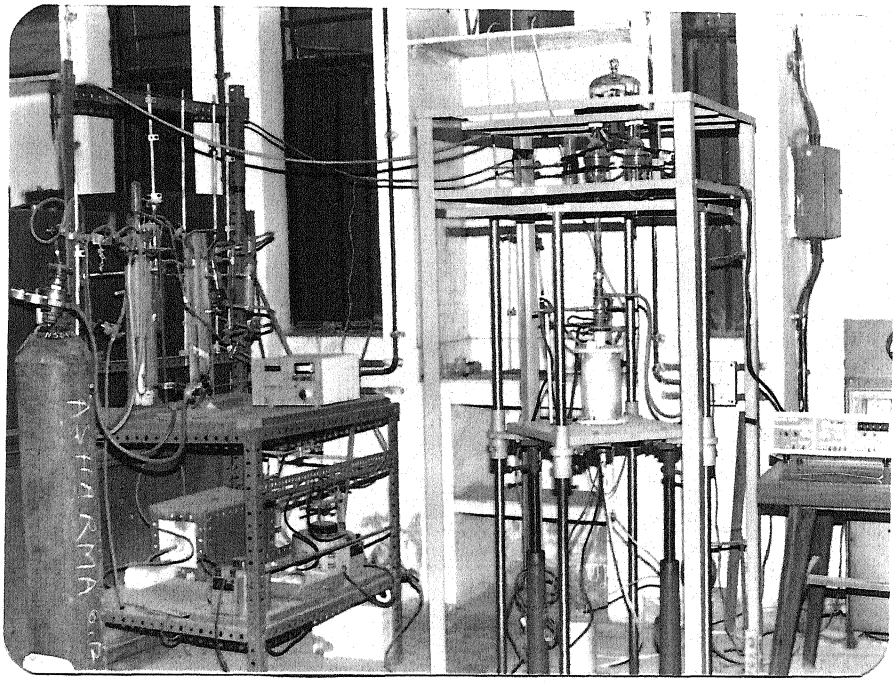

Fig.3.1: Photograph of the experimental set-up

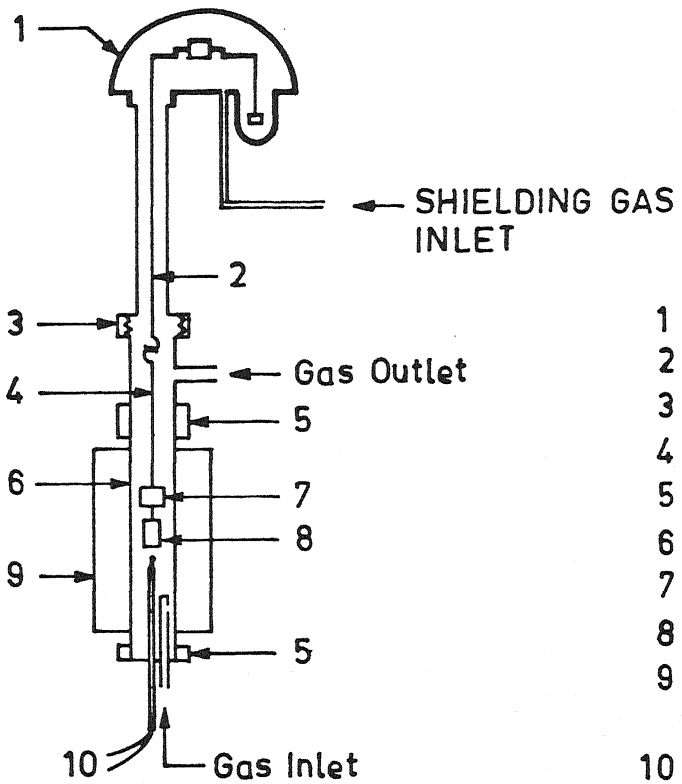

1 Cahn Balance
2 Inconel Rod
3 Screw Cap
4 Hanging Arrangement
5 Cooling Arrangement
6 Alumina Tube
7 Platinum Cylinder
8 Sample
9 Platinum-Rhodium Wound Furnace
10 Platinum-Platinum-10 % Rhodium Thermocouple

Fig.3.2: Schematic diagram of the thermogravimetry set-up with Cahn electrobalance

temperature of the furnace was controlled within ±2 K by a power proportionating indicating type temperature controller (Indotherm Instrument Pvt. Ltd., Bombay), actuated by a Pt/Pt-10 pct Rh thermocouple. The thermocouple emf was measured by a four-digit millivolt meter (Vaisehika Electron Devices, Ambala Cantt, Type 7707). A recrystallized alumina tube (17 mm i.d. and 370 mm length) acted as reaction chamber. The alumina tube was fitted with two brass heads (one at the top and the other at the bottom) to provide air tight fitting covers. Continuous water cooling through copper tube protected brazed joints in brass heads from high temperatures. Thermocouple and gas inlet tube were inserted through the bottom of the furnace. Silicone rubber 'O' rings and silicone sealant were employed to make the set-up leak proof. Temperature profiling of the furnace showed that a constant temperature zone of about 25 to 30 mm could be obtained at the centre of the furnace.

3.2.2 Cahn Electrobalance

The Cahn 1000 (Cahn Instruments, USA) is an automatic recording and sensitive weight measurement instrument (Figs.3.1 and 3.2). Its weighing capacity is upto 100 g and is sensitive to changes in weight as small as 1 μg as per specification. The maximum weight change that it can record is 10 g. The output signal is electrical.

The balance has two parts. The control unit houses all electrical controls for the balance, measures and displays the output of the balance. The other part is the weighing unit which measures the actual weight. The control unit was connected to a strip chart recorder (Digital Electronics Ltd., Bombay, Type:

Omniscribe B 5000) to register changes of weight continuously during the reaction as function of time.

3.2.3 Gas Train

The purpose of the gas train was to monitor the flow rates of the gases, purify them from probable impurities present, and to mix gases in different proportions as required. Fig.3.3 shows the line diagram of the gas train. Various gases and gas mixtures at 1 atmospheric pressure were employed in the present investigation. They were oxygen, nitrogen, and mixtures of oxygen-nitrogen, oxygen-argon, nitrogen-argon and nitrogen- carbon dioxide. Hydrogen gas was employed for regenerating BTS catalyst (BASF, Germany) intermittently.

Gases were passed through bubbler and capillary flow meter. Each gas from the cylinder was analysed in a Gas Chromatograph (Chromatograph Instrument Co., Baroda) by thermal conductivity detector (TCD) using Carbosieve S-II and Silica gel adsorbent columns to detect impurities. No peaks for impurity could be detected from the chromatogram which indicated that the extent of impurities, if any were very small (less than 0.5 pct). Except oxygen all other gases were passed through the BTS catalyst furnace kept at 460K. The BTS catalyst pellets (5 x 5 mm cylinder) contain 30 pct of copper in a very finely dispersed form, stabilized on ceramic substrate. Owing to its very high surface area, the fine copper particles remove oxygen efficiently from gases at a relatively low temperature. Gases were then passed through Ascarite column to remove carbon dioxide. This column was removed when carbon dioxide was employed in some experiments. Next, gases were

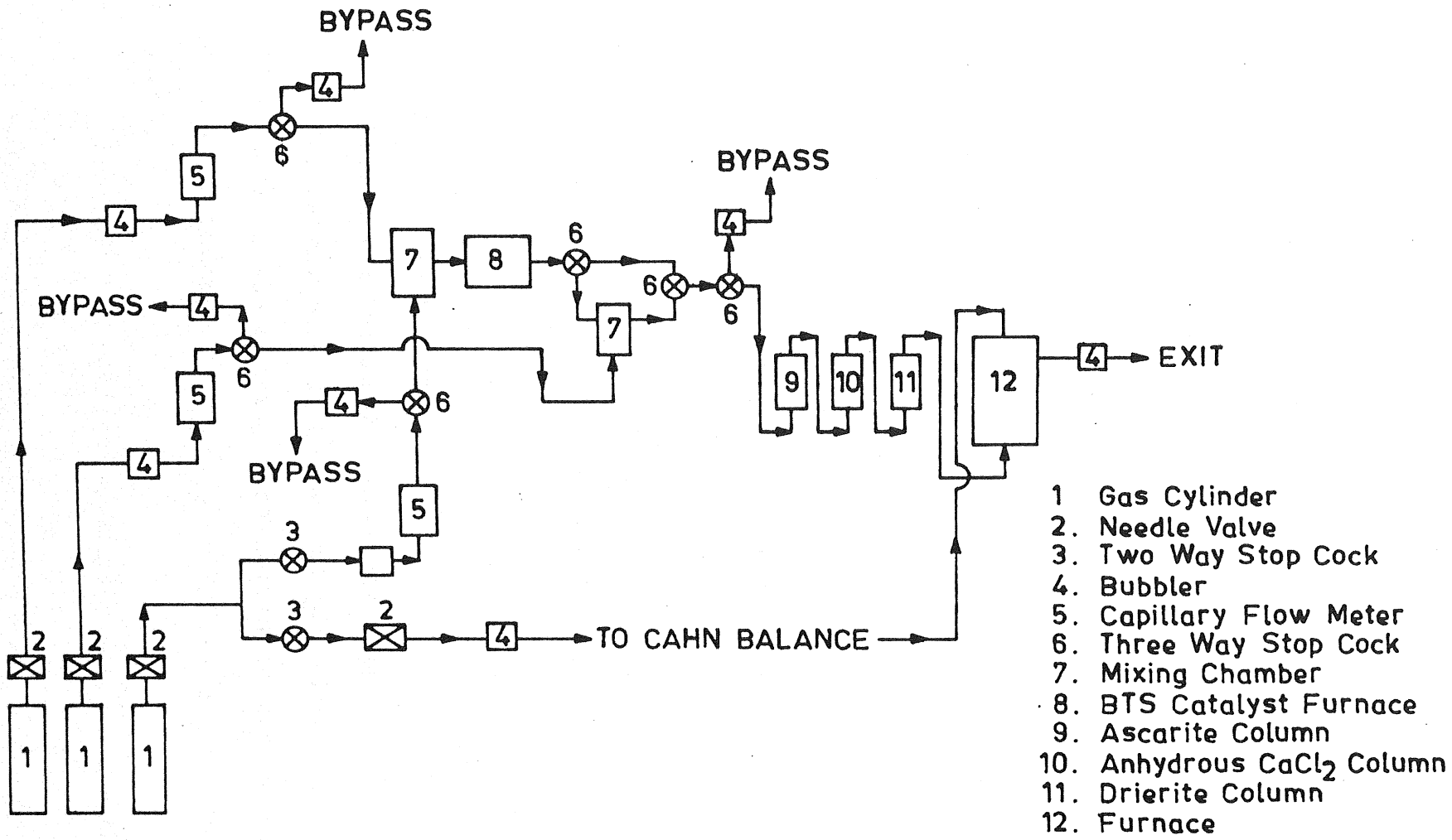

Fig.3.3: Schematic diagram of the gas train used with thermogravimetry set-up

passed through anhydrous calcium chloride and Drierite ($CaSO_4$) columns successively before introduction into the reaction chamber. Drierite has a low equilibrium residual water vapour pressure and therefore, it was used after the anhydrous calcium chloride column in the gas train for efficient removal of moisture.

Individual capillary flowmeters were calibrated by soap bubble meter. Results were fitted by linear regression analysis and the equations are given in Table 3.2, where $\dot{V}$ is gas flow rate in cm^3s^{-1} (STP), and h is height difference in the flowmeter, cm.

Table 3.2 Calibration Equations for Flowmeters at STP

Gas	Equation
Ar	$\dot{V} = 1.0847h + 0.3303$
N_2	$\dot{V} = 1.3901h + 0.4403$
O_2	$\dot{V} = 0.0992h + 0.1078$
CO_2	$\dot{V} = 0.1149h + 0.0222$
Ar	$\dot{V} = 0.0964h + 0.0221$

3.3 EXPERIMENTAL PROCEDURE

3.3.1 Isothermal Oxidation Kinetic Studies

Before arriving at the actual procedure a few trial runs were carried out. These trial runs helped in the following ways, besides familiarization with the handling of balance and accessories.

(i) Initially oxidation samples were tied with a Pt-wire

and hung inside the furnace. This caused vibration under flowing gases and produced disturbances in the strip chart recorder. This problem was taken care of by modifying the sample hanging assembly. A platinum cylinder (12 mm diameter and 6 mm long) was tied at the lower part of the Pt-wire. The cylinder kept the hanging assembly vertical and straight, and helped to dampen vibration. Fig.3.4 shows the hanging assembly.

(ii) An idea regarding weight gain values was obtained. Thus desirable meter and recorder range settings could be ascertained.

(iii) Sample introduction and removal times were standardized.

(iv) Gas flow rate was also standardized.

Instrument settings:

(a) Cahn electrobalance

Pct sample weight	: off
Meter and recorder range (MRR)	: 1 mg and 10 mg
Weight suppression range (WS)	: 10 g
Output	: 10 mV
Filter	: on/off (as necessary)
Auto range expander	: off

(b) Recorder:

Voltage scale	: 10 mV full scale
Chart speed	: 2.5 mm min^{-1}

Oxidation experiments were carried out isothermally. Experimental set-up and arrangements have been shown in Figs.(3.1)

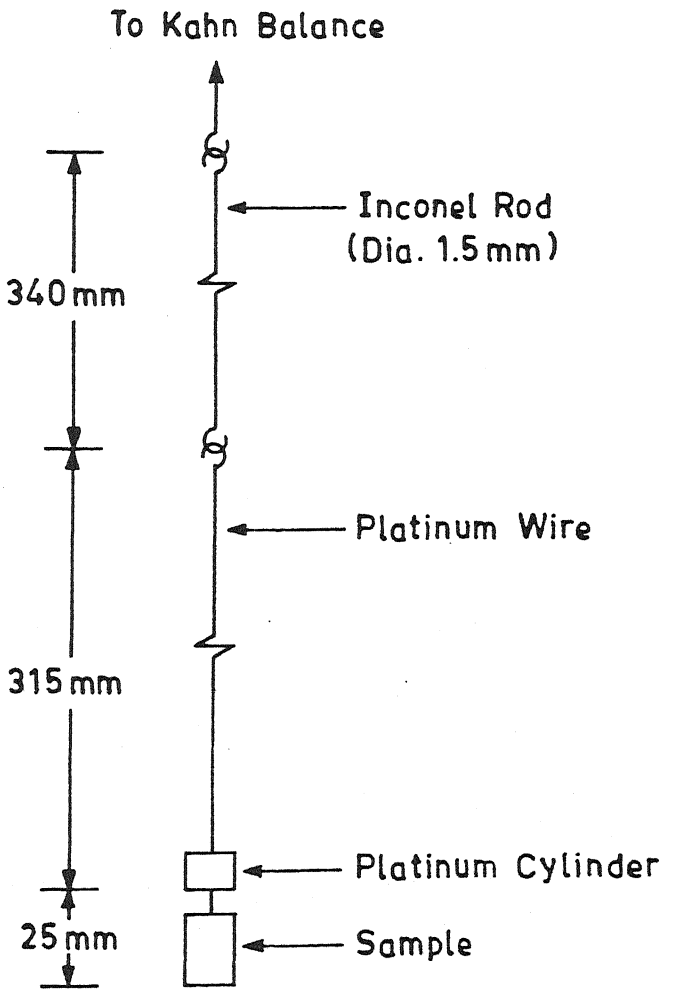

Fig.3.4: Sample hanging assembly for thermogravimetry

to (3.4). After the furnace attained the test temperature, sufficient time (20 to 30 minutes) was allowed for the stabilization of temperature. The furnace was then flushed with the test gas or gas mixture (when gas mixture was the reactant) to remove all entrapped air and to maintain test environment condition inside the furnace before introduction of the sample. A very low flow rate of argon or nitrogen was maintained continuously through balance chamber to protect the balance from hot reactive furnace gases.

The furnace was in lowered position initially. The oxidation sample with freshly prepared surfaces was weighed outside in analytical balance, and then attached to the end of the hanging assembly (Fig. 3.4). Then the assembly was hung from the Cahn electrobalance and introduced inside the furnace with a gas flow of 1.67 $cm^3 s^{-1}$ (STP). The sample was then quickly brought into the hot zone by raising the furnace with the help of jacks to proper position, and the whole system was made gas tight by tightening screw-cap on brass head. The sample temperature and furnace temperature were equalized by allowing some more time (4 to 5 minutes).

This corresponded to initial weight in balance, and the recorder was set at zero position by adjusting the weight suppression of the Cahn balance controller. Any change in weight occurring during oxidation was recorded as function of time by the strip chart recorder. After oxidation for the required length of time, flow of reactive gas was stopped. The cap was then unscrewed and the furnace was disconnected from the balance and

lowered down by jacks. The sample was taken out, cooled to room temperature, weighed in outside balance and kept in a plastic vial, wrapped with tissue paper for further studies. In some cases the outer scale spalled off upon cooling during removal from the furnace as well as outside the furnace. Spalled mass outside the furnace was collected and weighed together wherever possible.

3.3.2 Oxidation Followed by Pretreatment

Few experiments were conducted in changing environments. This helped to gain a better understanding of the role of constituents of the reactive gases in the oxidation process. These experiments were conducted at 1300K. Sample was exposed for 1 hr in one type of gas (pretreatment), before switching over to the other gas or gas mixture. When pretreatment was over the first gas was diverted to the bypass. The next gas or gas mixture whose flow had already been established through the bypass, was now introduced into the furnace through a three-way stop cock. The pen position at this moment in the chart recorder was taken as corresponding to zero weight gain for the new atmosphere. The whole operation was executed within 3 to 4 minutes time. These experiments were carried out in the following three ways :

(i) 1 hr pretreatment in nitrogen, then atmosphere replaced by oxygen

(ii) 1 hr pretreatment in nitrogen, then atmosphere replaced by 20 pct O_2 + 80 pct N_2 gas mixture

(iii) 1 hr pretreatment in oxygen, then atmosphere replaced by 20 pct O_2 + 80 pct N_2 gas mixture

3.3.3 Oxidation/Nitridation Tests With Getter in Reaction Chamber

Essential purpose of these experiments was to carry out blank runs in ultra-pure argon, and to obtain some information about nitriding behaviour of Ti_3Al-based alloys. Oxidation in 20 O_2 + 80 N_2 gas mixture can lead to nitride layer formation beneath the oxide scale. To gain more information on nitride formation, all three alloys were exposed to dry nitrogen passed through purifying gas train. However in addition to nitridation, considerable oxidation also occurred. These showed that the impurity (i.e. oxygen) level of nitrogen could not be kept low enough by BTS catalyst to avoid any formation of stable oxides of Al and Ti.

So, it was decided that nitrogen gas would be passed through a getter column, placed inside the reaction chamber in addition to usual purification. In this context zirconium metal was considered as an efficient getter element since it is very reactive and possesses capacity of removing oxygen in gas to an extremely low level. Thermodynamic calculations showed that it is able to give very low p_{O_2}. A special arrangement was made for this purpose inside the furnace. A closely fitted quartz tube (i.d. = 13.5 mm and o.d. = 15.6 mm) was placed inside the alumina reaction tube. The length of the quartz tube was such that the thermocouple tip remained outside it. The tube was then packed with drillings of pure zirconium crystal bar (Foote Mineral Co., Exton, USA) through which nitrogen gas would be passed during experiments.

In these experiments the furnace was switched on, and test temperature was attained after about 120 minutes with nitrogen flow

at a rate of 6.7 cm^3s^{-1} (STP), keeping the furnace opening closed by a rubber stop cock. The flow rate was increased still further during introduction of the sample inside the furnace. Once the system was made gas tight using screw-cap arrangement, the flow rate was reduced to 1.67 cm^3s^{-1} (STP) before balance controller output was on. After exposing the sample for required length of time, the furnace was switched off and the sample removed from the furnace with high flow rate of gas. The furnace was then cooled under flowing gas.

The purpose of heating and cooling under flowing gas was to prevent ignition of the getter metal at high temperature due to oxygen ingress into the system. The condition of the getter column was checked intermittently. Fresh zirconium drillings was used when the yellow coloration due to formation of zirconium nitride changed to blue-black by oxidation. Initial and final (before discarding) weights of getter elements were taken to get an idea about the amount of oxygen/nitrogen consumed by the getter metal.

A few blank runs were also carried out at 1200K in argon, following the same procedure as discussed above.

3.4 TECHNIQUES OF SCALE CHARACTERIZATION

Once the oxide scale is formed on the materials on exposure to reactive environment, it is necessary to know the composition, nature etc. of scale to understand the scale formation kinetics. Therefore, characterization of scale constituted an important component of the present study. The various techniques adopted are discussed in the following sections.

3.4.1 Visual Observation of Scales

In the present study, the alloys were exposed to various gases at high temperatures. The resulting scales were observed by unaided eye or by low magnification microscope after the sample was taken out of furnace. This type of examination is important, because subsequent microscopic examination could be carried out only at specific locations on a section. Only visual observation provides information about variation over a macroscopic scale on the specimen surface.

Observations regarding scale colour, scale adherence (or spalling characteristics) and uniformity were recorded. Some topological observations of scales on the wide faces of samples were also recorded for scale porosity, nodule formation etc., using a low magnification (50X) portable microscope, attached with external illuminating system (Vaiseshika Electron Devices, Ambala Cantt., Type 7002).

3.4.2 X-Ray Diffraction Studies of Scales

Most of the oxidized/nitrided samples were selected for X-ray diffraction (XRD) studies to identify the scales formed. An ISO Debyeflex 2002 diffractometer with monochromator (Rich-Seifert and Co., Germany) was employed. Samples were employed as such, because in most of the cases the scale thickness was low. Hence preparation of powder from very thin scale for XRD was difficult. XRD studies of some control specimens (i.e. polished and unoxidized) of each alloys were also carried out. Most of the specimens were scanned at low speed with low count rate, but it was varied sometimes. The settings of the X-ray diffractometer were as

follows :

(i)	Radiation	:	CuK_{α}
(ii)	Scan speed (2θ)	:	1.2 and 3 degrees min^{-1}
(iii)	Chart speed	:	12 and 30 mm min^{-1}
(iv)	Counts per minute	:	5K and 10K
(v)	Time constant	:	10 sec
(vi)	Current	:	20 mA
(vii)	Voltage	:	30 kV

3.4.3 Physical and Chemical Examinations of Scales under Scanning Electron Microscope

A scanning electron microscope (SEM) (JEOL JSM 840A) was employed for microscopic examination of nature and composition of scale. This consisted of the following :

1. Topological observation of scales

The SEM was used for topological observation of the wide faces of specimens after exposure, which had been subjected to XRD studies. Various aspects of topology like morphology, porosity etc. of external scale were recorded. The morphologies of scales after spalling (whenever this occurred) were also observed. The scales were mostly poor electrical conductors and therefore, in order to prevent building of space charge during SEM observation, a very thin silver coating was provided on the outer surface by sputtering in order to make it conducting. Morphological observations were made at various locations and photographs were taken at various magnifications.

2. Cross sectional metallography of scales

Topological observation is inadequate as well as

inconclusive in such cases where multilayer scale forms. In the present study, the alloys exhibited multilayer scale formation, observed by several earlier investigators as well. Therefore, observation of scale cross section was important as it could reveal the different products formed as layers. If the scales are strongly adherent to the substrate, then the thicknesses of the scales can also be estimated from cross sectional observation.

Cross sectional observation involved slicing the oxidized sample in transverse direction, mounting and polishing of a section. The scale is likely to detach from the specimen due to polishing stresses. Hence, in order to prevent spalling, the oxidized specimen must be mounted. So, the samples selected for cross sectional observation were cold mounted using epoxy. Before mounting, most of the samples were cut into two pieces along the transverse direction.

In this mounting technique, the die was greased with glycerine (for easy removal of mounted sample), the specimen was properly positioned, and the cold setting powder was poured into the die. The setting liquid was added dropwise for consolidation of the powder. It was kept for few hours, and then the mount was removed from the die.

The cross sections of the samples were prepared by conventional grinding and polishing technique with great care. Samples were ground through 220, 400 and 600 grit SiC paper applying only mild pressure in order to prevent scale detachment or spallation, and to cause less damage to the scale in view of their friable nature. The final polishing was performed with a suspension

Electroless nickel plating provides a continuous build up of metal coating on a substrate by simple immersion in a suitable aqueous solution. Details are available in literature[87-90].

3.4.4 Optical Metallography of Scale Cross Sections

Morphological observations of scale of a few samples were carried out under a Leitz Metallux 3 (Leitz Wetzlar, Germany) optical microscope. Metallographic samples were prepared following the method discussed earlier. Micrographs of the scales were recorded. However, due to the poor resolution of scale/alloy and scale/epoxy interfaces, this type of examination yielded mostly no useful result.

3.4.5 Microhardness Testing

The purpose of microhardness testing was to measure the hardness from the scale/alloy interface to the interior of the alloy in order to observe the variation in hardness values as a function of distance. A 160 Microhardness Tester attached to a Carl Zeiss Jena vertical incident light microscope (GDR) was employed for this purpose. Microhardness values along the cross sections of polished samples were taken by a square diamond pyramid indentor using an optimised load of 20g. A number of trials using different loads such as 60g, 40g and 10g were conducted before arriving at an optimised load. Photographs of indented surfaces were also taken.

CHAPTER 4

RESULTS AND DATA PROCESSING

4.1 CHARACTERIZATION OF AS-RECEIVED ALLOYS

Titanium aluminide alloys obtained from various sources were characterized by optical metallography and Energy Dispersive X-ray (EDX) analysis attached to a JEOL JSM 840A Scanning Electron Microscope (SEM). The procedure has already been discussed in sec.3.1.3. The alloys i.e. Ti-25Al, Ti-24Al-15Nb and Ti-25Al-11Nb, are designated as alloys A,B, and C respectively. The compositions are expressed in atom pct. Equivalent weight pct. are also noted in Table 3.1.

The X-ray diffraction (XRD) pattern for Ti-25Al (alloy A) revealed the presence of Ti_3Al only. Fig.4.1 presents optical micrographs of as-received alloys. Fig.4.1a shows a typical cast microstructure of alloy A. Fig.4.1b reveals two phase $\alpha_2+\beta$ structure of Ti-24Al-15Nb (alloy B) with prior β grain boundaries. Fig. 4.1c shows slightly elongated grains of α_2 (light) and intergranular β (dark) in rolled sheet of Ti-25Al-11Nb (alloy C). XRD patterns for alloys B and C revealed presence of Ti_3Al. However, a few peaks could not be identified for both the alloys.

Alloys A and B were procured in as cast condition and employed as such. These were melted four times to eliminate inhomogeneity. Even then it was decided to check their chemical homogeneity. Fig. 4.2 presents elemental EDX line scans of Ti, Al and Nb for Ti-24Al-15Nb. The figure indicates attainment of chemical

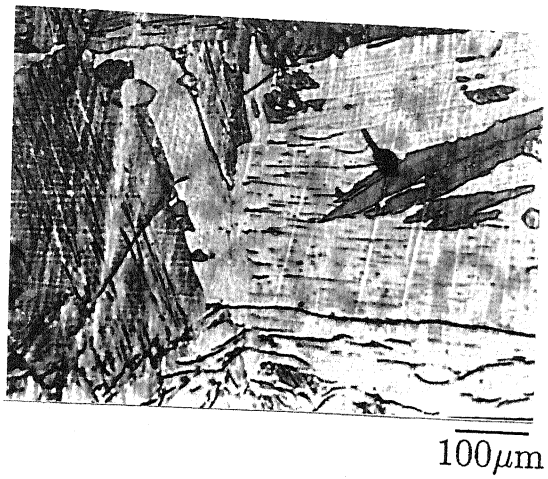

(a)

100μm

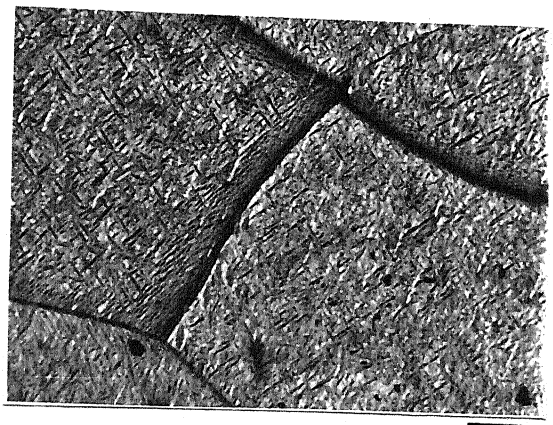

(b)

200μm

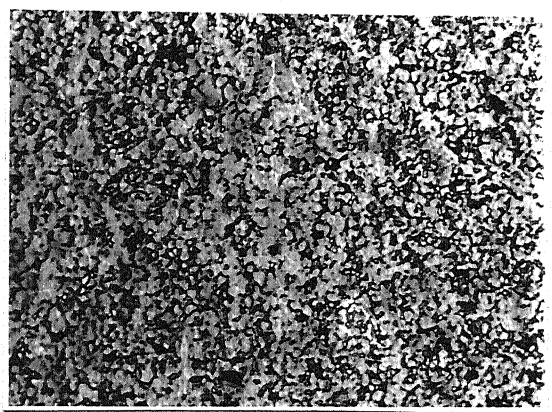

(c)

50μm

Fig.4.1: Optical microstructures of as received alloys (a) Ti-25Al, (b) Ti-24Al-15Nb, (c) Ti-25Al-11Nb

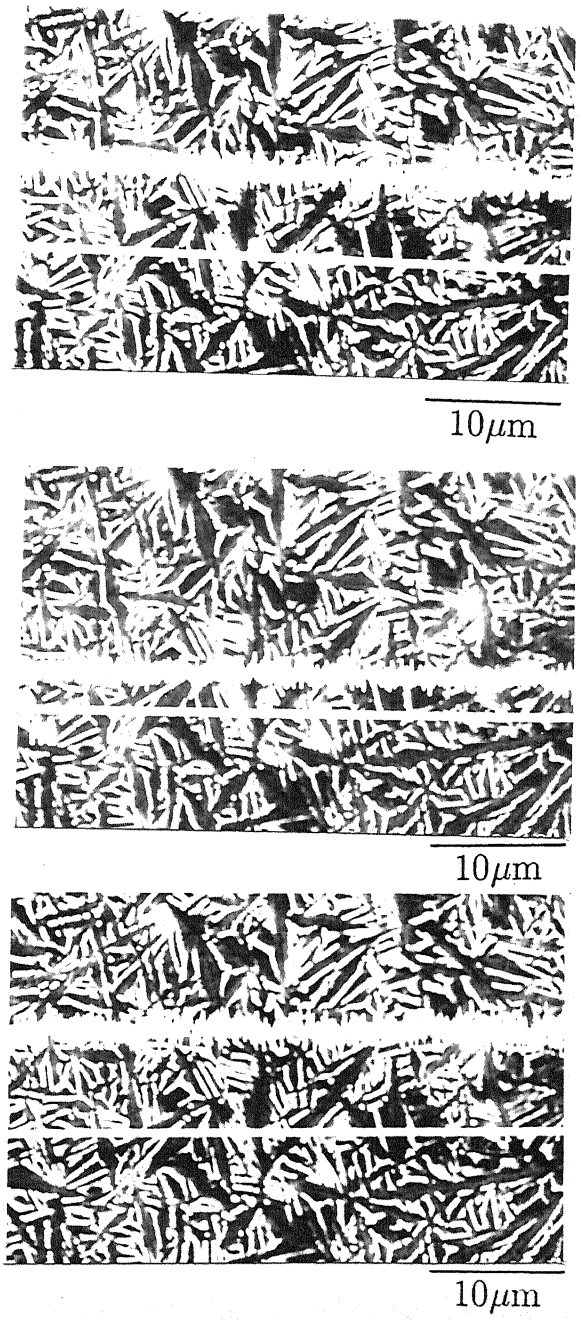

Fig.4.2: EDX elemental line scans of as received Ti-24Al-15Nb alloy for (a) titanium, (b) aluminium, (c) niobium

homogeneity in the alloy. Similar observation was made for alloy A also. Alloy C had been rolled and heat treated by the manufacturer and hence was taken as homogeneous.

4.2 THERMOGRAVIMETRY

In the present study, isothermal weight gain of samples upon exposure to various gas compositions were measured as function of time using a Cahn 1000 electrobalance and a strip chart recorder. Experimental procedure has been presented in sec.3.3. Various gases and gas mixtures employed were oxygen, nitrogen, oxygen-nitrogen, oxygen-argon, nitrogen-argon, and nitrogen-carbon dioxide, at a total pressure of 1 atmosphere. As mentioned in sec.3.2.3, all gases were dried by passing through anhydrous $CaCl_2$ and Drierite, and except for CO_2, freed from CO_2 by Ascarite. Nitrogen and argon gases were further passed through BTS catalyst furnace to remove oxygen inpurity. The experiments were carried out over the temperature range of 1000 to 1300K. Time of exposure in reactive environments ranged between 4 to 6 hr mostly. However in some cases 10 hr and 24 hr exposure times were also employed. Duplicate experiments were carried out for oxidation in oxygen to check reproducibility.

Tables (4.1) through (4.4) include the experimental conditions for oxidation and nitridation studies. Tables 4.1(a) to 4.1(c) are for the alloys A, B and C respectively exposed in oxygen, whereas Tables (4.2) through (4.4) are for other gases and gas mixtures as well as for sequential oxidation. Experimental data for weight gain per unit surface area of the specimen ($\frac{\Delta W}{A}$) at various exposure time (t) are presented in Appendix A. The spalled amount was added to

Table 4.1(a) Experimental Conditions and Salient Features of Oxidation of Ti-25Al Alloy in Oxygen

Experiment Number*	Temp. (K)	Rate const, k_p ($kg^2m^{-4}s^{-1}$)	Total exposure time (10^3 s)	Scale Characteristics					X-ray diffraction	
				Estimated thickness (μm)	Spalling	Colour	Porousness/ uniformity	Other features	Major phase	Minor phase
A1	1000	1.36×10^{-10}	85.5	2.1	no	mostly bluish white	very tiny pores, uniform	-	matrix	TiO_2, Al_2O_3
A2	1100	2.66×10^{-9}	18.0	4.3	no	bluish white	dense, uniform	-	TiO_2, matrix	Al_2O_3
A2r	1100	2.78×10^{-9}	15.42	4.0	no	do	do	-	-	-
A3	1150	1.34×10^{-8}	37.5	13.7	considerable	grey, bluish black (spalled area)	tiny pores, uniform	some cracks in the scale	-	-
A3r	1150	1.22×10^{-8}	32.76	12.3	do	do	do	-	-	-
A4	1200	4.20×10^{-8}	20.16	18.2	considerable	light yellow, bluish black (spalled area)	larger pores, non-uniform	-	-	-
A4r	1200	5.49×10^{-8}	20.4	20.6	do	do	do	-	TiO_2, matrix	Al_2O_3
A5	1250	9.58×10^{-8}	10.38	19.3	considerable	yellowish white, bluish black (spalled area)	larger pores	-	-	-
A5r	1250	1.18×10^{-7}	13.8	25.3	do	do	do	-	-	-
A6	1300	4.50×10^{-7}	16.8	54.3	minor but outer scale loose	yellow, bluish black (spalled area)	larger pores, slightly non-uniform	-	-	-
A6r	1300	4.37×10^{-7}	9.0	37.8	do	do	do	-	TiO_2	Al_2O_3, matrix

* A indicates alloy A (Ti-25Al) and, r indicates reproducibility test

Table 4.1(b) Experimental Conditions and Salient Features of Oxidation of Ti-24Al-15Nb Alloy in Oxygen

Experiment Number*	Temp. (K)	Rate const, k_p ($kg^2m^{-4}s^{-1}$)	Total exposure time (10^3 s)	Scale Characteristics					X-ray diffraction	
				Estimated thickness (μm)	Spalling	Colour	Porousness/ uniformity	Other features	Major phase	Minor phase
B1	1000	1.26×10^{-10}	86.1	2.0	no	dark grey	tiny pores, non-uniform	-	matrix	TiO_2, Al_2O_3
B2	1100	5.77×10^{-10}	21.6	2.2	no	dark blue	dense, uniform	some cracks in the scale	matrix	TiO_2, Al_2O_3
B2r	1100	4.82×10^{-10}	10.8	1.4	no	do	do	do	-	-
B3	1150	1.96×10^{-9}	27.3	4.6	no	blue	tiny pores, non-uniform white patch	-	-	-
B3r	1150	1.48×10^{-9}	13.5	2.8	no	do	porous	-	-	-
B4	1200	1.34×10^{-8}	21.3	10.4	no	blue	tiny pores, uniform white spots	-	TiO_2	Al_2O_3, matrix
B4r	1200	1.40×10^{-8}	21.3	10.3	no	do	do	-	-	-
B5	1250	5.40×10^{-8}	19.6	19.3	minor but poorly adhered	bluish white deep black (spalled area)	tiny pores, non-uniform	-	-	-
B5r	1250	3.98×10^{-8}	24.6	18.9	do	do	do	-	-	-
B6	1300	9.30×10^{-8}	17.4	24.7	minor	bluish white deep black (spalled area)	tiny pores, slightly non-uniform	some cracks	TiO_2, matrix	Al_2O_3
B6r	1300	1.02×10^{-7}	14.4	23.3	do	do	do	do	-	-

* B indicates alloy B (Ti-24Al-15Nb) and, r indicates reproducibility test

Table 4.1(c) Experimental Conditions and Salient Features of Oxidation of Ti-25Al-11Nb Alloy in Oxygen

Experiment Number*	Temp. (K)	Rate const, k_p ($kg^2 m^{-4} s^{-1}$)	Total exposure time (10^3 s)	Scale Characteristics					X-ray diffraction	
				Estimated thickness (μm)	Spalling	Colour	Porousness/ uniformity	Other features	Major phase	Minor phase
C1	1000	1.37×10^{-10}	86.4	2.1	no	greyish blue	tiny pores, non-uniform	some white spots	matrix	TiO_2, Al_2O_3
C2	1100	6.16×10^{-10}	14.4	1.8	no	deep blue	dense, non-uniform	-	matrix	TiO_2, Al_2O_3
C2r	1100	3.58×10^{-10}	14.4	1.4	no	do	do	-	-	-
C3	1150	1.55×10^{-9}	16.2	3.1	no	blue	dense, uniform	-	-	-
C3r	1150	1.45×10^{-9}	15.6	2.9	no	do	do	-	-	-
C4	1200	7.64×10^{-9}	15.6	6.6	no	greyish blue	dense, non-uniform	some cracks	-	-
C4r	1200	8.34×10^{-9}	15.6	6.9	no	do	do	do	-	-
C5	1250	3.95×10^{-8}	16.14	15.3	no	grey	tiny pores, uniform	-	-	-
C5r	1250	3.25×10^{-8}	15.6	13.8	no	do	do	some cracks	-	-
C6	1300	8.98×10^{-8}	15.6	23.3	minor	greyish blue, deep black (spalled area)	larger pores, non-uniform	-	TiO_2,	Al_2O_3, matrix
C6r	1300	1.06×10^{-7}	13.8	23.7	-	-	-	-	-	-

* C indicates alloy C (Ti-25Al-11Nb) and, r indicates reproducibility test

Table 4.2 Experimental Conditions and Salient Features of Oxidation in Nitrogen and Nitrogen Containing Gas Mixtures

Experiment Number[+]	Temp. (K)	Rate const, k_p ($kg^2m^{-4}s^{-1}$)	Total exposure time (10^3 s)	Scale Characteristics					X-ray diffraction	
				Estimated thickness (μm)	Spalling	Colour	Porousness/ uniformity	Other features	Major phase	Minor phase
A7 (N_2)	1300	1.78×10^{-8}	36.0	15.6	no	bluish white	pores, uniform	-	TiO_2	Al_2O_3, TiN
A8[*] (N_2)	1200	7.11×10^{-10}	18.0	2.1	no	light grey	larger pores, non-uniform	some black patches	TiN, matrix	TiO_2
A9[*] (N_2)	1300	3.64×10^{-9}	17.4	4.9	no	bluish grey	larger pores, uniform	-	TiO_2, TiN, matrix	Al_2O_3
A10 (20 vol% O_2 +80 vol% N_2)	1150	8.76×10^{-9}	15.0	6.9	considerable	bluish white, dark grey (spalled area)	tiny pores	-	TiO_2, matrix	TiN
A11 (20 vol% O_2 +80 vol% N_2)	1200	5.09×10^{-8}	15.6	16.8	considerable	yellowish white, greyish blue (spalled area)	tiny pores	-	-	-
A12 (20 vol% O_2 +80 vol% N_2)	1300	6.05×10^{-7}	18.0	67.4	considerable	yellow, bluish white, (spalled area)	porous	-	TiO_2	Al_2O_3, matrix
A13 (95 vol% N_2 +5 vol% CO_2)	1300	2.35×10^{-6}	18.0	126.2	considerable	yellow, creamy (spalled area)	clustered pores, large pores in spalled area	some globular spots, spalling exposed metal at edges	TiO_2	Al_2O_3
B7 (N_2)	1300	5.09×10^{-9}	36.0	8.3	no	bluish white	tiny pores, uniform	some cracks	TiO_2, matrix	Al_2O_3, TiN

Contd. Table 4.2

Experiment Number[+]	Temp. (K)	Rate const, k_p ($kg^2 m^{-4} s^{-1}$)	Total exposure time (10^3 s)	Scale Characteristics					X-ray diffraction	
				Estimated thickness (μm)	Spalling	Colour	Porousness/ uniformity	Other features	Major phase	Minor phase
B8* (N_2)	1200	2.14×10^{-11}	43.2	0.6	no	largely bluish white	tiny pores	-	matrix, TiN	TiO_2
B9* (N_2)	1300	1.94×10^{-9}	18.0	3.6	no	bluish grey	larger pores, uniform	-	TiO_2, TiN	matrix
B10 (20 vol% O_2 +80 vol% N_2)	1100	6.16×10^{-11}	86.7	1.4	no	blue	porous, non-uniform	some bright spots	matrix	TiO_2, TiN, Al_2O_3
B11 (20 vol% O_2 +80 vol% N_2)	1150	1.69×10^{-10}	19.2	1.1	no	mostly blue	non-uniform	some bright spots	matrix	TiO_2, TiN, Al_2O_3
B12 (20 vol% O_2 +80 vol% N_2)	1200	8.09×10^{-10}	17.4	2.3	no	blue	tiny pores, non-uniform	some bright spots	TiO_2, matrix	TiN, Al_2O_3
B13 (20 vol% O_2 +80 vol% N_2)	1250	2.48×10^{-9}	21.6	4.5	no	greyish blue	porous, non-uniform	grey patches	TiO_2, matrix	TiN, Al_2O_3
B14 (20 vol% O_2 +80 vol% N_2)	1300	4.82×10^{-9}	14.4	5.4	no	greyish blue	tiny pores, slightly non-uniform	-	TiO_2, matrix	Al_2O_3, TiN
B15 (50 vol% O_2 +50 vol% N_2)	1200	8.08×10^{-10}	15.6	2.1	no	deep blue	non-uniform	-	TiO_2, matrix	Al_2O_3, TiN
B16 (80 vol% O_2 +20 vol% N_2)	1200	2.90×10^{-9}	14.4	3.9	no	greyish blue	tiny pores, non-uniform	-	TiO_2	Al_2O_3, TiN, matrix

Contd. Table 4.2

Experiment Number+	Temp. (K)	Rate const, k_p ($kg^2 m^{-4} s^{-1}$)	Total exposure time (10^3 s)	Scale Characteristics					X-ray diffraction	
				Estimated thickness (μm)	Spalling	Colour	Porousness/ uniformity	Other features	Major phase	Minor phase
B17 (95 vol% N_2 +5 vol% CO_2)	1300	3.97×10^{-9}	21.6	5.6	no	grey	tiny pores, slightly non-uniform	some globular white spots	TiO_2, matrix	Al_2O_3, TiN
B18 (20 vol% N_2 +80 vol% Ar)	1300	3.97×10^{-9}	21.6	5.7	no	dark grey	tiny pores, uniform	some white spot	-	-
C7 (N_2)	1300	5.91×10^{-9}	35.7	9.0	no	greyish blue	tiny pores	-	TiO_2,	Al_2O_3, TiN, matrix
C8 (20 vol% O_2 +80 vol% N_2)	1300	1.10×10^{-8}	21.6	9.3	minor	greyish blue, brown (spalled area)	tiny pores	-	TiO_2,	Al_2O_3, TiN, matrix

+ A, B, C indicate alloy A (Ti-25Al), alloy B (Ti-24Al-15Nb) and alloy C (Ti-25Al-11Nb) respectively

* experiment using getter element

Table 4.3 Experimental Conditions and Salient Features of Oxidation in Oxygen and Argon Gas Mixtures

Experiment Number[+]	Temp. (K)	Rate const, k_p ($kg^2m^{-4}s^{-1}$)	Total exposure time (10^3 s)	Scale Characteristics					X-ray diffraction	
				Estimated thickness (μm)	Spalling	Colour	Porousness/ uniformity	Other features	Major phase	Minor phase
A14 (20 vol% O_2 +80 vol% Ar)	1200	5.29×10^{-8}	15.6	17.2	considerable	yellowish white, black (spalled area)	tiny pores	-	-	-
A15* (Ar)	1200	7.70×10^{-9}	18.0	7.5	no	light grey	tiny pores	some black patches	-	-
B19 (80 vol% O_2 +20 vol% Ar)	1200	1.06×10^{-8}	15.6	7.8	no	greyish blue	tiny pores	some cracks, many white spots	TiO_2	Al_2O_3, matrix
B20 (50 vol% O_2 +50 vol% Ar)	1200	9.78×10^{-9}	15.6	7.0	no	greyish blue	tiny pores	some cracks, many white spots	TiO_2	Al_2O_3, matrix
B21 (20 vol% O_2 +80 vol% Ar)	1200	5.94×10^{-9}	11.88	4.9	no	greyish blue	non-uniform	some cracks, white spots	TiO_2	Al_2O_3, matrix
B22* (Ar)	1200	1.22×10^{-9}	16.2	2.7	no	mostly bluish grey	tiny pores, non-uniform	some bright spots	-	-

+ A, B indicate alloy A (Ti-25Al) and alloy B (Ti-24Al-15Nb) respectively

* experiment using getter element

Table 4.4 Experimental Conditions and Salient Features of Sequential Oxidation in Changing Environments

Experiment Number+	Temp. (K)	Rate const, k_p ($kg^2m^{-4}s^{-1}$)*	Total** exposure time (10^3 s)	Scale Characteristics					X-ray diffraction	
				Estimated thickness (μm)	Spalling	Colour	Porousness/ uniformity	Other features	Major phase	Minor phase
A16 (1 hr in N_2 then O_2)	1300	4.28×10^{-7}	21.45	55.2	minor	yellow, bluish white (spalled area)	porous, loosely adhered	some cracks	TiO_2	Al_2O_3
A17 (1 hr in N_2 then 20 vol% O_2+80 vol% N_2)	1300	6.13×10^{-7}	17.67	63.4	considerable	yellow, greyish blue (spalled area)	porous	-	TiO_2	Al_2O_3
A18 (1 hr in O_2 then 20 vol% O_2+80 vol% N_2)	1300	1.62×10^{-7}	17.67	61.3	considerable	yellow, greyish blue (spalled area)	porous	-	TiO_2	Al_2O_3
B23 (1 hr in N_2 then O_2)	1300	4.76×10^{-8}	35.39	26.6	minor	yellow, black (spalled area)	tiny pores, non-uniform	-	TiO_2	Al_2O_3, matrix
B24 (1 hr in N_2 then 20 vol% O_2+80 vol% N_2)	1300	2.54×10^{-9}	17.67	5.6	no	greyish blue	tiny pores, uniform	some globular white spots	TiO_2	Al_2O_3, TiN, matrix
B25 (1 hr in O_2 then 20 vol% O_2+80 vol% N_2)	1300	3.50×10^{-9}	18.0	14.7	no	greyish blue	tiny pores,	some white patches	TiO_2	Al_2O_3, TiN, matrix

+ A, B indicate alloy A (Ti-25Al) and alloy B (Ti-24Al-15Nb) respectively

* pretreatment data excluded

** including pretreatment time

subsequent weight gain values for further processing of data, wherever spalling occurred during the experiment. Fig.4.3 shows some typical $(\frac{\Delta W}{A})$ vs t plots of alloy A (Ti-25Al). Very little spalling occured during oxidation of alloy A at 1300K which could be detected from sudden loss of weight in the recorded data as indicated in Fig.4.3.

4.3 MEASUREMENT ERRORS

4.3.1 Errors in Temperature Measurement

A Pt/Pt-10% Rh thermocouple, placed inside the reaction chamber, allowed furnace temperature control within ±2K at the constant temperature zone. The measurement thermocouple was placed within 10-15 mm below the sample in the constant temperature zone. Axial temperature profiling in and around hot zone showed that the sample temperatures were likely to differ from control temperature by about ±2K. Furthermore, the thermocouples were calibrated against standard thermocouple, and the measuring instrument was also checked against precision potentiometer from time to time. Thus, considering all sources of error in temperature measurement, the overall temperature measurement error may be taken as ±3K.

4.3.2 Errors in Weight Gain Measurement

The Cahn 1000 electrobalance was sensitive to changes in weight as small as 4 μg. Precautions were taken for damping vibration of the sample hanging assembly for attainment of such sensitivity in measurement. The initial and final weights of the sample were also taken separately in an analytical balance to cross check weight gain values against those obtained from the chart. The

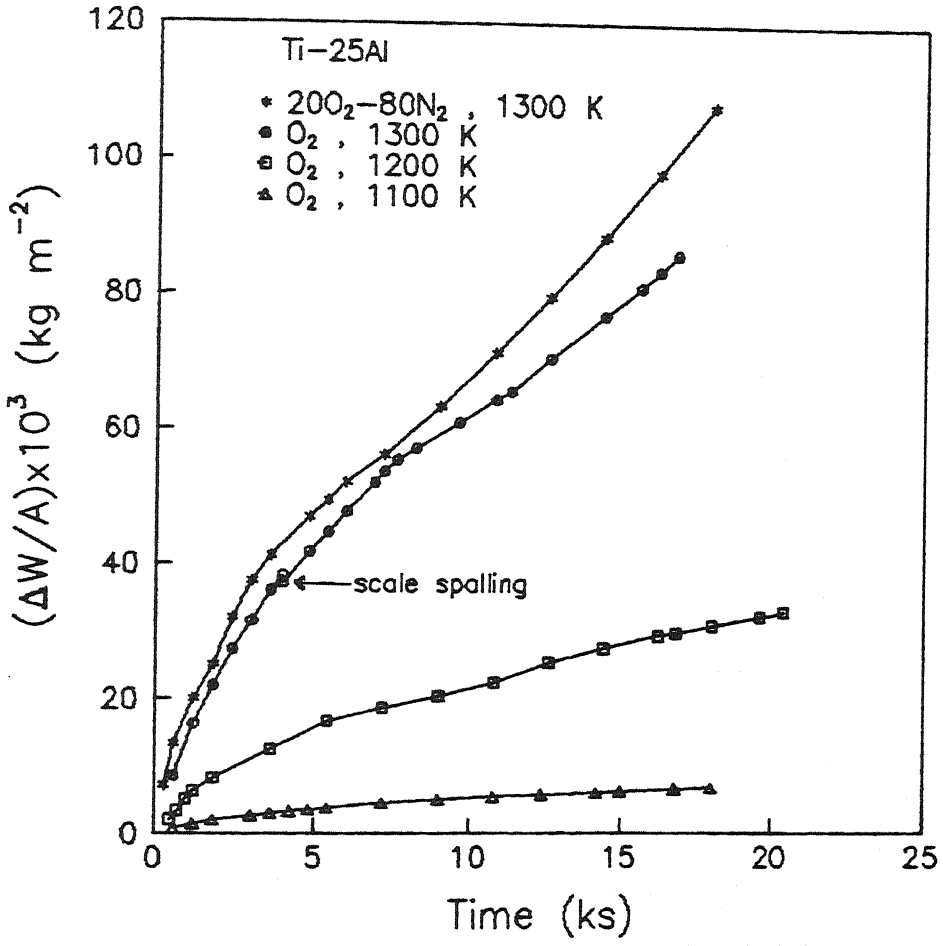

Fig.4.3: Some typical weight gain ($\frac{\Delta W}{A}$) versus time plots for oxidation of Ti-25Al alloy

actual weight gain values were 2 to 5 pct higher than those obtained from the chart. Higher the temperature of exposure, higher was the difference. This difference may partly be due to weight gain during introduction and withdrawal of the sample from the furnace. The hanging assembly (Fig.3.4) was made of Pt-wire and Pt-cylinder. Therefore any weight gain due to its oxidation under the present experimental conditions could be considered as negligible.

To check reproducibility of weight gain values, each oxidation experiment performed at temperatures from 1100-1300K in dry CO_2-free oxygen was repeated two times. Figs.(4.4) and (4.5) illustrate the nature of reproducibility of weight gain per unit surface area ($\frac{\Delta W}{A}$) vs time of exposure data for alloys A (Ti-25Al) and B (Ti-24Al-15Nb) respectively. It may be noted that weight gain data were fairly reproducible for both the alloys at lower temperature whereas at higher temperature the reproducibility was relatively less.

4.4 EVALUATION OF RATE CONSTANT

As stated in chapter 2 that there are few rate laws viz. parabolic, linear, paralinear etc. Literature review showed that most of the investigators employed parabolic rate law as the basis of interpretation of the weight gain vs time data (although oxidation of titanium aluminides did not exhibit a singular rate law as discussed in sec. 2.5.1). Hence parabolic rate law was first considered as the basis of data processing and interpretation of results in this investigation as well. However, as will be shown later that the parabolic law was obeyed by experimental data only

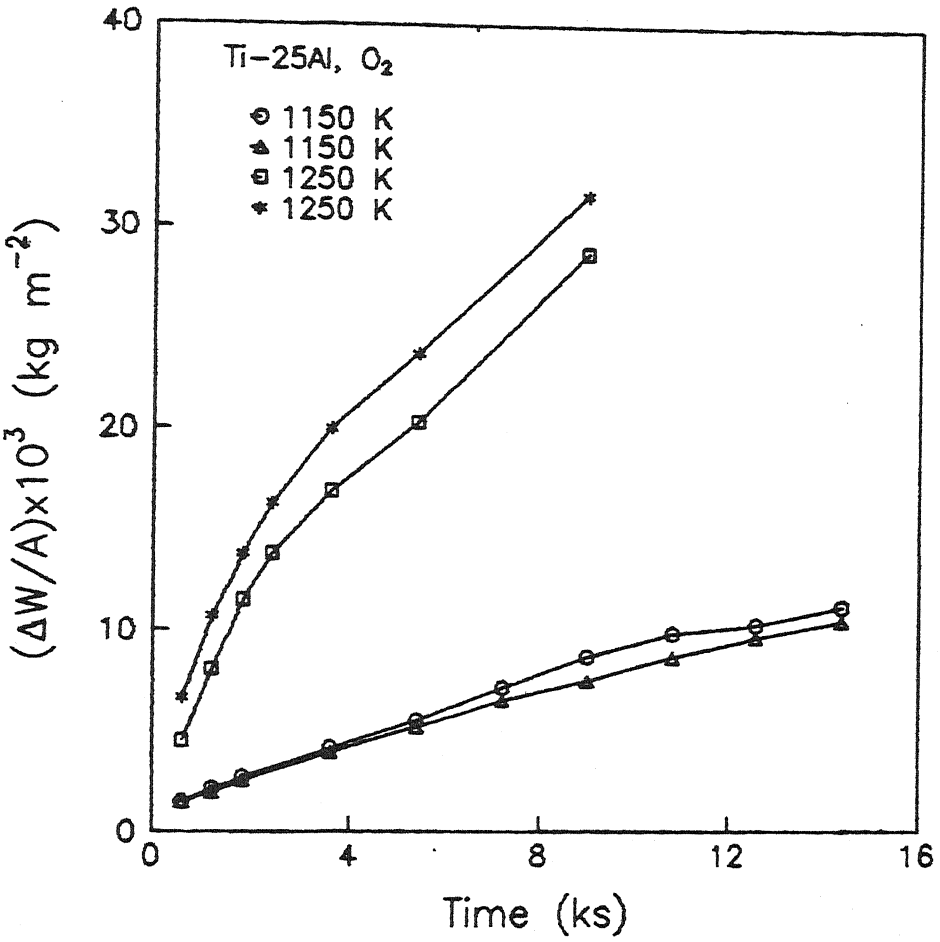

Fig.4.4: Reproducibility of $(\frac{\Delta W}{A})$ for oxidation of Ti-25Al alloy in oxygen

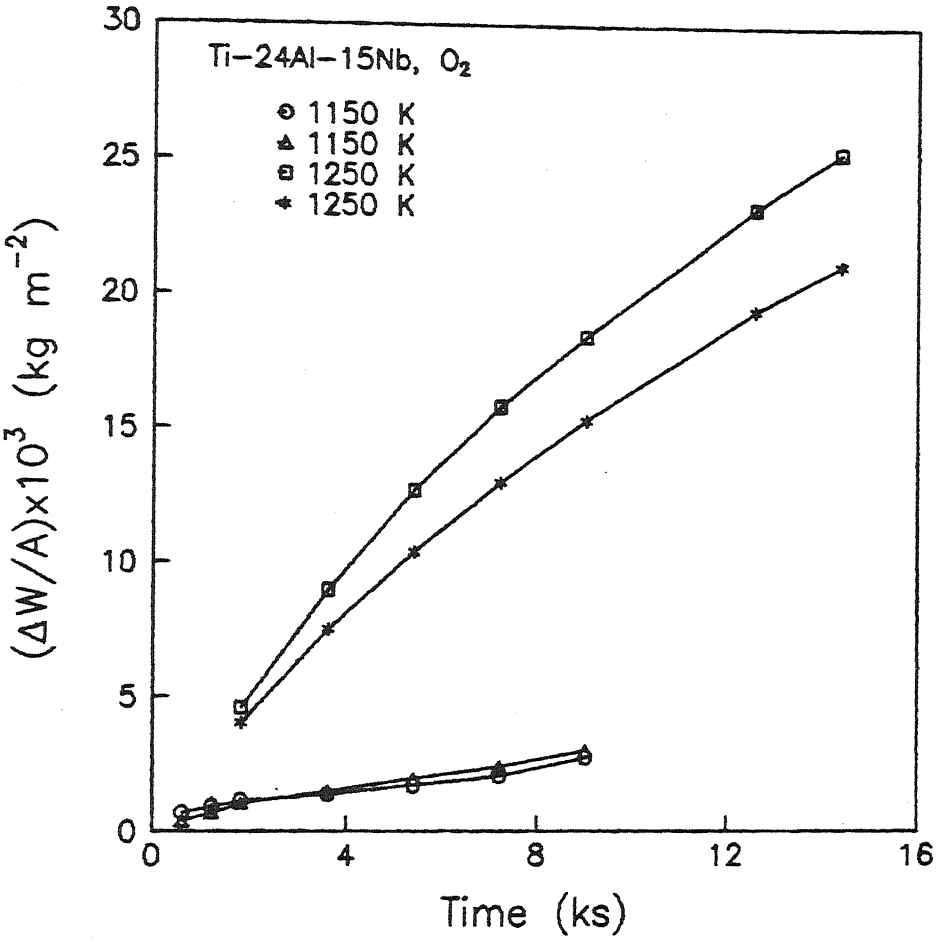

Fig.4.5: Reproducibility of $(\frac{\Delta W}{A})$ for oxidation of Ti-24Al-15Nb alloy in oxygen

approximately. Significant deviations were found. Hence, determination of rate constant was carried out by three methods. These methods as well as their comparisons and relative evaluations have been presented in this section.

4.4.1 Determination of Parabolic Rate Constant (k_p)

The parabolic rate constant (k_p) is related to weight gain per unit surface area of specimen ($\frac{\Delta W}{A}$) and exposure time (t) as :

$$(\frac{\Delta W}{A})^2 = k_p t \qquad \ldots(2.6)$$

The rate constant k_p was obtained from the slope of the linear regression fitted line of $(\frac{\Delta W}{A})^2$ vs t plot. The values are included in Tables (4.1) to (4.4) for various experiments. Figs.(4.6) and (4.7) show the nature of fit of parabolic rate law for some experiments. It is clear from the figures that in general, experimental data deviated from regression fitted lines with a definite pattern. It means that scatter was not random. It may also be concluded that obedience to parabolic rate law was only approximate.

4.4.2 Determination of Instantaneous Parabolic Rate Constants (k_i)

High temperature oxidation of alloys is a complex phenomenon. The reaction rate is governed by several external factors (viz. temperature, gas composition etc.), and also by the structure and composition of the reaction products (i.e. the scale). Therefore, it is quite likely that any single rate law such as parabolic may not be obeyed well. It may be illustrated from the

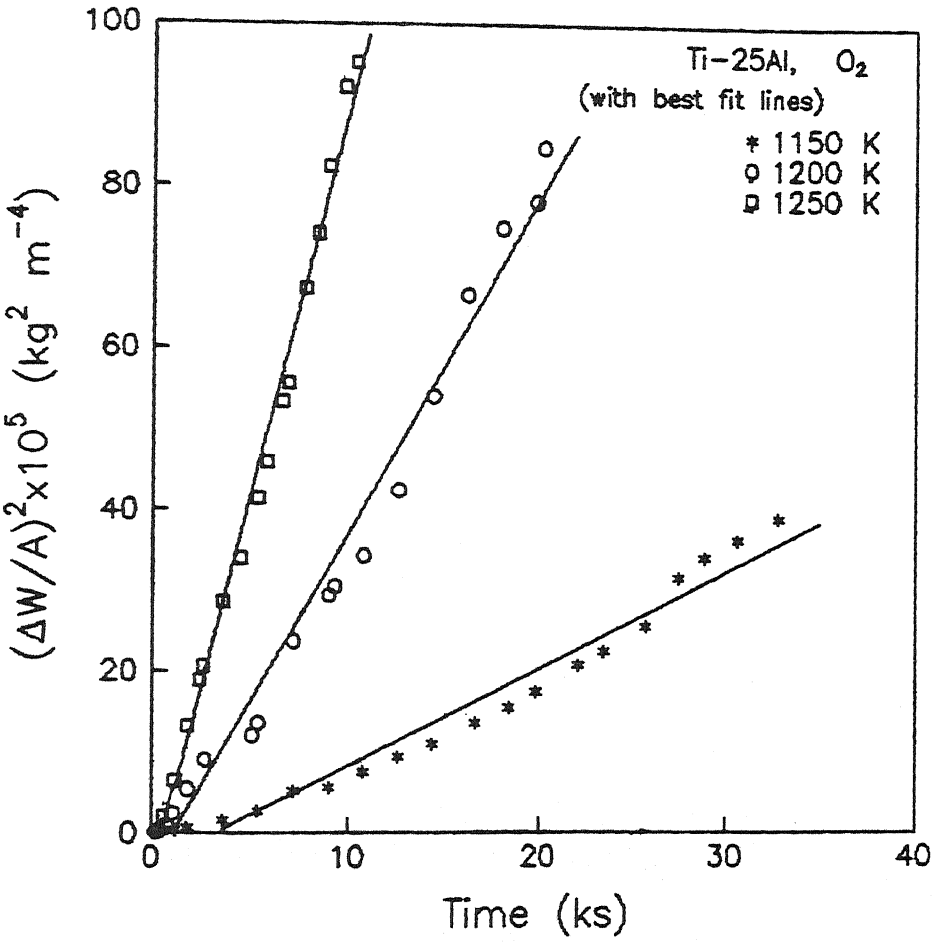

Fig.4.6: $(\frac{\Delta W}{A})^2$ versus time plots for oxidation of Ti-25Al alloy

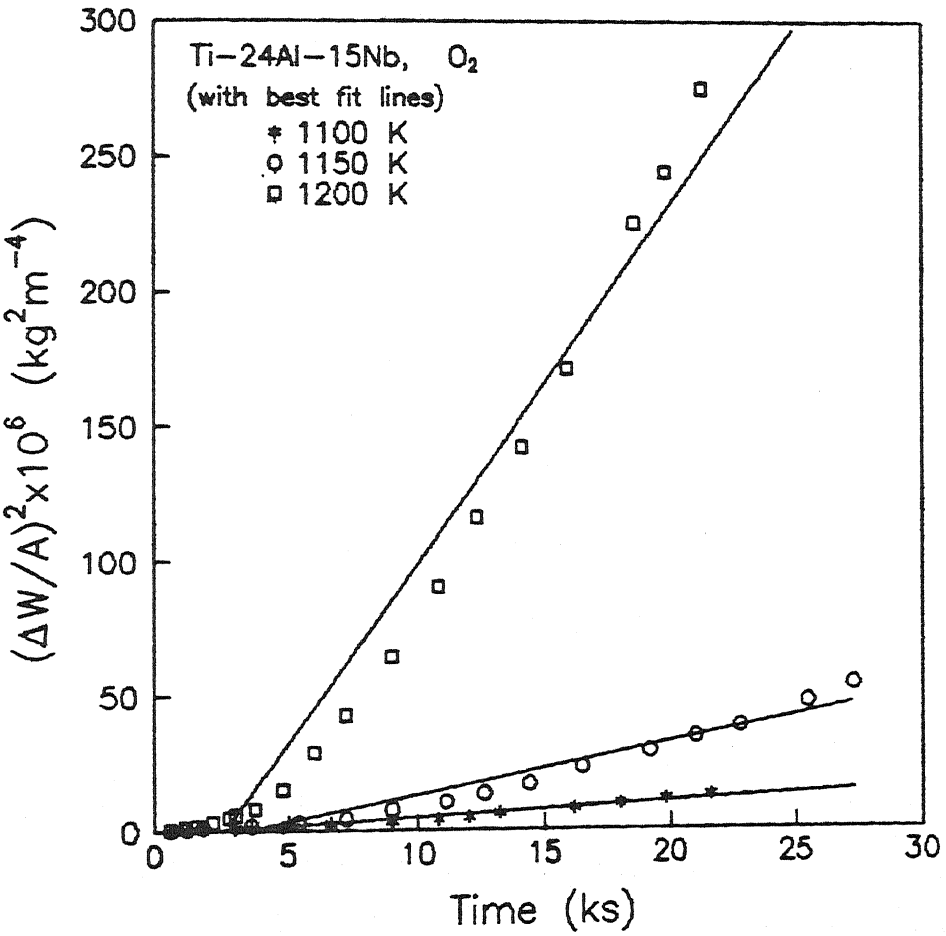

Fig.4.7: $(\frac{\Delta W}{A})^2$ versus time plots for oxidation of Ti-24Al-15Nb alloy

instantaneous parabolic rate constant values. For this purpose $(\frac{\Delta W}{A})^2$ vs t data were fitted by a fourth order polynomial curve expressed as :

$$(\frac{\Delta W}{A})^2 = a_1 + a_2 t + a_3 t^2 + a_4 t^3 + a_5 t^4 \qquad \ldots(4.1)$$

where a_1, a_2, a_3, a_4 and a_5 are constants. Eq.4.1 was then differentiated at any time instant to obtain the instantaneous rate constant (k_i) at that time instant, (i.e. $d[(\frac{\Delta W}{A})^2]/dt$). The program for calculation of instantaneous rate constant and other rate constants is presented in Appendix B.

In a recent study, Wallace et al[63] plotted k_i as function of time (sec. 2.5.1). If the nature and properties of the scales remain the same all throughout an experiment, and parabolic law is obeyed then k_i would be independent of time. The reason for its variation with time in some experiments may be attributed to variation of scale characteristics with time, provided there has been no spalling.

Figs.(4.8) and (4.9) present a few sample curves of k_i as function of time(t). Fig.4.8 shows that for some experiments k_i was approximately independent of time. However, Fig.4.9 shows that k_i vs t curves mostly deviated from parabolic behaviour. Moreover, the natures of deviation did not have any systematic pattern. These only confirm the complexity of the oxidation behaviour.

Variation of k_i with t may be due to first of all random errors in data which cause data points to scatter around a mean line. However, examination of the Fig.4.9 as well as for other experiments (not presented here) reveal that the variation of k_i with t is not due to random errors. Rather they exhibit some

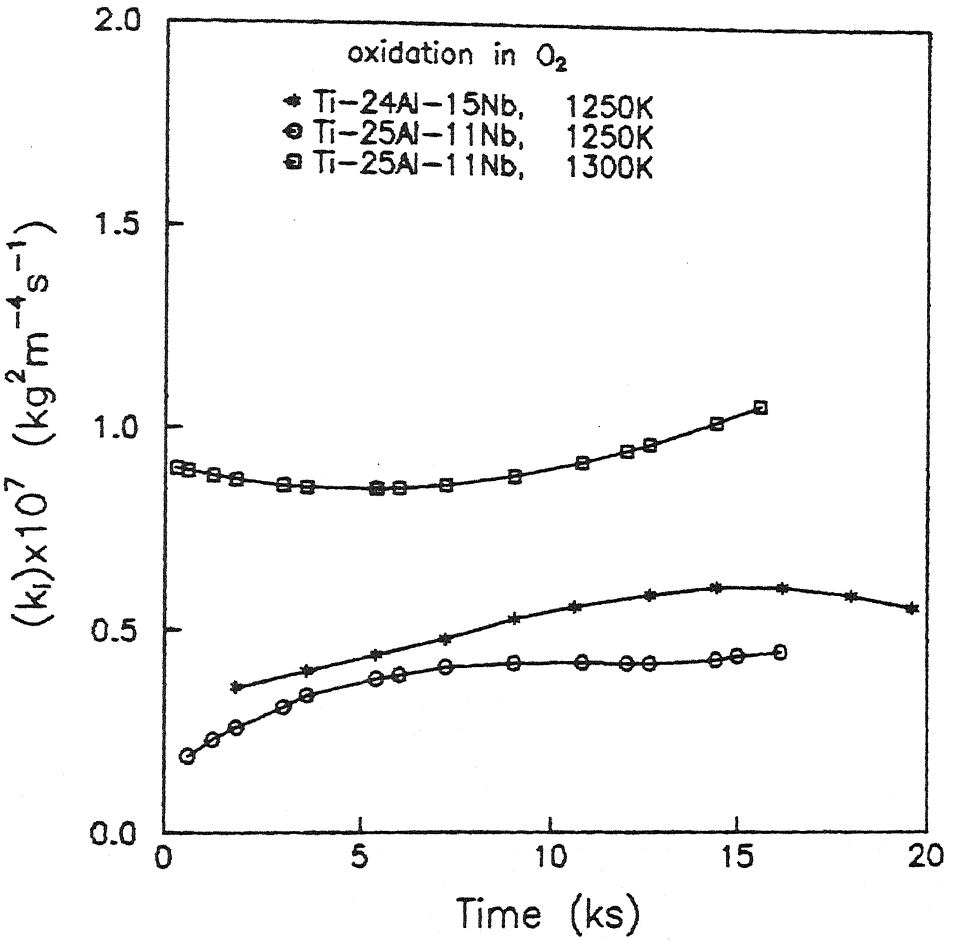

Fig.4.8: k_i versus time plots showing agreement with parabolic rate law

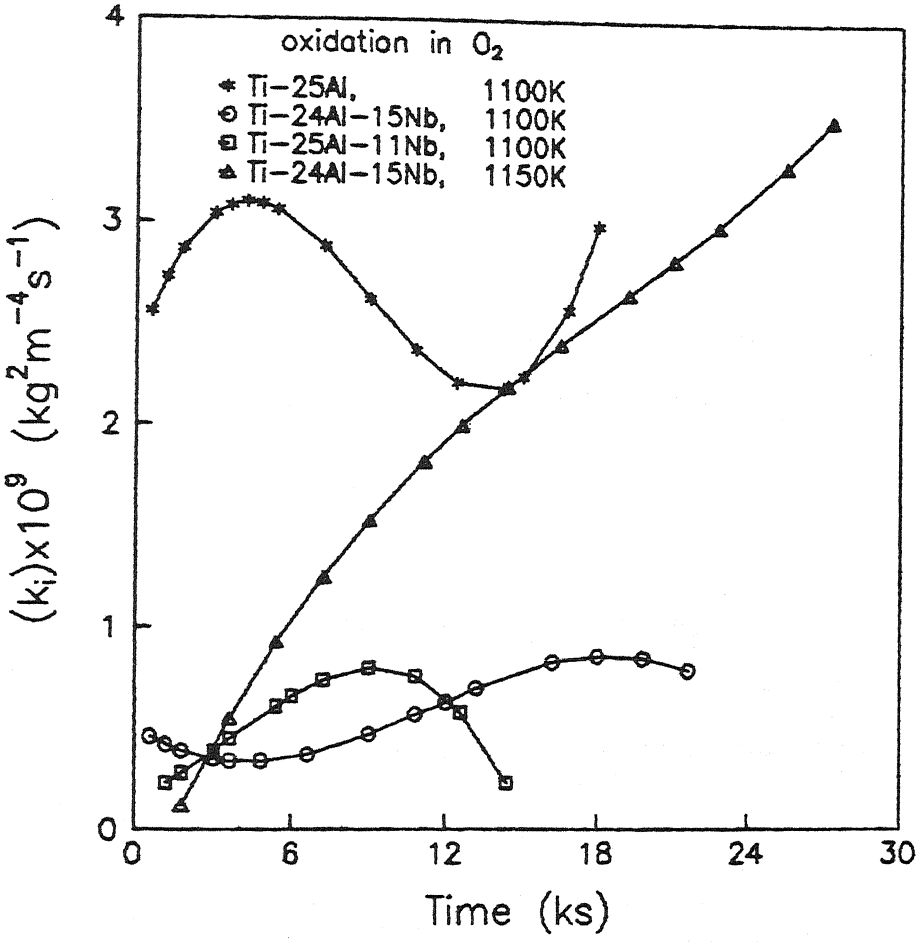

Fig.4.9: k_i versus time plots showing disagreement with parabolic rate law

trends and hence are attributed to some changes taking place in the samples during progress of the experiments.

The parabolic rate law is theoretically valid only under idealized condition as stated in the assumptions listed in sec. 2.3.4. If those assumptions remain valid throughout the duration of an experiment then only instantaneous rate constant (k_i) would be independent of t. The observed behaviour patterns show that for most experiments it is not the case. It is difficult to pinpoint the causes. However, in general it can be ascribed to variation in uniformity, and or nature and composition of scale with progress of oxidation. These may be due to changes in scale porousness, adherence, nature of defects, cracking etc. Attempts would be made later on to try to explain few very anomalous behaviour on the basis of structural examinations.

4.4.3 Comparison of Averaged k_i (k_p') With k_p

The overall parabolic rate constant for an experiment may be obtained by averaging the values of instantaneous rate constant (k_i) as per the following equation :

$$k_p' = \sum_{i=1}^{N} k_i \, t_i \; / \sum_{i=1}^{N} t_i \qquad \ldots(2.40)$$

where k_p' is really k_p as per Eq.2.6, but determined from k_i. N is the number of data points in an experiment and t_i is instantaneous time.

k_p and k_p' strictly speaking should be the same. However, some difference may arise due to the non-standard behaviour of $(\frac{\Delta W}{A})$ vs t .

curves. Table 4.5 presents values of k_p and k'_p for most of the experiments conducted in oxygen. Fig.4.10 compares log k_p with log k'_p . It may be noted that most of the data points lie on 1:1 line or very close to it. Hence, the agreement is considered to be very good. It may be further concluded that it does not matter by which method overall parabolic rate constant (k_p) is obtained.

4.4.4 Determination of Rate Constant by Power Law Fitting

In view of various patterns of deviations from the parabolic behaviour, it was decided to process the experimental data also assuming power law as follows :

$$\left(\frac{\Delta W}{A}\right)^m = k_m t \qquad \ldots(4.2)$$

or, $$\log \left(\frac{\Delta W}{A}\right) = \frac{1}{m} \log k_m + \frac{1}{m} \log t \qquad \ldots(4.3)$$

Schaeffer[65] also processed weight gain data vs time in a similar way. The above is a purely empirical data fitting. Rate constant (k_m) and m are to be evaluated from linear regression analysis of log $\left(\frac{\Delta W}{A}\right)$ vs log t data for each experiment. The inverse of slope will give the value of m and k_m can be obtained from the intercept of the best fit line.

Table 4.5 includes m and k_m for different experiments carried out in oxygen and those in other gases and gas mixtures are presented in Table 4.6. Parabolic rate law corresponds to a value of m=2 and linear rate law corresponds to a value of m=1. Tables (4.5) and (4.6) show that values of m lie between 1 to 1.86. Therefore, as a generalization the oxidation behaviour is

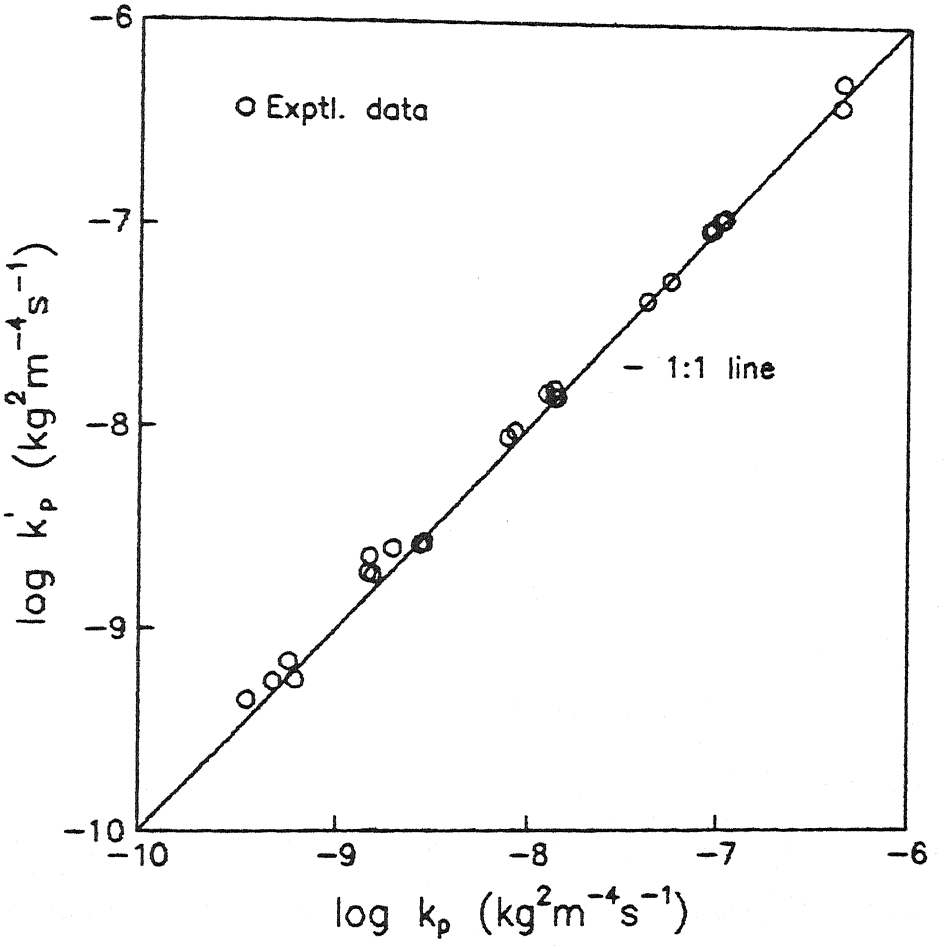

Fig.4.10: Comparison of k_p' and k_p for oxidation in oxygen

'paralinear'. Although parabolic rate law in general has been the basis of interpretation of earlier investigators, observed nature was reported to be following mixed kinetics by some investigators[49,61,72,81]. Schaeffer[65] found that the values of m ranged from 1.18 to 2.13 during oxidation of Ti_3Al-based alloys, and concluded that the oxidation kinetics was to be treated as a mixed one, except for values of m close to 2. However, it is to be noted that the departure from parabolic law need not be due to mixed kinetics alone. It may very well be caused by change of scale characteristics with time thus changing the diffusivities of ionic/molecular species across the scale with progress of reaction. In that case, even though oxidation rate may be controlled by diffusion through the oxide scale, the value of m may significantly differ from 2.

Tables (4.5) and (4.6) also present k_m/k_p values. k_m was always larger than k_p or k_p' i.e. k_m/k_p was always greater than 1, and ranged between 2.3 and 302. Figs.(4.11) and (4.12) present data plots of k_m/k_p as function of m for exposure in O_2 and in other gases respectively. The figures exhibit considerable scatter. However, the trend is evident, i.e. as m decreases k_m/k_p increases. In other word the discrepancy between k_m and k_p depends on the extent of departure of the value of m from 2. Fig.4.13 presents m as function of temperature for alloys A (Ti-25Al), B (Ti-24Al-15Nb) and C (Ti-25Al-11Nb) oxidized in oxygen.

The values of m exhibited lot of scatter and significant irreproducibility amongst duplicate sets. Also no trend could be observed with variation of temperature. Reproducibility of

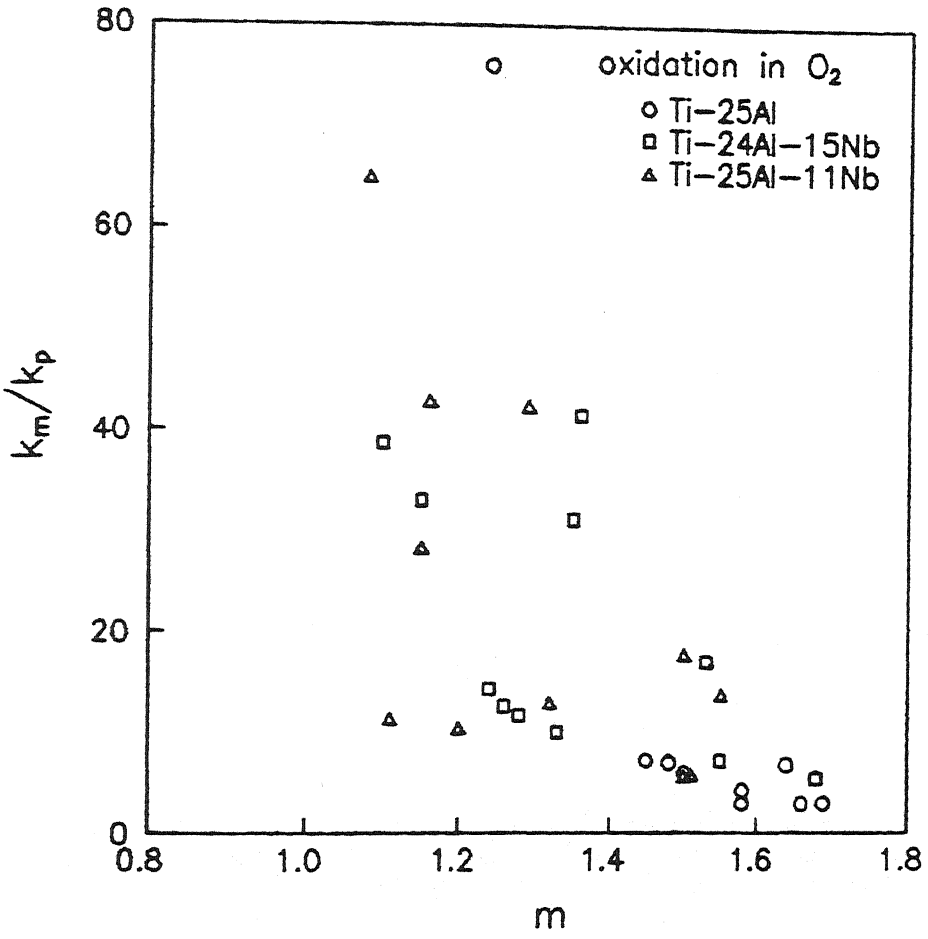

Fig.4.11: Variation of k_m/k_p with m for oxidation in oxygen

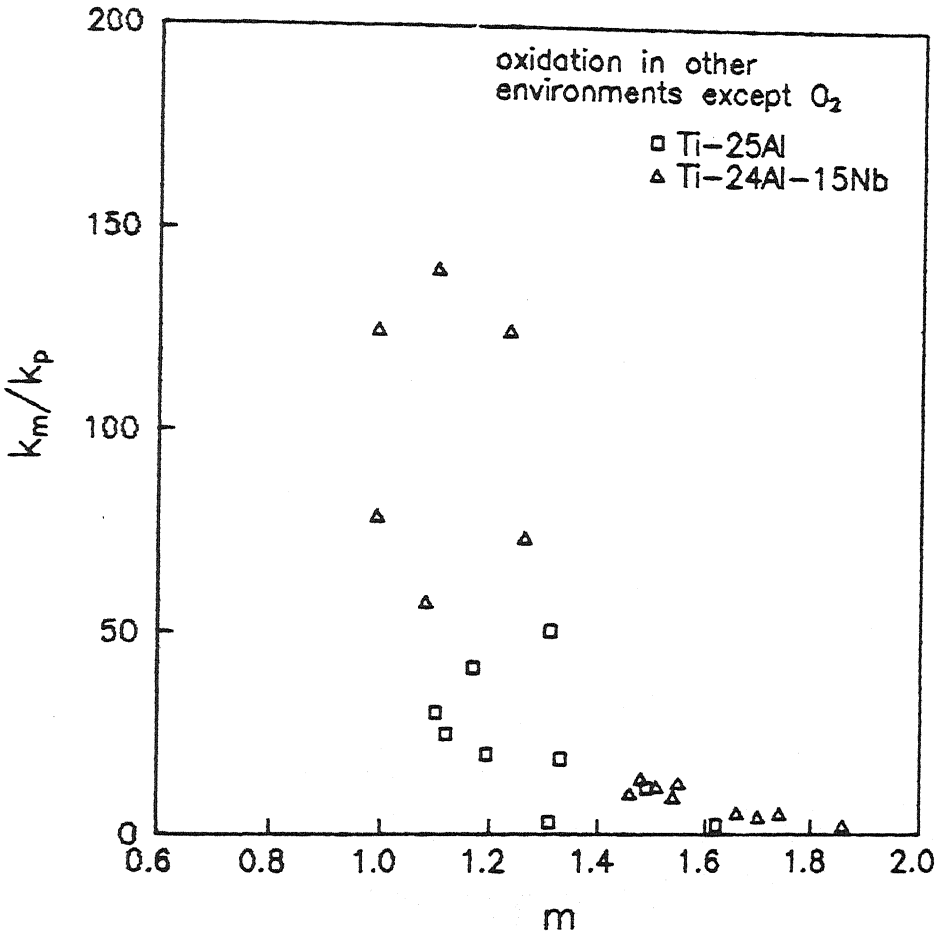

Fig.4.12: Variation of k_m/k_p with m for oxidation in gases and gas mixtures other than oxygen

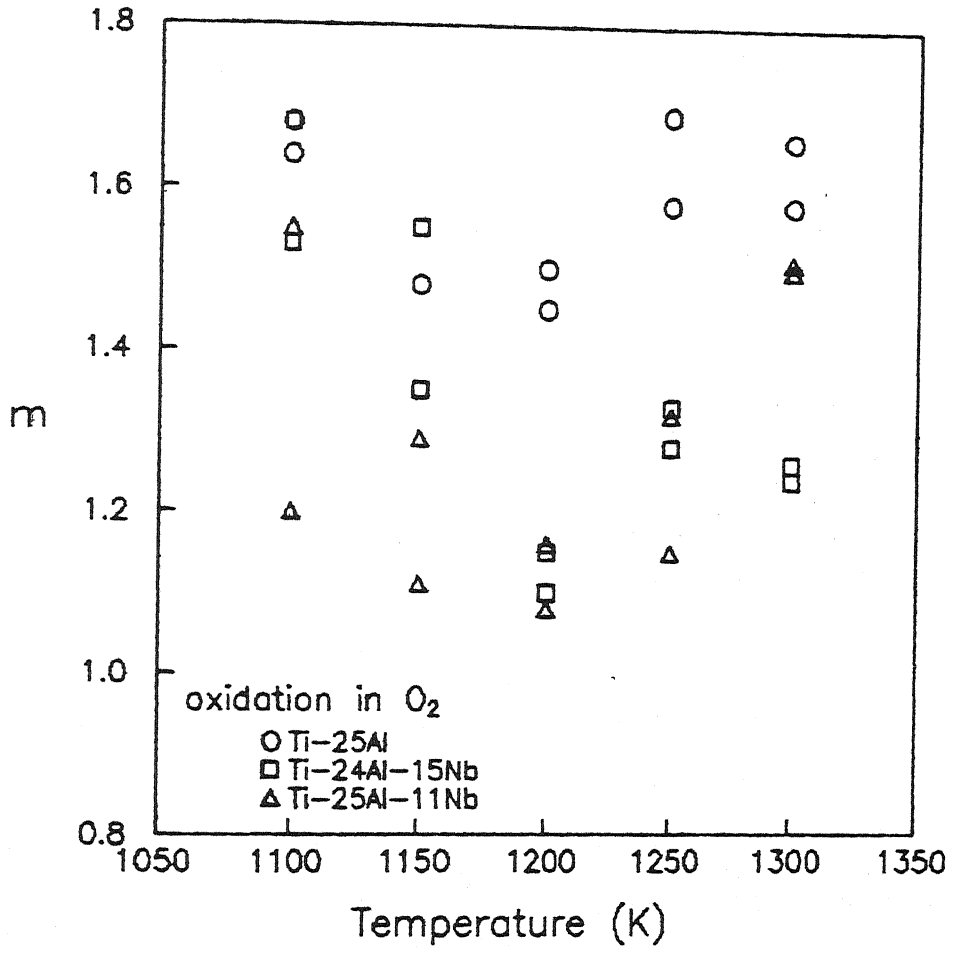

Fig.4.13: Variation of m as function of temperature for duplicate sets for oxidation of Ti-25Al, Ti-24Al-15Nb and Ti-25Al-11Nb alloys in oxygen

Table 4.5 Rate Constants and Other Parameters for Oxidation in Oxygen

Expt. No.	k_p ($kg^2\ m^{-4}\ s^{-1}$)	k'_p ($kg^2\ m^{-4}\ s^{-1}$)	m	k_m	k_m/k_p
A1	1.36×10^{-10}	-	1.24	1.04×10^{-8}	76.0
A2	2.66×10^{-9}	2.61×10^{-9}	1.68	1.45×10^{-8}	5.5
A2r	2.78×10^{-9}	2.66×10^{-9}	1.64	1.88×10^{-8}	6.8
A3	1.34×10^{-8}	1.42×10^{-8}	1.48	9.53×10^{-8}	7.1
A3r	1.22×10^{-8}	1.48×10^{-8}	1.48	8.54×10^{-8}	7.0
A4	4.20×10^{-8}	4.23×10^{-8}	1.45	3.04×10^{-7}	7.2
A4r	5.49×10^{-8}	5.39×10^{-8}	1.50	3.26×10^{-7}	6.0
A5	9.58×10^{-8}	-	1.58	4.07×10^{-7}	4.3
A5r	1.18×10^{-7}	-	1.69	3.46×10^{-7}	3.0
A6	4.50×10^{-7}	5.29×10^{-7}	1.58	1.33×10^{-6}	3.0
A6r	4.37×10^{-7}	3.93×10^{-7}	1.66	1.27×10^{-6}	3.0
B1	1.26×10^{-10}	-	1.36	5.22×10^{-9}	41.4
B2	5.77×10^{-10}	6.87×10^{-10}	1.68	3.14×10^{-9}	5.4
B2r	4.82×10^{-10}	5.46×10^{-10}	1.53	8.19×10^{-9}	17.0
B3	1.96×10^{-9}	2.53×10^{-9}	1.55	1.41×10^{-8}	7.2
B3r	1.48×10^{-9}	2.28×10^{-9}	1.35	4.61×10^{-8}	31.1
B4	1.34×10^{-8}	1.55×10^{-8}	1.10	5.19×10^{-7}	38.7
B4r	1.40×10^{-8}	1.40×10^{-8}	1.15	4.62×10^{-7}	33.0
B5	5.40×10^{-8}	-	1.28	6.32×10^{-7}	11.7
B5r	3.98×10^{-8}	-	1.33	3.98×10^{-7}	10.0
B6	9.30×10^{-8}	9.68×10^{-8}	1.24	1.33×10^{-6}	14.3
B6r	1.02×10^{-7}	1.07×10^{-7}	1.26	1.29×10^{-6}	12.6

Contd. Table 4.5

Expt. No.	k_p ($kg^2\ m^{-4}\ s^{-1}$)	k'_p ($kg^2\ m^{-4}\ s^{-1}$)	m	k_m	k_m/k_p
C1	1.37×10^{-10}	-	1.50	2.43×10^{-9}	17.7
C2	6.16×10^{-10}	5.57×10^{-10}	1.20	6.42×10^{-8}	10.4
C2r	3.58×10^{-10}	4.51×10^{-10}	1.55	4.95×10^{-9}	13.8
C3	1.55×10^{-9}	1.85×10^{-9}	1.11	1.76×10^{-7}	11.4
C3r	1.45×10^{-9}	1.92×10^{-9}	1.29	6.13×10^{-8}	42.3
C4	7.64×10^{-9}	8.85×10^{-9}	1.10	5.01×10^{-7}	65.0
C4r	8.34×10^{-9}	9.64×10^{-9}	1.20	3.57×10^{-7}	42.8
C5	3.95×10^{-8}	-	1.32	5.13×10^{-7}	13.0
C5r	3.25×10^{-8}	-	1.15	9.20×10^{-7}	28.3
C6	8.98×10^{-8}	9.47×10^{-8}	1.51	5.17×10^{-7}	5.8
C6r	1.06×10^{-7}	1.10×10^{-7}	1.50	6.02×10^{-7}	5.7

Table 4.6 Rate Constant and Other Parameters in Other Gases and Gas Mixtures

Expt. No.	k_p ($kg^2\ m^{-4}\ s^{-1}$)	m	k_m	k_m/k_p
A7	1.78×10^{-8}	1.20	3.54×10^{-7}	20.0
A8*	7.11×10^{-10}	1.31	3.60×10^{-8}	50.6
A9*	3.64×10^{-9}	1.49	4.24×10^{-8}	11.6
A10	8.76×10^{-9}	1.17	3.62×10^{-7}	41.3
A11	5.09×10^{-8}	1.12	1.26×10^{-6}	25.0
A12	6.05×10^{-7}	1.62	1.41×10^{-6}	2.3
A13	2.35×10^{-6}	1.31	7.01×10^{-6}	3.0
B7	5.09×10^{-9}	1.46	5.30×10^{-8}	10.4
B8*	2.14×10^{-11}	1.74	1.12×10^{-10}	5.2
B9*	1.94×10^{-9}	1.48	2.72×10^{-8}	14.0
B10	6.16×10^{-11}	1.23	7.69×10^{-9}	125.0
B11	1.69×10^{-10}	1.10	5.11×10^{-8}	302.3
B12	8.09×10^{-10}	1.55	1.05×10^{-8}	13.0
B13	2.48×10^{-9}	1.54	2.35×10^{-8}	10.0
B14	4.82×10^{-9}	1.86	1.13×10^{-8}	2.3
B15	8.08×10^{-10}	1.26	5.95×10^{-8}	74.0
B16	2.90×10^{-9}	1.51	3.45×10^{-8}	12.0
B17	3.97×10^{-9}	1.66	2.16×10^{-8}	5.4
B18	3.97×10^{-9}	1.70	1.74×10^{-8}	4.4
C7	5.91×10^{-9}	1.51	4.76×10^{-8}	8.1
C8	1.10×10^{-8}	1.50	9.96×10^{-8}	9.1
A14	5.29×10^{-8}	1.10	1.60×10^{-6}	30.2
A15*	7.70×10^{-9}	1.33	1.45×10^{-7}	19.0
B19	1.06×10^{-8}	0.99	8.35×10^{-7}	79.0
B20	9.78×10^{-9}	1.08	5.64×10^{-7}	58.0
B21	5.94×10^{-9}	0.99	7.42×10^{-7}	125.0
B22*	1.22×10^{-9}	1.10	1.71×10^{-7}	140.2

experimental data was fairly good as may be followed from the $(\frac{\Delta W}{A})$ vs t curves for few duplicate sets in Figs.(4.4) and (4.5). Hence, so much scatter in the values of m amongst duplicate sets of experiments can be attributed to a large extent to the empirical nature of the equation for evaluation of m and k_m. If that is so, then the values of k_p amongst duplicate sets should exhibit better reproducibility as compared to the values of k_m. Fig.4.14 presents comparison of k_p and k_m amongst duplicate sets of the experiments carried out to test the reproducibility of measurements. It may be noted from Fig.4.14 that k_p values for duplicate experiments lie on 1:1 line or very close to it. However, the departure of rate constant k_m for duplicate sets from 1:1 line was larger in general.

These findings confirm that evaluation of rate constant on the basis of parabolic law is more reliable as compared to the use of the empirical Eq.4.2. Moreover it has already been stated that;

(i) parabolic rate constant k_p has a theoretical basis,

and (ii) the earlier investigators have employed it, and hence is to be used for comparison with literature any way.

Hence, the parabolic rate constant k_p shall be employed for further discussion of results from now onwards.

4.5 VISUAL OBSERVATION AND X-RAY DIFFRACTION STUDIES OF SCALES

As mentioned previously in chapter 3, various features of the scales were observed by unaided eyes or using a low magnification (50X) portable microscope. Most of the samples were also subjected to X-ray diffraction (XRD) studies to identify the different phases present in the scales. Various features of scales observed visually and results of X-ray diffraction studies have also been included in

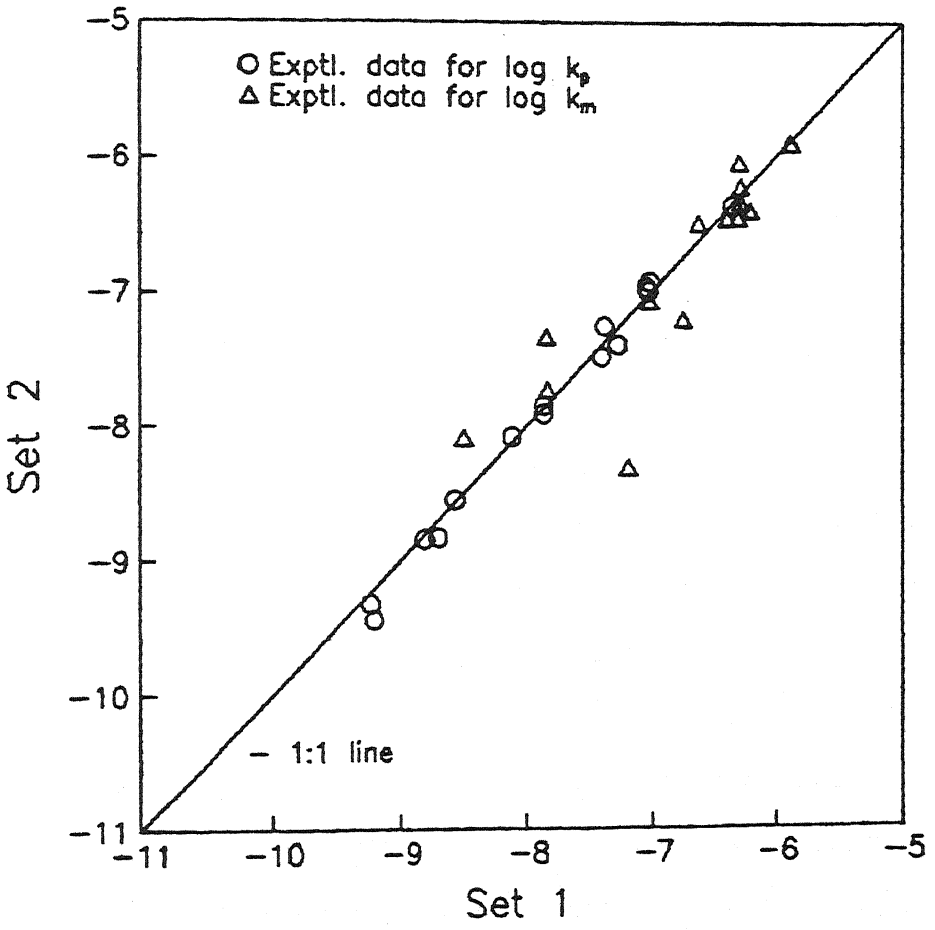

Fig.4.14: Comparison of log k_p and log k_m amongst duplicate experiments

Tables (4.1) to (4.4). Observations on scale morphologies by SEM and chemical analyses of scales by EDX will be discussed later.

As the Tables (4.1) to (4.4) show, the estimated scale thickness (x) varied from less than 1 μm to as high as 126 μm. The following relation was employed to estimate x :

$$x = \frac{\Delta W}{A} \frac{1}{\rho_{ox} \text{ (wt pct oxygen in scale)}} \qquad \ldots(4.4)$$

where ρ_{ox} is the average density of the oxide scale (taken as 4000 kg m^{-3}) and average weight pct of oxygen in the scale was taken to be 40. Since these assumptions are approximations, estimated values of x are approximate. Even then they have been useful for qualitative and semiquantitative interpretation of results.

Spalling of scale was mostly observed with alloy A where colour of outermost scale, which spalled off, was predominantly yellow. Scale spallation occurred during withdrawal of specimens from the furnace, cooling outside the furnace, and also during subsequent characterization studies. Alloys B (Ti-24Al-15Nb) and C (Ti-25Al-11Nb) showed mostly bluish and grey adherent scales in general. The scales were largely porous and non-uniform in all samples. Qualitatively speaking, the extent of scale porousness was higher at higher temperatures, particularly for alloy A (Ti-25Al).

Some special features such as scale cracking, globule formation etc. were also observed. These have been recorded as 'other features' in Tables (4.1) to (4.4). Metallic lustre and grinding marks were noticed where the scale thickness was pretty low (say less than 3 μm). However, these are not included in the tables.

CHAPTER 5

DISCUSSION OF RESULTS

As mentioned already the alloys employed in the present investigation for high temperature oxidation studies, were Ti-25Al, Ti-24Al-15Nb and Ti-25Al-11Nb. These have been designated as alloys A, B and C respectively. Emphasis was given for alloy B since this alloy had not been studied well earlier. Some experiments were also carried out to elucidate nitriding behaviour of these alloys.

The experimental conditions have already been summarized in Tables (4.1) to (4.4) in chapter 4. Some experimental results including XRD findings have also been presented there. Methods of processing weight gain vs time data have been fully presented and discussed in sec.4.4. Sources of errors and extent of errors expected have been indicated as well. The interpretations of the results will be taken up in this chapter. For this purpose in addition to results presented in chapter 4, observations and elemental analyses of scale cross sections by SEM and EDX will also be considered. Discussions would be separated on the basis of gas/gas mixture employed in the experiments.

5.1 OXIDATION BEHAVIOUR IN OXYGEN ATMOSPHERE

5.1.1 Variation of Parabolic Rate Constant k_p with Temperature

Some earlier investigators attempted to correlate the overall parabolic rate constant (k_p) and temperature through

Arrhenius-type equation :

$$k_p = k_o \exp(-Q/RT) \qquad \ldots(5.1)$$

where R is the universal gas constant, k_o is pre-exponential factor, T is temperature in K, and Q is activation energy.

However, Q can be taken as activation energy from fundamental view point if only one kinetic step controls rate. For mixed control kinetics, Q can not be called activation energy in a fundamental sense. It is then just a temperature coefficient. Parabolic rate law assumes control of oxidation rate by diffusion through the oxide scale. Even if in the present study this assumption is valid in the entire temperature range, Q may not represent true activation energy. The nature and composition of the scale depend on temperature. This is evident from Tables 4.1(a) to 4.1(c). Observations of scale topology by SEM revealed different scale morphologies at different temperatures. Other evidences for the same have also been discussed in sec.4.4 in connection with validity of various rate laws.

Therefore, the properties of medium of diffusion for any of these alloys vary with temperature. The effect of this variation on rate of oxidation would get incorporated in variation of rate with temperature, and consequently the value of Q. Hence, Q is nothing but a temperature coefficient and not true activation energy. For this reason Welsch and Kahveci[61] had used the symbol Q_{eff} instead of Q, where Q_{eff} was termed as 'effective activation energy'.

Fig.5.1 shows experimentally determined values of log k_p as function of 1/T for oxidation in oxygen for all the three alloys. The slopes of the linear best fit lines of data points provided the

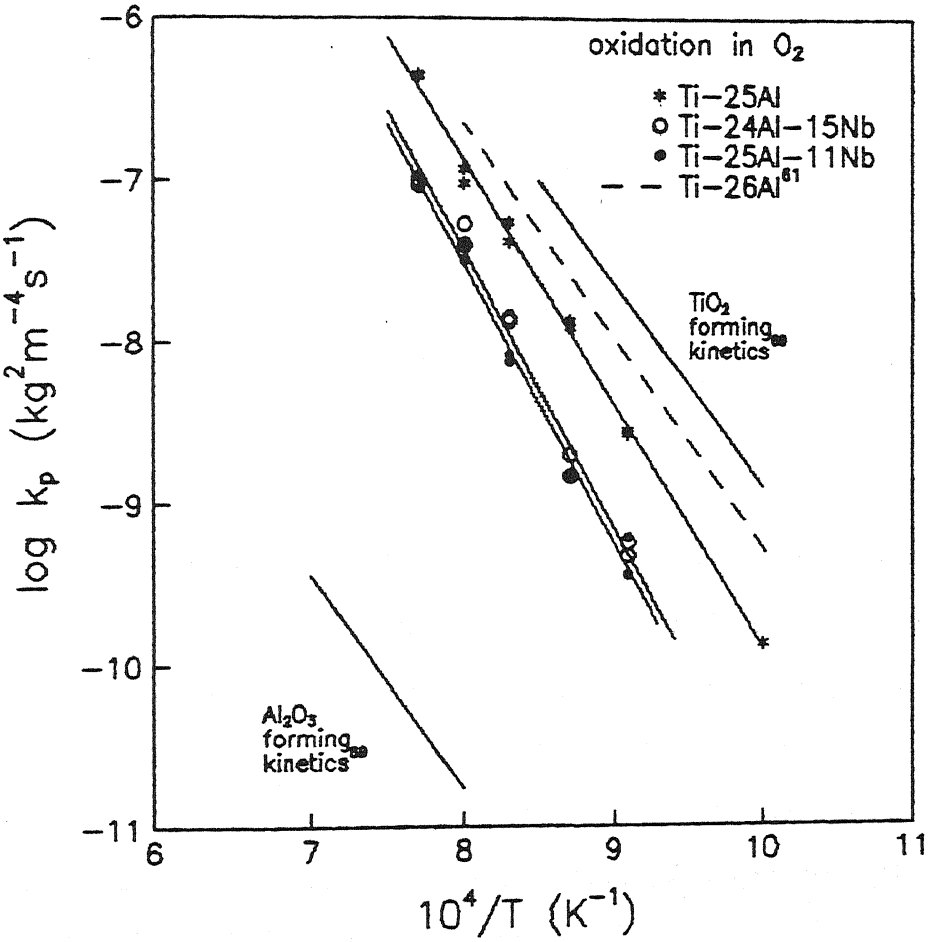

Fig.5.1: log k_p versus 1/T plots for oxidation of Ti-25Al, Ti-24Al-15Nb, and Ti-25Al-11Nb alloys in oxygen

values of Q_{eff}. As may be noted the values of Q_{eff} obtained are 289, 329 and 330 kJ/mole for alloys A (Ti-25Al), B (Ti-24Al-15Nb) and C (Ti-25Al-11Nb) respectively. It may be noted that rates of oxidation of alloys B and C were almost the same at same temperature. On the other hand, the rates for alloy A were 2 to 8 times higher than alloys B or C except at 1000K. It may also be noted from Tables 4.1(a) to 4.1(c) that k_p values for alloys B and C are almost equal to that for alloy A at 1000K. This means that actual values of k_p at 1000K are about one order of magnitude larger than those predicted by log k_p vs 1/T plots for alloys B and C. Efforts would be made later to explain this. However, the data at 1000K for alloys B and C have been excluded in regression fitting of log k_p vs 1/T data.

Table 5.1 lists the experimentally obtained Q_{eff} values for oxidation in oxygen as well as those in a gas mixture containing 20 pct O_2 and 80 pct N_2 for the present investigation. Welsch and Kahveci[61] compiled the Q_{eff} values for oxidation of Ti and Ti-Al binary alloys as well as activation energies for diffusion of oxygen in Ti, TiO_2 and Al_2O_3. In another paper Liu and Welsch[91] surveyed and tabulated the diffusion data for oxygen in rutile. These have also been presented in Table 5.1.

5.1.2 Oxidation of Ti-25Al in Oxygen

As mentioned already, it may be noted from Table 4.1(a) that the nature of scales changed with change of temperature. Scales formed in Ti-25Al(alloy A) were adherent at lower temperatures, whereas at higher temperatures (above 1100K) either considerable scale spallation occurred or loosely adherence.

Table 5.1 Effective Activation Energies (Q_{eff}) of Oxidation and Diffusion

a) present study

System*	Gas composition	Q_{eff} (kJ/mole)
Ti-25Al(alloy A)	oxygen	289
Ti-24Al-15Nb(alloy B)	oxygen	329
Ti-25Al-11Nb(alloy C)	oxygen	330
Ti-25Al(alloy A)	20 pct O_2 + 80 pct N_2	351
Ti-24Al-15Nb(alloy B)	20 pct O_2 + 80 pct N_2	274

b) other sources[61,64,68,77,91]

System*	Q_{eff} (kJ/mole)
Oxidation of Ti	235 to 265
Oxidation of Ti-2.6 Al	183
Oxidation of Ti-16 Al	209
Oxidation of Ti-25 Al	269
Oxidation of Ti-25 Al	255
Oxidation of Ti-34 Al	299
Oxidation of Ti-49 Al	419
Oxygen diffusion in TiO_2	251
Oxygen diffusion in TiO_2	234
Titanium diffusion in TiO_2	257
Oxygen diffusion in Al_2O_3 above 1473K	587
Oxygen fast diffusion paths in Al_2O_3	241
Aluminium diffusion in polycrystalline Al_2O_3	477
Oxidation of Ti-25Al-10Nb-3V-1Mo in air	248
Oxidation of Ti-2.27 Nb	215

* alloy compositions in atom pct

Moreover, the scales were generally porous and non-uniform. In one specimen cracks were observed in the scale. Colour of scales changed with variation of temperature as well. Spalled scales were largely yellowish. Below that the adherent subscale was bluish. The spalled yellow scale was mostly TiO_2 as identified by XRD.

Fig.5.2 shows SEM photographs of morphological features of surface oxides. At lower temperatures the oxide crystals were equiaxed and smaller in size. At 1300K, randomly oriented rod like TiO_2 crystals could be observed which might have caused void and pore formation. Umakoshi et al[22] reported similar morphological observation on TiAl oxidized at 1273K. Some sintering of oxide grain also occurred at 1300K as evidenced by formation of globules at the surface. Kofstad et al[57] also observed recrystallization and sintering of outer TiO_2 layers formed in titanium above 1223K.

X-ray diffraction results of some oxidized specimens presented in Table 4.1(a) showed that TiO_2 was the dominant oxide in the scale with Al_2O_3 as the minor phase. Matrix peaks were also present in the diffraction patterns. This indicates that X-ray beam was able to penetrate the oxide scales. This was again facilitated by spallation of outer layer in thicker scales. The matrix peaks were identified comparing the diffraction pattern of reference (unoxidized) sample.

Fig.5.1 gives some insight into the kinetics and mechanism of oxidation of binary Ti-Al and ternary Ti-Al-Nb alloys. The observed k_p values are expected to lie in between those for purely TiO_2 and purely Al_2O_3 forming kinetics, as reported in literature. The figure shows that the kinetics for Ti-Al binary was close to that

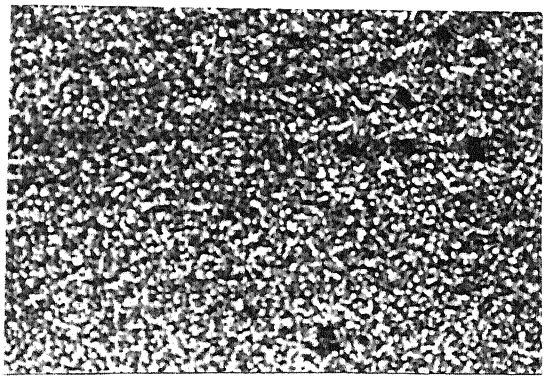

(a)

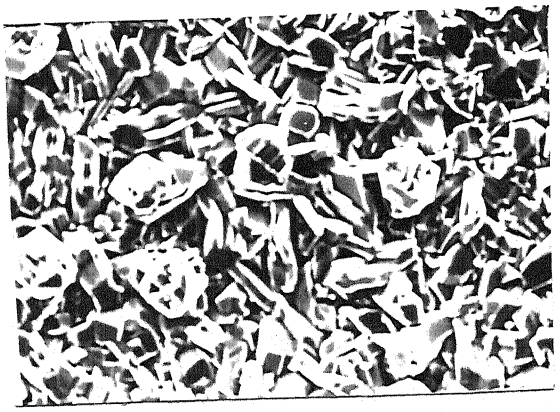

(b)

Fig.5.2: SEM micrographs of surface oxides formed on Ti-25Al alloy after exposure in oxygen showing (a) fine equiaxed grains at 1100K (b) large non-equiaxed grains with partial sintering at 1300 K

for TiO_2 formation, and it was more so at higher temperatures. The dashed line is after Welsch and Kahveci[61] for oxidation of Ti-26Al alloy showing similar behaviour. Hence the results of the present investigation are consistent with literature reports qualitatively speaking.

The Q_{eff} value for oxidation of alloy A in oxygen was 289 kJ/mole. It may be noted from Fig.5.1, that oxidation rates were lower over the entire temperature range than those reported by Welsch and Kahveci[61]. This indicates that the scales were more protective for the present study. This was also reflected by higher values of Q_{eff} compared to those reported by others[61,68] (Table 5.1).

The scales formed at all temperatures were found to consist of TiO_2 as the major oxide and Al_2O_3 as minor one. From Table 2.5, the values of ΔG^o per mole O_2 at 1300K are as follows :

Al_2O_3 : -840 kJ, TiO : -792 kJ, TiO_2 : -638 kJ, Nb_2O_5 : -475 kJ.

Hence Al_2O_3 is the most stable oxide out of the above followed by TiO, TiO_2 and Nb_2O_5 in decreasing order. However as discussed in sec.2.4.2 that the real criteria of stability is chemical potential of oxygen in equilibrium with the alloy and oxide, and it depends on activities of Ti, Al and Nb in the alloy as well. The above values show that TiO_2 is less stable as compared to TiO. Even then all investigations including the present study have reported formation of TiO_2 and not TiO. The explanation lies in the fact that ΔG^o for oxidation of TiO into TiO_2 is highly negative. For example at 1300K :

$$TiO(s) + 1/2\ O_2(g) = TiO_2(s) \qquad \ldots(5.2)$$

$$\Delta G^{O} = (-2 \times 638 + 792)/2 \text{ kJ/mole}$$

$$= -242 \text{ kJ/mole}$$

Several earlier studies had shown that TiO_2 is an n-type conducting oxide and defect is oxygen ion vacancy. Therefore, addition of cations of valence lower than 4 (valence of Ti in TiO_2) should increase oxygen ion vacancy concentration, thus increasing oxidation rate of Ti. Welsch and Kahveci[61] reported that at Al content below 25 atom pct, Q_{eff} of oxidation was below that of oxygen diffusion in TiO_2 (Table 5.1). This was proposed to be due to transport through fast diffusion paths or an increase in oxygen ion vacancy concentration by possible doping effect of Al in TiO_2. At higher Al level (above 25 atom pct), Q_{eff} lies between those for oxygen diffusion in TiO_2 and Al_2O_3. This was attributed to formation of distinct Al_2O_3 sublayer. However, this layer was observed not to give much protection because the scale was not dense and transport occurred through fast diffusion paths. In the present investigation also, Al_2O_3 was detected in scale both by XRD as well as EDX.

It may be further noted from Table 5.1 that the values of Q_{eff} for diffusion of oxygen and titanium in TiO_2 as well as diffusion of oxygen in titanium lie within the overall range of Q_{eff} values for oxidation of titanium and Ti_3Al. From this it may broadly be concluded that oxidation was controlled by diffusion. Since, a fraction of weight gain was due to oxygen dissolution in the alloy, diffusion of oxygen in the alloy besides diffusion through the scale would also be involved to some extent.

5.1.3 Comments on k_i vs Scale Thickness (x) Curves

In sec.4.4.2 some plots of k_i vs t were presented and discussed (Figs.(4.9) and (4.10)). In general, k_i varied with time. As discussed already, the reason for this variation may be attributed to variation of scale characteristics with time. Therefore, it may be possible to provide some further insight into the phenomena provided the variation of k_i is plotted as function of scale thickness (x), and not t. A given instant of time, x can be calculated from Eq.4.4. Fig.5.3 shows one such plot for oxidation of alloy A (Ti-25Al) at 1300K in oxygen. Although at other temperatures k_i vs x plots revealed different natures but they did not vary much, and hence are not being presented.

Fig.5.4 presents SEM photograph of morphology of retained scale along the cross section of alloy A oxidized in oxygen at 1300K. As recorded in Table 4.1(a), outer scale was loosely adherent to the alloy and spalled during subsequent examinations. It may be noted from Fig.5.4 that the retained scale was about 20μm thick. The colour of retained scale was bluish black whereas spalled outer scale was yellow. It indicates that natures of two layers were different. This has been reflected in the k_i vs x plot as well. The maximum in the curve is approximately at 20μm thickness of scale (Fig.5.3). The decrease in rate after attaining maxima may be due to gap formation between the inner and outer scale, which reduced the rate of diffusion through the scale. The increase of rate at the end could be due to cracking in the scale caused by generation of growth stress (sec.2.3.9).

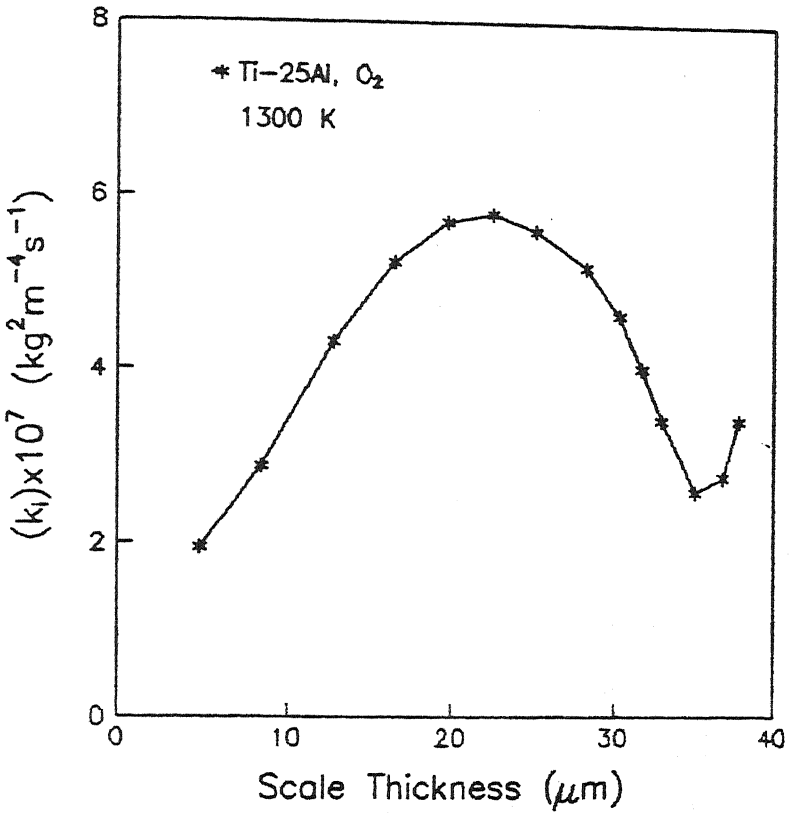

Fig.5.3: Plot of k_i versus scale thickness of Ti-25Al alloy at 1300 K

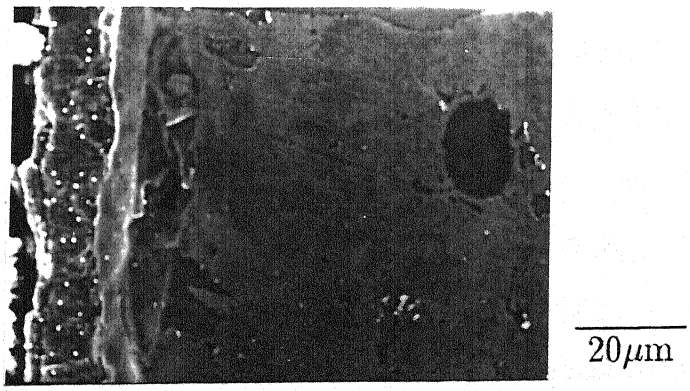

Fig.5.4: SEM micrograph of cross section of retained scale of Ti-25Al alloy oxidized in oxygen at 1300 K

5.1.4 Oxidation of Niobium Containing Alloys

Fig.5.1 also presents log k_p vs 1/T plots for alloys B (Ti-24Al-15Nb) and C (Ti-25Al-11Nb). Comparison of these with that of alloy A (Ti-25Al) shows that niobium improved oxidation resistance of Ti_3Al. The presence of niobium had been observed to be beneficial in enhancing oxidation resistance by earlier investigators as well with a few exceptions, as discussed under literature review (sec.2.6.1) and presented in Fig.2.13 and Table 2.6.

Again it is clear from Fig.5.1 that log k_p vs 1/T plots of all the three alloys lie in between lines for purely TiO_2 and purely Al_2O_3 forming kinetics indicating mixed oxide formation. The amount of Al present in Ti-Al alloys decides whether Al_2O_3 or TiO_2 formation will predominantly govern the kinetics of oxidation. In this regard several investigators[60,61,68] compared observed k_p values for oxidation of titanium aluminides with purely Al_2O_3 and TiO_2 forming kinetics. This has been shown in Fig.2.13. Increasing aluminium content or addition of nibium to Ti_3Al or TiAl tend to shift the kinetics towards Al_2O_3 formation.

Although niobium provided enhanced oxidation resistance in the present study but alloys B and C containing 15 and 11 atom pct Nb respectively showed not much of a difference in the kinetic behaviour. As Tables 4.1(b) and 4.1(c) shows, the k_p values at all temperatures were approximately the same for alloys B and C. This is in agreement with the observation that oxidation resistance became independent of Nb above 10 atom pct as reported by Singheiser et al[75].

X-ray diffraction results presented in Tables 4.1(b) and

4.1(c) reveal that in alloy B above 1200K, TiO_2 was the dominant oxide in the scale with Al_2O_3 as the minor constituent. Thermodynamic analysis as presented earlier (sec.5.1.2) shows that oxidation of TiO into TiO_2 is favourable in the present condition. This explains the absence of TiO in the scale. At lower temperatures X-ray signals of TiO_2 and Al_2O_3 were comparable. In alloy C, observations were almost similar. Matrix peaks identified as Ti_3Al were also present in oxidized samples of both the alloys. A few peaks could not be identified both for alloys B and C.

Table 5.1 gives Q_{eff} values determined in the investigation for oxidation of Ti-24Al-15Nb (alloy B) and Ti-25Al-11Nb (alloy C) in oxygen. The values are 329 and 330 kJ/mole for alloys B and C respectively. Close values of k_p of both the alloys are again reflected in identical Q_{eff} values. To the author's knowledge, Q_{eff} values for similar alloys have not been reported in literature. Hence comparison with literature is not possible. However, Q_{eff} value for oxidation of Ti-2.27Nb (atom pct) alloy reported to be 215 kJ/mole by Chen and Rosa[77]. The Q_{eff} values for alloys B and C are also higher as compared to that for alloy A (289 kJ/mole). This is in conformity with lower k_p values in these alloys as compared to that for alloy A. All of these indicate a more protective scale for niobium containing alloys.

The scales formed in these alloys were mostly bluish, adherent and comparatively thinner than those formed in alloy A (i.e. without Nb) in comparable exposure times. Smaller thickness is due to lower oxidation rates in alloys B and C. Scale porousness and non-uniformity were less than those of alloy A. Fig.5.5 shows EDX

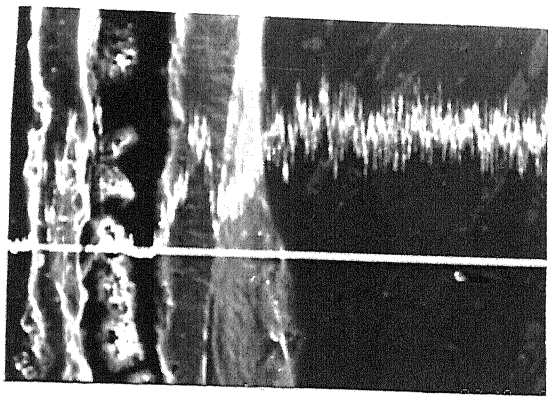

(a)

20μm

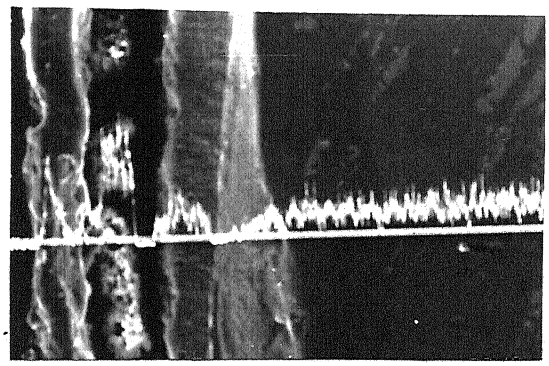

(b)

20μm

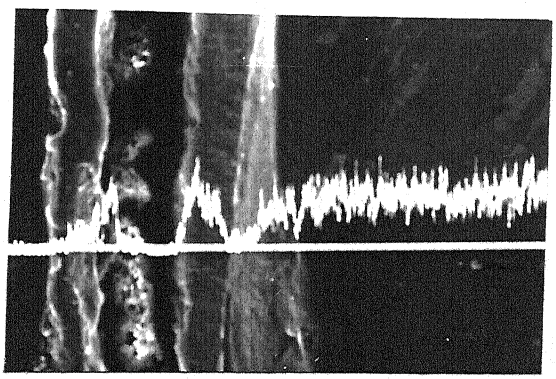

(c)

20μm

Fig.5.5: EDX elemental line scans of scale cross section of Ti-24Al-15Nb alloy oxidized in oxygen at 1300 K for (a) titanium, (b) aluminium, (c) niobium

elemental line scans of Ti,Al and Nb in the cross section of scale formed on alloy B at 1300K in oxygen. The presence of Al and Nb in the scale is evident in addition to Ti. However, niobium oxide could not be detected by XRD. Similar observations have been reported by other investigators[78]. Closer observation of the figure shows that the scale was multilayered. The sequence of scale formed from outer to inner portion was TiO_2+Al_2O_3/TiO_2+Nb-oxide/Al_2O_3/ TiO_2+Al_2O_3+Nb-oxide. Beneath that was the oxygen enriched alloy substrate depleted with Ti, Al and Nb. EDX elemental scans of scale in the present study showed almost similar sequence of scale formation as observed by Welsch and Kahveci[61].

The beneficial role of Nb has been explained in different ways in literature (sec.2.6.1). In this regard possible doping effect of niobium in reducing or modifying defect concentration of TiO_2 was proposed by some investigators[61,62,64,68,74]. According to others[45,49,67,72,73] niobium promotes Al_2O_3 formation, thus enhancing oxidation resistance. Welsch and Kahveci[61] reported that the greater protectiveness of Nb-containing alloys was due to formation of a relatively dense Ti-Nb oxide compound layer rather than a heterogeneous and porous mixtures of TiO_2 and Al_2O_3. In the present investigation no niobium oxide was detected by XRD. However elemental concentration map for Nb revealed the presence of Nb with TiO_2 in the scale. Therefore possible doping effect of Nb in reducing or modifying defect concentration of TiO_2, proposed by some earlier investigators may be taken as one of the causes promoting oxidation resistance of Nb-containing alloys.

5.1.5 Comments on Oxidation at 1000K

The actual values of k_p for alloys B and C at 1000K were about an order of magnitude higher than those predicted by log k_p vs 1/T plots. The following is a list of k_p values obtained experimentally as reported in Tables 4.1(b) and 4.1(c) as well as by extrapolation of log k_p vs 1/T plots (Fig.5.1) for alloys B (Ti-24Al-15Nb) and C (Ti-25Al-11Nb).

k_p ($kg^2\ m^{-4}\ s^{-1}$)

	Experimental	Extrapolated
Alloy B	1.26×10^{-10}	1.35×10^{-11}
Alloy C	1.37×10^{-10}	1.08×10^{-11}

The higher k_p values than expected could possibly be attributed to the nature of scale formed in these alloys at this temperature, as compared to other temperatures. SEM surface scale morphology as shown in Fig.5.6 as well as Table 4.1(b), show that the scale was non-uniform and did not cover the entire specimen surface even after an exposure of 86.1 ks (24 hr) at 1000K. Due to this the underlying alloy structure was quite discernible in some region. At other temperatures the scale covered the specimen surface, hence underlying alloy microstructure was not revealed.

As mentioned earlier, the present alloys have high solubility for oxygen. So, significant fraction of weight gain at initial stage will be due to oxygen dissolution in the alloy. Rate of dissolution will be faster if there is no scale to hinder transport

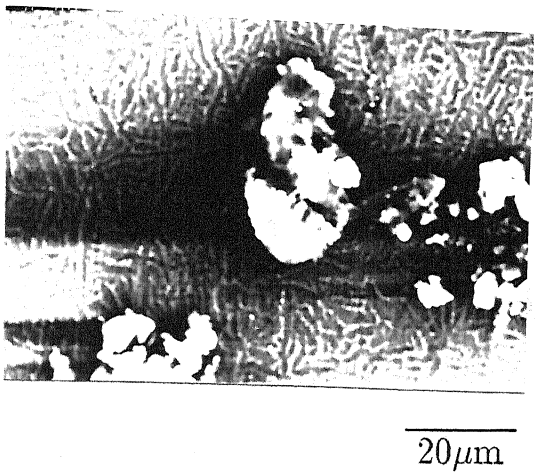

Fig.5.6: SEM micrograph of surface of scale formed on Ti-24Al-15Nb alloy after oxidation in oxygen for 86.1 ks at 1000 K

of oxygen into the alloy. Diffusion coefficient of oxygen through Nb-containing alloy B (presented later on) obtained for the present study was several orders of magnitude higher than that through TiO_2 at 1300K[91]. It may thus be concluded that faster rate at 1000K was primarily due to faster dissolution rate than oxide formation.

5.2 INFLUENCE OF OXYGEN PARTIAL PRESSURE ON OXIDATION BEHAVIOUR

5.2.1 General

In the present study some experiments were also conducted to find out the influence of partial pressure of oxygen (p_{O_2}) on the oxidation behaviour of titanium aluminides. To the author's knowledge no systematic study on this aspect has been reported so far in literature for Ti_3Al-based alloys.

Either Ar or N_2 was mixed with O_2 to generate atmosphere with varying p_{O_2}. This type of experiment was carried out at an intermediate temperature of 1200K with the major emphasis on alloy B (Ti-24Al-15Nb). p_{O_2} values were 0.2, 0.5 and 0.8 atmosphere. The total pressure of gas mixture was 1 atmosphere. Tables (4.2) and (4.3) include the experimental conditions and some features of oxidation of these experiments (Expt. Nos. B12, B15, B16 and B19, B20, B21 for alloy B, and Expt. Nos. A11, A14 for alloy A). It may be noted that in alloy A (Ti-25Al), k_p values for oxidation at 1200K was approximately the same in O_2 (Expt. No. A4), and at p_{O_2} = 0.2 atm. either in N_2-O_2 gas mixture or in Ar-O_2 gas mixture. Therefore, experiments in varying p_{O_2} were not persued further for alloy A.

5.2.2 Oxidation in O_2-Ar Gas Mixture

Fig.5.7 presents $(\frac{\Delta W}{A})^2$ vs t plot for O_2-Ar gas mixtures at 1200K for alloy B. As stated in sec.4.4.2 if the parabolic rate law is obeyed well then the instantaneous rate constant (k_i) should be independent of time. Fig.5.8 presents k_i vs t plots for the above. It shows k_i varying greatly with time and hence obedience to parabolic law was poor.

Fig.5.9 is a plot of log k_p vs log p_{O_2} illustrating the dependence of oxidation rate of alloy B on p_{O_2} at 1200K. The figure also includes the k_p for oxidation in oxygen for comparison. The slope of the least square fitted line was 0.49 for oxidation in Ar-O_2 gas mixtures indicating k_p to be proportional to square root of p_{O_2}. No such findings are available in the literature. However, Becker et al[49] observed that the weight gain curves during oxidation of TiAl (Ti-36 wt pct Al) alloys in O_2 and O_2-Ar gas mixtures fell into one scatter band which existed at least over the pressure range of 0.01-1 bar O_2. Based on this study they concluded that the influence of oxygen pressure on the oxidation rate in N_2-free atmosphere was negligible.

Examination of Fig.5.8 shows that at the initial stage of oxidation, k_i was approximately the same at all the p_{O_2} levels. However, they differed significantly at the latter stages of oxidation. Although TiO_2 was the major oxide formed in Ar-O_2 gas mixtures, but Al_2O_3 was present in the scale for all the conditions studied (Table 4.3). From the peak intensities observed in XRD studies it appeared that the amount of Al_2O_3 in the scale increased

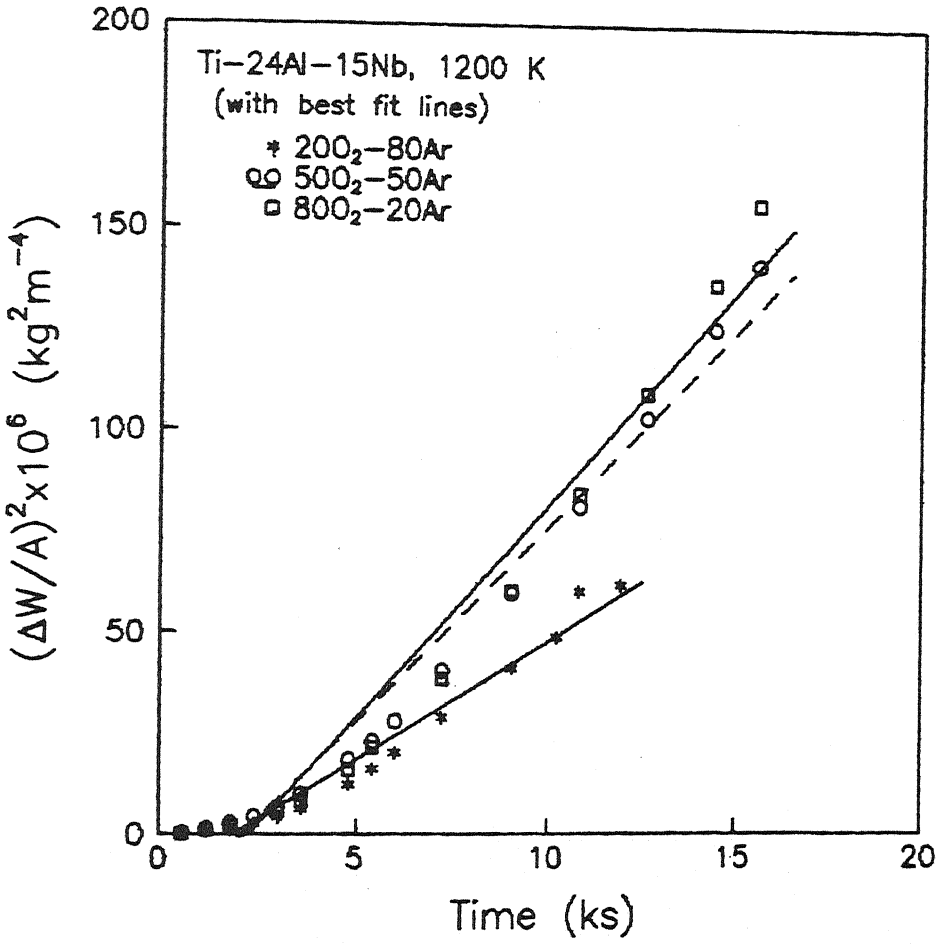

Fig.5.7: $(\frac{\Delta W}{A})^2$ versus time plots for oxidation of Ti-24Al-15Nb alloy exposed to oxygen-argon mixtures at 1200 K

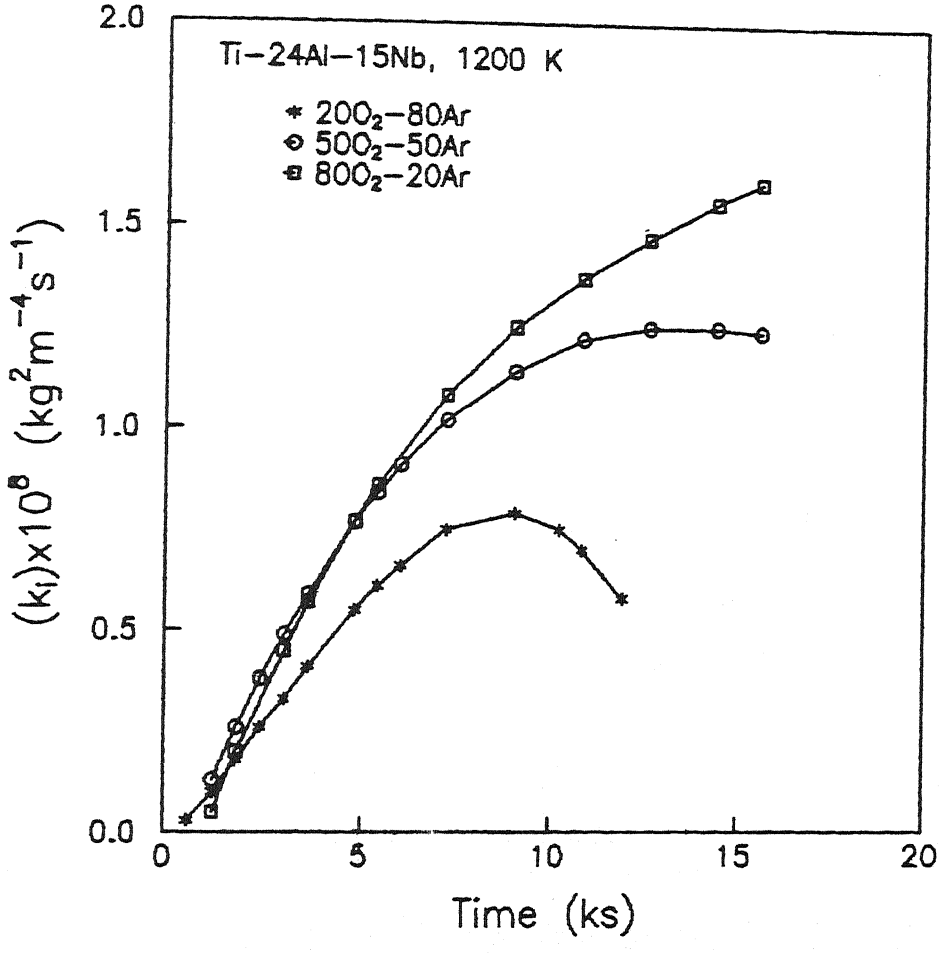

Fig.5.8: Plots of k_i versus time for oxidation of Ti-24Al-15Nb alloy exposed to oxygen-argon mixtures at 1200 K

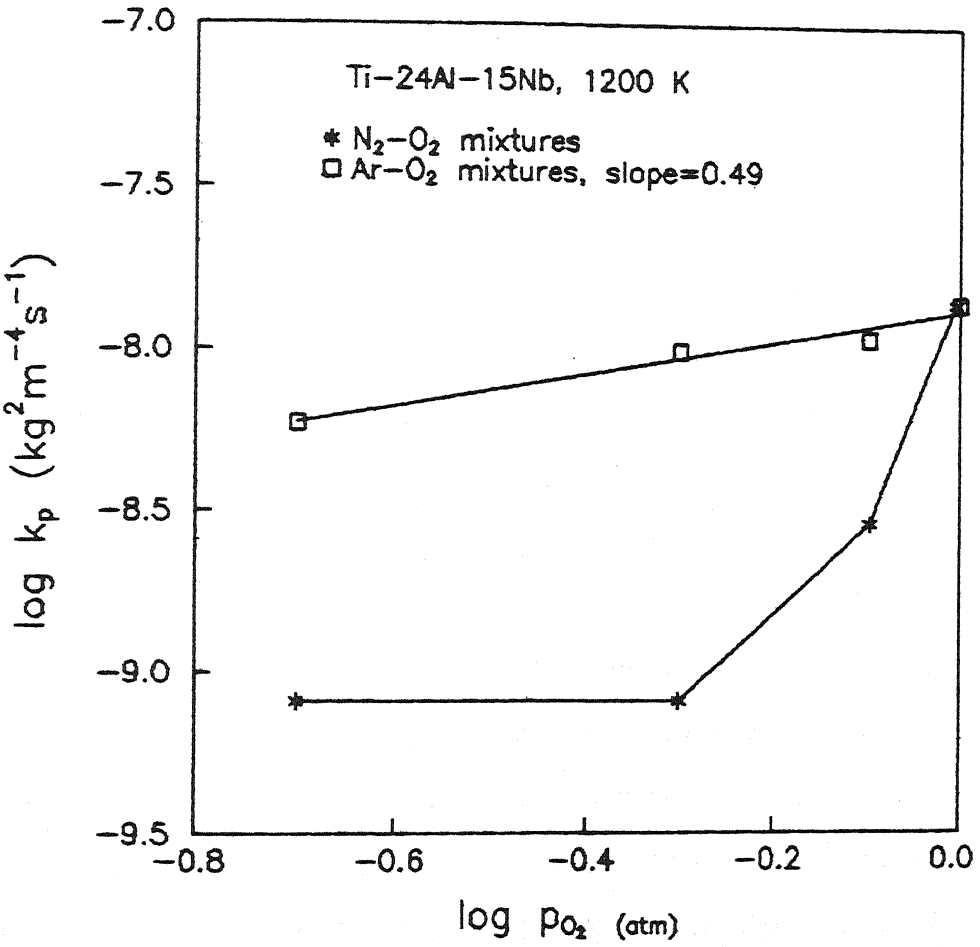

Fig.5.9: log k_p versus log p_{O_2} plots in oxygen-argon and oxygen-nitrogen mixtures for Ti-24Al-15Nb alloy at 1200 K

with decreasing p_{O_2}. This can in principle explain the differing values of k_i at latter stages of oxidation, which was reflected in the linear regression fitted values of parabolic rate constant (k_p).

Fig.5.10 presents SEM photograph of scale surface morphology for specimen exposed to O_2-Ar mixture with 80 pct O_2. The phase exhibiting rod like crystals is TiO_2 and the white equiaxed crystals growing on TiO_2 is Al_2O_3. Also the scale was not compact but had lots of pores. Visual observations also showed porous nature of top layer of the scale with some cracks (Table 4.3).

Pilling-Bedworth ratio for oxidation of titanium to TiO_2 has been reported to be in the range of 1.7 to 1.78[31]. Since alloy B is titanium rich, it is expected that the ratio would not differ too much from it and would be larger than 1.5. It predicts a dense oxide scale (sec.2.3.9) possibly with crack formation due to large compressive stresses. However, the observations here did not show dense scale. Some cracks were however present. The porous nature may be attributed to outward growth of the scale due to predominance of cationic diffusion. This is reflected in the formation of Al_2O_3 over TiO_2 crystals in Fig.5.10. The abnormal increase of k_i with time may be attributed to the porous nature of scale and consequent easy accessibility of gaseous oxygen molecules inside the scale layer. However, on the basis of the data, change in ionic permeability of scale with time also can not be ruled out.

5.3 INFLUENCE OF NITROGEN ON OXIDATION BEHAVIOUR

Fig.5.11 shows $(\frac{\Delta W}{A})^2$ vs t plots for oxidation experiments in O_2-N_2 gas mixtures at 1200K for alloy B (Ti-24Al-15Nb). Fig.5.12

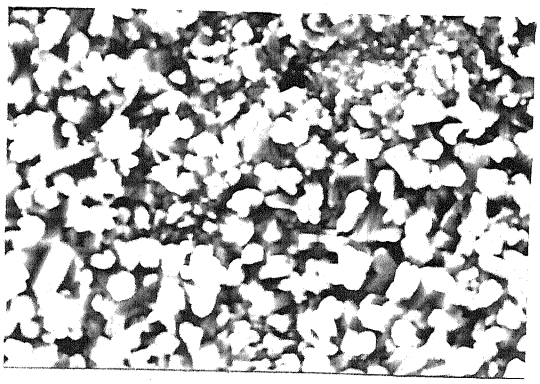

Fig.5.10: SEM micrograph of surface of scale formed on Ti-24Al-15Nb alloy exposed to 20 pct Ar-80 pct O_2 mixture at 1200 K

presents a few plots of instantaneous rate constant (k_i) vs t for the above. The obedience to parabolic law ranged from satisfactory to poor. Fig.5.9 presents log k_p vs log p_{O_2} plot for oxidation in O_2-N_2 mixtures for alloy B. k_p decreased approximately by an order of magnitude when p_{O_2} was lowered from 1 to 0.5 atm, and then became almost independent of p_{O_2}. This is in contrast to the behaviour in O_2-Ar gas mixtures, where the change was much less.

Some experiments were also performed in 20 pct O_2 + 80 pct N_2 gas mixture for alloy B at some temperatures in the range of 1100 to 1300K. It was stated earlier that alloy A (Ti-25Al) did not exhibit significant change in k_p with change in p_{O_2} in the gas mixtures. Hence only few experiments were performed in alloy A with O_2-N_2 mixture. However to compare the effect of temperature with alloy B, a few experiments were also conducted with alloy A in 20 O_2 + 80 N_2 gas mixture at 3 temperatures (1150K, 1200K, 1300K).

Fig.5.13 shows the plots of log k_p vs 1/T for alloys A and B in 20 O_2 + 80 N_2. For comparison, the plots for alloys A and B in oxygen are also included in the same figure. In addition the lines for purely TiO_2 forming kinetics and purely Al_2O_3 forming kinetics from literature are also shown. The values of Q_{eff} are listed in Table 5.1. It may be noted that in O_2-N_2 mixture the values of Q_{eff} were 351 and 274 kJ/mole respectively for alloys A and B. These are in contrast to the values obtained for oxidation in oxygen where the relative values are in the reverse order, viz. 289 and 329 kJ/mole for alloys A and B respectively.

The values of k_p were similar in magnitude for alloy A both in

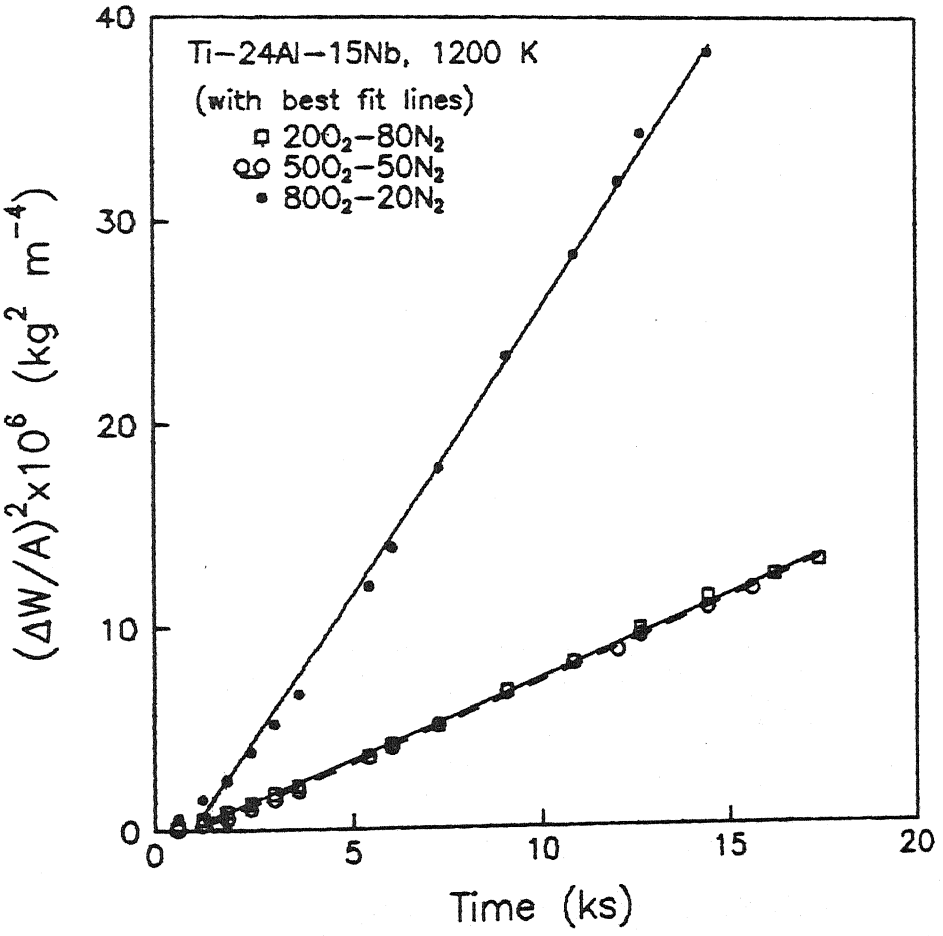

Fig.5.11: $(\frac{\Delta W}{A})^2$ versus time plots for oxidation of Ti-24Al-15Nb alloy exposed to oxygen-nitrogen mixtures at 1200 K

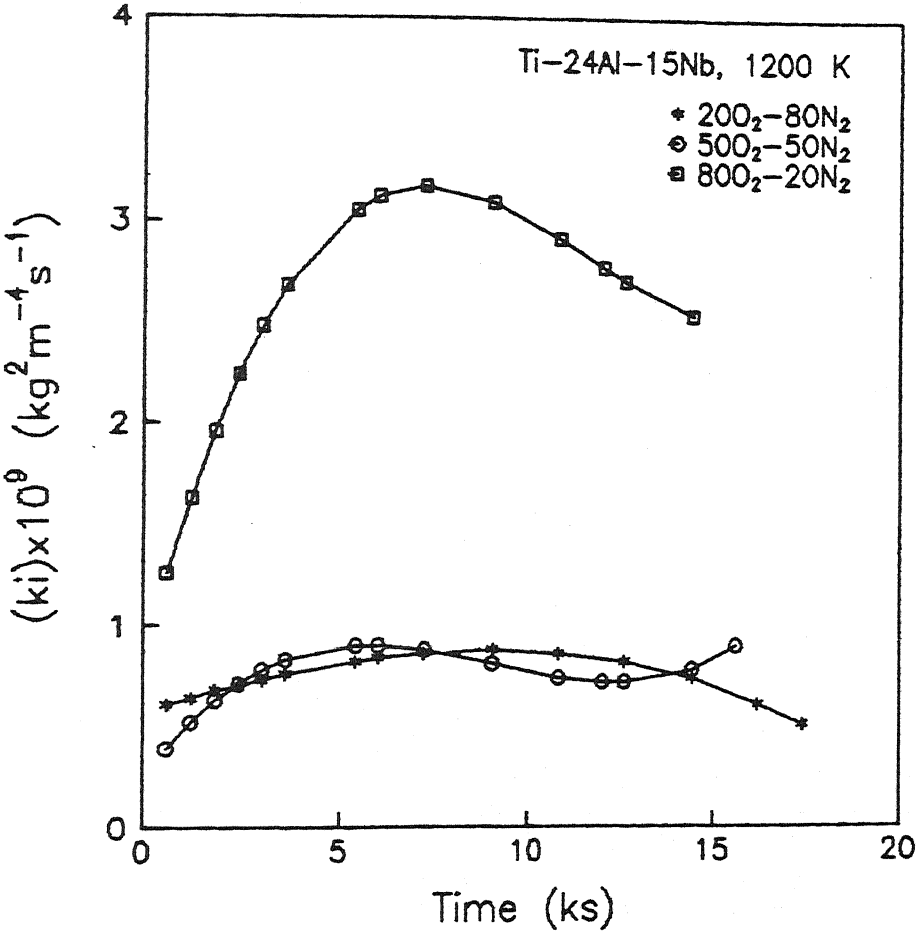

Fig.5.12: Plots of k_i versus time for oxidation of Ti-24Al-15Nb alloy exposed to oxygen-nitrogen mixtures at 1200 K

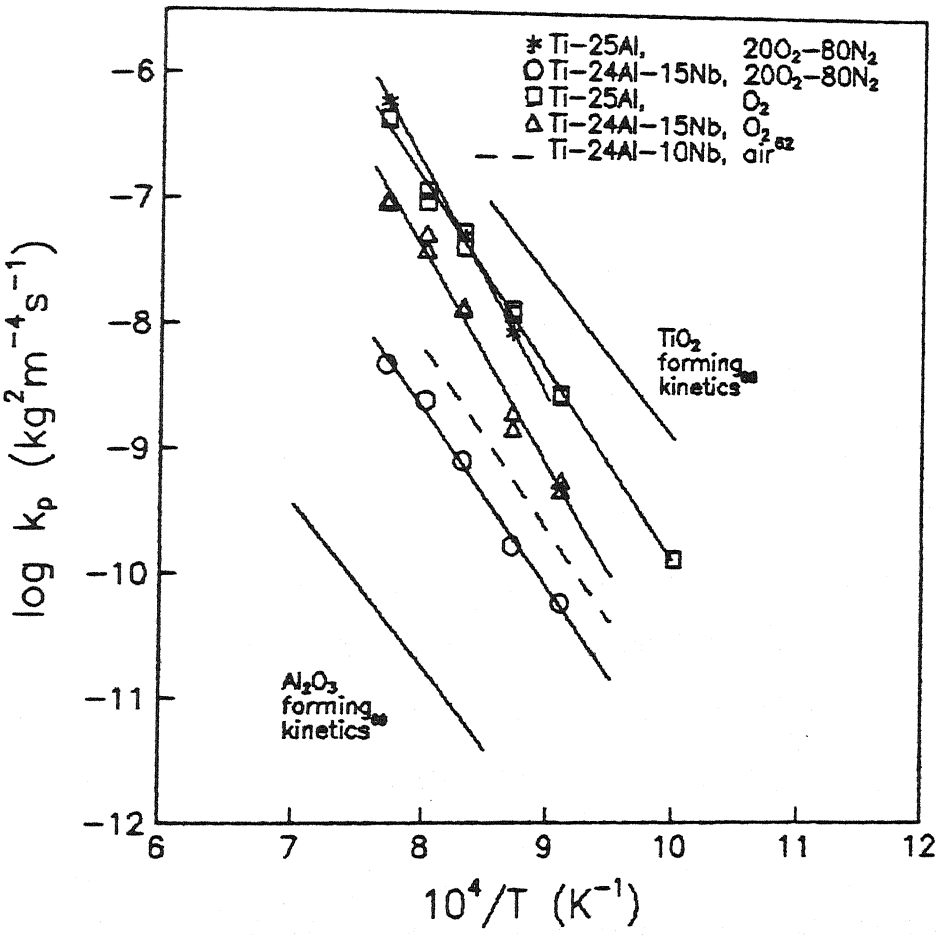

Fig.5.13: log k_p versus 1/T plots for oxidation of Ti-25Al, Ti-24Al-15Nb alloys in 20 pct O_2 80 pct N_2 mixture

O_2-N_2 mixture and in O_2. However for alloy B, k_p was approximately an order of magnitude lower in 20 O_2 + 80 N_2 at all temperatures as compared to those in O_2. One experiment (No. C8) for alloy C (Ti-25Al-11Nb) was also carried out in 20 O_2 + 80 N_2 gas mixture at 1300K. There also k_p was observed to be an order of magnitude lower than that in O_2. Fig.5.13 also includes the data obtained by Sankaran et al[62] for oxidation of Ti-24Al-15Nb in air. Their data lie between those of alloy A (Ti-25Al) and alloy B (Ti-24Al-15Nb) in the present investigation.

As already discussed in sec.5.1.4 that niobium enhanced oxidation resistance of Ti_3Al. Further enhancement of resistance in 20 O_2 + 80 N_2 gas mixture can be attributed to the presence of nitrogen in the atmosphere. Some investigators tried to assess the influence of nitrogen on oxidation kinetics in Ti-Al-Nb based alloy system. The data were generally very limited. The findings were also contradictory. Some observed a retardation effect of nitrogen on rate whereas some others found enhancement of rate in presence of nitrogen. These have been reported in chapter 2 (sec.2.6.2).

5.3.1 Formation of TiN in Scale

Fig.5.14 presents X-ray diffraction patterns of scales for alloys A, B and C at 1300K for reference. For alloys B and C, examination of the scale by XRD revealed presence of TiN in the scale formed in O_2 - N_2 mixture in addition to TiO_2 and Al_2O_3 (Table 4.2). In contrast TiN could not be detected in scale of alloy A for experiment in 20 O_2 + 80 N_2 gas mixture at higher temperature (1300K) however, weak signals for TiN was detected at lower temperature (1150K). For alloys B and C, a few peaks could

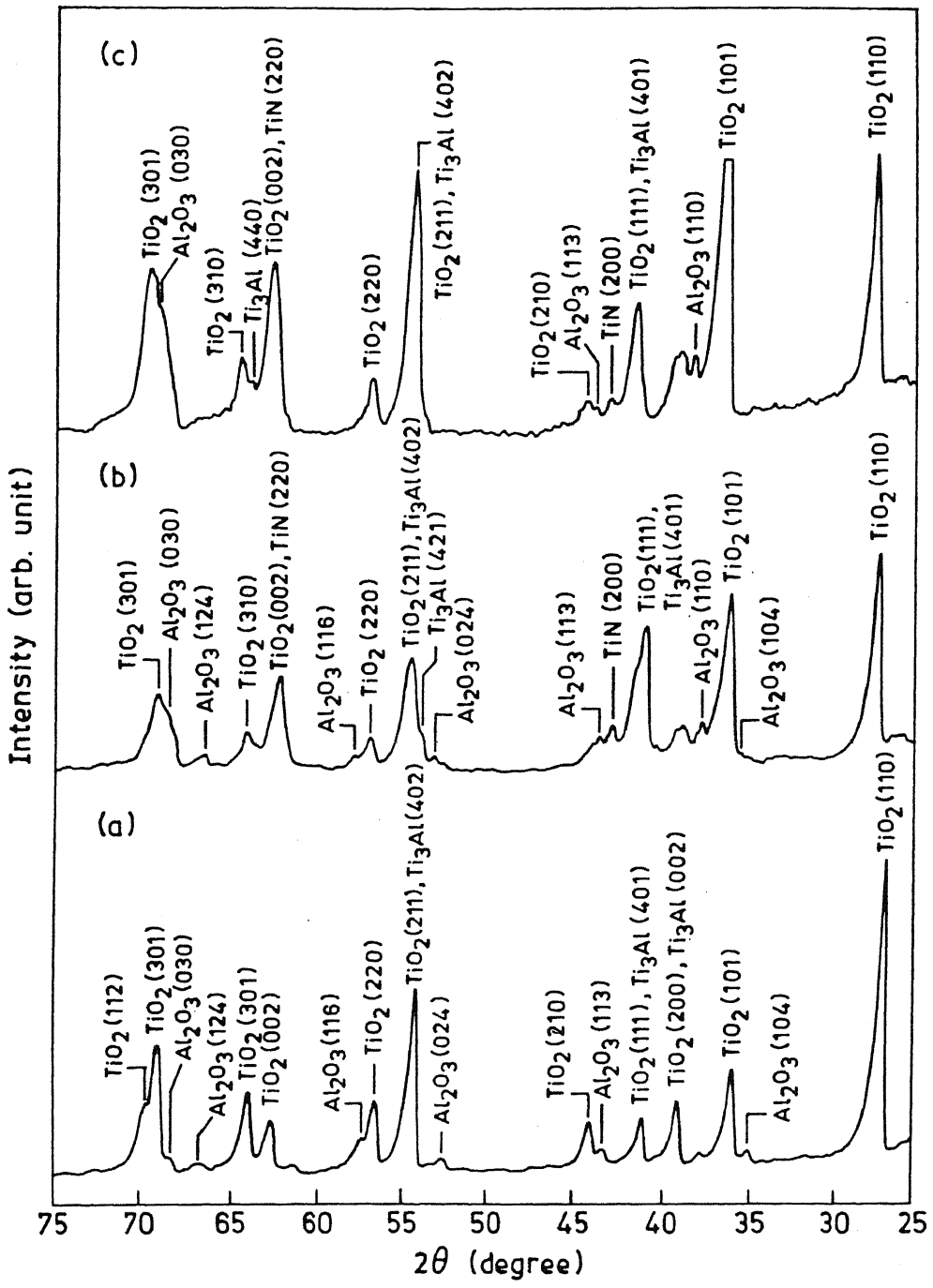

Fig.5.14: X-ray diffraction patterns of scales formed in 20 pct O_2-80 pct N_2 mixture at 1300 K for alloys (a) Ti-25Al, (b) Ti-24Al-15Nb, (c) Ti-25Al-11Nb

not be identified in the diffraction patterns. Formation of TiN seems to have played the beneficial role in lowering the oxidation rate in alloys B and C. Rawe and Rosa[58] attributed this to the barrier qualities of TiN layer. As already stated that development of a dense protective scale is possible only when the Pilling-Bedworth ratio (PBR) is sightly above 1. TiN satisfies this requirement, since PBR is approximately 1.1[82]. Secondly, the nitrides in general, including TiN are more metallic in nature, and hence would be able to accommodate more stresses before cracking. These, in principle, are expected to make TiN more protective for oxidation. Thirdly, although no data for diffusivity of oxygen through TiN are available to the author's knowledge, it is expected that it will be much lower as compared to oxygen diffusion through oxide. All these support the viewpoint that TiN would act as barrier to oxidation.

Wiedemann et al[78] detected TiN by XRD in the scale formed on Ti-25Al-11Nb (atom pct) upon oxidation in air at 1255K. Although they detected TiN as the only nitride phase, they proposed the thin nitride layer near the substrate to be composed of titanium and niobium nitride. The outermost scale was a mixture of titanium and aluminium oxides, below which there was a region of titanium oxide and a mixture of titanium and niobium oxide (not identified by XRD) formed on top of nitride layer.

Wallace et al[64] also detected TiN by XRD in Ti-25Al-10Nb -3V-1Mo (known as super α_2) oxidized in air from 973 to 1273K. Here again TiN was observed to form near the scale/alloy interface. They observed TiN layer to be 1.1 μm thick at 1173K, which did not grow

further during the period from 24 to 100 hr. They also confirmed TiN formation by electron probe microanalysis (EPMA). The outermost layer was Al_2O_3 while the middle layer (top of TiN) was TiO_2 doped with niobium. SEM and EDX examinations of surface oxide revealed the presence of TiO_2 particles along with Al_2O_3. This indicated that Al_2O_3 did not form as a continuous layer.

Schaeffer et al[65] observed a leyer of Ti(O,N,C) by secondary ion mass spectroscopy (SIMS) and X-ray photoelectron spectroscopy (XPS) after oxidation of Ti-25Al-10Nb-3V-1Mo and Ti-24.5Al-12.5Nb-1.5Mo in air in the temperature range between 866 and 978K. This layer was white in appearance and formed near the scale/alloy interface. The mixed nature of Ti(O,N,C) layer could be expected due to the fact that TiO, TiN and TiC are isomorphous interstitial compounds. The internal scale was consistent with Al_2O_3 and some TiO_2 for 12.5Nb-1.5Mo alloy whereas surface oxide was a heterogeneous mixtue of oxides of Ti, Al, Nb etc.

Becker et al[49] carried out interference layer metallography and EPMA measurements along the scale cross sections formed by oxidation of TiAl in air. They identified two different nitride layers viz. TiN and Ti_2AlN beneath the Al_2O_3 layer in the scale. The innermost layer was TiN and outside that was Ti_2AlN and single Al_2O_3 layer was the outermost scale. Rawe and Rosa[58] also found TiN to be the innermost layer as well as very thin.

Fig.5.15 presents cross sectional micrographs as well as elemental maps of Ti, Al and Nb by SEM and EDX for alloy B in 20 O_2 + 80 N_2 gas mixture at 1300K for the present investigation. It reveals the following :

(i) presence of a gap at/near the scale/alloy interface, presumably due to the tendency of detachment as a result of growth stresses

(ii) a thin white layer at the outermost scale presumably that of Al_2O_3

(iii) presence of both Ti and some Nb but very little Al in the inside scale

and (iv) no separate layer which could be taken as TiN.

Efforts were made to carry out some examinations by electron probe microanalysis (EPMA) because this instrument is capable of detecting low atomic elements viz. nitrogen and oxygen. However, no success was obtained because of non-availability/malfunctioning of the equipment during the entire course of the present investigation. Hence it was not possible to confirm whether TiN was present as a separate layer and also the location of its formation in the scale. The presence of Al_2O_3 at the exterior of the scale in alloys Ti-25Al-10Nb-3V-1Mo and TiAl respectively in air have also been reported by Wallace et al[64] and Becker[49].

Table 4.2 shows that, for alloy A (Ti-25Al) the outer bluish white/yellow scales formed in 20 O_2 + 80 N_2 gas mixture at all temperatures were not adherent to the substrate. The retained scales after spalling were compact, dark grey in colour except at 1300K, where it was white and scale was more porous. As stated earlier TiN could not be detected in the scale formed at 1300K. The estimated thickness of scale was 67 μm (Table 4.2). Although outer yellow scale spalled off almost completely, the retained scale was also thick and it may be that X-rays could not penetrate the

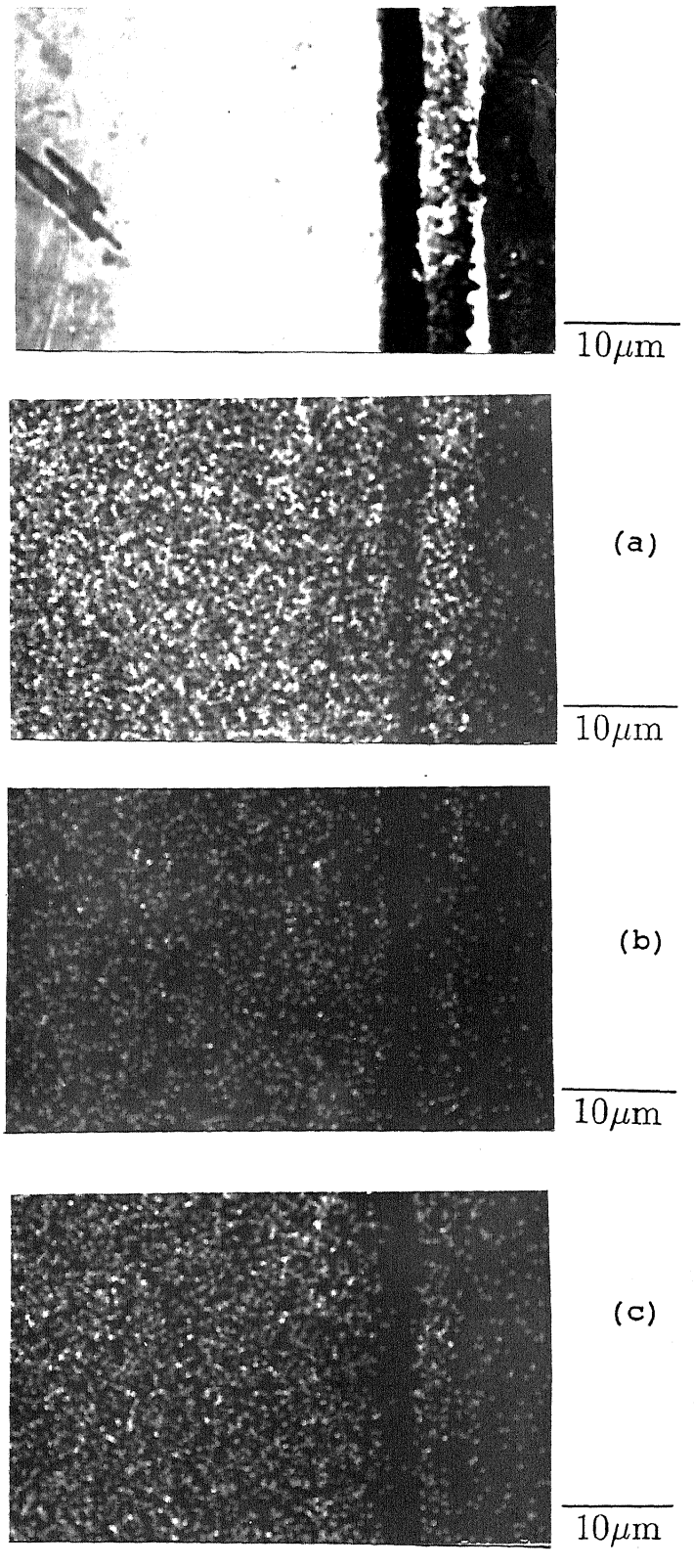

Fig.5.15: SEM micrograph and EDX elemental maps of scale cross section of Ti-24Al-15Nb alloy exposed in 20 pct O_2-80 pct N_2 mixture at 1300 K for (a) titanium, (b) aluminium, (c) niobium

retained scale completely and generate signals from TiN layer at the alloy/scale interface.

Whatever may be, the scales were not protective in alloy A as compared to those in alloy B for same experimental conditions. TiN was detected in the scale for alloy A at 1150K but no beneficial effect was observed. Some other investigators[68,80] also did not observe any nitrogen bearing phase in TiAl alloy upon oxidation in air. Fig.5.16 shows surface oxide morphology of spalled scale after oxidation of alloy A in 20 O_2 + 80 N_2 gas mixture at 1300K. It may be noted from the figure that some sintering of oxide grains took place as observed in the scale formed in oxygen at the same temperature (Fig.5.2).

It may be noted that niobium oxide could not be detected by XRD in the present investigation but presence of niobium in the scale is evident from SEM EDX. This may be taken as an evidence that niobium ions were present as dissolved in TiO_2 rather than as separate phase. This observation is in line with that already made in connection with oxidation in oxygen. As concluded in sec.5.1.4 the doping effect of niobioum ion is expected to slow down oxygen ion diffusion through oxide and hence would promote oxidation resistance. The presence of an Al_2O_3-rich (possibly only Al_2O_3) layer in the outermost scale for oxidation in 20 O_2 + 80 N_2 gas mixture for alloy B is expected to provide additional protection to oxidation. Hence it is concluded that the significantly lower rate in oxidation for Nb-containing alloy in 20 O_2 + 80 N_2 gas mixture seems to be due to the beneficial effect of TiN as well as Al_2O_3.

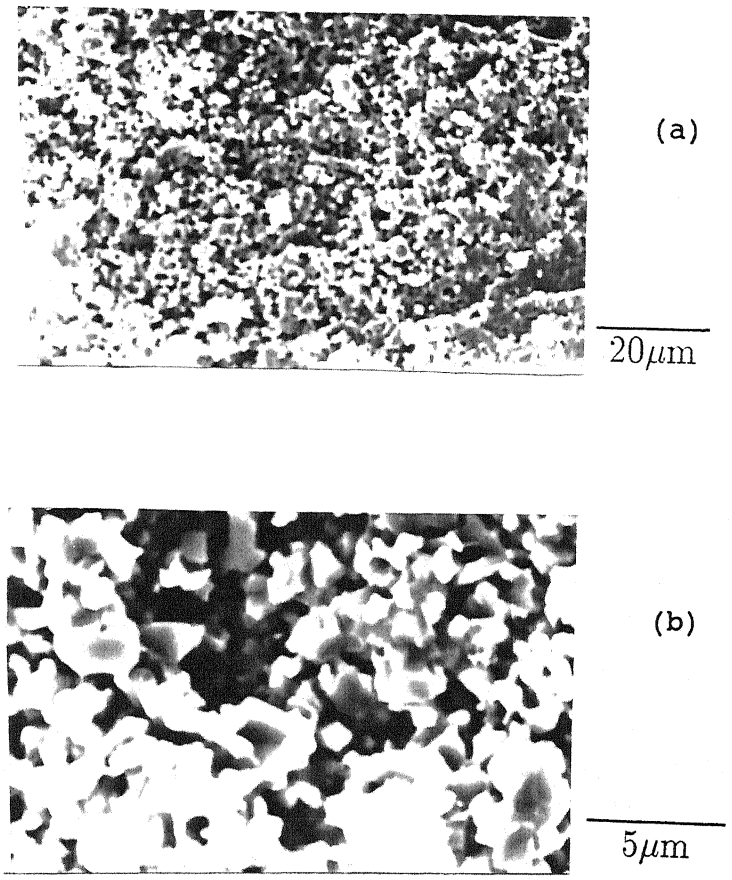

Fig.5.16: SEM micrographs of spalled scale of Ti-25Al alloy exposed in 20 pct O_2-80 pct N_2 mixture at 1300 K (a) at lower magnification, (b) at higher magnification showing some sintering of oxide grains

The reason for formation of outer Al_2O_3 layer seems to be due to enhanced diffusion of aluminium through niobium doped TiO_2. As per Kofstad[92] the solubility of Al_2O_3 in TiO_2 decreases as the oxygen potential increases. At surface the oxygen potential is high so aluminium oxide diffusing through the oxide would tend to precipitate there. Wiedemann et al[78] explained the presence of Al_2O_3 at the surface by this mechanism. On the other hand, Schaeffer[65] tried to explain this by relative increase of concentration of Al as compared to that of Ti due to the formation of Ti(O,N,C) layer. According to him increased Al concentration increases Al supply to the scale, thus facilitating Al_2O_3 formation. However this line of reasoning is not clear.

Becker et al[49] found a build up of Al concentration in the alloy beneath the Ti_2AlN layer and attributed this to the difficulty of diffusion of aluminium ions through the nitride layer. If that is so then the formation of outer Al_2O_3 layer in their experiment can not be explained. As already mentioned that doping of TiO_2 by niobium oxide decreases concentration of oxygen ion vacancy and hence is expected to retard inward diffusion of O^{2-}. This would tend to promote outward growth of scale, and hence formation of Al_2O_3-rich layer at top. It also suggests that perhaps TiN was not present as a single impervious layer but might have been present as patches in niobium doped TiO_2. Becker et al[49] studied TiAl, but alloy B had niobium as well. That way situation in the present study was similar to that of Wiedemann et al[78] who studied oxidation of Ti-25Al-11Nb (atom pct) in air. The latter reported presence of a thin layer of mixed titanium and niobium nitrides adjacent to scale/alloy interface.

Again, $Al_2O_3 + 2TiN = 2AlN + TiO_2 + TiO$ ...(5.6)

$\Delta G^o_6 = [-1/2 \times 792 - 638 - 354] - [3/2 \times (-840) - 407]$ kJ/mole

$= 279$ kJ/mole

On the basis of the above reaction (5.6) it may be noted that TiN is stabler than AlN in contact with aluminium and titanium oxides. This is in conformity with formation of TiN rather than AlN in some experiments. Thermodynamic analysis for reaction (5.3) shows that TiO is much more stable as compared to TiN. For example at 1300K, $\left(\frac{p_{O_2}}{p_{N_2}} \right)_{actual} < 3.4 \times 10^{-16}$ for formation of TiN in preference to TiO. Therefore, a principal question is how can TiN form at all? Obviously it is a transient phenomenon, and as per literature reports it forms as a thin layer adjacent to alloy surface. Attainment of such low $\left(\frac{p_{O_2}}{p_{N_2}} \right)$ ratio is possible if :

(i) either oxygen diffusion through the scale is orders of magnitude lower compared to that of nitrogen

or (ii) both oxygen and nitrogen reach the surface from the gas phase at comparable rates but oxygen gets consumed primarily in dissolution in alloy and/or internal oxidation of Al to Al_2O_3.

It seems from evidences available in literature that the latter mechanism is more dominant. The diffusivity of oxygen is atleast an order of magnitude larger compared to that of nitrogen in α-Ti. Possibility of formation of Al_2O_3 precipitates at or near the alloy surface is from study by Becker et al[49], who found enrichment of aluminium at the surface of the alloy in presence of

TiN. MÜnster and Schlamp[93] studied the oxidation of TiN in the temperature range of 898 to 1348K in oxygen, and found the rates to be significantly lower than those for pure titanium. This study indicates that TiN, once formed, is likely to resist its conversion to oxides by oxidation.

5.4 NITRIDING BEHAVIOUR

Experiments carried out in 20 O_2 + 80 N_2 gas mixture led to TiN formation in alloys B and C at all temperatures. However, no nitride could be detected in alloy A at 1300K. To gain more information on nitride formation, all three alloys (alloys A,B and C) were exposed at 1300K to nitrogen freed from O_2, CO_2 and moisture by passing through purifying gas train.

The parabolic rate constants (k_p) in nitrogen, as recorded in Table 4.2 (Expt Nos. A7, B7 and C7), were approximately 15 to 25 times lower than those in oxygen. However, X-ray results of these experiments show that in addition to nitridation, significant oxidation also occurred. This is because oxygen level in nitrogen gas could not be kept low enough by the BTS catalyst for avoiding formation of stable oxides of aluminium and titanium.

So, to obtain a very low p_{O_2}, after usual purification, nitrogen was passed through a getter column placed inside the reaction chamber. Zirconium drillings were used for gettering purpose since it possesses the capacity of removing oxygen in gas to an extremely low level. Details have already been presented in sec.3.3.3. These experiments were conducted for alloys A and B at 1200 and 1300K. Table 4.2 presents rate constants (k_p) and other features of these experiments (Nos. A8*, A9*, B8* and B9*). For

convenience of discussion some data are again reproduced in Table 5.2.

Use of getter lowered the rates only approximately 3 to 5 times as compared to those without getter for both the alloys A (Ti-25Al) and B (Ti-24Al-15Nb) at 1300K. As may be noted from the Table 5.2, the lowering of k_p in N_2 (with getter) as compared to that in O_2 was more at 1300K than at 1200K for alloy A. For alloy B this happened in the other way. The presence of TiO_2 in the scale for both the alloys reveals that in addition to nitridation, oxidation also occurred. This only indicates that gettering was not as effective as expected.

In order to understand whether presence of nitrogen was hindering gettering action by zirconium, a few experiments were conducted in argon using getter column at 1200K (Expt.Nos. A15*, B22*). Here again some weight gain was recorded. The parabolic rate constants (k_p) were only approximately an order of magnitude lower than those in oxygen for both alloy A and B (Table 5.2). It confirmed that getter element could not remove oxygen impurity present in argon efficiently to prevent oxidation.

The experimental data and observations in nitrogen and in oxygen point out that the nitridation rate constant (k_p) for both the alloys A and B were lowered by one to two orders of magnitude as compared to those for oxidation. McDonald and Wallwork[94] had also reported that nitridation rates of pure titanium in the temperature range between 823 and 1273K were much lower than those of oxidation. This is in agreement with findings of the present investigation.

Table 5.2 Experimental Conditions and Salient Results of Some Experiments in N_2, O_2-N_2, O_2-Ar, and Ar

Expt.(+) No.	Gas Composition	Temp. (K)	$\left(\frac{k_p}{k_{p,O_2}}\right)$**	X-ray Diffraction(++) Major phase	Minor phase
A7	N_2	1300	0.04	TiO_2	Al_2O_3,TiN
A8*	N_2	1200	0.015	TiN,M	TiO_2
A9*	N_2	1300	0.008	TiO_2,TiN,M	Al_2O_3
A11	20 O_2 + 80 N_2	1200	1.06	-	-
A12	20 O_2 + 80 N_2	1300	1.36	TiO_2	Al_2O_3,M
A15*	Ar	1200	0.16	-	-
A14	20 O_2 + 80 Ar	1200	1.10	-	-
B7	N_2	1300	0.05	TiO_2,M	Al_2O_3,TiN
B8*	N_2	1200	0.002	M,TiN	TiO_2
B9*	N_2	1300	0.02	TiO_2,TiN	M
B12	20 O_2 + 80 N_2	1200	0.06	TiO_2,M	TiN,Al_2O_3
B14	20 O_2 + 80 N_2	1300	0.05	TiO_2,M	Al_2O_3,TiN
B22*	Ar	1200	0.09	-	-
B21	20 O_2 + 80 Ar	1200	0.43	TiO_2	Al_2O_3,M
B18	20 N_2 + 80 Ar	1300	0.04	-	-
C7	N_2	1300	0.06	TiO_2	Al_2O_3,TiN,M
C8	20 O_2 + 80 N_2	1300	0.11	TiO_2	Al_2O_3,TiN,M

(+) A, B, C denote alloys A, B and C respectively

* experiment using getter element

** k_p = parabolic rate constant for the given experiment and k_{p,O_2} = k_p for the same alloy at same temperature in oxygen

(++) M denotes Ti_3Al

Again from Table 5.2 it may be noted that k_p for alloy B in purified Ar (using getter) was approximately 5 times lower than that in 20 O_2 + 80 Ar mixture at 1200K. On the other hand k_p value at 1200K in purified N_2 (using getter) was approximately 30 times lower as compared to that in 20 O_2 + 80 N_2 gas mixture. Also k_p in 20 O_2 + 80 N_2 mixture was 7 times lower than that in 20 O_2 + 80 Ar mixture. This again demonstrates significant retarding effect of nitrogen on rate for alloy B, and confirms conclusions in sec.5.3.1.

5.5 SEQUENTIAL EXPOSURE TO DIFFERENT GASES

The presence of nitrogen in the oxidizing environment proved to be beneficial in the present study for lowering of rates for alloy B. Some experiments were also performed in changing environments for further elucidation of the role of nitrogen. For this purpose both alloys A (Ti-25Al) and B (Ti-24Al-15Nb) were exposed in one type of gas for 1 hr (i.e. pretreatment), and then switched over to other gas or gas mixtures. These experiments were carried out at 1300K. Details have been presented in sec.3.3.2.

Fig.5.17 presents the weight gain data for alloy A for oxidation in oxygen after nitrogen pretreatment, whereas Fig.5.18 presents weight gain data for oxidation in 20 O_2 + 80 N_2 gas mixture after pretreatment in nitrogen as well as in oxygen. For comparison, the weight gain data for oxidation in oxygen and in 20 O_2 + 80 N_2 without pretreatent have been included in the Figs.(5.17) and (5.18) respectively. The experimental conditions and some salient features of these experiments have already been listed in Table 4.4.

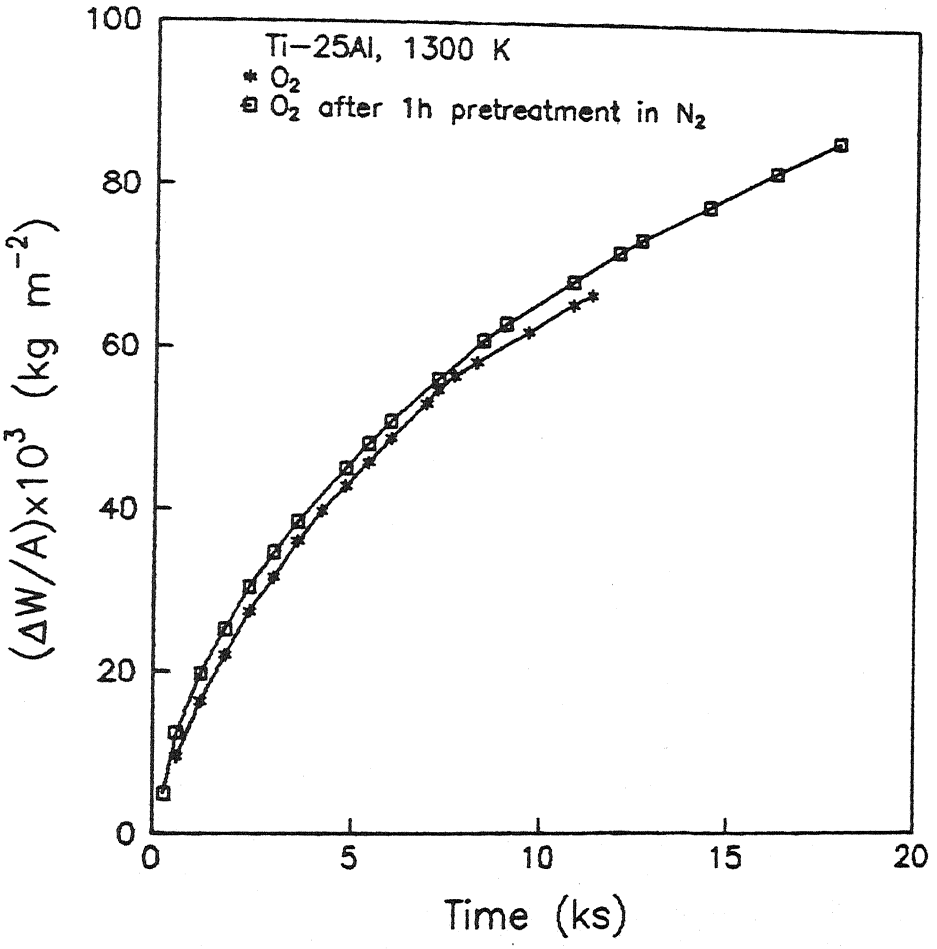

Fig.5.17: Plots of $(\frac{\Delta W}{A})$ versus time of Ti-25Al alloy for oxidation in oxygen at 1300 K with or without nitrogen pretreatment

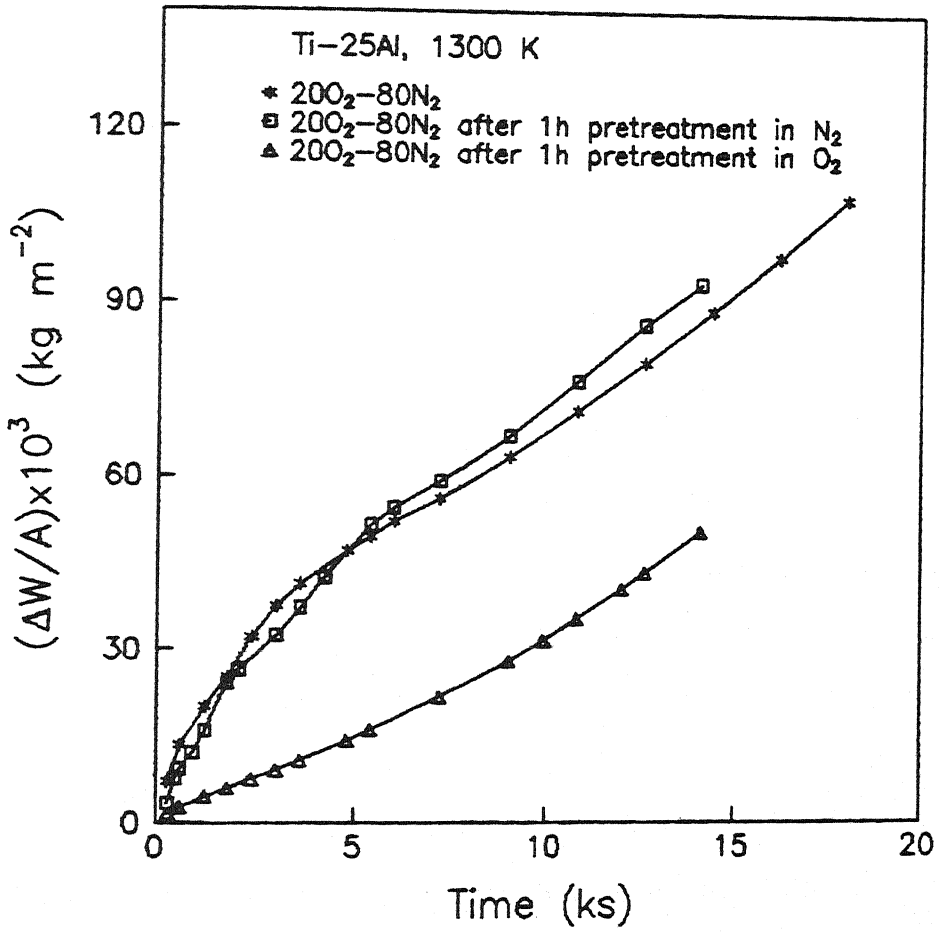

Fig.5.18: Plots of $(\frac{\Delta W}{A})$ versus time of Ti-25Al alloy for oxidation in 20 pct O_2-80 pct N_2 mixture at 1300 K after oxygen and nitrogen pretreatment and without any pretreatment

It is clear from the Figs.(5.17) and (5.18) that nitrogen pretreatment displayed virtually no beneficial role for alloy A whereas oxygen pretreatment was observed to be effective in lowering weight gain. The scales consisted of non-adherent yellow outer scale with adherent, non-compact greyish blue subscale. The scales formed in these conditions consisted of TiO_2 as the major and Al_2O_3 as minor phase. No TiN could be detected by XRD. From X-ray intensities it was observed that the amount of Al_2O_3 was more in oxygen pretreated specimen than that of nitrogen pretreated specimen. This might have provided some protection resulting in decreased weight gain. Examination of scale by SEM did not provide any further information about mechanism.

On the contrary Choudhury et al[68] observed N_2 to be detrimental during exposure of oxygen pretreated Ti-36Al (wt pct) alloys either in N_2 or air at 1223K. The preoxidation time was 24 hr. The XRD analyses did not reveal presence of N_2 containing phases in the oxidized sample. They proposed that N_2 might have caused breakdown of protective alumina scale.

Fig.5.19 presents the weight gain data for oxidation of alloy B in oxygen after nitrogen pretreatment, whereas Fig.5.20 shows the weight gain data for oxidation in 20 O_2 + 80 N_2 gas mixture after pretreatrent in N_2 and O_2. Again for comparison purposes the weight gain plots of oxidation of alloy B in O_2 and in 20 O_2 + 80 N_2 gas mixture without any pretreatment, have been included in Figs.(5.19) and (5.20) respectively. Table 4.4 summarizes the experimental conditions and some features of these experiments.

It is evident from Figs.(5.19) and (5.20) that nitrogen

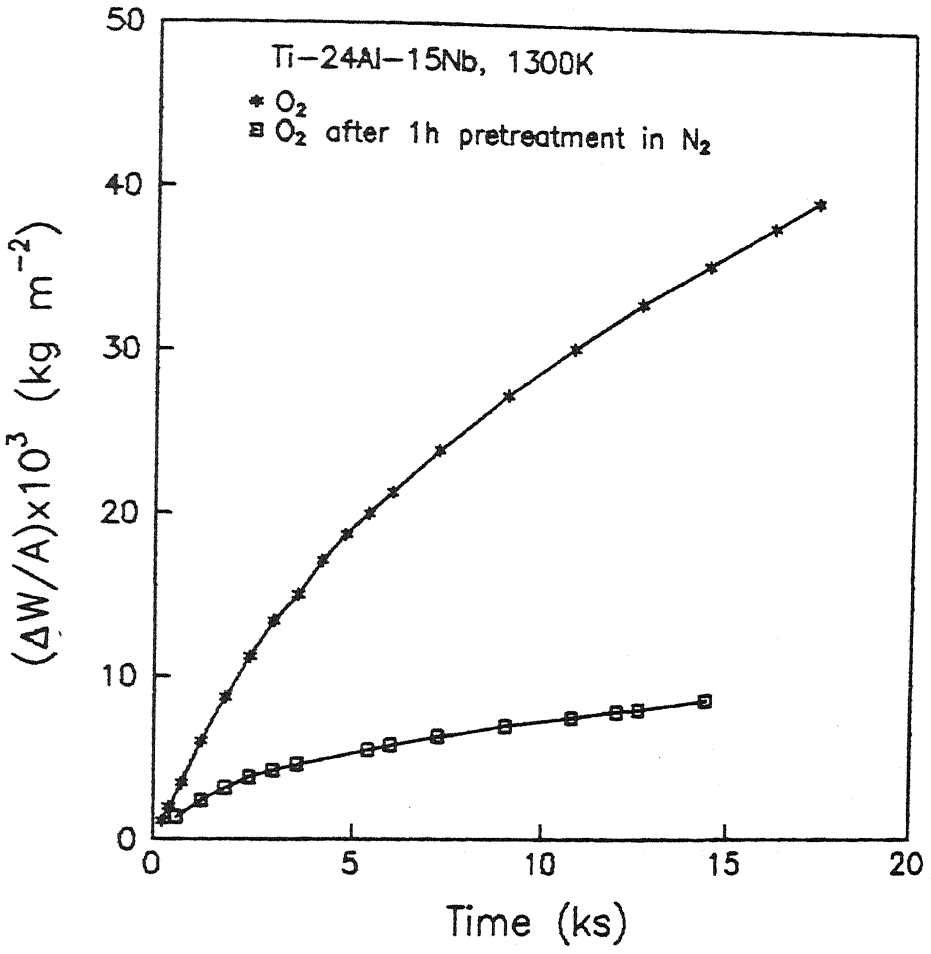

Fig.5.19: Plots of $(\frac{\Delta W}{A})$ versus time of Ti-24Al-15Nb alloy for oxidation in oxygen at 1300 K with or without nitrogen pretreatment

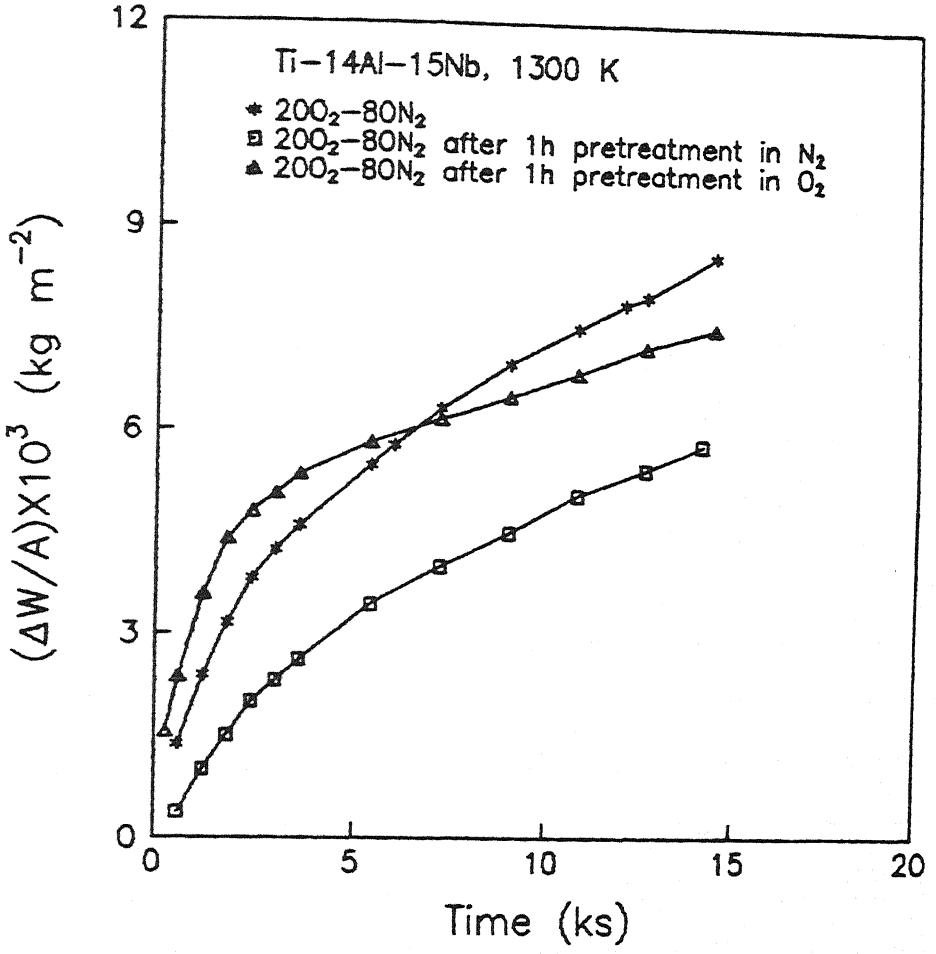

Fig.5.20: Plots of $(\frac{\Delta W}{A})$ versus time of Ti-24Al-15Nb alloy for oxidation in 20 pct O_2-80 pct N_2 mixture at 1300 K after oxygen and nitrogen pretreatment and without any pretreatment

pretreatment proved to be beneficial for alloy B in lowering weight gain during oxidation either in O_2 or in 20 O_2 + 80 N_2 gas mixture. The scales were mostly greyish blue, adherent and compact. The XRD studies revealed the presence of TiN in the specimens formed upon exposure to 20 O_2 + 80 N_2 gas mixture after pretreatment either in N_2 or O_2. However TiN could not be detected in the specimen oxidized in oxygen after N_2 pretreatment.

Beneficial effect of nitrogen on alloy B by retardation of weight gain has already been discussed in sec.5.3. The additional beneficial effect in sequential exposure may thus be attributed to the initial nitride layer formed during N_2 pretreatment period. Since it has been discussed in sec.5.3. already, no further discussions is necessary here.

5.6 EXPERIMENTS IN N_2-CO_2 GAS MIXTURE

These experiments were aimed to demonstrate the role of CO_2 in the oxidation behaviour of Ti_3Al-based titanium aluminides. Choudhury et al[68] commented that rapid oxidation rates of TiAl in air was due to N_2 and not caused by other impurities such as CO, CO_2 etc in the air. To verify the role of CO_2, alloy A (Ti-25Al) as well as alloy B (Ti-24Al-15Nb) were exposed to a gas mixture containing 95 pct N_2 and 5 pct CO_2 at 1300K (Expt. Nos. A13 and B17). The gas was passed through BTS furnace, anhydrous $CaCl_2$ and Drierite to remove oxygen and moisture.

For alloy A, rapid oxidation rates with a rate constant (k_p) of 2.36 x 10^{-6} $kg^2m^{-4}s^{-1}$ was obtained in N_2-CO_2 gas mixture against 1.78 x 10^{-8} $kg^2m^{-4}s^{-1}$ in N_2. Furthermore, the k_p was even approximately 5 times larger than that found in O_2 (Expt. No. A6).

Fig.5.4 has already presented cross sectional SEM photograph for oxidation of alloy A in oxygen at 1300K. Fig.5.21 shows the same in N_2-CO_2 gas mixture. The unusually high rate in the latter seems to be due to highly porous nature of the scale. The scale formed in presence of CO_2 was much thicker comprising a nonadherent yellow outer scale beneath which was a creamy inner scale. The outer scale spalled off considerably exposing metallic parts at some edges. The inner scale was porous with larger pore size than the outer scale. The XRD pattern revealed the presence of only TiO_2 and Al_2O_3 in the scale.

Fig.5.22 shows instantaneous rate constant (k_i) vs time plots for alloy A in experiments with N_2-CO_2, O_2 and N_2 at 1300K. For N_2-CO_2 as well as N_2 the large increase in k_i with time continuously is noteworthy. This may be attributed to increase in scale permeability and porousness with time. It may be noted that the value of m was 1.31 only for N_2-CO_2 when fitted with empirical equation (4.2). This was fairly close to linear rate of oxidation. Although similar k_i vs t plot was obtained for experiment in N_2, with value of m = 1.2, the rate was much lower. It has already been discussed in earlier sections that nitridation rates are lower than oxidation rates in these alloys and that explains this difference.

An important issue here is the enhancement of scale cracking, porosity and spallation in N_2-CO_2 atmosphere as compared to that in oxygen. Carbon dioxide is much less stable compared to titanium and aluminium oxides. Hence carbon dioxide is as much of an oxidizing agents as O_2. Its dissociation is likely to give rise to formation of CO or carbon. If carbon forms at the outer surface of the scale

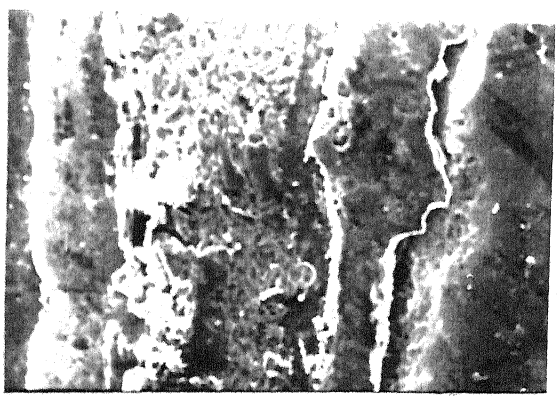

Fig.5.21: SEM micrograph of scale cross section of Ti-25Al alloy exposed in nitrogen containing 5 pct carbon dioxide at 1300 K

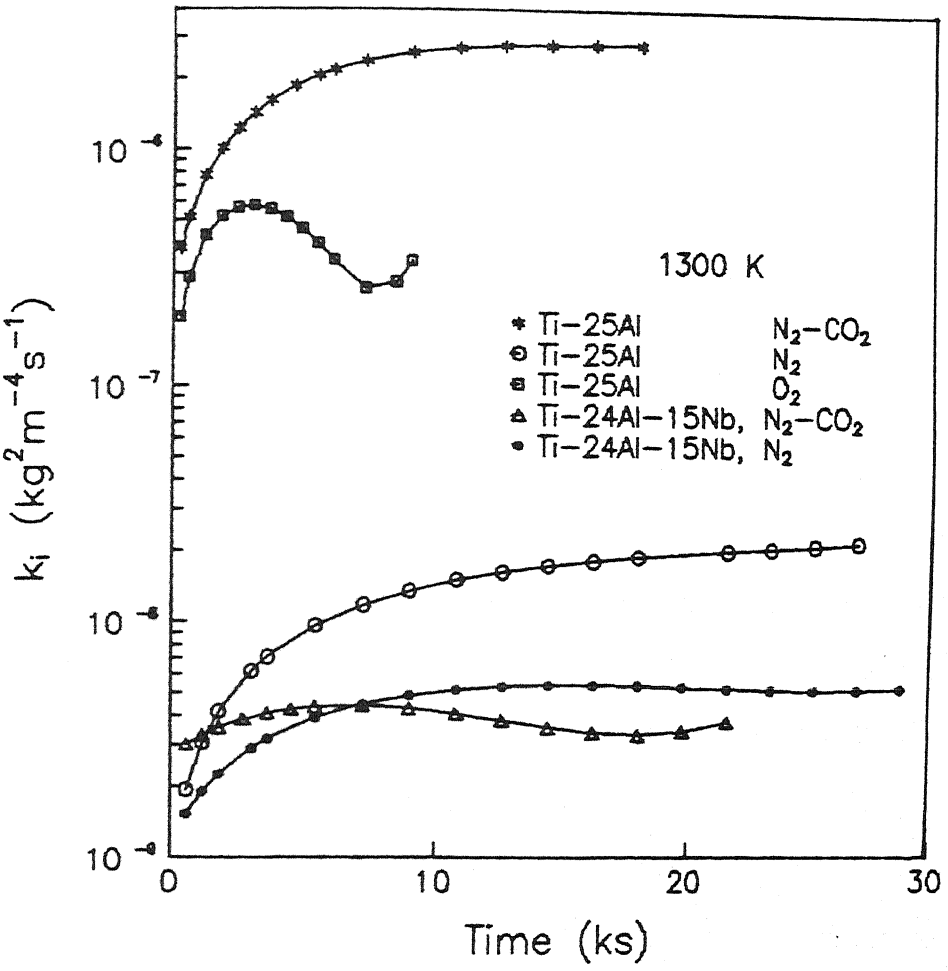

Fig.5.22: k_i versus time plots of Ti-25Al and Ti-24Al-15Nb alloys exposed to various environments at 1300 K

it is unlikely to have any effect on nature of scale. However, due to scale cracking and porousness carbon dioxide can diffuse to the interior of the scale and possibly may come in contact with alloy as well. Formation of carbon or a carbide like titanium carbide in the interior of the scale may be leading to generation of additional stresses causing this behaviour.

The effect of CO_2 on alloy B was observed to be negligible. The parabolic rate constant (k_p) was 3.97×10^{-9} $kg^2m^{-4}s^{-1}$ in N_2-CO_2 gas mixture as compared to 5.09×10^{-9} $kg^2m^{-4}s^{-1}$ in N_2, thus indicating similar rates. The nature of scales were also similar in both the cases with thin, adherent and compact scales. k_i vs time plots in Fig.5.22 demonstrate good agreement with parabolic law as is expected of a dense scale retaining uniformity with time. Both the scales constituted TiN and Al_2O_3 as minor phases in addition to TiO_2 as major oxide. Strong signals/reflections for matrix were also present in the XRD patterns. The nature of scale formed in this condition was similar to that obtained in nitrogen containg atmosphere. Here carbon dioxide was not able to penetrate and react directly with the alloy. Hence its role as an oxidant was restricted near the outer surface of the scale. The oxygen potential in the gas due to presence of CO_2 can not be estimated properly. The dissociation of CO_2 into CO and oxygen is represented as :

$$CO_2(g) = CO(g) + \frac{1}{2} O_2(g) \qquad \ldots(5.7)$$

and

$$K_7 = \frac{p_{CO}\, p_{O_2}^{1/2}}{p_{CO_2}} \qquad \ldots(5.8)$$

At high temperature, the equilibrium of the above reaction may be assumed. From free energy data at 1300K, $K_7 = 1.47 \times 10^{-7}$. Assuming that the gas did not have any oxygen before introduction into the furnace, $p_{CO} = 2\ p_{O_2}$ from stoichiometry of reaction (5.7). This gives us a value of equilibrium p_{O_2} in the gas as equal to 2.38×10^{-6} atm. As discussed in sec.5.4 that the BTS catalyst furnace was not able to lower oxygen to such a low level. Hence, addition of CO_2 to N_2 would not increase oxygen potential in nitrogen. In other words, so far as alloy B is concerned, CO_2 behaved like an inert gas.

5.7 SUBSURFACE MICROHARDNESS PROFILING AND DETERMINATION OF DIFFUSIVITIES IN THE ALLOYS

5.7.1 Subsurface Microhardness Profiles

Only some selected samples were considered for this. Microhardness measurements were taken from the scale/alloy interface to the interior of the alloy on the cross section of polished specimen. A diamond pyramid indentor with an optimised load of 20g was employed. The measurements were taken at magnification of 600X. Only for sample B exposed in oxygen at 1300K (Expt.No.B6), 30g load was used since at 20g load the indentations nearer to the interface were very small. The length of diagonal of the indentation was measured and microhardness values (MHv) were obtained using the following relation :

$$MHv = \frac{1854.4\ L}{d^2} \qquad \ldots(5.9)$$

here, L is load in g, and d is the length of diagonal in μm. The istance between two indentations was measured in μm from the entre to centre of the indentations. Fig.5.23 shows a SEM hotograph of an indented surface.

Figs.(5.24) to (5.27) present the microhardness profiles as unction of distance from scale/alloy interface to illustrate the ubscale hardening effect. Figs.(5.24) and (5.25) contain hardness alues for alloys A and B respectively, measured after exposure in xygen at different temperatures for approximately the same time. For alloy B a distinct hardness contour was obtained at 1300K. At other temperatures the hardness data lie within a scatter band with no discernible subscale hardening. In alloy A, although a higher value of hardness was obtained near the scale/alloy interface but no distinct hardness contour could be obtained due to large scatter in the experimental data.

As Figs.(5.26) and (5.27) reveal, the nature of hardness profiles were similar for both the alloys A (Ti-25Al) and B (Ti-24Al-15Nb) exposed to nitrogen at 1300K. The hardness values near the interface were approximately 900kg/mm^2 for alloy B and 750kg/mm^2 for alloy A. In 20 O_2 + 80 N_2 gas mixture, alloy A exhibited a subscale hardening with a distinct hardness contour. No such behaviour was observed for alloy B. On the contrary, the average hardness data were surprisingly higher compared to those for other conditions.

Subsurface hardening and microhardness measurements in titanium alloys by other investigators have been reviewed in sec. 2.7.1. Causes of subsurface hardening and consequent

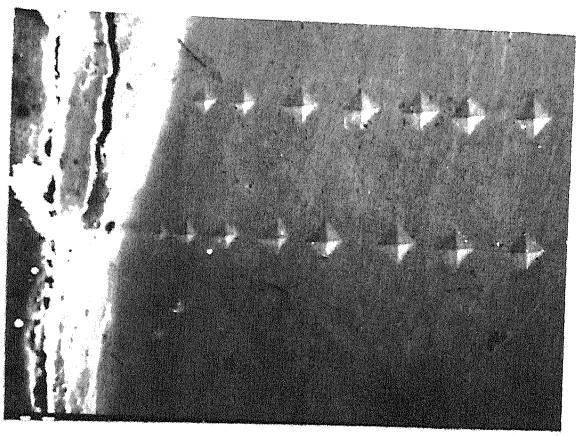

Fig.5.23: SEM micrograph of a typical indented surface after microhardness testing

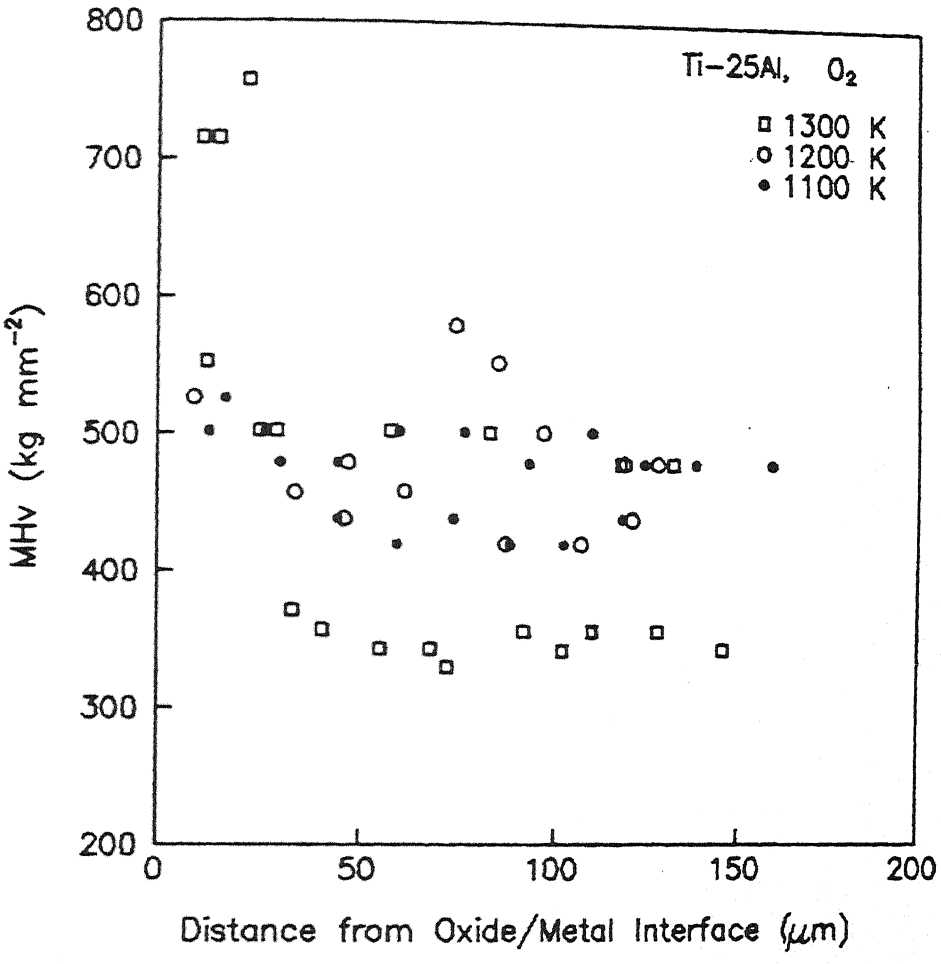

Fig.5.24: Microhardness profiles of Ti-25Al alloy exposed to oxygen at various temperatures

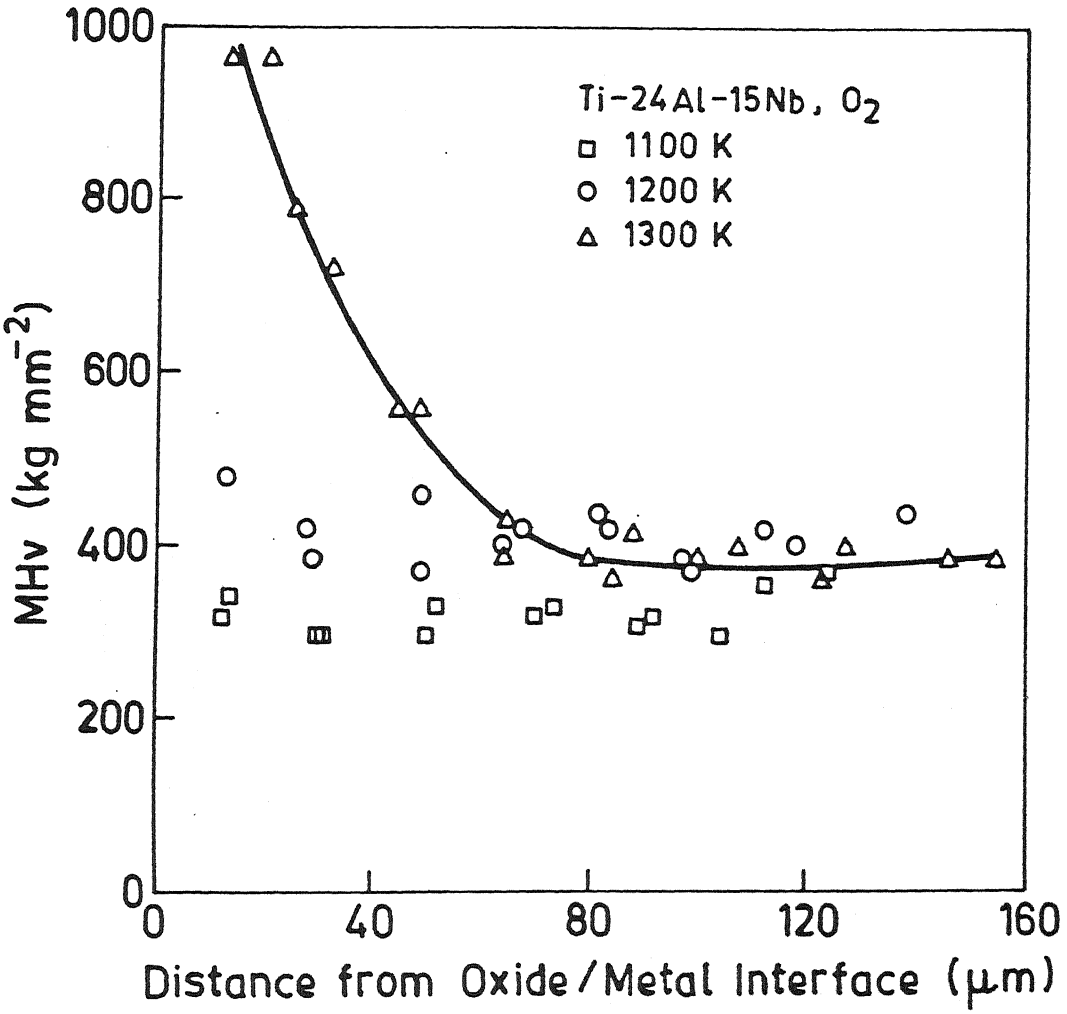

Fig.5.25: Microhardness profiles of Ti-24Al-15Nb alloy exposed to oxygen at various temperatures

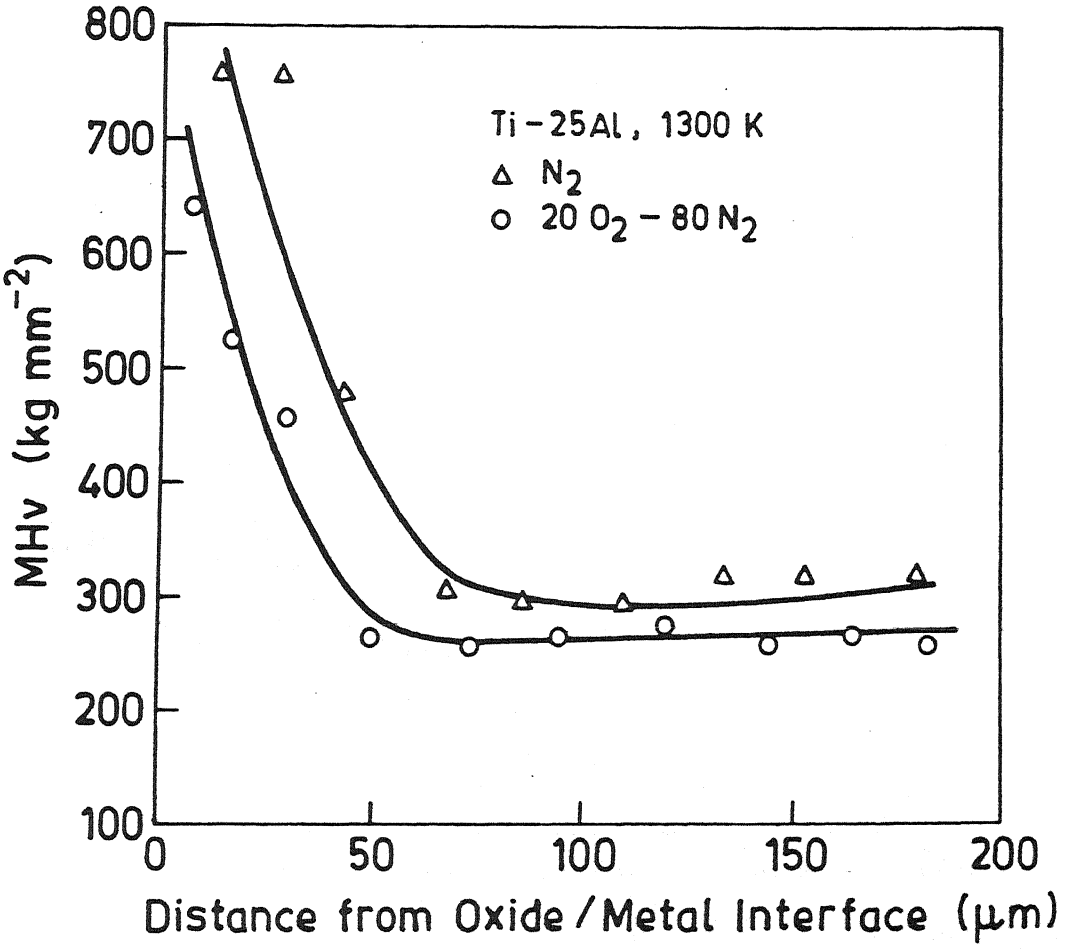

Fig.5.26: Microhardness profiles of Ti-25Al alloy exposed to nitrogen and 20 pct O_2-80 pct N_2 mixture at 1300 K

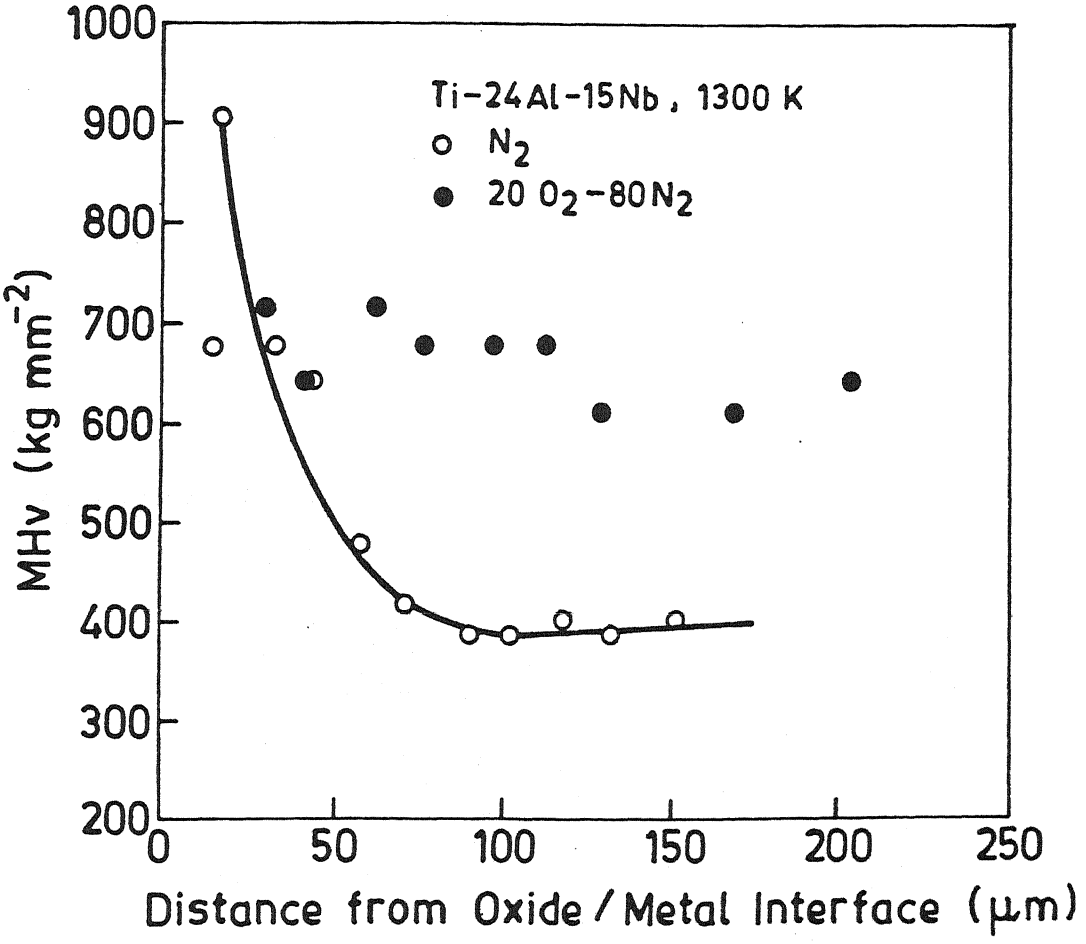

Fig.5.27: Microhardness profiles of Ti-24Al-15Nb alloy exposed to nitrogen and 20 pct O_2-80 pct N_2 mixture at 1300 K

embrittlement are dissolution of oxygen or nitrogen and internal oxidation of alloys.

Wallace et al[63] did not observe a clear increase in hardness value near the oxide/alloy interface for Ti-33Al-6Nb-1.4Ta (wt pct) after exposure in air at 1173K for 24 hr. Chaze and Coddet[59] observed the additive beneficial role of nitrogen and alloying elements (e.g. Al, Cr) in Ti in lowering the amount of dissolved oxygen. It may be noted here that alloy A exhibited lower hardness in O_2 - N_2 gas mixture compared to that in O_2 or nitrogen. This is in agreement with the findings of chaze and Coddet[59].

5.7.2 Determination of Diffusivities in the Alloys

From Figs.(5.24) to (5.27) it may be noted that depth of hardened subsurface zones varied from 50 to 80 μm. Attributing this variation to diffusion of oxygen and nitrogen into the alloys, estimation of diffusivity was made. Since the specimen surfaces were flat and the depths of diffusion fields were very small compared to the thickness of samples, it may be treated as unsteady diffusion through a semi-infinite flat specimen. The following assumptions were made further :

(i) single phase

(ii) no internal oxidation in diffusion field

(iii) constant D

(iv) constant C_s , i.e. $C_s \neq f(t)$

(v) concentration (C) α microhardness

The diffusion equation is :

$$\frac{C - C_o}{C_s - C_o} = 1 - \text{erf}\left(\frac{z}{2\sqrt{Dt}}\right) = \text{erfc}\left(\frac{z}{2\sqrt{Dt}}\right) \qquad \ldots(5.10)$$

where C = concentration of diffusing species at z after exposure time t, kg m^{-3}

C_o = bulk concentration, kg m^{-3}

C_s = surface concentration, kg m^{-3}

z = distance from alloy/scale interface, 10^{-6} m

t = time, s

and D = diffusivity (i.e. diffusion coefficient), $m^2 s^{-1}$

It may be noted from Figs.(5.24) to (5.27) that, for some experiments either the variation of microhardness with distance had too much scatter or too little variation. Determination of diffusivity for these would be unreliable. Only a few samples showed distinct hardness contours. As shown in Figs.(5.25) to (5.27), smooth curves were drawn through data points and diffusivity determination were made using Eq.5.10.

The technique consisted of picking up a pair of points on the smoothened microhardness vs distance curve and then follow the procedure noted below :

For two given points 1 and 2, the parameter Y_{12} could be obtained using Eq.5.10 and assumptions (iv) and (v) as,

$$Y_{12} = \left(\frac{C_1 - C_o}{C_s - C_o}\right) / \left(\frac{C_2 - C_o}{C_s - C_o}\right) = \frac{C_1 - C_o}{C_2 - C_o} = \frac{(MHv)_1 - (MHv)_o}{(MHv)_2 - (MHv)_o} \quad \ldots(5.11)$$

where $(MHv)_1$ = microhardness value at point 1, kg mm^{-2}

$(MHv)_2$ = microhardness value at point 2, kg mm^{-2}

and, $(MHv)_o$ = bulk microhardness value, kg mm^{-2}

Again,
$$Y_{12} = \frac{\text{erfc}\left(\frac{z_1}{2\sqrt{Dt}}\right)}{\text{erfc}\left(\frac{z_2}{2\sqrt{Dt}}\right)} \qquad \ldots(5.12)$$

For a given experiment only D is unknown in the Eq.5.12. Using error function table and by trial and error solution, values of D were obtained.

Table 5.3 presents the values of D at 1300K as obtained by the above procedure. From one curve several pairs of data points were chosen to obtain a set of diffusivity values. These have also been presented in Table 5.3. It may be noted that largest and smallest D values for a given experiment differed by approximately a factor of 3. This may be considered as fairly good in view of many simplifying assumptions.

Assumptions (i), (ii) and (iv) are questionable. Particularly alloys B (Ti-24Al-15Nb) and C (Ti-25Al-11Nb) can not be considered single phase since Nb stabilizes high temperature β phase. Al has strong affinity for oxygen, so formation of Al_2O_3 in the diffusion layer is likely to occur. Internal oxidation has been reported by some investigators[45,61] in Ti-Al (upto 50 atom pct Al) as well as in Ti-Al-Nb alloys. However Wiedemann et al[78] did not observe internal oxidation in Ti-25Al-11Nb (atom pct) alloy. Also the assumption of constant surface concentration (C_s) may not be valid.

Values of D_{av} also have been presented in Table 5.3. These may be taken as the diffusivity values determined from microhardness measurements in the present study. For the sake of comparison, some

values of diffusivities have also been compiled from literature sources. In Table 5.3 it may be noted that the values obtained in the present investigation are very close to those reported in literature for nitrogen and oxygen. Strafford and Towell[82] calculated diffusion coefficient of nitrogen in titanium following the technique as has been employed for the present study. The D values of nitrogen in alloys A and B for the present investigation were very close to those obtained by them. Diffusivities of oxygen in α-Ti were found to be approximately 2 orders of magnitude higher than those of nitrogen.

Table 5.3 Diffusion Coefficient of Oxygen and Nitrogen in Titanium and its Alloys

a) present study, at 1300K

System*	Gas composition	D (m^2s^{-1})	D_{av} (m^2s^{-1})
Ti-25Al(alloy A)	nitrogen	$3.12x10^{-14}$, $1.8x10^{-14}$, $9.82x10^{-15}$	$1.97x10^{-14}$
Ti-25Al(alloy A)	20 O_2+80 N_2	$8.67x10^{-14}$, $5.17x10^{-14}$, $3.07x10^{-14}$, $2.69x10^{-14}$	$4.9x10^{-14}$
Ti-24Al-15Nb (alloy B)	oxygen	$3.9x10^{-14}$, $3.7x10^{-14}$, $1.47x10^{-14}$, $1.16x10^{-14}$	$2.56x10^{-14}$
Ti-24Al-15Nb (alloy B)	nitrogen	$4.3x10^{-14}$, $2.93x10^{-14}$, $3.31x10^{-14}$, $8.51x10^{-15}$	$2.86x10^{-14}$

b) other sources

System*	Diffusing species	D (m^2s^{-1})	Temp. (K)	References
α-Ti	oxygen	$1.29x10^{-12}$	1300	91
Ti-2.27Nb	oxygen	$2.53x10^{-12}$	1300	77
Ti-25Al	oxygen	$3.40x10^{-13}$	1373	81
Ti-25Al-11Nb	oxygen	$3x10^{-14}$	1300	78
α-Ti	nitrogen	$3.21x10^{-14}$	1273	82
Ti-25Al	aluminium	$8x10^{-15}$	1373	81

* alloy composition in atom pct

CHAPTER 6

SUMMARY AND CONCLUSIONS

In the present investigation high temperature isothermal oxidation of three Ti_3Al-based alloys, viz., Ti-25Al, Ti-24Al-15Nb and Ti-25Al-11Nb (atom pct) has been studied. Some experiments have also been conducted to elucidate nitriding behaviour of these alloys. Various gases and gas mixtures employed were oxygen, nitrogen, oxygen-nitrogen, oxygen-argon and nitrogen-carbon dioxide at a total pressure of 1 atmosphere. The experiments in oxygen were carried out at several temperatures in the range of 1000 to 1300K, and in other gases and gas mixtures at two temperatures, viz. 1200 and 1300K. Out of the two niobium containing alloys, emphasis was given on Ti-24Al-15Nb, since this composition has not been properly investigated so far. Time of exposure in reactive environments ranged between 4 to 6 hr mostly. However, in some cases, 10 hr and 24 hr exposure times were also employed.

Polished samples of length, width and thickness within the ranges of 13 to 16 mm, 9 to 12 mm and 0.5 to 1.5 mm respectively, were employed for experiments. Sample inside the furnace was hung from a Cahn 1000 electrobalance to measure weight gain as function of time. The scales formed after exposure were examined by visual observation, X-ray diffraction, scanning electron microscope with energy dispersive X-ray analysis, and optical microscope. In addition, microhardness measurements were also made in the alloys adjacent to alloy/scale interface after some experiments.

6.1 DETERMINATION OF RATE CONSTANTS AND ASSESSMENT OF APPLICABILITY OF PARABOLIC RATE LAW AND POWER LAW OF OXIDATION

Weight gain per unit surface area of sample $(\frac{\Delta W}{A})$ vs time of exposure (t) data were processed by the following methods to determine rate constants for reaction in different gaseous environments and temperature. The principal reaction was oxidation. However in nitrogen bearing atmosphere some nitridation also occurred. Several experiments were repeated. Reproducibility of data amongst duplicate sets were satisfactory.

Method 1

The parabolic rate law was assumed, and accordingly the parabolic rate constant (k_p) was determined by linear regression fitting of $(\frac{\Delta W}{A})^2$ vs t data as per the following equation :

$$(\frac{\Delta W}{A})^2 = k_p t \qquad \ldots(2.6)$$

Method 2

Instantaneous parabolic rate constant (k_i), defined as; $k_i = \frac{d\,[(\frac{\Delta W}{A})^2]}{dt}$, was determined by regression fitting of $(\frac{\Delta W}{A})$ vs t data with the following fourth order polynomial,

$$(\frac{\Delta W}{A})^2 = a_1 + a_2 t + a_3 t^2 + a_4 t^3 + a_5 t^4 \qquad \ldots(4.1)$$

and then taking derivative of the same at various values of t. Average value of k_i (i.e. k_p') was determined as follows :

$$k_p' = \sum_{i=1}^{N} k_i t_i \Big/ \sum_{i=1}^{N} t_i \qquad \ldots(2.40)$$

Method 3

$(\frac{\Delta W}{A})$ vs t data were fitted with an empirical power law type relation viz.,

$$(\frac{\Delta W}{A})^m = k_m t \qquad \ldots(4.2)$$

where k_m and m were obtained by linear regression fitting of log $(\frac{\Delta W}{A})$ vs log t data.

The following conclusions were arrived at on the basis of the above data fitting exercise :

(i) Basically k_p and k_p' are the same. Only the procedure of determination is different. Good agreement was obtained between k_p and k_p' which indicates that reliability of evaluation of k_p was independent of method employed.

(ii) If parabolic rate law is obeyed well then k_i should be independent of time. However it was not so and k_i varied with time. Moreover the nature of variation did not have any systematic pattern. These indicated the complexity of the oxidation behaviour, and the variation may be attributed to variation of nature and properties of scale with time. Hence, to sum up, obedience to parabolic law was approximate only.

(iii) The values of exponent (m) of power law equation ranged between 1 to 1.86. For parabolic law the value of m should be 2. So, as a generalization the oxidation behaviour can be considered to be 'paralinear'.

(iv) The values of m exhibited large scatter as well as significant irreproducibility amongst duplicate sets. Also no trend

could be observed with variation of temperature.

(v) k_m/k_p was always greater then 1 and ranged between 2.3 and 302. Plots of k_m/k_p as function of m showed considerable scatter. However, as expected from mathematical considerations, a definite trend of increasing k_m/k_p with decreasing m was evident.

(vi) Reproducibility of parabolic rate constant (k_p) values amongst duplicate sets was good. Thus it may be concluded that parabolic rate law is more reliable in interpreting weight gain vs time data of the present investigation as compared to k_m. Hence k_p was adopted as a measure of rate for further interpretation of results.

6.2 OXIDATION BEHAVIOUR IN OXYGEN

(i) The parabolic rate constant (k_p) for oxidation of Ti-24Al-15Nb and Ti-25Al-11Nb in oxygen were almost the same at the same temperature. In general k_p values for Ti-25Al were 2 to 8 times larger as compared to those for Nb-containing alloys in the temperature range of 1100 to 1300K. However at 1000K the k_p values for all the three alloys were approximately the same.

(ii) Temperature dependence of k_p followed Arrhenius type equation. The 'effective activation energy' (Q_{eff}) was 289 kJ/mole for Ti-25Al in the temperature range of 1000 to 1300K. For Ti-24Al-15Nb and Ti-25Al-11Nb, Q_{eff} values were 329 and 330 kJ/mole respectively in the range of 1100 to 1300K.

(iii) The greyish or bluish scales were usually observed to be adherent and protective than the yellowish scales. In general, the scales were porous. However these were thinner, compact, and adherent for Nb-containing alloys. On the other hand Ti-25Al showed

significant scale spallation above 1100K.

(iv) The scales formed on these alloys were predominantly composed of TiO_2. However Al_2O_3 was also present as minor oxide. The outer scale in Ti-25Al was TiO_2, whereas in Nb-containing alloys it was mostly a mixture of Al_2O_3 and TiO_2. Nb was also detected by EDX in the inner scale. Improved oxidation resistance of Nb-containing alloys was attributed at least partially to the doping effect of Nb in reducing defect concentration of TiO_2.

6.3 OXIDATION AND NITRIDATION BEHAVIOUR IN N_2-O_2, O_2-Ar, N_2, and, N_2-CO_2 ATMOSPHERES

(i) At 1200K, in O_2-Ar gas mixtures, k_p for Ti-24Al-15Nb was found to be proportional to square root of p_{O_2} in the range of 0.2 to 1 atm. However in O_2-N_2 mixture, decrease of k_p was much more and approximately by an order of magnitude when p_{O_2} was lowered from 1 to 0.5 atm, and then became almost independent of p_{O_2}. On the other hand in Ti-25Al, k_p values were approximately the same for O_2-Ar as well as O_2-N_2 gas mixtures as in only O_2.

(ii) In 20 pct O_2 + 80 pct N_2 gas mixture, k_p for Ti-24Al-15Nb was approximately an order of magnitude lower at all temperatures as compared to those in O_2. However for Ti-25Al, k_p was similar in magnitude both in O_2-N_2 mixture and in O_2. Q_{eff} for oxidation of Ti-24Al-15Nb in 20 O_2 + 80 N_2 mixture was 274 kJ/mole in the temperature range of 1100 to 1300 K. However, for Ti-25Al, Q_{eff} was 351 kJ/mole in the temperature range between 1150 and 1300K.

(iii) For Nb-containing alloys, in addition to TiO_2 and Al_2O_3, TiN was also detected in the scales formed in O_2-N_2 mixture. TiN

could not be detected in scale formed in Ti-25Al at 1300K, but was detected at 1150K. This nitride layer seemed to have played an additional beneficial role in improving oxidation resistance of Nb-containing alloys whereas it showed no effect in Ti-25Al.

(iv) k_p in nitrogen for all alloys were found to be 15 to 25 times lower than those in oxygen at 1300K. However some oxidation also occurred. Use of getter lowered the rates only 3 to 5 times. Blank run in argon using getter showed some weight gain thus indicating that even gettering was not effective in removing traces of oxygen in the gas. To sum up, the rates of nitridation were slower than rates of oxidation by one to two orders of magnitude.

(v) In sequential oxidation studies at 1300K, nitrogen pretreatment was observed to be beneficial for Ti-24Al-15Nb in lowering weight gain during oxidation in oxygen and O_2-N_2 gas mixture. For Ti-25Al, N_2-pretreatment showed no effect. Presence of nitrogen in gas mixture has already been found to be beneficial for Nb-containing alloys. Thus additional beneficial effect may be attributed to the initial nitride layer formed during N_2-pretreatment. On the other hand O_2-pretreatment was beneficial for Ti-25Al only. Amount of Al_2O_3 was more in O_2-pretreated specimen than that in N_2-pretreated specimen. This seemed to have lowered the rate.

(vi) For Ti-25Al rapid weight gain was recorded in N_2 containing 5 pct CO_2. k_p was more than 130 times larger as compared to that in only nitrogen. k_p was even 5 times larger than that in oxygen. The scale formed in the gas mixture was much thicker, non-adherent and porous which resulted in scale permeability and

cracking and rapid oxidation by CO_2. On the other hand, the effect of CO_2 on Ti-24Al-15Nb was negligible, and the scale was compact and adherent. Thermodynamic considerations enabled explanation of the differing behaviours in the two alloys, and showed that in the latter case, CO_2 behaved as an inert gas only.

6.4 CONCLUDING REMARKS

(i) Microhardness measurements were carried out and considerable subscale hardening was observed in Ti-25Al and Ti-24Al-15Nb alloys after oxidation in O_2 at 1300K. Hardening was also observed after exposure either in N_2 or 20 pct O_2 + 80 pct N_2 gas mixture at 1300K for both the alloys. From hardness profiles, the values of diffusion coefficient (D) were evaluated assuming diffusion through a semi-infinite flat specimen and some other simplifying assumptions. Using error function table and trial and error solution, values of D were obtained. The D values in oxygen and nitrogen atmospheres were found to be almost the same for both the alloys. For example, at 1300K, D in Ti-24Al-15Nb were 2.56×10^{-14} and 2.86×10^{-14} $m^2 s^{-1}$ for oxygen and nitrogen respectively. The values are close to those reported in literature.

(ii) TiO_2 was the dominant oxide in the scale in almost all the conditions studied.

(iii) k_p, Q_{eff}, nature of scale etc. were compared with literature wherever possible. Findings were sometime in agreement, but not always.

(iv) Nb-containing alloys showed superior oxidation resistance as compared to that without Nb, irrespective of gas composition employed.

(v) Nitridation rates of these alloys were more than an order of magnitude lower than the oxidation rates.

6.5 SUGGESTIONS FOR FURTHER WORK

Some suggestions having bearing with the present study are as follows.

(i) For further understanding of the role of nitrogen and nitride formation, use of electron probe microanalyser (EPMA) would be very desirable. EPMA would also be useful in obtaining concentration profiles of oxygen and nitrogen in the alloy. This would allow determination of extent of dissolution of above elements in the alloy as well as diffusion coefficient more effectively. EPMA would also help further understanding of the scale.

(ii) Some investigations may be performed to assess the role of other alloying elements on oxidation behaviour.

(iii) Information on thermodynamic and phase diagram of the alloy as well as oxide phases are not satisfactorily available. Scope exists for further studies on these aspects.

(iv) To gain better understanding about transient phenomena, some experiments may be carried out with much longer exposure time.

(v) It would be desirable to perform more experiments to assess more comprehensively the role of carbon dioxide.

(vi) Cyclic oxidation studies are expected to provide more information on relative oxidation resistance of the alloys.

REFERENCES

1. R.W. Cahn : *Met. Mater. Process*, 1989, vol.1, pp.1.

2. R.L. Fleisher, D.M. Dimiduk, and H.A. Lipsitt : *Amer. Mater. Sci.*, 1989, vol.19, pp.231.

3. J.B. McAndrew and C.R. Simcoe : WADD Technical Report 60-99, Wright Patterson Air Force Base, 1960.

4. M.J. Blackburn, D.L. Ruckle, and C.E. Bevan : AFWAL Technical Report 78-18, Wright Patterson Air Force Base, 1978.

5. C.H. Ward : *Intl. Mater. Rev.*, 1993, vol.38, pp.79-101.

6. C.T. Liu, J.O. Stiegler, and F.H. Froes : *Metals Handbook*, ASM Intl., 10th edition, 1990, vol.2, pp.913-42.

7. J. Kumpfert and C.H. Ward : *Advanced Aerospace Materials*, H. Buhl, ed., MRE; Springer-Verlag, 1992, pp.73-83.

8. H.A. Lipsitt : *High Temperature Ordered Intermetallic Alloys*, C.C. Koch, C.T. Liu and N.S. Stoloff, eds., MRS, Pittsburgh, PA, 1985, vol.39, pp.351-64.

9. R.G. Rowe : *High Temperature Aluminides and Intermetallic*, S.H. Whang, C.T. Liu, D.P. Pope, and J.O. Stiegler, eds., TMS/ ASM INTERNATIONAL, Warrendale, PA, 1990, pp.375-401.

10. D.A. Koss, D. Banerjee, D.D. Lukasak, and A.K. Gogia : *High Temperature Aluminides and Intermetallic*, S.H. Whang, C.T. Liu, D.P. Pope, and J.O. Stiegler, eds.,TMS/ASM INTERNATIONAL, Warrendale, PA, 1990, pp.175-96.

11. F.H. Froes, C. Suryanarayan, and D. Eliezer : *ISIJ Intl.*, 1991, vol.31, pp.1235-48.

12. Y.W. Kim and F.H. Froes : *High Temperature Aluminides and Intermetallics*, S.H. Whang, C.T. Liu, D.P. Pope, and J.O. Stiegler, eds., TMS/ASM INTERNATIONAL,Warrendale, PA, 1990, pp.465-92.

13. D.M. Dimiduk, D.B. Miracle, Y.W. Kim and M.G. Mendiratta : *ISIJ Intl.*, 1991, vol.31, pp.1223-34.

14. F.H. Froes : *Space Age Metals Technology*, SAMPE, Covina, CA, 1988, pp.1-19.

15. J.M. Larsen, K.A. Williams, S.J. Balsone, and M.A. Stucke : *High Temperature Aluminides and Intermetallic*, S.H. Whang, C.T. Liu, D.P. Pope, and J.O. Stiegler, eds., TMS/ASM INTERNATIONAL, Warrendale, PA, 1990, pp.521-56.

16. P.L. Martin, M. Mendiratta, and H.A. Lipsitt : *Metall. Trans. A*, 1983, vol.14A, pp.2170-74.

17. N.S. Stoloff and R.G. Davies : *Prog. Mater. Sci.*, 1966, vol. 13, pp.1.

18. H.A. Lipsitt, D. Shechtman, and R.E. Schafrik : *Metall. Trans. A*, 1980, vol.11A, pp.1369-75.

19. S.M.L. Sastry and H.A. Lipsitt : *Titanium' 80 Science and Tech.*, H. Kimura and O. Izumi, eds., TMS-AIME, Warrendale, PA, 1980, vol.2, pp.1231-43.

20. D. Banerjee, T.K. Nandy, and A.K. Gogia : *Scripta Metall.*, 1987, vol.21, pp.597-600.

21. M. Khobaib and F.W. Vahldiek : *Space Age Metals Technology*, SAMPE Metals and Metals Processing Intl. Conf. Proc., F.H. Froes and R.A. Cull, eds., Dayton, Ohio, 1988, vol.2, pp.262-70.

22. Y. Umakoshi, M. Yamaguchi, T. Sakagami, and T. Yamane : *J. Mater. Sci.*, 1989, vol.24, pp.1599-1603.

23. S.J. Balsone : *Oxidation of High-Temperature Intermetallics*, T. Grobstein and J. Doychak, eds., TMS, Warrendale, PA, 1989, pp.219-34.

24. Y. Saitoh and K. Mino : *Mater. Trans. JIM*, 1993, vol.34, pp. 393-95.

25. J. Subrahmanyam : *J. Mat. Sci.*, 1988, vol.23, pp.1906-10.

26. D.L. Anton, D.M. Shah, D.N. Duhl, and A.F. Giamei : *J. Metals*, 1989, vol.41, No.7, pp.12-17.

pp.1-16.

43. C. Wagner : *Z. Elektrochem.*, 1959, vol.63, pp.772.

44. K.L. Luthra : *Oxid. Metals*, 1991, vol.36, pp.475-90.

45. G.H. Meier, D. Appalonia, R.A. Perkins, and K.T. Chiang : *Oxidation of High-Temperature Intermetallics*, T. Grobstein and J. Doychak, eds., TMS, Warrendale, PA, 1988, pp.185-93.

46. J.L. Murray and H.A. Wriedt : *Binary Alloy Phase Diagrams*, T.B. Massalski and B. Thaddeus, eds., ASM, Metals Park, Ohio, 1986.

47. M. Pajunen and J. Kivilahti : *Z. Metallkd.*, 1992, vol.83, pp.17-20.

48. V.V. Glazova : *Doklady Akad. Nauk SSSR*, 1965, vol.164, pp.567-570 (see ref.44).

49. S. Becker, A. Rahmel, M. Schorr, and M. Schütze : *Oxid. Metals*, 1992, vol.38, pp.425-64.

50. A. Rahmel and P.J. Spencer : *Oxid. Metals*, 1991, vol.35, pp.53-68.

51. M.X. Zhang, K.C. Hsieh, J. DeKock, and Y.A. Chang : *Scripta Metall.*, 1992, vol.27, pp.1361-66.

52. M. Hoch and R.Y. Lin : *Ternary Alloys - A Comprehensive Compendium of Evaluated Constitutional Data and Phase Diagrams*, G. Petzow and G. Effenberg, eds., MSI, VCH, FRG, 1993, vol.8, pp.79-88.

53. O. Kubaschewski, E.L. Evans and C.B. Alcock : *Metallurgical Thermochemistry*, 4th ed., Pergamon Press, Oxford, vol.1, 1967.

54. E.T. Turkdogan : *Physical Chemistry of High Temperature Technology*, Academic Press, 1980.

55. C.E. Wicks and F.E. Block : *Thermodynamic Properties of 65 Elements - Their Oxides, Halides, Carbides and Nitridies*, Burean of Mines, Bulletin 605, U.S. Government Printing Office, Washington D.C., 1963.

56. A.E. Palty, H. Margolin, and J.P. Nielsen : *Trans. Amer. Soc.*

Metals, Amer. Soc. for Metals, 1954, vol.64, pp.312-28.

57. P. Kofstad, P.B. Anderson, and O.J. Krudtaa : *J. Less Common Metals*, 1961, vol.3, pp.89-97.

58. R.L. Rawe and C.J. Rosa : *Oxid. Metals*, 1980, vol.14, pp. 549-66.

59. A.M. Chaze and C. Coddet : *J. Less Common Metals*, 1986, vol. 124, pp.73-84.

60. A.I. Kahveci, G. Welsch, and G.E. Wasielewski : *Proc. of 6th World Conf. on Titanium*, P. Lacombe, R. Tricot, and G. Béranger, eds., Soc. Francaise de Méitallurgie, France, 1988, vol.2, pp.1015-1019.

61. G. Welsch and A.I. Kahveci : *Oxidation of High-Temperature Intermetallics*, T. Grobstein and J. Doychak, eds., TMS, Warrendale, PA, 1988, pp.207-18.

62. S.N. Sankaran, R.K. Clark, J. Unnam, and K.E. Wiedemann : NASA Tech. Paper, TP3012, 1990, pp.22.

63. T.A. Wallace, R.K. Clark, S.N. Sankaran, and K.E. Wiedemann : *Environmental Effects on Advanced Materials*, R.H. Jones and R.E. Ricker, eds., TMS, Warrendale, PA, 1991, pp.79-89.

64. T.A. Wallace, R.K. Clark, K.E. Wiedemann, and S.N. Sankaran : *Oxid. Metals*, 1992, vol.37, pp.111-24.

65. J.C. Schaeffer : *Scripta Metall.*, 1993, vol.28, pp.791-96.

66. R.A. Perkins, K.T. Chiang and G.H. Meier : *Scripta Metall.*, 1987, vol.21, pp.1505-10.

67. R.A. Perkins, K.T. Chiang, G.H. Meier, and R. Miller : *Oxidation of High-Temperature Intermetallics*, T. Grobstein and J. Doychak, eds., TMS, Warrendale, PA, 1988, pp.157-69.

68. N.S. Choudhury, H.C. Graham and J.W. Hinze : *Proc. of Symp. on Properties of High Temperature Alloys*, Z.A. Foroulis and F.S. Pettit, eds., Electrochem. Soc. Proc., 1976, vol.77-1, pp.668-80.

69. Y.W. Kim : *J. Metals*, 1989, vol.41, No.7, pp.24-30.

70. K. Hirukawa, H. Mabuchi, and Y. Nakayama : *Scripta Metall.*, 1991, vol.25, pp.1211-16.

71. R. Prescott and M.J. Graham : *Oxid. Metals*, 1992, vol.38, pp.233-53.

72. K. Maki, M. Shioda, M. Sayashi, T. Shimizu, and S. Isobe : *Second Intl. ASM Conf. on High Temperature Aluminides and Intermetallics*, II, Proc. Conf., California, USA, 1991.

73. M. Hoch : Unpublished Research (see ref.68).

74. K. Hauffe : *Oxidation of Metals*, Plenum Press, 1965.

75. L. Singheiser, H.W. Grünling, and K. Schneider : *High Temperature Materials for Power Engg., II Proc. Conf.*, Liége, Belgium, 1990, pp.1687-1702.

76. G. Chen, Z. Sun, and Z. Zhou : *Corrosion*, 1992, vol.48, pp. 939-46.

77. Y.S. Chen and C.J. Rosa : *Oxid. Metals*, 1980, vol.14, pp. 147-165.

78. K.E. Wiedemann, S.N. Sankaran, R.K. Clark, and T.A. Wallace : *Oxidation of High-Temperature Intermetallics*, T. Grobstein and J. Doychak, eds., TMS, Warrendale, PA, 1988, pp.195-206.

79. M.P. Brady, R.J. Hanrahan, Jr., S.P. Elder Randall, and E.D. Verink, Jr. : *Scripta Metall.*, 1992, vol.26, pp.767-70.

80. A. Takasaki, K. Ojima, Y. Taneda, T. Hoshiya, and A. Mitsuhashi : *J. of Mat. Sci.*, 1993, vol.28, pp.1067-73.

81. Y. Shida and H. Anada : *Mater. Trans. JIM*, 1993, vol.34, pp.236-42.

82. K.N. Strafford and J.M. Towell : *Oxid. Metals*, 1976, vol.10, pp.41-67.

83. D.W. McKee : *High Temperature Ordered Intermetallic Alloys V*, Mat. Res. Soc. Symp. Proc., MRS, 1993, vol.288, pp.953-58.

84. P. Grahale, B. Heine, and E. Fromm : Max-Planck Institut für Metallforschung, Dornier Luft-fahrt, Werkst, Korros, 1991,

vol.42, pp.12-18.

85. J.L. Smialek, M.A. Gedwill, and P.K. Brindley : *Scripta Metall.*, 1990, vol.24, pp.1291-96.

86. *Metals Handbook*, ASM, Metals Park, Ohio, 8th ed., 1972, vol.7, pp.321-34.

87. G.G. Gawrilov : *Chemical (Electroless) Nickel Plating*, Portcullis Press Ltd., Redhill, Surrey, 1979.

88. W.D. Fields, R.N. Duncan, and J.R. Zickgraf : *Metals Handbook*, ASM, Metals Park, Ohio, 9th ed., 1982, vol.5, pp.219-43.

89. K.R. Trethewey and J. Chamberlain : *Corrosion for Students of Science and Engineering*, John Longman Scientific and Technical, 1988.

90. D.S. Rickerby and A. Matthews : *Advanced Surface Coatings- a Handbook of Surface Engineering*, D.C. Rickerby and A. Matthews, eds., Blackie, Chapman and Hall, New York, 1991.

91. Z. Liu and G. Welsch : *Metall. Trans. A*, 1988, vol.19A, pp.1121-25.

92. P. Kofstad : *Nonstoichiometry, Diffusion, and Electrical Conductivity in Binary Metal Oxides*, New York, Wiley Interscience, 1972, pp.146-48.

93. A. Münster and G. Schlamp : *Z. Phys. Chem.*, Leipzig, 1957, vol.13, pp.76.

94. N. R. McDonald and G. R. Wallwork : *Oxid. Metals*, 1970, vol.2, pp.263.

APPENDIX A

WEIGHT GAIN PER UNIT SURFACE AREA VERSUS TIME DATA

Experiment No. = A1
Temperature (K) = 1000.00
Sample area (m sq.) =0.3990E-03

Time (ks)	dW/A (kg/m sq.)
1.80	0.155E-03
3.60	0.271E-03
7.20	0.451E-03
10.80	0.622E-03
14.40	0.772E-03
18.00	0.927E-03
21.60	0.112E-02
25.20	0.130E-02
28.80	0.142E-02
32.40	0.158E-02
36.00	0.173E-02
39.60	0.190E-02
43.20	0.202E-02
46.80	0.213E-02
50.40	0.222E-02
54.00	0.239E-02
57.60	0.255E-02
64.80	0.269E-02
72.00	0.291E-02
79.20	0.323E-02
85.50	0.334E-02

Experiment No. = A2
Temperature (K) = 1100.00
Sample area (m sq.) =0.4470E-03

Time (ks)	dW/A (kg/m sq.)
0.60	0.805E-03
1.20	0.143E-02
1.80	0.206E-02
3.00	0.268E-02
3.60	0.304E-02
4.20	0.331E-02
4.80	0.358E-02
5.40	0.385E-02
7.20	0.456E-02
9.00	0.501E-02
10.80	0.546E-02
12.42	0.573E-02
14.22	0.609E-02
15.00	0.626E-02
16.80	0.662E-02
18.00	0.680E-02

Experiment No. = A2r
Temperature (K) = 1100.00
Sample area (m sq.) =0.3880E-03

Time (ks)	dW/A (kg/m sq.)
0.60	0.825E-03
1.20	0.144E-02
1.80	0.196E-02
2.22	0.227E-02
3.42	0.309E-02
5.40	0.392E-02
6.60	0.433E-02
7.80	0.485E-02
8.40	0.495E-02
10.20	0.536E-02
11.40	0.557E-02
12.72	0.588E-02
14.82	0.629E-02
15.42	0.639E-02

Experiment No. = A3
Temperature (K) = 1150.00
Sample area (m sq.) =0.4140E-03

Time (ks)	dW/A (kg/m sq.)
0.60	0.150E-02
1.20	0.213E-02
1.80	0.271E-02
3.60	0.415E-02
5.40	0.551E-02
7.20	0.715E-02
9.00	0.870E-02
10.80	0.986E-02
12.60	0.103E-01
14.40	0.112E-01
16.20	0.123E-01
18.00	0.133E-01
19.80	0.144E-01
21.60	0.154E-01
23.40	0.164E-01
25.20	0.172E-01
27.00	0.180E-01
28.80	0.188E-01
30.60	0.195E-01
32.40	0.200E-01
34.20	0.207E-01
37.50	0.219E-01

Experiment No. = A3r
Temperature (K) = 1150.00
Sample area (m sq.) =0.4050E-03

Time (ks)	dW/A (kg/m sq.)
0.60	0.148E-02
1.20	0.198E-02
1.80	0.257E-02
3.60	0.393E-02
5.40	0.519E-02
7.20	0.652E-02
9.00	0.751E-02
10.80	0.869E-02
12.60	0.968E-02
14.40	0.105E-01
16.56	0.117E-01
18.36	0.124E-01
19.80	0.132E-01
21.96	0.144E-01
23.40	0.150E-01
25.56	0.160E-01
27.36	0.178E-01
28.80	0.185E-01
30.60	0.191E-01
32.76	0.198E-01

Experiment No. = A4
Temperature (K) = 1200.00
Sample area (m sq.) =0.4080E-03

Time (ks)	dW/A (kg/m sq.)
0.24	0.118E-02
0.42	0.186E-02
0.78	0.304E-02
1.08	0.490E-02
1.80	0.735E-02
2.70	0.951E-02
5.10	0.110E-01
5.40	0.117E-01
7.20	0.154E-01
9.00	0.172E-01
9.30	0.175E-01
10.80	0.185E-01
12.60	0.206E-01
14.40	0.232E-01
16.20	0.258E-01
18.00	0.274E-01
19.80	0.279E-01
20.16	0.291E-01

Experiment No. = A4r
Temperature (K) = 1200.00
Sample area (m sq.) =0.4370E-03

Time (ks)	dW/A (kg/m sq.)
0.48	0.211E-02
0.72	0.339E-02
0.96	0.513E-02
1.20	0.632E-02
1.80	0.824E-02
3.60	0.125E-01
5.40	0.167E-01
7.20	0.186E-01
9.00	0.204E-01
10.80	0.224E-01
12.60	0.254E-01
14.40	0.275E-01
16.20	0.294E-01
16.80	0.298E-01
18.00	0.309E-01
19.56	0.323E-01
20.40	0.330E-01

Experiment No. = A5
Temperature (K) = 1250.00
Sample area (m sq.) =0.4070E-03

Time (ks)	dW/A (kg/m sq.)
0.60	0.452E-02
1.20	0.806E-02
1.80	0.115E-01
2.40	0.138E-01
2.58	0.143E-01
3.60	0.169E-01
4.50	0.185E-01
5.40	0.203E-01
5.88	0.214E-01
6.60	0.231E-01
6.90	0.236E-01
7.80	0.259E-01
8.40	0.272E-01
9.00	0.287E-01
9.78	0.304E-01
10.38	0.309E-01

Experiment No. = A5r
Temperature (K) = 1250.00
Sample area (m sq.) =0.4030E-03

Time (ks)	dW/A (kg/m sq.)
0.30	0.357E-02
0.60	0.665E-02
1.20	0.107E-01
1.80	0.138E-01
2.40	0.163E-01
3.00	0.185E-01
3.30	0.194E-01
3.60	0.200E-01
4.32	0.214E-01
4.80	0.225E-01
5.40	0.237E-01
6.00	0.252E-01
7.20	0.278E-01
9.00	0.316E-01
10.80	0.349E-01
12.00	0.372E-01
12.60	0.383E-01
13.80	0.405E-01

Experiment No. = A6
Temperature (K) = 1300.00
Sample area (m sq.) =0.4060E-03

Time (ks)	dW/A (kg/m sq.)
0.60	0.946E-02
1.20	0.163E-01
1.80	0.220E-01
2.40	0.274E-01
3.00	0.316E-01
3.60	0.361E-01
4.20	0.398E-01
4.80	0.429E-01
5.40	0.458E-01
6.00	0.488E-01
6.90	0.531E-01
7.20	0.548E-01
7.62	0.565E-01
8.22	0.582E-01
9.60	0.620E-01
10.80	0.654E-01
11.28	0.666E-01
12.60	0.715E-01
14.40	0.778E-01
15.60	0.820E-01
16.20	0.843E-01
16.80	0.869E-01

Experiment No. = A6r
Temperature (K) = 1300.00
Sample area (m sq.) =0.3960E-03

Time (ks)	dW/A (kg/m sq.)
0.30	0.768E-02
0.60	0.134E-01
1.20	0.203E-01
1.80	0.263E-01
2.40	0.316E-01
3.00	0.361E-01
3.60	0.404E-01
4.20	0.453E-01
4.80	0.486E-01
5.40	0.508E-01
6.00	0.527E-01
7.20	0.560E-01
8.40	0.588E-01
9.00	0.604E-01

Experiment No. = A7
Temperature (K) = 1300.00
Sample area (m sq.) =0.4000E-03

Time (ks)	dW/A (kg/m sq.)
0.60	0.850E-03
1.20	0.150E-02
1.80	0.205E-02
3.00	0.315E-02
3.60	0.365E-02
5.40	0.535E-02
7.20	0.695E-02
9.00	0.840E-02
10.80	0.995E-02
12.60	0.113E-01
14.40	0.125E-01
16.20	0.137E-01
18.00	0.150E-01
19.80	0.160E-01
21.60	0.172E-01
23.40	0.183E-01
25.20	0.191E-01
27.00	0.201E-01
28.80	0.212E-01
30.60	0.222E-01
32.40	0.231E-01
34.20	0.241E-01
36.00	0.250E-01

Experiment No. = A8*
Temperature (K) = 1200.00
Sample area (m sq.) =0.4010E-03

Time (ks)	dW/A (kg/m sq.)
0.60	0.274E-03
1.20	0.449E-03
1.80	0.579E-03
2.40	0.868E-03
3.60	0.113E-02
5.40	0.158E-02
7.20	0.193E-02
9.00	0.224E-02
10.80	0.259E-02
12.60	0.280E-02
14.40	0.308E-02
16.20	0.329E-02
18.00	0.340E-02

Experiment No. = A9*
Temperature (K) = 1300.00
Sample area (m sq.) =0.4070E-03

Time (ks)	dW/A (kg/m sq.)
0.60	0.786E-03
1.20	0.133E-02
1.80	0.172E-02
2.40	0.205E-02
3.00	0.242E-02
3.60	0.268E-02
5.40	0.348E-02
7.20	0.423E-02
9.00	0.493E-02
10.80	0.571E-02
12.60	0.633E-02
14.40	0.690E-02
16.20	0.742E-02
17.40	0.780E-02

Experiment No. = A10
Temperature (K) = 1150.00
Sample area (m sq.) =0.3990E-03

Time (ks)	dW/A (kg/m sq.)
0.60	0.652E-03
1.20	0.145E-02
1.80	0.195E-02
3.00	0.311E-02
3.60	0.366E-02
5.40	0.511E-02
7.20	0.637E-02
9.00	0.757E-02
10.80	0.872E-02
12.60	0.982E-02
14.40	0.108E-01
15.00	0.111E-01

Experiment No. = A11
Temperature (K) = 1200.00
Sample area (m sq.) =0.4290E-03

Time (ks)	dW/A (kg/m sq.)
0.60	0.149E-02
1.20	0.280E-02
1.80	0.420E-02
2.76	0.653E-02
3.12	0.718E-02
3.72	0.876E-02
5.40	0.124E-01
7.20	0.157E-01
9.00	0.186E-01
10.80	0.211E-01
12.60	0.235E-01
14.40	0.256E-01
15.60	0.269E-01

Experiment No. = A12
Temperature (K) = 1300.00
Sample area (m sq.) =0.3990E-03

Time (ks)	dW/A (kg/m sq.)
0.30	0.722E-02
0.60	0.134E-01
1.20	0.201E-01
1.80	0.252E-01
2.40	0.321E-01
3.00	0.375E-01
3.60	0.413E-01
4.80	0.470E-01
5.40	0.495E-01
6.00	0.521E-01
7.20	0.561E-01
9.00	0.633E-01
10.80	0.712E-01
12.60	0.795E-01
14.40	0.884E-01
16.20	0.979E-01
18.00	0.108E+00

Experiment No. = A13
Temperature (K) = 1300.00
Sample area (m sq.) =0.4160E-03

Time (ks)	dW/A (kg/m sq.)
0.30	0.962E-02
0.60	0.153E-01
1.20	0.250E-01
1.80	0.341E-01
2.40	0.424E-01
3.00	0.513E-01
3.60	0.598E-01
4.50	0.723E-01
5.40	0.835E-01
6.00	0.903E-01
7.20	0.104E+00
9.00	0.124E+00
10.80	0.143E+00
12.60	0.159E+00
14.40	0.174E+00
16.20	0.188E+00
18.00	0.202E+00

Experiment No. = A14
Temperature (K) = 1200.00
Sample area (m sq.) =0.4120E-03

Time (ks)	dW/A (kg/m sq.)
0.60	0.126E-02
1.26	0.282E-02
1.56	0.335E-02
2.40	0.524E-02
3.24	0.723E-02
5.40	0.121E-01
7.20	0.158E-01
9.00	0.191E-01
10.80	0.221E-01
12.60	0.245E-01
14.40	0.266E-01
15.00	0.270E-01
15.60	0.276E-01

Experiment No. = A15*
Temperature (K) = 1200.00
Sample area (m sq.) =0.4190E-03

Time (ks)	dW/A (kg/m sq.)
0.60	0.878E-03
1.20	0.157E-02
1.80	0.206E-02
3.00	0.297E-02
3.60	0.336E-02
4.50	0.390E-02
5.40	0.444E-02
7.20	0.550E-02
9.00	0.660E-02
10.80	0.762E-02
12.60	0.872E-02
14.40	0.983E-02
16.20	0.109E-01
18.00	0.120E-01

Experiment No. = A16
Temperature (K) = 1300.00
Sample area (m sq.) =0.3960E-03

Time (ks)	dW/A (kg/m sq.)
0.30	0.495E-02
0.60	0.124E-01
1.20	0.197E-01
1.80	0.252E-01
2.40	0.304E-01
3.00	0.347E-01
3.60	0.385E-01
4.80	0.451E-01
5.40	0.481E-01
6.00	0.509E-01
7.20	0.561E-01
8.40	0.609E-01
9.00	0.630E-01
10.80	0.682E-01
12.00	0.719E-01
12.60	0.735E-01
14.40	0.777E-01
16.20	0.820E-01
17.88	0.859E-01

Experiment No. = A17
Temperature (K) = 1300.00
Sample area (m sq.) =0.3760E-03

Time (ks)	dW/A (kg/m sq.)
0.30	0.340E-02
0.48	0.766E-02
0.60	0.936E-02
0.90	0.121E-01
1.20	0.159E-01
1.80	0.243E-01
2.10	0.265E-01
3.00	0.324E-01
3.60	0.372E-01
4.20	0.424E-01
5.40	0.515E-01
6.00	0.545E-01
7.20	0.591E-01
9.00	0.669E-01
10.80	0.763E-01
12.60	0.861E-01
14.10	0.932E-01

Experiment No. = A18
Temperature (K) = 1300.00
Sample area (m sq.) =0.4110E-03

Time (ks)	dW/A (kg/m sq.)
0.30	0.151E-02
0.60	0.273E-02
1.20	0.453E-02
1.80	0.603E-02
2.40	0.764E-02
3.00	0.915E-02
3.60	0.108E-01
4.80	0.142E-01
5.40	0.160E-01
7.20	0.218E-01
9.00	0.280E-01
9.90	0.315E-01
10.80	0.353E-01
12.00	0.405E-01
12.60	0.433E-01
14.10	0.504E-01

Experiment No. = B1
Temperature (K) = 1000.00
Sample area (m sq.) =0.3270E-03

Time (ks)	dW/A (kg/m sq.)
1.80	0.208E-03
3.60	0.281E-03
7.20	0.520E-03
10.80	0.758E-03
14.40	0.966E-03
18.00	0.109E-02
21.60	0.120E-02
25.20	0.139E-02
28.80	0.150E-02
32.40	0.167E-02
36.00	0.182E-02
39.60	0.197E-02
43.20	0.206E-02
46.80	0.222E-02
50.40	0.240E-02
57.60	0.263E-02
64.80	0.267E-02
73.80	0.283E-02
79.20	0.301E-02
86.10	0.325E-02

Experiment No. = B2
Temperature (K) = 1100.00
Sample area (m sq.) =0.4000E-03

Time (ks)	dW/A (kg/m sq.)
0.60	0.400E-03
1.20	0.600E-03
1.80	0.800E-03
3.00	0.100E-02
3.60	0.110E-02
4.80	0.130E-02
6.60	0.160E-02
9.00	0.180E-02
10.80	0.200E-02
12.00	0.220E-02
13.20	0.250E-02
16.20	0.280E-02
18.00	0.310E-02
19.80	0.335E-02
21.60	0.355E-02

Experiment No. = B2r
Temperature (K) = 1100.00
Sample area (m sq.) =0.3580E-03

Time (ks)	dW/A (kg/m sq.)
0.60	0.391E-03
1.20	0.447E-03
1.80	0.670E-03
3.60	0.117E-02
4.80	0.145E-02
6.00	0.156E-02
7.20	0.168E-02
9.00	0.201E-02
10.80	0.223E-02

Experiment No. = B3
Temperature (K) = 1150.00
Sample area (m sq.) =0.3480E-03

Time (ks)	dW/A (kg/m sq.)
0.60	0.690E-03
1.20	0.920E-03
1.80	0.115E-02
3.60	0.138E-02
5.40	0.172E-02
7.20	0.207E-02
9.00	0.276E-02
11.10	0.322E-02
12.60	0.368E-02
14.40	0.414E-02
16.50	0.483E-02
19.20	0.540E-02
21.00	0.586E-02
22.80	0.621E-02
25.50	0.690E-02
27.30	0.736E-02

Experiment No. = B3r
Temperature (K) = 1150.00
Sample area (m sq.) =0.3470E-03

Time (ks)	dW/A (kg/m sq.)
0.60	0.403E-03
1.20	0.692E-03
1.80	0.104E-02
3.60	0.150E-02
5.40	0.196E-02
6.00	0.207E-02
7.20	0.242E-02
9.00	0.300E-02
10.80	0.346E-02
12.00	0.392E-02
12.60	0.415E-02
13.50	0.450E-02

Experiment No. = B4
Temperature (K) = 1200.00
Sample area (m sq.) =0.3790E-03

Time (ks)	dW/A (kg/m sq.)
0.60	0.844E-03
1.14	0.127E-02
1.50	0.137E-02
2.16	0.179E-02
2.76	0.222E-02
3.00	0.243E-02
3.72	0.285E-02
4.80	0.391E-02
6.00	0.538E-02
7.20	0.654E-02
9.00	0.802E-02
10.80	0.950E-02
12.30	0.108E-01
14.10	0.119E-01
15.90	0.131E-01
18.60	0.150E-01
19.80	0.156E-01
21.30	0.166E-01

Experiment No. = B4r
Temperature (K) = 1200.00
Sample area (m sq.) =0.3570E-03

Time (ks)	dW/A (kg/m sq.)
0.60	0.896E-03
1.38	0.157E-02
1.80	0.190E-02
2.40	0.235E-02
3.60	0.347E-02
5.40	0.538E-02
7.20	0.728E-02
9.00	0.885E-02
10.80	0.103E-01
12.60	0.117E-01
14.40	0.129E-01
16.20	0.141E-01
18.00	0.154E-01
19.50	0.161E-01
21.30	0.165E-01

Experiment No. = B5
Temperature (K) = 1250.00
Sample area (m sq.) =0.3830E-03

Time (ks)	dW/A (kg/m sq.)
1.80	0.460E-02
3.60	0.898E-02
5.40	0.127E-01
7.20	0.158E-01
9.00	0.184E-01
10.62	0.206E-01
12.60	0.232E-01
14.40	0.253E-01
16.20	0.276E-01
18.00	0.295E-01
19.62	0.309E-01

Experiment No. = B5r
Temperature (K) = 1250.00
Sample area (m sq.) =0.3670E-03

Time (ks)	dW/A (kg/m sq.)
1.80	0.403E-02
3.60	0.752E-02
5.40	0.104E-01
7.20	0.130E-01
9.00	0.153E-01
10.80	0.172E-01
12.60	0.194E-01
14.40	0.211E-01
16.20	0.228E-01
18.00	0.244E-01
19.80	0.259E-01
21.60	0.277E-01
23.40	0.289E-01
24.60	0.302E-01

Experiment No. = B6
Temperature (K) = 1300.00
Sample area (m sq.) =0.3580E-03

Time (ks)	dW/A (kg/m sq.)
0.24	0.112E-02
0.42	0.201E-02
0.72	0.346E-02
1.20	0.603E-02
1.80	0.872E-02
2.40	0.112E-01
3.00	0.134E-01
3.60	0.150E-01
4.20	0.171E-01
4.80	0.187E-01
5.40	0.200E-01
6.00	0.213E-01
7.20	0.239E-01
9.00	0.273E-01
10.80	0.302E-01
12.60	0.330E-01
14.40	0.354E-01
16.20	0.378E-01
17.40	0.394E-01

Experiment No. = B6r
Temperature (K) = 1300.00
Sample area (m sq.) =0.3440E-03

Time (ks)	dW/A (kg/m sq.)
0.24	0.128E-02
0.60	0.314E-02
0.84	0.453E-02
1.08	0.547E-02
1.32	0.674E-02
1.80	0.907E-02
2.82	0.135E-01
3.72	0.164E-01
4.80	0.194E-01
5.40	0.209E-01
6.00	0.224E-01
7.20	0.249E-01
9.00	0.285E-01
10.80	0.317E-01
12.60	0.345E-01
13.20	0.356E-01
13.68	0.362E-01
14.40	0.373E-01

Experiment No. = B7
Temperature (K) = 1300.00
Sample area (m sq.) =0.3410E-03

Time (ks)	dW/A (kg/m sq.)
0.60	0.762E-03
1.20	0.135E-02
1.80	0.188E-02
3.00	0.264E-02
3.60	0.293E-02
5.40	0.375E-02
7.20	0.475E-02
9.00	0.557E-02
10.80	0.633E-02
12.60	0.704E-02
14.40	0.757E-02
16.20	0.821E-02
18.00	0.886E-02
19.80	0.944E-02
21.60	0.991E-02
23.40	0.104E-01
25.20	0.109E-01
27.00	0.110E-01
28.80	0.116E-01
30.60	0.120E-01
32.40	0.126E-01
34.20	0.128E-01
36.00	0.133E-01

Experiment No. = B8*
Temperature (K) = 1200.00
Sample area (m sq.) =0.2710E-03

Time (ks)	dW/A (kg/m sq.)
0.60	0.590E-04
1.20	0.133E-03
1.80	0.177E-03
3.60	0.236E-03
5.40	0.266E-03
7.20	0.280E-03
9.00	0.295E-03
10.80	0.347E-03
14.40	0.369E-03
18.00	0.443E-03
21.60	0.531E-03
25.20	0.635E-03
28.80	0.708E-03
32.40	0.797E-03
36.00	0.856E-03
39.60	0.923E-03
43.20	0.959E-03

Experiment No. = B9*
Temperature (K) = 1300.00
Sample area (m sq.) =0.3120E-03

Time (ks)	dW/A (kg/m sq.)
0.60	0.577E-03
1.20	0.955E-03
1.80	0.124E-02
2.40	0.153E-02
3.00	0.167E-02
3.60	0.200E-02
5.40	0.255E-02
7.20	0.310E-02
9.00	0.363E-02
10.80	0.417E-02
12.60	0.463E-02
14.40	0.505E-02
16.20	0.542E-02
18.00	0.578E-02

Experiment No. = B10
Temperature (K) = 1100.00
Sample area (m sq.) =0.3210E-03

Time (ks)	dW/A (kg/m sq.)
3.60	0.125E-03
7.20	0.343E-03
10.80	0.623E-03
14.40	0.735E-03
15.60	0.798E-03
19.20	0.928E-03
21.90	0.100E-02
25.80	0.110E-02
29.10	0.115E-02
32.70	0.121E-02
36.00	0.132E-02
39.60	0.144E-02
43.20	0.150E-02
46.80	0.162E-02
50.40	0.172E-02
54.00	0.181E-02
57.00	0.189E-02
60.90	0.194E-02
64.80	0.196E-02
75.60	0.198E-02
86.70	0.218E-02

Experiment No. = B11
Temperature (K) = 1150.00
Sample area (m sq.) =0.3700E-03

Time (ks)	dW/A (kg/m sq.)
1.20	0.151E-03
1.80	0.189E-03
2.40	0.270E-03
3.00	0.335E-03
3.60	0.432E-03
5.40	0.616E-03
7.20	0.757E-03
9.00	0.962E-03
10.80	0.115E-02
12.60	0.132E-02
14.40	0.141E-02
15.00	0.145E-02
16.20	0.155E-02
18.00	0.165E-02
19.20	0.170E-02

Experiment No. = B12
Temperature (K) = 1200.00
Sample area (m sq.) =0.3600E-03

Time (ks)	dW/A (kg/m sq.)
0.60	0.378E-03
1.20	0.722E-03
1.80	0.933E-03
2.40	0.114E-02
3.00	0.133E-02
3.60	0.147E-02
5.40	0.190E-02
6.00	0.204E-02
7.20	0.226E-02
9.00	0.260E-02
10.80	0.286E-02
12.00	0.304E-02
12.60	0.313E-02
14.40	0.336E-02
16.20	0.352E-02
17.40	0.362E-02

Experiment No. = B13
Temperature (K) = 1250.00
Sample area (m sq.) =0.3620E-03

Time (ks)	dW/A (kg/m sq.)
0.60	0.696E-03
1.20	0.114E-02
1.80	0.147E-02
2.40	0.177E-02
3.00	0.207E-02
3.60	0.233E-02
5.40	0.306E-02
6.00	0.325E-02
7.20	0.363E-02
9.00	0.419E-02
10.80	0.471E-02
12.00	0.496E-02
12.60	0.518E-02
14.40	0.568E-02
16.20	0.614E-02
18.00	0.651E-02
19.80	0.684E-02
21.60	0.714E-02

Experiment No. = B14
Temperature (K) = 1300.00
Sample area (m sq.) =0.3350E-03

Time (ks)	dW/A (kg/m sq.)
0.60	0.137E-02
1.20	0.239E-02
1.80	0.316E-02
2.40	0.382E-02
3.00	0.424E-02
3.60	0.460E-02
5.40	0.549E-02
6.00	0.579E-02
7.20	0.633E-02
9.00	0.699E-02
10.80	0.752E-02
12.00	0.788E-02
12.60	0.800E-02
14.40	0.860E-02

Experiment No. = B15
Temperature (K) = 1200.00
Sample area (m sq.) =0.3890E-03

Time (ks)	dW/A (kg/m sq.)
0.60	0.216E-03
1.20	0.509E-03
1.80	0.761E-03
2.40	0.103E-02
3.00	0.123E-02
3.60	0.139E-02
5.40	0.189E-02
6.00	0.201E-02
7.20	0.226E-02
9.00	0.259E-02
10.80	0.285E-02
12.00	0.295E-02
12.60	0.307E-02
14.40	0.328E-02
15.60	0.341E-02

Experiment No. = B16
Temperature (K) = 1200.00
Sample area (m sq.) =0.4110E-03

Time (ks)	dW/A (kg/m sq.)
0.60	0.793E-03
1.20	0.124E-02
1.80	0.156E-02
2.40	0.197E-02
3.00	0.229E-02
3.60	0.259E-02
5.40	0.346E-02
6.00	0.373E-02
7.20	0.421E-02
9.00	0.483E-02
10.80	0.532E-02
12.00	0.564E-02
12.60	0.586E-02
14.40	0.619E-02

Experiment No. = B17
Temperature (K) = 1300.00
Sample area (m sq.) =0.3520E-03

Time (ks)	dW/A (kg/m sq.)
0.60	0.966E-03
1.20	0.165E-02
1.80	0.233E-02
2.70	0.290E-02
3.60	0.347E-02
4.50	0.398E-02
5.40	0.443E-02
7.20	0.517E-02
9.00	0.597E-02
10.80	0.659E-02
12.60	0.710E-02
14.40	0.750E-02
16.20	0.795E-02
18.00	0.830E-02
19.80	0.869E-02
21.60	0.903E-02

Experiment No. = B18
Temperature (K) = 1300.00
Sample area (m sq.) =0.3520E-03

Time (ks)	dW/A (kg/m sq.)
0.60	0.977E-03
1.20	0.178E-02
1.80	0.231E-02
2.40	0.283E-02
3.00	0.323E-02
3.60	0.360E-02
5.40	0.457E-02
7.20	0.528E-02
9.00	0.586E-02
10.80	0.637E-02
12.60	0.689E-02
14.40	0.740E-02
16.20	0.791E-02
18.00	0.836E-02
19.80	0.878E-02
21.60	0.918E-02

Experiment No. = B19
Temperature (K) = 1200.00
Sample area (m sq.) =0.3420E-03

Time (ks)	dW/A (kg/m sq.)
0.60	0.491E-03
1.20	0.107E-02
1.80	0.140E-02
3.00	0.236E-02
3.60	0.285E-02
4.80	0.400E-02
5.40	0.463E-02
7.20	0.620E-02
9.00	0.776E-02
10.80	0.917E-02
12.60	0.105E-01
14.40	0.116E-01
15.60	0.125E-01

Experiment No. = B20
Temperature (K) = 1200.00
Sample area (m sq.) =0.3960E-03

Time (ks)	dW/A (kg/m sq.)
0.60	0.626E-03
1.20	0.115E-02
1.80	0.165E-02
2.40	0.207E-02
3.00	0.260E-02
3.60	0.315E-02
4.20	0.373E-02
4.80	0.429E-02
5.40	0.480E-02
6.00	0.528E-02
7.20	0.636E-02
9.00	0.773E-02
10.80	0.900E-02
12.00	0.981E-02
12.60	0.102E-01
14.40	0.112E-01
15.60	0.119E-01

Experiment No. = B21
Temperature (K) = 1200.00
Sample area (m sq.) =0.3870E-03

Time (ks)	dW/A (kg/m sq.)
0.60	0.413E-03
1.20	0.827E-03
1.80	0.129E-02
2.40	0.165E-02
3.00	0.207E-02
3.60	0.253E-02
4.80	0.351E-02
5.40	0.403E-02
6.00	0.450E-02
7.20	0.537E-02
9.00	0.641E-02
10.20	0.698E-02
10.80	0.775E-02
11.88	0.786E-02

Experiment No. = B22*
Temperature (K) = 1200.00
Sample area (m sq.) =0.3290E-03

Time (ks)	dW/A (kg/m sq.)
0.60	0.207E-03
1.20	0.438E-03
1.80	0.657E-03
2.40	0.875E-03
3.00	0.107E-02
3.60	0.128E-02
5.40	0.184E-02
7.20	0.236E-02
9.00	0.287E-02
10.80	0.319E-02
12.60	0.357E-02
14.40	0.398E-02
16.20	0.438E-02

Experiment No. = B23
Temperature (K) = 1300.00
Sample area (m sq.) =0.3400E-03

Time (ks)	dW/A (kg/m sq.)
0.60	0.176E-03
1.20	0.647E-03
1.80	0.106E-02
3.00	0.212E-02
3.60	0.259E-02
5.40	0.494E-02
6.00	0.624E-02
7.20	0.794E-02
9.00	0.101E-01
10.80	0.116E-01
12.00	0.129E-01
12.60	0.136E-01
14.40	0.166E-01
16.20	0.196E-01
18.00	0.225E-01
19.80	0.254E-01
21.60	0.269E-01
23.40	0.290E-01
25.20	0.310E-01
27.00	0.330E-01
28.80	0.351E-01
30.60	0.372E-01
31.80	0.385E-01

Experiment No. = B24
Temperature (K) = 1300.00
Sample area (m sq.) =0.3200E-03

Time (ks)	dW/A (kg/m sq.)
0.60	0.375E-03
1.20	0.100E-02
1.80	0.150E-02
2.40	0.200E-02
3.00	0.231E-02
3.60	0.262E-02
5.40	0.344E-02
7.20	0.400E-02
9.00	0.450E-02
10.80	0.506E-02
12.60	0.544E-02
14.10	0.581E-02

Experiment No. = B25
Temperature (K) = 1300.00
Sample area (m sq.) =0.2950E-03

Time (ks)	dW/A (kg/m sq.)
0.30	0.156E-02
0.60	0.237E-02
1.20	0.359E-02
1.80	0.441E-02
2.40	0.481E-02
3.00	0.508E-02
3.60	0.536E-02
5.40	0.583E-02
7.20	0.617E-02
9.00	0.651E-02
10.80	0.685E-02
12.60	0.725E-02
14.40	0.753E-02

Experiment No. = C1
Temperature (K) = 1000.00
Sample area (m sq.) =0.3140E-03

Time (ks)	dW/A (kg/m sq.)
1.80	0.255E-03
3.60	0.408E-03
7.20	0.701E-03
10.80	0.917E-03
14.40	0.111E-02
18.00	0.124E-02
21.60	0.144E-02
25.20	0.152E-02
28.80	0.167E-02
32.40	0.186E-02
36.00	0.196E-02
39.60	0.217E-02
43.20	0.224E-02
46.80	0.245E-02
50.40	0.257E-02
57.60	0.275E-02
64.80	0.287E-02
72.00	0.294E-02
79.20	0.313E-02
86.40	0.341E-02

Experiment No. = C2
Temperature (K) = 1100.00
Sample area (m sq.) =0.3350E-03

Time (ks)	dW/A (kg/m sq.)
0.60	0.239E-03
1.20	0.358E-03
1.80	0.478E-03
3.00	0.776E-03
3.60	0.955E-03
5.40	0.143E-02
6.00	0.155E-02
7.20	0.173E-02
9.00	0.209E-02
10.80	0.245E-02
12.60	0.269E-02
14.40	0.281E-02

Experiment No. = C2r
Temperature (K) = 1100.00
Sample area (m sq.) =0.3310E-03

Time (ks)	dW/A (kg/m sq.)
0.60	0.302E-03
1.20	0.423E-03
1.80	0.483E-03
3.00	0.725E-03
3.60	0.846E-03
5.40	0.103E-02
6.00	0.115E-02
7.20	0.127E-02
9.00	0.151E-02
10.80	0.181E-02
12.60	0.199E-02
14.40	0.230E-02

Experiment No. = C3
Temperature (K) = 1150.00
Sample area (m sq.) =0.3320E-03

Time (ks)	dW/A (kg/m sq.)
0.60	0.241E-03
1.20	0.482E-03
1.80	0.723E-03
3.00	0.120E-02
3.60	0.127E-02
5.40	0.193E-02
6.00	0.211E-02
7.20	0.235E-02
9.00	0.295E-02
10.80	0.343E-02
12.60	0.398E-02
14.40	0.452E-02
16.20	0.494E-02

Experiment No. = C3r
Temperature (K) = 1150.00
Sample area (m sq.) =0.3210E-03

Time (ks)	dW/A (kg/m sq.)
0.60	0.374E-03
1.20	0.623E-03
1.80	0.810E-03
3.00	0.118E-02
3.60	0.137E-02
5.40	0.193E-02
7.20	0.231E-02
9.00	0.280E-02
10.80	0.330E-02
12.60	0.386E-02
14.40	0.436E-02
15.00	0.449E-02
15.60	0.467E-02

Experiment No. = C4
Temperature (K) = 1200.00
Sample area (m sq.) =0.3640E-03

Time (ks)	dW/A (kg/m sq.)
0.60	0.549E-03
1.80	0.137E-02
3.00	0.225E-02
3.60	0.275E-02
5.40	0.429E-02
6.00	0.473E-02
7.20	0.571E-02
9.00	0.692E-02
10.80	0.791E-02
12.00	0.857E-02
12.60	0.890E-02
14.40	0.978E-02
15.60	0.105E-01

Experiment No. = C4r
Temperature (K) = 1200.00
Sample area (m sq.) =0.3650E-03

Time (ks)	dW/A (kg/m sq.)
0.60	0.712E-03
1.20	0.126E-02
1.80	0.164E-02
3.00	0.263E-02
3.60	0.312E-02
5.40	0.460E-02
6.00	0.510E-02
7.20	0.608E-02
9.00	0.740E-02
10.80	0.833E-02
12.00	0.910E-02
12.60	0.942E-02
14.40	0.104E-01
15.60	0.111E-01

Experiment No. = C5
Temperature (K) = 1250.00
Sample area (m sq.) =0.3100E-03

Time (ks)	dW/A (kg/m sq.)
0.60	0.181E-02
1.20	0.374E-02
1.80	0.529E-02
3.00	0.800E-02
3.60	0.903E-02
5.40	0.122E-01
6.00	0.132E-01
7.20	0.148E-01
9.00	0.172E-01
10.80	0.192E-01
12.00	0.205E-01
12.60	0.211E-01
14.40	0.229E-01
15.00	0.235E-01
16.14	0.245E-01

Experiment No. = C5r
Temperature (K) = 1250.00
Sample area (m sq.) =0.3120E-03

Time (ks)	dW/A (kg/m sq.)
0.36	0.769E-03
0.54	0.122E-02
1.02	0.263E-02
1.80	0.449E-02
3.60	0.808E-02
5.40	0.110E-01
6.00	0.118E-01
7.20	0.135E-01
9.00	0.156E-01
10.80	0.176E-01
12.00	0.187E-01
12.60	0.194E-01
14.40	0.210E-01
15.60	0.221E-01

Experiment No. = C6
Temperature (K) = 1300.00
Sample area (m sq.) =0.3310E-03

Time (ks)	dW/A (kg/m sq.)
0.30	0.211E-02
0.60	0.471E-02
1.20	0.882E-02
1.80	0.117E-01
3.00	0.155E-01
3.60	0.170E-01
5.40	0.209E-01
6.00	0.221E-01
7.20	0.244E-01
9.00	0.276E-01
10.80	0.303E-01
12.00	0.320E-01
12.60	0.328E-01
14.40	0.356E-01
15.60	0.372E-01

Experiment No. = C6r
Temperature (K) = 1300.00
Sample area (m sq.) =0.3080E-03

Time (ks)	dW/A (kg/m sq.)
0.30	0.247E-02
0.60	0.506E-02
1.20	0.948E-02
1.80	0.126E-01
3.00	0.169E-01
3.60	0.186E-01
5.40	0.227E-01
6.00	0.242E-01
7.20	0.265E-01
9.00	0.299E-01
10.80	0.331E-01
12.00	0.351E-01
12.60	0.361E-01
13.80	0.379E-01

Experiment No. = C7
Temperature (K) = 1300.00
Sample area (m sq.) =0.3500E-03

Time (ks)	dW/A (kg/m sq.)
0.60	0.914E-03
1.20	0.154E-02
1.80	0.200E-02
3.00	0.280E-02
3.60	0.320E-02
5.40	0.423E-02
7.20	0.514E-02
9.00	0.594E-02
10.80	0.669E-02
12.60	0.726E-02
14.40	0.794E-02
16.20	0.851E-02
18.00	0.914E-02
19.80	0.971E-02
21.60	0.103E-01
23.40	0.109E-01
25.20	0.114E-01
27.00	0.119E-01
28.80	0.125E-01
30.60	0.130E-01
32.40	0.135E-01
34.20	0.140E-01
35.70	0.144E-01

Experiment No. = C8
Temperature (K) = 1300.00
Sample area (m sq.) =0.3330E-03

Time (ks)	dW/A (kg/m sq.)
0.60	0.126E-02
1.20	0.228E-02
1.80	0.324E-02
3.00	0.480E-02
3.60	0.541E-02
5.40	0.703E-02
6.00	0.751E-02
7.20	0.841E-02
9.00	0.961E-02
10.80	0.105E-01
12.60	0.114E-01
14.40	0.123E-01
16.20	0.130E-01
18.00	0.138E-01
19.80	0.144E-01
21.60	0.150E-01

APPENDIX B

PROGRAM FOR CALCULATION OF VARIOUS RATE CONSTANTS

```
C-----------------------------------------------------------------------
C       T= TEMPERATURE (K)
C       L= SAMPLE NO.
C       M= MAXIMUM NO. OF EXP. SETS
C       N= NO. OF DATA
C       AREA=GEOMETRIC SURFACE AREA OF SAMPLE
C       X= TIME
C       W= WT. GAIN
C-----------------------------------------------------------------------
        IMPLICIT REAL *8(A-H,O-Z)
        COMMON/DATA/W(30),X(30,2),XT(30,2),Y1(30,2),Y(30,2),YB(30,2)
        COMMON/LEAST/AM,AK,N,J
        REAL *8 YT(30,2)
        REAL *8 AX(10),FF(3),DF(3),DEF(3,2),XI(3,2),AXI(3),SIGMA(3)
        REAL *8 A0(3),A1(3),A2(3),A3(3),A4(3),YI(30,2),SLOPE(30,2)
        REAL *8 A(5,5),B(5,5),C(5,1),D(5,1),BB(5,5),E(5,5),DEFI(3,2)
        REAL *8 SUMX(30),SUMSX(30),SUMCX(30),SUMFOX(30),SUMFX(30)
        REAL *8 SUMSIX(30),SUMX7(30),SUMX8(30),SUMY(30),SUMXY(30)
        REAL *8 SUMSXY(30),SUMCXY(30),SUMX4Y(30),AREA1(3)
C-----------------------------------------------------------------------
        OPEN (UNIT=21, FILE='C:\DATA1.IN')
        OPEN (UNIT=22, FILE='C:\DATA1.DAT')
        OPEN (UNIT=23, FILE='C:\DATA1A.OUT')
        OPEN (UNIT=24, FILE='C:\DATA1B.OUT')
C
        MM=0
5       MM=MM+1
        LL=0
10      READ (21,*) T
        IF (T .EQ. 9999.0) GO TO 99
C        T=T+273.00
C15      LL=LL+1
        J=0
20      READ (21,*) L,M
25      J=J+1
        READ (21,*) N,AREA1(J)
        AREA=AREA1(J)*1.D-4
        DO 30 I=1,N
        READ (21,*) XT(I,J),W(I)
30      CONTINUE
        DO 40 I=1,N
        X(I,J)=XT(I,J)*60.0
        W(I)=W(I)*1.D-6
        Y1(I,J)=W(I)/AREA
        YT(I,J)=625.0*Y1(I,J)
        Y(I,J)=Y1(I,J)**2
40      CONTINUE
C-------
        CALL LSTSQR
C-------
        SUMX(J)=0.0
        SUMSX(J)=0.0
        SUMCX(J)=0.0
        SUMFOX(J)=0.0
        SUMFX(J)=0.0
        SUMSIX(J)=0.0
        SUMX7(J)=0.0
        SUMX8(J)=0.0
        SUMY(J)=0.0
        SUMXY(J)=0.0
```

```
      SUMSXY(J)=0.0
      SUMCXY(J)=0.0
      SUMX4Y(J)=0.0
      DO 50 I=1,N
      SUMX(J)=SUMX(J)+X(I,J)
      SUMSX(J)=SUMSX(J)+X(I,J)**2
      SUMCX(J)=SUMCX(J)+X(1,J)**3
      SUMFOX(J)=SUMFOX(J)+X(I,J)**4
      SUMFX(J)=SUMFX(J)+X(I,J)**5
      SUMSIX(J)=SUMSIX(J)+X(I,J)**6
      SUMX7(J)=SUMX7(J)+X(I,J)**7
      SUMX8(J)=SUMX8(J)+X(I,J)**8
C
      SUMY(J)=SUMY(J)+Y(I,J)
      SUMXY(J)=SUMXY(J)+X(I,J)*Y(I,J)
      SUMSXY(J)=SUMSXY(J)+X(I,J)**2*Y(I,J)
      SUMCXY(J)=SUMCXY(J)+X(I,J)**3*Y(I,J)
      SUMX4Y(J)=SUMX4Y(J)+X(I,J)**4*Y(I,J)
50    CONTINUE
      A(1,1)=REAL(N)/SUMY(J)
      A(1,2)=SUMX(J)/SUMY(J)
      A(1,3)=SUMSX(J)/SUMY(J)
      A(1,4)=SUMCX(J)/SUMY(J)
      A(1,5)=SUMFOX(J)/SUMY(J)
C
      A(2,1)=SUMX(J)/SUMXY(J)
      A(2,2)=SUMSX(J)/SUMXY(J)
      A(2,3)=SUMCX(J)/SUMXY(J)
      A(2,4)=SUMFOX(J)/SUMXY(J)
      A(2,5)=SUMFX(J)/SUMXY(J)
C
      A(3,1)=SUMSX(J)/SUMSXY(J)
      A(3,2)=SUMCX(J)/SUMSXY(J)
      A(3,3)=SUMFOX(J)/SUMSXY(J)
      A(3,4)=SUMFX(J)/SUMSXY(J)
      A(3,5)=SUMSIX(J)/SUMSXY(J)
C
      A(4,1)=SUMCX(J)/SUMCXY(J)
      A(4,2)=SUMFOX(J)/SUMCXY(J)
      A(4,3)=SUMFX(J)/SUMCXY(J)
      A(4,4)=SUMSIX(J)/SUMCXY(J)
      A(4,5)=SUMX7(J)/SUMCXY(J)
C
      A(5,1)=SUMFOX(J)/SUMX4Y(J)
      A(5,2)=SUMFX(J)/SUMX4Y(J)
      A(5,3)=SUMSIX(J)/SUMX4Y(J)
      A(5,4)=SUMX7(J)/SUMX4Y(J)
      A(5,5)=SUMX8(J)/SUMX4Y(J)
C
      CALL GJORD(5,A)
      C(1,1)=1.0
      C(2,1)=1.0
      C(3,1)=1.0
      C(4,1)=1.0
      C(5,1)=1.0
      CALL MATMUL (A,5,  C,5,  5,5,1,  D,5)
C
      A0(J)=D(1,1)
      A1(J)=D(2,1)
      A2(J)=D(3,1)
      A3(J)=D(4,1)
      A4(J)=D(5,1)
      DO 60 I=1,N
      YR(I,J)=A0(J)+A1(J)*X(I,J)+A2(J)*X(I,J)**2+A3(J)*X(I,J)**3
     1  +A4(J)*X(I,J)**4
60    CONTINUE
```

```
C------ Calculation of instantaneous rates  -------------------------
        DO 500 I=1,N
        SLOPE(I,J)=A1(J)+2.0*A2(J)*X(1,J)+3.0*A3(J)*X(1,J)**2
     1  +4.0*A4(J)*X(I,J)**3
500      CONTINUE
C------ Calculation of standard deviation (SIGMA)  -------------------
65      SUMZ=0.0
        DO 70 I=1,N
        SUMZ=SUMZ+(Y(I,J)-YB(I,J))**2
70      CONTINUE
        SIGMA(J)=SQRT(SUMZ/(FLOAT(N-2)))
C------ Calculation of average rate const [AVKP] ---------------------
        SUMKP=0.0
        STIME=0.0
        DO 333 I=1,N
        SUMKP=SUMKP+SLOPE(I,J)*X(I,J)
        STIME=STIME+X(I,J)
333     CONTINUE
        AVKP=SUMKP/STIME
C-------------------------------------------------------------------------
C        WRITE(22,80) L,T,J,AREA
C80      FORMAT(/80('*')/2X,'Sample No.=',I2,34X,'Temp.(K)=',F7.2
C     1  /2X,'Exp. Set=',I2,31X,'Sample Area (m sq.)=',E10.4/)
        WRITE(22,80) T,AREA
80      FORMAT(/80('*')/30X,'Expt. No.= B11'/'Temp.(K)=',F7.2,
     1  30X,'Sample Area (m sq.) =',E10.4)
        WRITE (22,90) A0(J),A1(J),A2(J),A3(J),A4(J),SIGMA(J),AVKP
90      FORMAT ('A0=',E10.4,3X,'A1=',E10.4,3X,'A2=',E10.4,
     1  3X,'A3=',E10.4,3X,'A4=',E10.4/'Std.Dev.=',E10.4/
     2  'Average rate const =',E11.3/80('-'))
        WRITE(22,100)
100     FORMAT('S.No.',3X,'Time(S)',7X,'dW/A',4X,'th(micron)',3X,
     1  'Y(actual)',4X,'Y(Best Fit)',1X,'Inst. Rate Const.')
        DO 110  I=1,N
        WRITE (22,120) I,X(I,J),Y1(I,J),YT(I,J),Y(I,J),YB(I,J),
     1  SLOPE(I,J)
120     FORMAT(I2,2X,E12.3,1X,E12.3,2X,F7.2,2X,E12.3,2X,E12.3,1X,
     1  E12.3)
110     CONTINUE
C-------------------------------------------------------------------------
        WRITE(23,580) T,AREA
580     FORMAT(/30('-')/4X,'Experiment No. = B11'/
     1  'Temperature (K)      =',1X,F7.2/'Sample area (m sq.) =',
     2  E10.4/30('-'))
        WRITE(23,590)
590     FORMAT('Time (ks)',6X,'dW/A (kg/m sq.)')
        DO 600  I=1,N
        XX=X(I,J)/1.D3
        WRITE (23,610) XX,Y1(I,J)
610     FORMAT(F8.2,7X,E12.3)
600     CONTINUE
        WRITE(23,620)
620     FORMAT(30('-'))
C-------------------------------------------------------------------------
        WRITE(24,900) T,AREA
900     FORMAT(/70('*')/24X,'Experiment No. = B11'/
     1  'Temperature (K) =',1X,F7.2,12X,'Sample area (m sq.) = ',
     2  E10.4/70('.'))
        WRITE (24,910) A0(J),A1(J),A2(J),A3(J),A4(J),SIGMA(J),AVKP
910     FORMAT ('Polynomial coefficients:'/'a=',E11.4,1X,'b=',
     1  E11.4,1X,'c=',E11.4,1X,'d=',E11.4,1X,'e=',
     2  E11.4/'Standard deviation =',E11.4/'Avg. rate const.=',
     3  E11.3/70('-'))
        WRITE(24,920)
920     FORMAT('Time (ks)',5X,'x (micron)',3X,'Y(actual)',5X,
     1  'Y(Best Fit)',1X,'Inst. Rate Const.')
```

```
      DO 930  I=1,N
      XX=X(I,J)/1.D3
      WRITE (24,940) XX,YT(I,J),Y(I,J),YB(I,J),
     1  SLOPE(I,J)
940   FORMAT(F8.2,6X,F7.2,3X,E12.3,3X,E12.3,2X,E12.3)
930   CONTINUE
      WRITE(24,950)
950   FORMAT(70('_'))
C-----------------------------
      IF (J .LT. M) GO TO 25
C-----------------------------------------------------------------------
      WRITE(22,210)
210   FORMAT(80('#')/)
C      IF (LL .LT.3) GO TO 15
      IF (MM .LT. 5) GO TO 5
99    STOP
      END
C-----------------------------------------------------------------------
C     SUBROUTINE FOR MATRIX INVERSION BY GAUSS JORDON METHOD
C-----------------------------------------------------------------------
      SUBROUTINE GJORD (N4,A)
      REAL*8 A(N4,N4)
      DO 50 K=1,N4
         DO 10 J=1,N4
            IF (J.EQ.K) GO TO 10
            A(K,J)=A(K,J)/A(K,K)
10       CONTINUE
         A(K,K)=1/A(K,K)
         DO 30 I=1,N4
            IF (I.EQ.K) GO TO 30
            DO 20 J=1,N4
               IF (J.EQ.K) GO TO 20
               A(I,J)=A(I,J)-A(K,J)*A(I,K)
20          CONTINUE
30       CONTINUE
         DO 40 I=1,N4
            IF (I.EQ.K) GO TO 40
            A(I,K)=-A(I,K)*A(K,K)
40       CONTINUE
50    CONTINUE
      RETURN
      END
C-----------------------------------------------------------------------
C          SUBROUTINE  FOR   MATRIX  MULTIPLICATION
C          matD (L X N) = matC(L X M) X matB(M X N)
C-----------------------------------------------------------------------
      SUBROUTINE MATMUL (B,IB,C,IC,L,M,N,D,ID)
      REAL*8 B(IB,M),C(IC,N),D(ID,N)
      DO I=1,L
         DO J=1,N
            D(I,J)=0.0
            DO K=1,M
               D(I,J)=D(I,J)+B(I,K)*C(K,J)
            ENDDO
         ENDDO
      ENDDO
      RETURN
      END
C-----------------------------------------------------------------------
      SUBROUTINE LSTSQR
      IMPLICIT REAL *8(A-H,O-Z)
      COMMON/DATA/W(30),X(30,2),XT(30,2),Y1(30,2),Y(30,2),YB(30,2)
      COMMON/LEAST/AM,AK,N,J
      DIMENSION YLOG(30,2),XLOG(30,2)
C-----------------------------------------------------------------------
      DO I=1,N
```

```
      YLOG(I,J)=DLOG(Y1(I,J))
      XLOG(I,J)=DLOG(X(I,J))
     ENDDO
     SUMY=0.0
     SUMX=0.0
     SUMXSQ=0.0
     SUMXY=0.0
     DO I=1,N
        SUMY=SUMY+YLOG(I,J)
           SUMX=SUMX+XLOG(I,J)
             SUMXSQ=SUMXSQ+XLOG(I,J)**2
          SUMXY=SUMXY+XLOG(I,J)*YLOG(I,J)
     ENDDO
     DENOM=(N*SUMXSQ-SUMX**2)
     A=(SUMY*SUMXSQ-SUMX*SUMXY)/DENOM
     B=(N*SUMXY-SUMX*SUMY)/DENOM
     AM=1.DO/B
     AA=A/B
     AK=DEXP(AA)
     RETURN
     END
C-----------------------------------------------------------------------
```

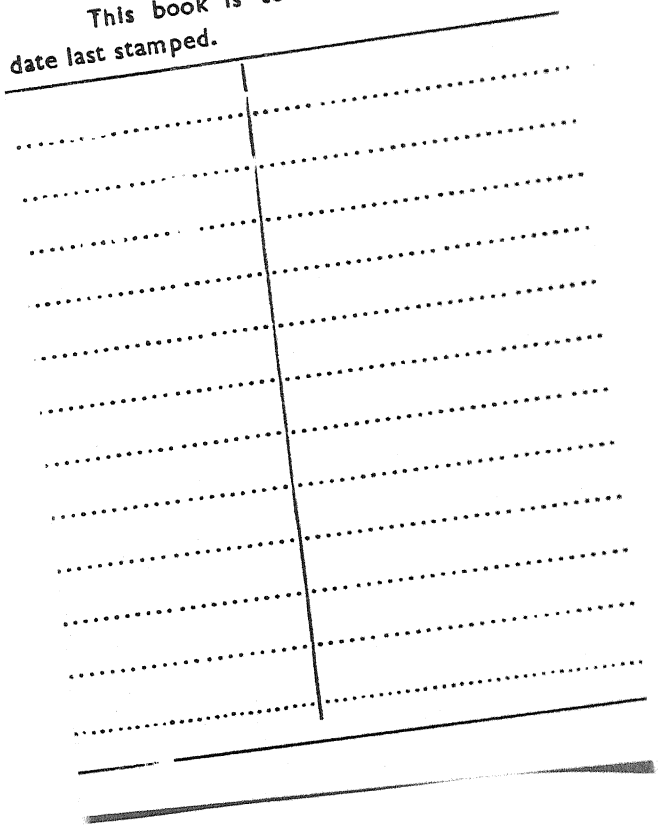

MME- 1995- D-RAY-MIG